BGSD-MO 7078

HARDWARE TEST PROGRAM FOR EVALUATION OF BASELINE RANGE/RANGE RATE SENSOR CONCEPT

PHASE II REPORT

CONTRACT
NAS8-36144

DECEMBER 1985

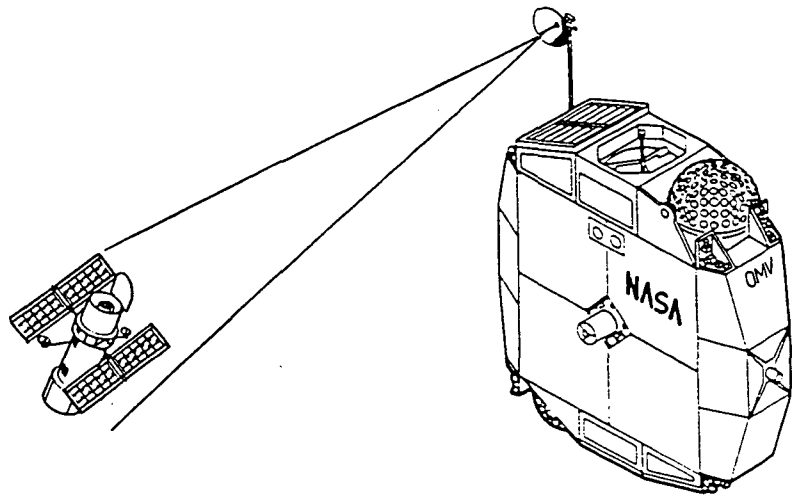

(NASA-CR-178710) HARDWARE TEST PROGRAM FOR EVALUATION OF BASELINE RANGE/RANGE RATE SENSOR CONCEPT (Allied Bendix Aerospace) 127 p HC A07/MF A01 CSCL 09B
N86-22129
Unclas
G3/60 16747

RECEIVED
NASA STI FACILITY
ACCESS DEPT.

FOR
NATIONAL AERONAUTICS AND
SPACE ADMINISTRATION
GEORGE C. MARSHALL
SPACE FLIGHT CENTER
MARSHALL SPACE FLIGHT CENTER
ALABAMA 35812

BY

ALLIED Bendix Aerospace

Bendix Guidance Systems Division
Mishawaka Operations
Mishawaka, Indiana 46544

BGSD-MO 7078

HARDWARE TEST PROGRAM FOR EVALUATION OF BASELINE RANGE/RANGE RATE SENSOR CONCEPT

PHASE II REPORT

CONTRACT NAS8-36144

DECEMBER 1985

PREPARED FOR:

NATIONAL AERONAUTICS & SPACE ADMINISTRATION
GEORGE C. MARSHALL SPACE FLIGHT CENTER
MARSHALL SPACE FLIGHT CENTER
ALABAMA 35812

PREPARED BY: _____
E. PERNIC
TEST COORDINATOR

APPROVED BY: _____
E. R. FEAGLER
PROJECT ENGINEER

APPROVED BY: _____
J. M. BUTTERFIELD
PROGRAM MANAGER

ALLIED Bendix Aerospace

Bendix Guidance Systems Division
Mishawaka Operations
Mishawaka, Indiana 46544

PREFACE

The Allied Corporation, Bendix Guidance Systems Division - Mishawaka Operations has prepared this report in fulfillment of Contract NAS8-36144 requirements. The report covers Phase II of the Hardware Test Program for evaluation for a range/range rate sensor concept for application with the Orbital Maneuvering Vehicle. During the six month Phase II effort, initiated 12 June 1985, an appropriately modified Bendix millimeter wave instrumentation radar served as the test bed for establishing range and range rate measurement accuracies, and radar signature characteristics of a typical spacecraft target, a one-third scale model of the Hubble Space Telescope.

TABLE OF CONTENTS

LIST OF TABLES

LIST OF FIGURES

SECTION 1.0

INTRODUCTION

During the past two and one-half years Bendix has been working with Marshall Space Flight Center (MSFC) on the conceptual design of an on-board sensor for application with the Orbital Maneuvering Vehicle (OMV). The proposed Range and Range Rate ($R/\dot{R}$) sensor would aid the OMV in performing rendezvous and docking maneuvers by providing independent measurements of range, range rate, and bearing to the target.

The Hardware Test Program was proposed to MSFC (BGSD-MO 6889) as one of the steps of a development program which has the objective of providing the space qualified sensor required for this application. The hardware test program is designed to reduce the technical risks associated with the $R/\dot{R}$ sensor design concept through a series of analyses and hardware tests utilizing appropriately modified Bendix brassboard radars.

Bendix was awarded contract NAS8-36144 by MSFC on 11 September 1984 to conduct the Hardware Test Program. Originally of six months duration, the program was extended through 11 December 1985 and expanded in scope to include a second phase of testing. The first phase of the test program, which covered the nine month period of 11 September 1984 through 11 June 1985, was successful in identifying risks associated with achieving the sensitivity required for initial target detection. A discussion of the Phase I effort, including a description for the test bed radar, tests performed, and test results, is presented in Technical Report, BGSD-MO 7035.

The test program Phase II effort, which is the subject of this report, provides additional design information in terms of $R/\dot{R}$ sensor performance when observing and tracking a typical spacecraft target. The target used in the test program was a one-third scale model of the Hubble Space Telescope (HST) available at the MSFC test site where the tests were performed. A modified Bendix millimeter wave radar served as the $R/\dot{R}$ sensor test bed for evaluation of range and range rate tracking performance, and generation of radar signature characteristics of the spacecraft target.

The Phase II program was directed at investigation of the $R/\dot{R}$ sensor radar "environment" during the final stages of rendezvous, in which the OMV is within 400′ to 50′ of the target. In this region the $R/\dot{R}$ sensor utilizes a high range resolution (3-1/3′) in order to achieve the required range and range rate tracking accuracy. Since the HST model is 15′ long, and has several surface discontinuities and appendages, the potential for an extended target signature characteristic exists.

The test series examined the signature characteristics of the HST model as a function of aspect angle and range. Major scatterers are defined by observing the target as a function of aspect angle. In a second series of tests, tracking performance is observed as a function of aspect angle. In the

final series of tests, the HST model is orientated in the docking position and the radar range and range rate tracking performance is evaluated as the radar was moved towards the target.

This report is presented in seven sections, following the Introduction, Section 2 presents a summary of program test results and conclusions. A detailed description of the Bendix test bed radar with accompanying instrumentation is presented in Section 3, and Section 4 describes the MSFC test site and facilities.

The test procedures used to establish background levels, and the calibration procedures used in the range accuracy tests and RCS (radar cross section) signature measurements, are presented in Section 5. A condensed version of the daily log kept during the 5 September through 17 September test period is presented in Section 6.

Section 7 contains the test program results starting with the RCS signature measurements, then continuing with range measurement accuracy test results and finally the range and range rate tracking accuracy test results.

SECTION 2.0

SUMMARY, CONCLUSIONS, AND RECOMMENDATIONS

The Hardware Test Program Phase II effort successfully achieved its two primary goals; establishing the key radar signature characteristics of a typical spacecraft target, and assessing the performance of the Bendix R/Ṙ test bed radar when tracking the representative target, a 1/3 scale model of the Hubble Space Telescope. Target signature and tracking performance data generated as a result of the test program provides an invaluable insight into the radar environment experienced by the R/Ṙ sensor during the final stages of the OMV rendezvous maneuver and initiation of the docking phase. Target detection and acquisition performance at initiation of the rendezvous maneuver can likewise be predicted by an appropriate scaling of the radar cross section data.

The radar-to-target range interval used during the testing (50′ to 350′) is representative of the transition from the rendezvous to the docking maneuver. During this phase of operation, the R/Ṙ sensor is operating in a high resolution mode to achieve the projected range measurement accuracy requirement of 6 inches. Results of the simulated docking maneuver tests indicate that the R/Ṙ sensor range and range rate measurement accuracy design goals of 0.5 ft/ and 0.1 ft/sec were achieved.

The range accuracy test series, in which the R/Ṙ sensor tracks the target as its orientation is varied in discrete steps, demonstrated the movement of tracking point with orientation, as anticipated. Likewise, the signature of the HST model was characteristic of the predominantly cylindrically shaped body with large scatterer returns at normal incidence and a lobing structure with alternating peaks and nulls as the angle moves away from normal incidence. A summary of test results is presented in Table 2-1.

A brief description of each of the test series listed in Table 2-1, including a summary of test results, conclusions and recommendations for further effort is presented in the following paragraphs.

2.1 RCS MEASUREMENTS

The radar cross section characteristics of the 1/3 scale model of the Hubble Space Telescope were measured with the Bendix W-Band R/Ṙ test bed radar. After calibration, RCS measurements of the spacecraft model were performed by observing the radar return signal through a series of contiguous 3-1/3′ range gates. The test data was processed in terms of the largest RCS value observed as a function of the aspect angle.

TABLE 2-1. TEST RESULT SUMMARY

• Radar Cross Section (RCS) Calibration	+28 dB
• HST Model RCS Measurements	
.. Body at normal incidence	>40 dB-m^2
.. Solar panels at normal incidence	36 dB-m^2
.. Overall for angles off normal	<-5 dB-m^2 to +25 dB-m^2
.. Overall 50% RCS value	5 dB-m2
• Range Measurement Calibration	
.. Mean range error	+.66 ft.
.. Standard deviation	.13 ft.
• Range Measurement Accuracy	
.. HST Model, Docking Orientation	.31 ft.
.. Other Orientations (see Table 7-2)	
• Tracking Accuracy Measurements	
.. Range Tracking Accuracy	.37 ft.
.. Range Rate Tracking Accuracy	.03 ft/sec.

2.1.1 RCS Calibration

The test bed radar was calibrated in terms of radar cross section by a two stage process. First, the radar was calibrated in terms of range gate (correlator) voltage vs. input power, as described in Section 5.3. The received power is then converted to RCS using the radar range equation. At the MSFC test site the test bed radar was calibrated using a standard point source target, a 300m^2 corner reflector. The measured RCS of the standard target was within 2 dB of the theoretical value.

2.1.2 HST Model RCS Measurements

The measured RCS of the HST model was a function of aspect angle, and displayed the general characteristics of a cylindrically shaped body. The maximum values of RCS were observed when the target was at normal incidence to the radar beam. As the aspect angle of the target was moved from the perpendicular, the RCS magnitude went through a lobing structure consisting of a series of peaks and valleys.

In addition to the main body response, which exceeded 40 dB-m^2, there were pronounced responses when the ends of the HST model were aligned with the R/$\dot{R}$ sensor boresight. Another predominant reflection was noted from the solar panels. A maximum RCS of 36 dB-m^2 was observed at normal incidence and the RCS gradually disappeared as the panel azimuth aspect angle moved away from perpendicular.

Also evident was a major return from the junction of the two cylinders comprising the body of the HST model. Distribution charts depicting the maximum observed RCS as a function of azimuth and elevation angles are presented in Figures 7-5 through 7-8. This data is likewise presented in Figures 7-33 and 7-34 in terms of distribution and density functions. The most frequently occurring RCS value was slightly above 5 dB-m^2 which corresponds to the 50% RCS value on the probability density function.

2.2 RANGE ACCURACY TESTS

Range accuracy tests were performed with a calibration reflector to establish radar measurement accuracy on the test sites and with the HST model to verify performance in both static and dynamic measurement scenarios.

2.2.1 Range Calibration

A trihedral corner reflector was used as a point-source target for range calibration. Results of the calibration procedure indicates a mean bias error of 0.66′ in the test setup. Although the test sample size is small, the 0.13′ standard deviation is equivalent to the least significant bit in the quantized radar range data. When determining range measurement accuracy, the bias noted during the calibration procedure is removed to indicate true range.

2.2.2 Static Test Results

The static tests were performed by observing the HST model with the tracking loops closed. The range tracking point was monitored as the model's orientation was changed in discrete steps. When the model was positioned to present a favorable tracking surface, such as presented by the docking mode orientations, the measured range accurately described the slant range to the surface. The results are repeatable and the measured range value can be verified independently.

As the aspect angle of the target changed the tracking point followed the predominant scatterer. When the aspect angle of the model was such that multiple reflectors were present within a given range gate, the tracking point will move as the result of any disturbance, such as that induced by wind. This is evident in the range accuracy tracking plots presented in Section 7.4.

2.2.3 Dynamic Test Results

The range measurement accuracy during a dynamic tracking scenario was evaluated during this series of tests. The docking position was used as the track point for approaches which were several degrees off boresite. Closure rates varied from 1 to 5 feet/second at slant ranges of approximately 350′ to 130′. By comparing the predicted radar slant range at several points along the radar route to the target with the actual radar measurements, a mean range differential of .37′ has been established as the dynamic range tracking error.

2.3 RATE TRACKING TESTS

The rate tests were conducted in conjunction with the dynamic range measurement tests discussed in Section 2.2.3. The rate output is based upon the doppler shift principle and is not derived from the range measurements through differential. The rate output is compared with a co-located laser measurement of the closing rate to determine the error. The maximum indicated mean rate error using this procedure is .025'/second.

2.4 CONCLUSIONS AND RECOMMENDATIONS

The measured 5 dB-m^2 average radar cross section of the 1/3 scale model of the HST corresponds to an average RCS of 14.5 dB-m^2 for the full-size HST. Since the $R/\dot{R}$ sensor design goal is detection of a 10 dB-m^2 target at 4.5 nmi, the detection range for targets the size of the HST would be increased to 5.8 nmi.

The demonstrated range and range rate measurement accuracies exceed the predicted $R/\dot{R}$ sensor requirements. During the simulated docking tests, the test bed $R/\dot{R}$ sensor maintained solid track of the HST model and the measured range and range rate accuracies of 0.3 ft. and 0.03 ft/sec, respectively, exceeded the corresponding predicted $R/\dot{R}$ sensor design requirements of 0.5 ft. and 0.1 ft/sec.

When the HST model's orientation was such that several scatterers were observed, the range tracking point was sensitive to slight motions of either the target or radar. This suggests that during initial acquisition when any target orientation is possible, the combined scatterers will generate glint and scintillation signature modulation components causing the target to fluctuate during the observation period.

It is recommended that the data processing and analysis effort continue with the objective of establishing a more detailed RCS model of the HST. In addition to the predominant scatterer data which has been processed to date, there is likewise RCS data on adjacent range bins which can be processed to identify other significant scatterers. Processing the remaining data would be the first step in developing an analytical model of the HST which would be used in target acquisition and tracking studies.

As an example of Bendix' previous experience in this area, a mathematical target model which included 22 scatterers was developed under a contract with Naval Weapons Center, China Lake, California. The computer program identified the tracking point in terms of ship aspect and rank order and was utilized in acquisition and tracking studies.

SECTION 3.0

SYSTEM CONFIGURATION

The test system setup used during testing at MSFC is shown in block diagram form in Figure 3-1. The primary tasks of each block in Figure 3-1 are briefly discussed in the following paragraphs.

XMTR/RCVR	Generation, transmission, reception, and conditioning of spread spectrum waveform.
DATA PROCESSOR	Contains circuits to process the received waveform for comparison with a delayed reference waveform and, in doing so, measures the target range and doppler shift (range rate).
RADAR COMPUTER	Controls the reference waveform delay; to provide finer granulation of the range function, it controls a delay applied to the received waveform. It also controls the doppler circuitry.
INSTRUMENTATION COMPUTER	Is the interface between the radar computer and the operator. It conditions and presents radar, positioner, and ranging laser data to the operator and the Instrumentation Recorder. It controls the radar via the radar computer and the tape recorder forward, record, and stop modes.
RANGING LASER	Furnished by MSFC, the laser provided an independent measure of target range and range rate data.
DISPLAYS: CRT, A-SCOPE, AND FREQUENCY COUNTER	The CRT presents radar and laser outputs and also test number, test elapsed time, clock time, and date. The A-scope provides an indication of target size and range on an oscilloscope. The frequency counter provides target acquisition and tracking performance information.

3.1 RADAR HARDWARE MODIFICATIONS

The W-Band CW radar was modified to the test bed configuration required for the test series, with the following considerations:

- Target extent of 15′
- 12 recorder channels for correlator outputs

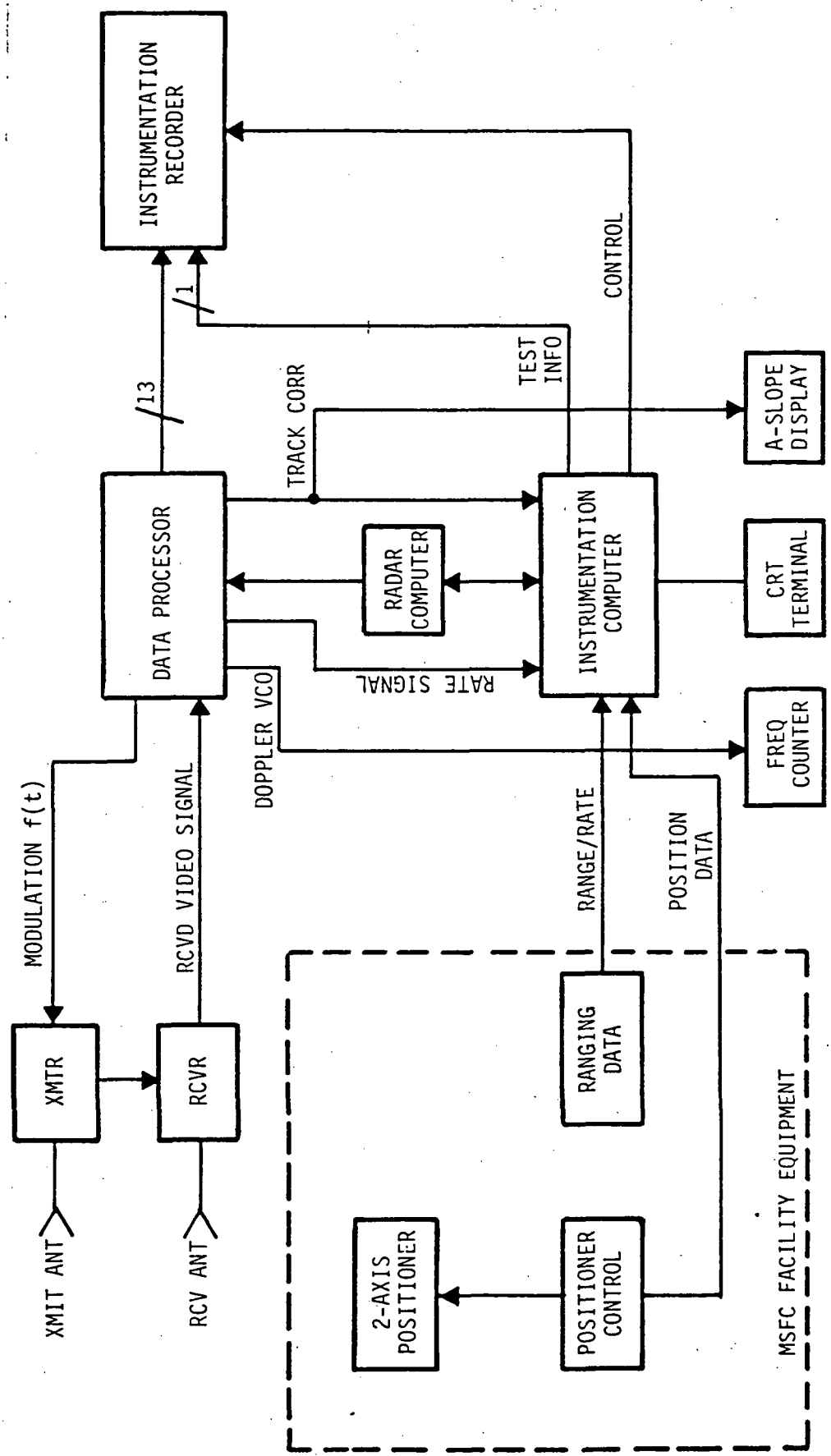

FIGURE 3-1 TEST SYSTEM

- .. 14 channels available
- .. 1 channel for digital test descriptor, etc.
- .. 1 channel for VCO signal for rate measure

- Provide range coverage which will easily include the target extent plus reasonable overlap

- A visual presentation of test rates available to the test operator

- Incorporation of an AFC circuit to accommodate relative target-radar motion

- Incorporation of a range error loop to track the target with relative motion

- Interface of the radar computer with an instrumentation computer which maintains overall test control

Based upon these considerations, the following radar modifications were incorporated:

- Transmitted bandwidth was changed to 150 MHz

  .. Resulting range resolution was 1 meter

- Correlator spacing equal to the range resolution of 1 meter

  .. Twelve contiquous correlators were incorporated to provide 39.4 ft. (12m) instantaneous range coverage

- A frequency-to-voltage converter monitoring the doppler offset oscillator was incorporated to provide a direct measurement of range rate

- An existing AFC circuit was incorporated and provided required performance for the test program

- The range tracker algorithm successfully used in the quiet altimeter program was incorporated for the HST test program

- An instrumentation computer was configured as the operator interface, and:

  .. Provided all test indication via a CRT terminal

  .. Simplified testing with minimal operator participation required to perform any test

  .. Maintained overall test control of the radar computer, the instrumentation recorder and the data written to the recorder

3.2 RADAR DESCRIPTION

The description of the radar test system with the changes incorporated is contained in this section. The pertinent radar parameters are listed in Table 3-1.

TABLE 3-1. RADAR PARAMETERS

PARAMETER	94 GHZ TEST RADAR
Operating Frequency	94 GHz
Antenna Gain	26 dB
Antenna Beamwidth	7^0
Peak Transmitter Power	18 dBm
Operating Range	1 m to 3 km
Transmitted Bandwidth	150 MHz
Range Resolution	1m
Sampling Rate	50 MHz
Observation Time	2 ms
Correlator Gain	36 dB
Duty Cycle	CW
Noise Figure Plus Losses	23 dB
Accuracy	$\pm$0.3 FT. (.09m)

3.2.1 Transmitter/Receiver (See Figure 3-2)

The transmitted signal originates at the 94 GHz oscillator. This oscillator is a Gunn-diode device selected for low noise characteristics. Long-term stability is enhanced by application of a 28 watt DC proportioning heater to the oscillator cavity; the set-point is held within 1^0C. The oscillator signal is coupled via a directional coupler to the biphase modulator. The directionally coupled port connects to the doppler offset generator discussed in the receiver section.

The modulator action is to add 180^o to the carrier phase when the input modulation function is a logic 1. The carrier output spectrum is a replica of the driving function provided sufficient drive current can be supplied to the diode in the modulator. The modulation function is a sampled noise signal. This signal contains all frequency components following a $(\sin x/x)^2$ envelope function. The transmitter must faithfully reproduce all these components in order to achieve efficient cross-correlation in the data processor.

The biphase modulator output is applied to an injection-locked Impatt amplifier. As long as the Impatt amplifier locks on the input spectrum, its output power is applied to that spectrum and not to the free running frequency of the amplifier itself. A good measure of modulator efficiency is the suppression of this natural frequency; the instrumentation radar being discussed herein has a carrier suppression of 25 dB.

The amplifier output is then applied to a variable 0-50 dB rotary-vane waveguide attenuator to provide transmit power control. This attenuator provides a readily calibrated control of transmit power. The attenuation required to prevent saturation of the receiver/data processor was determined by observation of the data processor output signals.

The circularly-polarized receive antenna is coupled to the first mixer via a circular-to-linear transition.

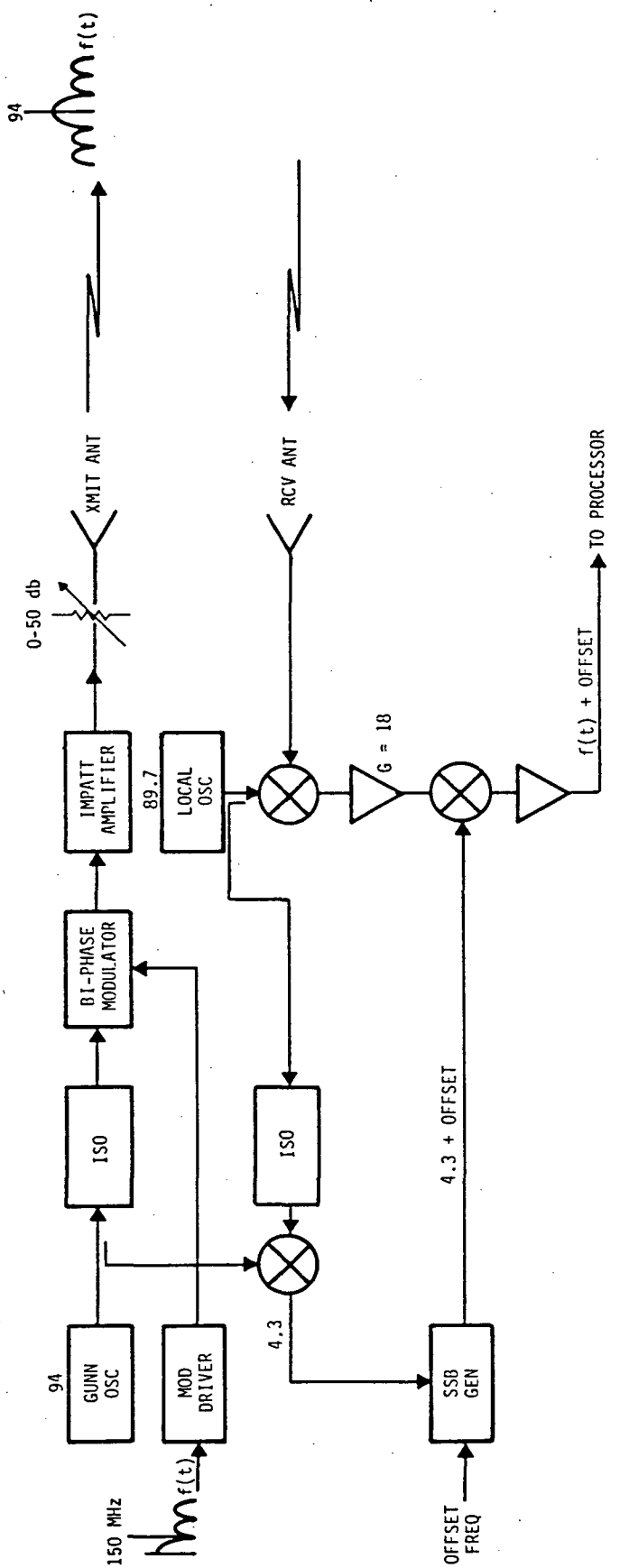

FIGURE 3-2 TRANSMITTER/RECEIVER

A dual conversion process is used in the receiver. The output of the first conversion is 4.3 GHz and the output of the second is 0.1 - 75 MHz video.

The LO signal for the first mixer stage is 89.7 GHz. This signal is generated with a Gunn oscillator. This oscillator signal is split using a 10 dB directional coupler. The -10 dB port output is then split in a waveguide magic tee; the in phase outputs of the magic tee are sent to the LO inputs at about a -3 dBm level.

The 20 dB receiver noise figure is primarily determined by the noise figure of the mixer and the low-noise 18 dB amplifier. The amplifier output is connected to the RF port of the second conversion mixer. The LO input of these mixers is centered at 4.3 GHz with 2.75 kHz doppler offset added as described in the next paragraph.

The 94 GHz transmit frequency is directionally coupled to a single port mixer where it is mixed with the 89.7 GHz first mixer LO frequency. The resulting 4.3 GHz output product is amplified and applied to a C-Band SSB modulator. The modulation input for the modulator is derived from a VCO controlled by the data processor AFC circuit. The control voltage is determined by the doppler shift encountered from the target. Since stationary targets generate no doppler shift the VCO remains at 2.75 kHz, and increases for incoming targets and decreases for outgoing targets.

The SSB modulator output of 4.3 GHz plus doppler offset, is mixed with the 4.3 GHz center frequency (plus video components of the form $[\text{SIN } X/X]^2$) in the second mixer stage. The resultant product is a sampled video spectrum, ideally a faithful reproduction of the biphase modulator drive signal of the form $(\text{SIN } X/X)^2$, wherein all frequencies are shifted by the 2.75 kHz doppler VCO frequency. This video signal is amplified to logic levels in a wide open, broadband 0.1-125 MHz amplifier. The amplifier output, being diode limited, is sent directly to an ECL-based correlator chain in the data processor.

3.2.2 Data Processor (See Figure 3-3)

The random waveform, which is applied to the biphase modulator and is digitally processed in the data processor, originates as the output of a high-gain video amplifier limiting on input noise. This output is sampled at a 150 MHz clock rate. The effect of sampling is to transform the broadband noise emanating from the amplifier into the sampled function with a $(\text{SIN } X/X)^2$ envelope. This function contains all frequency components of the sampled waveform; periodic nulls occur at 150 MHz intervals. The 3 dB bandwidth of the transmitted spectrum is equal to the sampling frequency. The highest frequency component present determines the minimum time interval between any two successive events; hence, the range resolution of 1m (resolution = C/2 times Transmitted BW).

The sampled noise waveform which operates the biphase modulator is effectively resampled at 50 MHz in the reference delay line. This means that only every third sample is saved for comparison with the received sample; this reduces the efficiency of the comparison process but doesn't affect range resolution.

ORIGINAL PAGE IS
OF POOR QUALITY

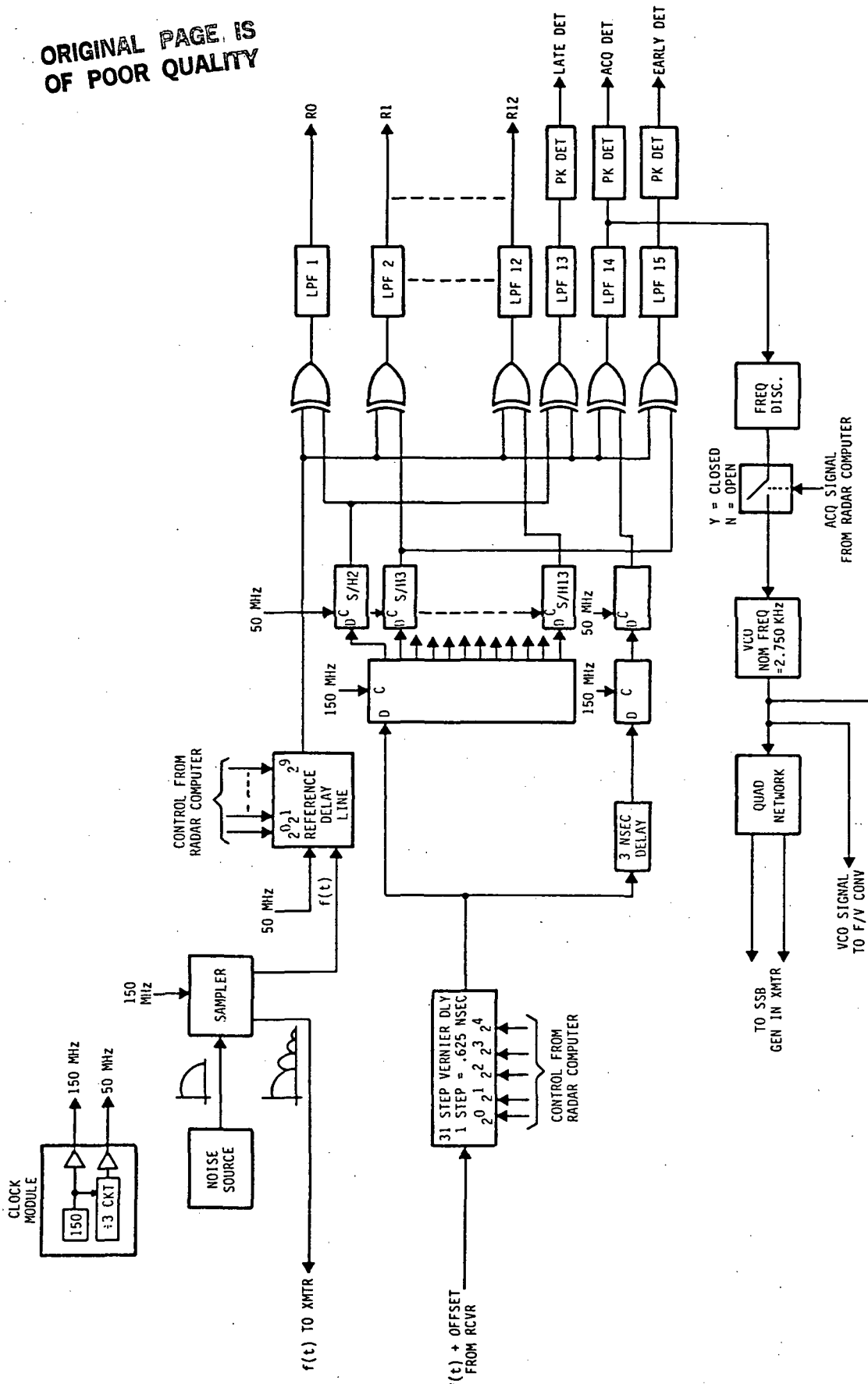

FIGURE 3-3 RADAR DATA PROCESSOR

The delay is obtained by holding the sample in a memory location for a specified number of clock periods. Up to to 1024 (10 bits) clock cycles at 50 MHz yields a maximum total delay of 6144 meters.

The amount of delay programmed can be successively stepped to generate a range sweep. Each step is the reciprocal of the clock period, or six meters (3 meters, 2-way). The delayed and sampled random noise waveform is then clocked out at 50 MHz to one input of a ECL exclusive-OR. This delayed waveform is referred to as the reference video.

3.2.2.1 Correlator

Correlation is achieved by multiplication of the target received signal and the delay reference signal and integration of the resulting product. Hence, the correlator output may be represented as a convolution of two sampled square waves which results in the the characteristic triangular shaped correlation functions. The circuit realization of the correlator is described in the following paragraphs.

The target video, whose generation was previously discussed in the RECEIVER section, is also delayed in a vernier delay line before the correlator. The purpose of these vernier delay is to introduce a finer delay increment than that generated in the reference video. The vernier delay is a hybrid network employing ECL technology. The amount of delay is programmed by 5 binary bits; the delay per step is .625 nanosecond (.094 meters, 2-way range). Hence, the interval during each clock cycle is divided into 32 smaller intervals. By successively stepping the vernier delay at X32 the reference delay step rate, the range delay interval can be covered in what is effectively .094m (.308') steps.

The delayed target video is then clocked through a shift register at a 150 MHz rate. Since the target video data appears at consecutive register outputs at intervals one clock cycle apart, the shift register acts like a tapped delay line with taps spaced 6.67 nsec apart.

This delay corresponds to a 2-way range of one meter. This shifted data is then resampled at 50 MHz to pick out the match for the samples "saved" in the reference delay line. This resampled data is inputted to the exclusive-OR as the target video logic input. The samples from the reference delay network line form the other logic input. Correlation is performed asynchronously due to the exclusive-OR logic action. The doppler offset on the target video appears as a 2.75 kHz modulation on the correlator output. The correlator output is then low-pass filtered before recording on analog magnetic tape.

To increase instantaneous range coverage for signature data, 12 correlators are connected in series, providing a total range coverage of 12 meters.

3.2.2.2 Range Error Loop

To provide early/late gates for a range error loop, the first two correlator outputs in the correlator string are used. The selection can be arbitrary; however, to easily synthesize an acquisition detector centered between the early/late gates, the first two were utilized.

The output of the vernier delay line branches to the acquisition detector circuit. It is first delayed by approximately 3 nanoseconds which is approximately 1/2 clock cycle. To keep all the samples lined up properly, the data is then shifted (effectively delayed by the same amount as in the main correlator string) at 150 MHz, then resampled at 50 MHz to pick out the right samples. This delayed, resampled data is the target video logic input to the acquisition detection correlator. This correlator output and the two correlator outputs straddling it in range are filtered and detected.

These detected outputs are sent to the radar computer. The radar computer sets the reference and vernier delays to maximize the acquisition detector output by forming a range discriminator with the early/late detected signals. The acquisition detector is connected to the vertical-deflection plates of an oscilloscope. The horizontal-deflection drive is an analog voltage converted from the digital range word used to set the reference and vernier delays. To form a range sweep, the full extent of the vernier delay is used (31 steps), then reset to zero at each reference delay step. The oscilloscope displays radar output versus range. The operator specifies the A-scope mode to observe the radar response over the selected range interval of interest.

3.2.2.3 Doppler VCO Control

During the range search mode, the incremental range delay is stopped when the acquisition detector output exceeds a threshold of about 9 dB above system noise. At this time, the ACQ signal is sent to the AFC loop to close the switch between the frequency discriminator and the VCO. The discriminator is centered at 2.750 kHz and provides a control signal to the VCO to normalize the acquisition correlator, hence all correlators, at the center frequency of 2.750 kHz. This approach worked satisfactorily because acquisition of the HST model was made with the radar and model both stationary.

After the AFC switch is closed, the range tracking loop is closed through the radar computer which fine tunes the range delay to equalize the early/late detector amplitudes.

3.2.2.4 Range Rate Indicator

For post-test analysis,the doppler offset oscillator frequency recorder on the Instrumentation Recorder (CH 14) can be compared with the correlator output frequency to arrive at a rate measurement. This luxury couldn't be easily provided for use during a test. A simplified approach used a frequency-to-voltage converter connected to the doppler offset oscillator output. The characteristics of this converter are shown in Figure 3-4. The center frequency was a nominal 2.750 kHz, with offset and gain adjustments to obtain a $\pm$10 VDC response around center at 1 VDC/191 Hz = 1VDC/ft/sec. The offset pot was available to the operator. Prior to start of a rate test, the operator adjusted the circuit to give a zero indicated rate. This adjustment compensated for minor drift in the AFC loop with temperature. By normalizing to zero rate, no frequency comparisons were required; this method gave excellent results.

INPUT	OUTPUT
F = 2.750 - 10•(191 Hz)	-10 VDC
F = 2.750 ± 0•(191 Hz)	0 VDC
F = 2.750 + 10•(191 Hz)	+10 VDC

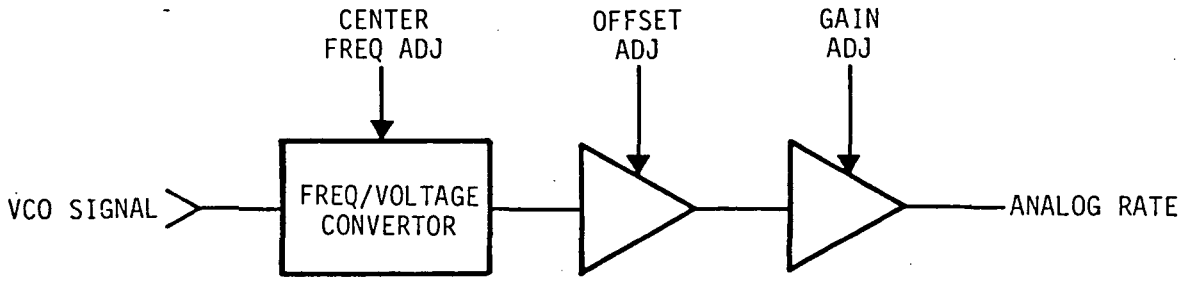

FIGURE 3-4 RATE OUTPUT CKT

3.3 INSTRUMENTATION RADAR COMPUTER(S)

The Instrumentation Radar originally contained a dual processor computer to provide for control and interface tasks. The radar controller processor was an Intel 8080 which worked in conjunction with an Intel 8085 operator interface processor. The operator interface was a 15 key hexadecimal keypad with an eight character LED display. This configuration could not supply the flexibility needed for this test series, which required data inputs from a Laser Range Finder and an IEEE 488 bus with model position information. In addition, control of an analog tape recorder and display of status information to the test operator was needed to provide good test control. For this reason a modification was made to the radar computer which basically eliminated the 8085 functions; these are now handled by an external 8086-based Single Board Computer. For the following description refer to Figure 3-5.

3.3.1 Hardware Description

The radar computer consists of four circuit boards that provide RAM, EPROM, data conversion, and external communications. The processor is an 8080 running at 2.0 MHz with 8K bytes of EPROM and 1024 bytes of RAM. The processor in turn controls 73 I/O lines, a 12 bit analog-to-digital converter and a 12 bit digital-to-analog converter. Connection to the outside world is by an 8 bit parallel bus to the SBC/86 computer. In addition, selected internal data used in the radar is "stolen" by the SBC for use in the operator information display.

ORIGINAL PAGE IS
OF POOR QUALITY

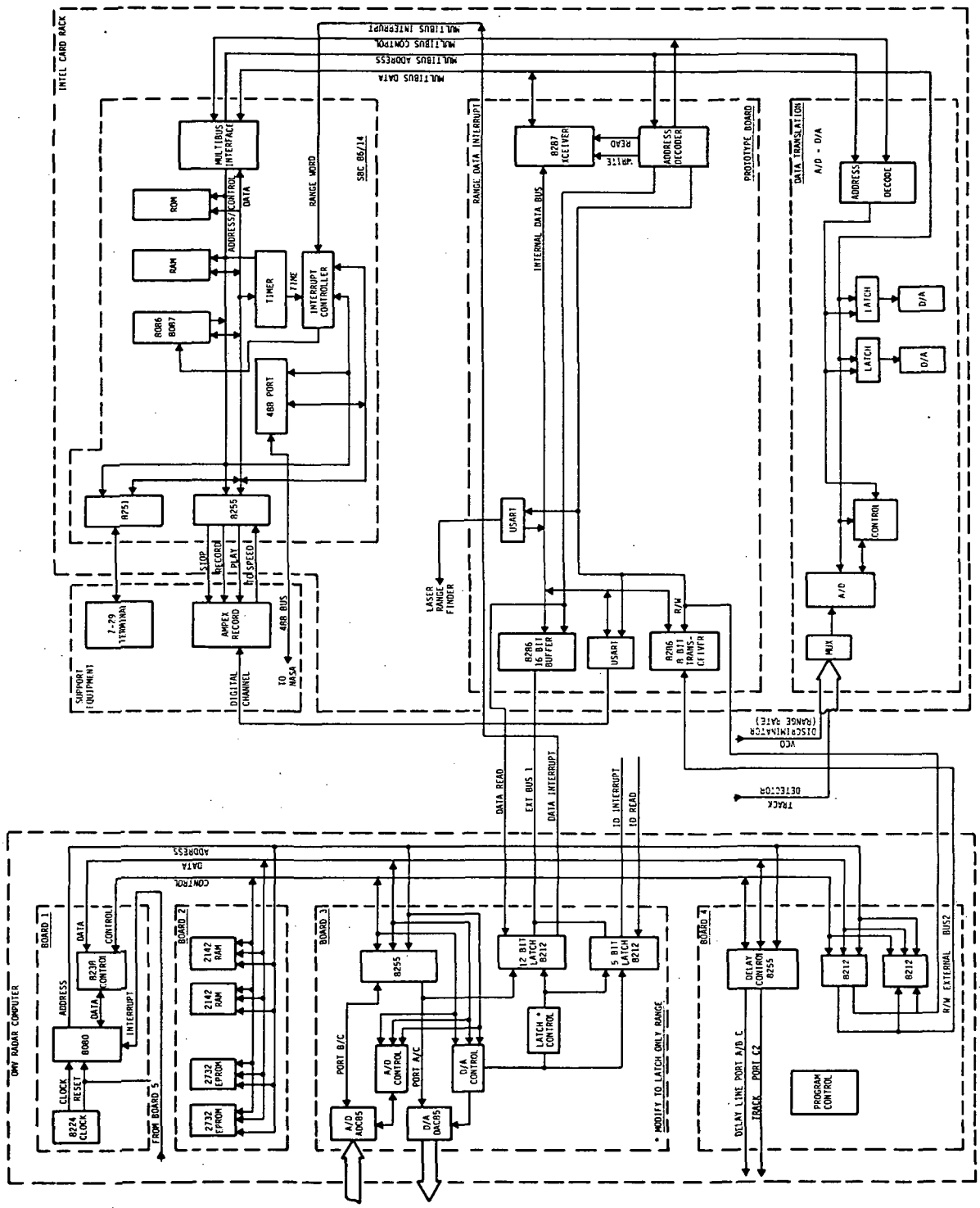

FIGURE 3-5 RADAR/INSTRUMENTATION COMPUTERS

The Instrumentation computer consists of an Intel SBC14/86 computer, an interface card and a 12 bit digitizing card. The SBC is made compatible with the IEEE 488 bus with the addition of an Intel Multimodule bus interface card. Each of the cards will be discussed separately.

The Single Board Computer uses an 8086 processor with an 8087 co-processor to perform floating point operations. The other support functions on the board include a serial port for communication with the terminal, a parallel port for control of the tape recorder, and a programmable timer which provides the real time clock. The IEEE 488 port is a plug in card that allows interfacing to the computer for control and data passing. This port was configured as a listener only.

External communications were conducted through the interface card which provided four different functions. The primary function was to communicate with the radar computer over an eight bit parallel two-way bus. A data stealing circuit latched data from the radar DAC for use in the terminal display for the operator. The interface to the Laser Range Finder is also found on this board. This interface is by way of a 300 baud USART. The fourth I/O port is a USART for providing serial "ASCII" data to the recorder. This data contained an ASCII test descriptor and selected binary data from the radar; it was recorded to identify each test.

The data conversion board uses a 12 bit A/D that digitized the track (acquisition) detector and the range rate data.

The interface between boards was via a Multibus I bus.

Further support items included a Zenith Z-29 smart terminal and an Ampex 14 channel analog recorder.

3.3.2 Software Description

Software support was an important part of the test control. Several features were incorporated to simplify test control and inform the operator of system status. Figure 3-6 shows the display presented to the operator during the data recording part of a test. The range, range rate, and track detector values come from the radar and show the status of the system and indicate if the data being recorded is valid. The turntable data displayed the position of the turntable as received over the 488 bus. This insured the operator that the model was positioned as expected for each test. The laser data also was external, combining over an RS232 bus from the laser range finder. The graph gave an easily interpreted display that allowed comparison between the laser standard and the radar to insure the radar was performing correctly. The graph of the track detector gives a visual presentation of the noise in the tracking loop and, as such, is a measure of goodness of track. Across the bottom of the terminal screen was date, current run number, elapsed time since start of test, and time of day.

ORIGINAL PAGE IS
OF POOR QUALITY

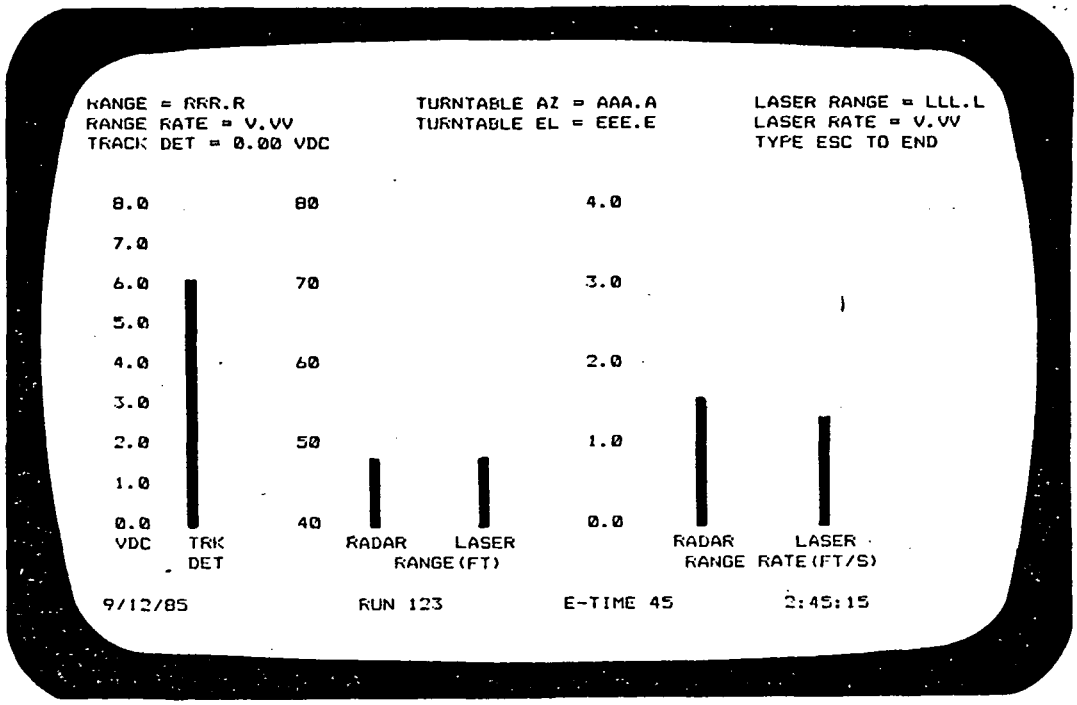

FIGURE 3-6. CRT DISPLAY

Much of the data displayed on the screen was also written to the tape on the "ASCII" channel. Table 3-2 tabulates the data that was stored in the data table that was available for output. The recorded data varied depending on the type of test being conducted. Table 3-2 shows which data was recorded for each test.

3.4 INSTRUMENTATION RECORDER

The recorder used was an Ampex PR 2230 operating at 15 ips. Control of the recorder modes STOP, FWD, and RECORD was via the Instrumentation Computer. The channel assignment was as follows:

CHANNEL	TYPE	DATA DESCRIPTION	MAXIMUM SIGNAL
1	FM	Test Descriptor	+5 VDC
2-13	DIR	Correlators R0-R11	10V p-p
14	FM	Reference Oscillator	1Vrms

TABLE 3-2. DATA TABLE

LOCATION	FUNCTION	ALL	TEST RECORD ON ACCURACY	RATE	PROFILE
BYTE-0	HOUR	X			
BYTE-1	MINUTES	X			
BYTE-2	SECONDS	X			
BYTE-3	RUN NUMBER HI	X			
BYTE-4	RUN NUMBER LOW	X			
BYTE-5	RANGE HI	X			
BYTE-6	RANGE LO	X			
BYTE-7	RANGE RATE HI		X	X	
BYTE-8	RANGE RATE LO		X	X	
BYTE-9	LASER RANGE HI 1	X			
BYTE-10	LASER RANGE HI 2	X			
BYTE-11	LASER RANGE LO 1	X			
BYTE-12	LASER RANGE LO 2	X			
BYTE-13	LASER RANGE RATE HI 1			X	
BYTE-14	LASER RANGE RATE HI 2			X	
BYTE-15	LASER RANGE RATE LO 1			X	
BYTE-16	LASER RANGE RATE LO 2			X	
BYTE-17	MSD TURNTABLE AZ				X
BYTE-18	2ND DIGIT TURNTABLE AZ				X
BYTE-19	3RD DIGIT TURNTABLE AZ				X
BYTE-20	4TH DIGIT TURNTABLE AZ				X
BYTE-21	5TH DIGIT TURNTABLE AZ				X
BYTE-22	MSD TURNTABLE EL				X
BYTE-23	2ND DIGIT TURNTABLE EL				X
BYTE-24	3RD DIGIT TURNTABLE EL				X
BYTE-25	4TH DIGIT TURNTABLE EL				X
BYTE-26	5TH DIGIT TURNTABLE EL				X
BYTE-27	EOT				X
BYTE-28	EOS BYTE 1 (00H)	X			
BYTE-29	EOS BYTE 2 (FFH)	X			

3.4.1 Tape Layout and Usage

Fifty foot leaders were left blank at each end of the tape to allow for handling and tape stretch.

A 25 foot section was then reserved for a calibration signal. The calibration standard was a frequency synthesized 2.750 kHz, 5V p-p signal applied to channels 2-13 simultaneously. The signal could then provide both an amplitude and frequency standard for playback.

The test data occupied the remainder of the tape; up to 4475' of tape was available for data.

To help distinguish between tests during data reduction, 15 second blank intervals were provided between tests. These were supplied by the instrumentation computer commanding the recorder to the FWD mode 5 seconds before issuing a RECORD command for 10-15 seconds. At the end of a data run, the RECORD command was dropped 10 seconds before the STOP command was given to the recorder. These intentionally programmed blank spots proved to be extremely useful during the signature runs; the positioner control was programmed to initialize the positioner to a new starting point for each data run during this time. Because of this complementary use of time, the signature testing proceeded very efficiently.

3.5 INSTALLATION

Because of the project schedule, it was desirable to arrive at the test site "ready to run." To accomplish this task, the system was mounted in, checked out in, and driven to the test area with the vehicle that was used on-site. The only on-site radar preparation required was to mount the XMTR/RCVR on its support. The radar system was mounted in a 15-passenger van and thoroughly checked out prior to departure to MSFC.

The van interior is shown in Figure 3-7. Equipment attachment points were furnished by a plywood pallet fastened to the van using the passenger seat bolt holes in the floor. A 19-inch equipment rack was used to house as much equipment as possible. This equipment was

- Equipment blower
- Radar data processor and computer
- Instrumentation computer
- Tape recorder calibration source
- Tape recorder monitor oscilloscope

The equipment used most frequently was closest to the operator. These were

- CRT terminal
- Instrumentation computer keyboard
- A-scope oscilloscope

In addition to these, MSFC supplied a television camera, video recorder, and monitor to record the HST model during testing. These are also shown in the photograph.

ORIGINAL PAGE IS
OF POOR QUALITY

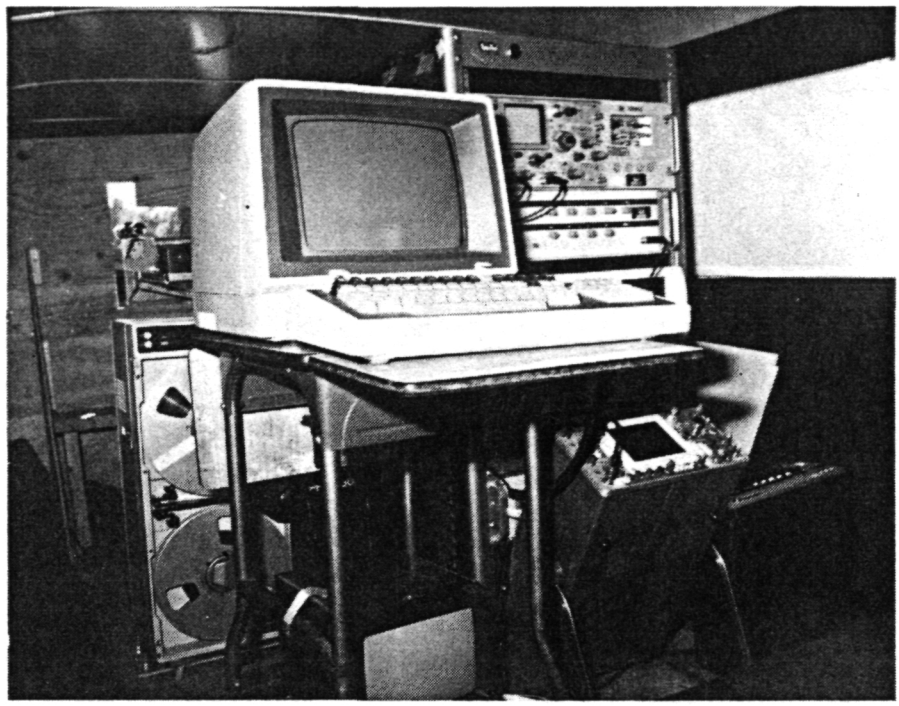

FIGURE 3-7. TEST VAN INTERIOR

A plywood bulkhead was installed at the rear of the van to enclose the equipment space as much as possible. This restricted the infiltration of outside air when the radar was in operation (the rear cargo doors were open during testing). Refer to Figure 3-8, it shows the bulkhead, the transmitter/receiver antenna set, the television camera mounted on top the transmitter/receiver and the telescope used for aiming. Electrical power and positioner data cabling are entering the van at the lower left corner of the cutout.

Because of the high heat and humidity in Alabama during the projected test time, a 7500 BTU/hr air conditioner was installed in the front passenger window. The mount was designed to be removable; it was installed after arrival on-site. To provide humidity control, the A/C was operated 24 hours/day. The laser mount was also clamped onto the front bumper after arrival, with subsequent attachment of the MSFC laser.

ORIGINAL PAGE IS
OF POOR QUALITY

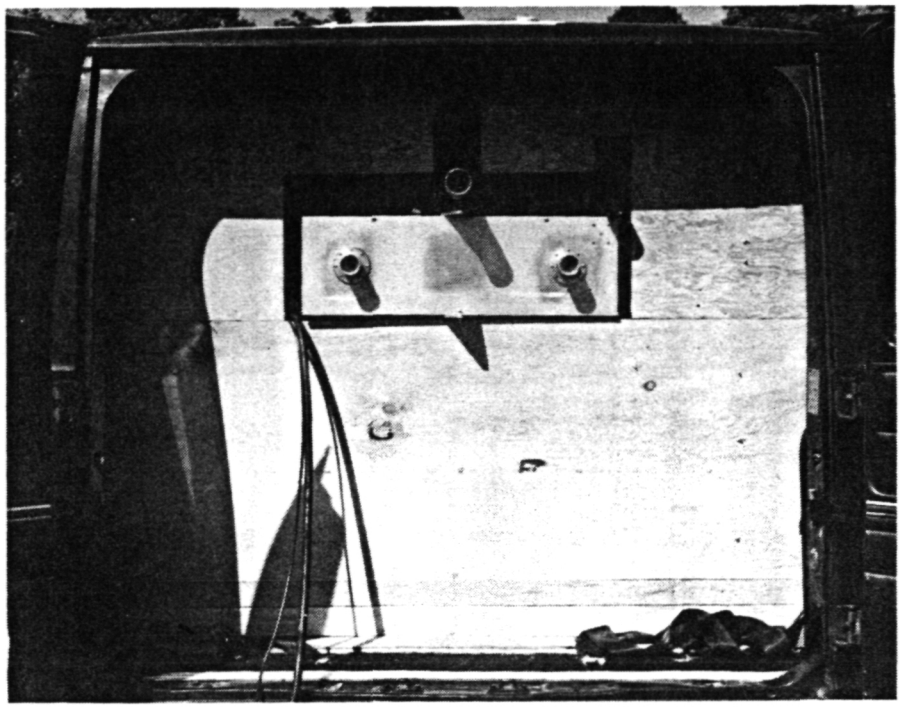

FIGURE 3-8. REAR BULKHEAD INSTALLATION

ORIGINAL PAGE IS
OF POOR QUALITY

SECTION 4.0

TEST SITE DESCRIPTION

The test site was located at MSFC Building 4194, the 400′ range of the two ranges available there being used for testing. Referring to Figure 4-1, the paved runway used for van placement runs from top/bottom at the center of the picture, the positioner being located at the near end of the runway. The gantry building to the right of the positioner was moved about twice as far away from the positioner during testing than is shown in Figure 4-1. The positioner control is located in Building 4194 in the foreground. Because of the transmitter building at the far end of the runway, the maximum range was limited to 350′. The runway was marked off in 50′ intervals from the positioner base center to facilitate radar van placement during testing.

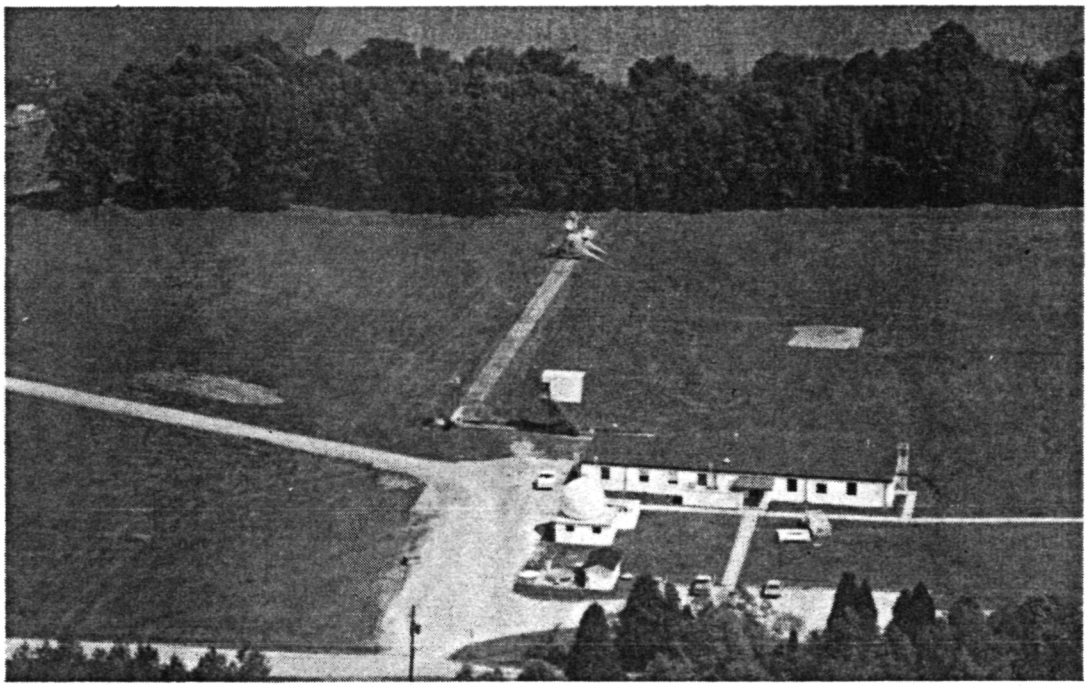

FIGURE 4-1. 400′ TEST RANGE

The relative location of the target and the test bed radar is shown in Figure 4-2. The target, which was a 1/3 scale model of the Hubble Space Telescope (HST), was mounted on the 2-axis positioner; the azimuth or elevation (tilt) aspect of the model HST was varied for each test. A laser was mounted on the front of the radar van to provide an independent measurement of range and range rate.

The radar slant range was varied by moving the van from 25′ to 350′ from the positioner base. The radar sighting point was in the axle support plane, midway between the supporting pylons.

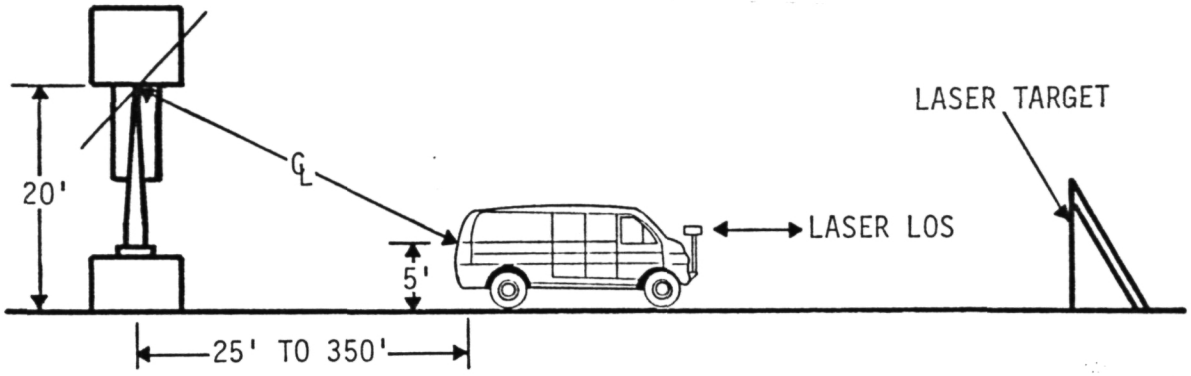

FIGURE 4-2. TEST SITE LAYOUT

A picture of the test setup is shown in Figure 4-3. Note that the model is mounted with the solar panels adjacent to the pylons on each side. Additional information on the testing setup is provided in Section 5.

FIGURE 4-3. TEST SETUP

4.1 MODEL ORIENTATION

The positioner sign convention used during testing is described in the following paragraphs.

4.1.1 Azimuth Convention

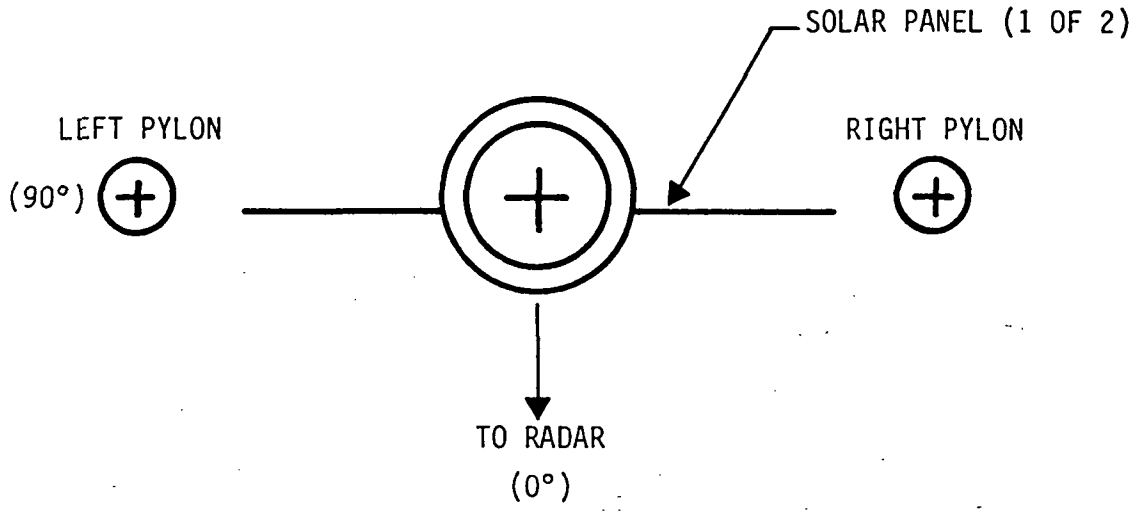

FIGURE 4-4. AZIMUTH CONVENTION

The positioner is shown at an azimuth position of 90°. Rotation in a CCW direction to 0° locates the left pylon closest to the radar. Typical positioner azimuth position was somewhere between 0° to 90°.

4.1.2 Elevation Convention

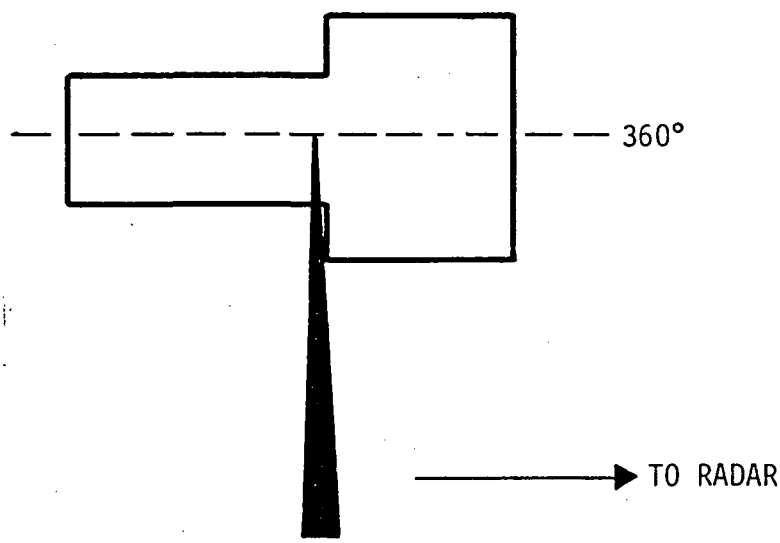

FIGURE 4-5. ELEVATION CONVENTION

The model orientation to place the larger end horizontal and closest to the radar occurred at an elevation of 360°. Clockwise elevation movement placed the large end down for an angle of 270°, with the small end closest to the radar corresponding to an angle of 180°. An apparent skew to the elevation data was observed. At 360° indicated angle, the measured model axis angle was 1.8° below horizontal. Other than at critical aspects where the ends of the model appeared as flat plates, this discrepancy caused no testing problem. To ensure the ends were orthogonal to the radar boresight at the critical aspects, the 1.8° correction factor was added to the requested elevation angle. This is illustrated in Table 4-1, which lists the requested angles to place the large end at boresight at the various test ranges.

TABLE 4-1. REQUESTED DEPRESSION ANGLES

RANGE	REQUIRED DEPRESSION ANGLE	REQUESTED DEPRESSION ANGLE
350'	357.5°	359.4°
200'	355.7°	357.5°
100'	351.5°	353.3°
50'	343.3°	345.1°
25'	329.0°	330.8°

4.1.3 Solar Panel Convention

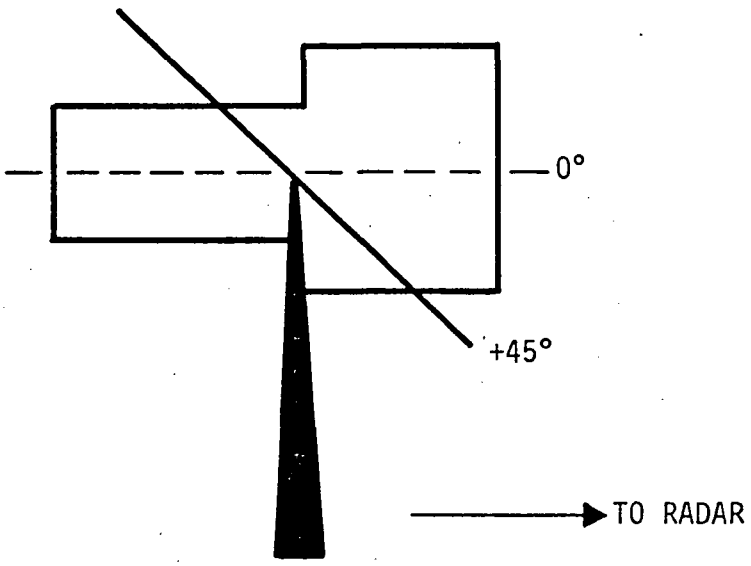

FIGURE 4-6. SOLAR PANEL CONVENTION

The model is shown in Figure 4-6 at an elevation of 360°, azimuth 0°, and solar panel position of +45°. The other solar panel position used was 0°, when the panels were aligned with the model major axis.

4.2 LASER CALIBRATION

The laser supplied by MSFC was mounted 5-3/4′ above the ground on a bracket attached to the front bumper. The van was positioned to put the radar antenna ground plane over the 350′ mark on the runway. The offsets due to van length and retro-reflector position were entered into the laser range computation to arrive at an indicated laser range of 350.00 feet. The laser measurement was also checked at ranges of 50′, 100′, and 200′. The laser measurement output was then cabled to the instrumentation computer for display and recording using an RS 232 interface.

4.3 TELEVISION CAMERA ALIGNMENT

Although the television camera boresite was not critical to the radar set-up, since the radar aimpoint was set with the antenna set telescope, reasonable care was exercised to position the selected aimpoint at the visual center of the television monitor. The television scene was recorded during portions of the range and signature testing and for all range rate tests.

SECTION 5.0

TEST PROCEDURES

The general test procedure used during the test program consisted of entering an appropriate set of test parameters, initiating a target search, and after target acquisition in range and doppler, initiating the test run. The test was terminated after the HST model had completed up to 90^{o} of rotation or 10-15 seconds of data had been recorded.

5.1 BACKGROUND MEASUREMENT

Measurements were performed to determine the effects of the positioner base, pylons, etc. A-scope surveys across the positioner location revealed a very large response from the positioner at all ranges. Based on these measurements, the pylons were covered with 2" thick, open-cell convoluted RAM (radar absorbing material) and the pylon supporting cross-piece front, top, and end surfaces covered with 3-1/2" pyramidal closed-cell absorber. The positioner base was also covered with the closed-cell absorber. Altogether, the positioner RCS was lowered 15-20 dB by the RAM.

The largest reduction in background interference was achieved with the addition of a radar fence across the test runway. Placement of the fence was not critical; generally it was set about 35 feet from the positioner.

The fence, provided by MSFC range personnel, was constructed of two 4' x 8' sheets of plywood, each piece covered with pyramidal absorber and styrofoam. The fence was intended for use at an operating frequency below W-Band; however, by placing each section at about 45^{o} to the runway, and forming a "bow" , the radar energy was deflected away from the large positioner base. The overall reduction in interference was about 40 dB, putting the largest component approximately 30 dB below system saturation.

Because the closed-cell RAM wasn't intended for exterior use, it was placed on the more accessible areas of the positioner. These easily reached areas were covered with a large sheet of plastic every evening to protect the absorber from overnight rains and heavy dew. Fortunately no rain occurred during the tests and no doubt added to the success of the covering technique.

5.2 RANGE ACCURACY CALIBRATION

Since the HST model extent encompassed several range cells, a short series of tests were performed to establish the radar range measurement accuracy using a point source target. A $300m^{2}$ reflector was placed on top of the left pylon with the azimuth turntable at 90^{o}. Close attention to align the reflector with the radar boresight wasn't required, since the purpose of these tests was to establish range measurement accuracy rather than RCS calibration.

The radar van was then positioned at various intervals from the turntable using range marks on the runway. The test ranges that were used in the range measurements calibration tests are listed in Table 5-1.

TABLE 5-1. LASER RANGES FOR RANGE ACCURACY

MARK	RANGE
1	50.04′
2	99.94′
4	200.01′
7	349.99′

The measurement setup is illustrated in Figure 5-1. The difference in the radar height and target height must be taken into account, as well as the 7.5′ shift in the reference point in the horizontal plane.

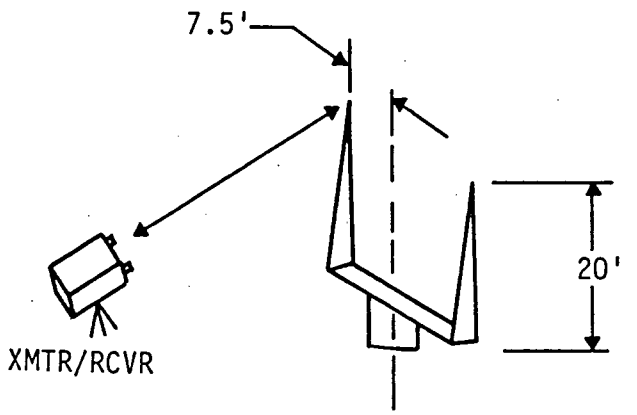

FIGURE 5-1. RANGE ACCURACY TEST SETUP

The target height is fixed at 20′. However, the radar height and range is determined by the geometry of its mount. The radar mount in the testing van was a tripod head with an elevation pivot which is below and behind the antennas as illustrated in Figure 5-2.

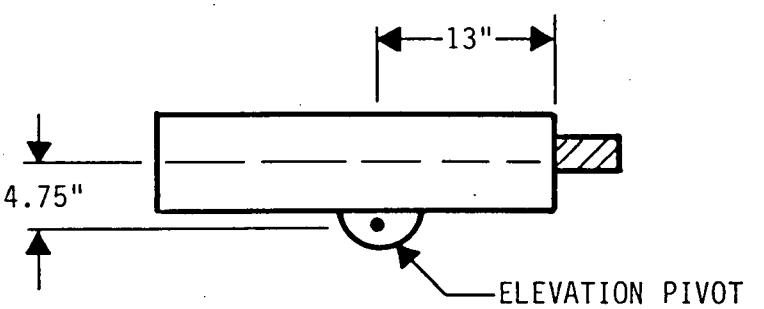

FIGURE 5-2. TRIPOD MOUNT

In computing the range between the radar and target it is necessary to account for the shift in radar height and range due to the pivot point placement, which was 13" back from and 4.75" under the center of the antenna plane (the ground plan is the zero range point). Slant range computation is performed in two steps as described below.

The first step establishes the range between the radar and target in the vertical plane as illustrated in Figure 5-3.

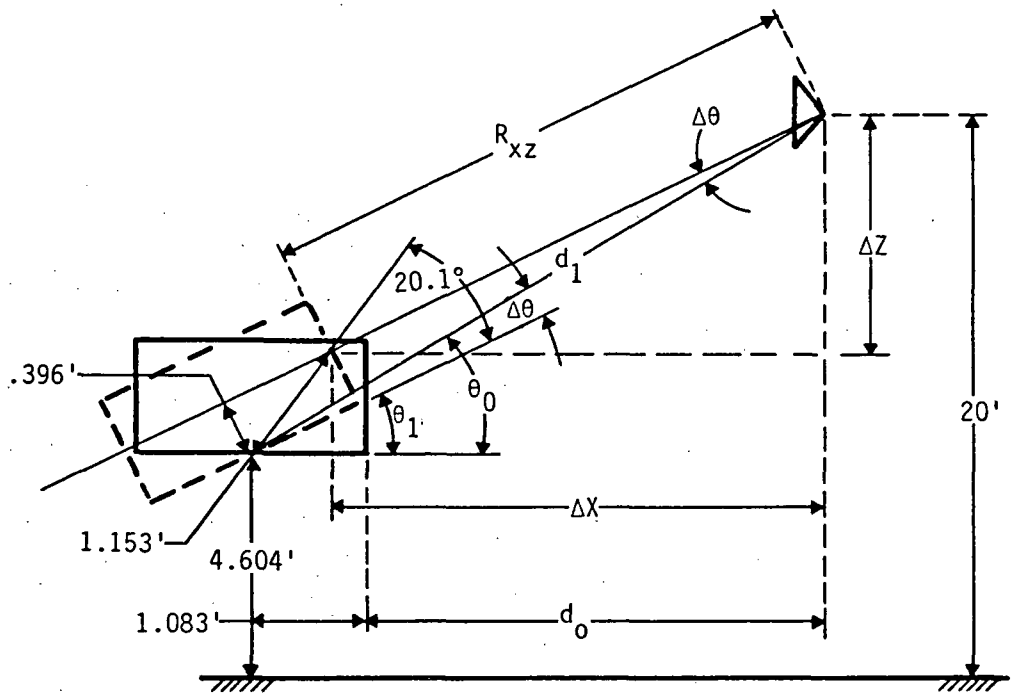

FIGURE 5-3. COMPUTATION OF RANGE

The second step completes the slant range computation by accounting for the 7.5′ displacement of the target in the horizontal plane. Computation of slant range for a laser measured range, d_o, of 50.04′ is presented below.

Evaluation of the horizontal plane range, R_{xy}, requires establishing the distances Δx and Δz, where,

$$\Delta x = d_o + 1.083' - 1.153' \cos (\theta_1 + 20.1^o) \quad (5\text{-}1)$$

$$\Delta z = (20' - 4.604') - 1.153' \sin (\theta_1 + 20.1^o) \quad (5\text{-}2)$$

where d_o = laser measured range

θ_1 = tilt angle of radar platform

The radar tilt angle, θ_1, is computed from the target line-of-sight angle w.r.t. the radar pivot point, θ_o, and the differential in angle between θ_o and θ_1, θ,

$$\theta_1 = \theta_o - \theta \tag{5-3}$$

Expressions for θ_o and θ,

$$\theta_o = \sin^{-1}((20' - 4.604')/d_1) = 16.76^o \tag{5-4}$$

$$\theta = \sin^{-1}(0.396'/d_1) = 0.43^o \tag{5-5}$$

$$d_1 = \sqrt{(d_o + 1.083')^2 + (20' - 4.604)^2} = 53.39' \tag{5-6}$$

and solving for θ_1, x, and z

$$\theta_1 = 0_o - \theta = 16.33^o \tag{5-7}$$

$$x = 50.04' + 1.083' - 1.153' \cos(36.43^o) = 50.19' \tag{5-8}$$

$$z = (20' - 4.604') - 1.153' \sin(36.43^o) = 14.71' \tag{5-9}$$

and the slant range to the target accounting for the 7.5' displacement in the horizontal plane becomes,

$$R = \sqrt{x^2 + (7.5')^2 + z^2} = 52.84' \tag{5-10}$$

The slant range for each of the ranges used in the range accuracy calibration tests was computed and the results of the accuracy tests are presented in Table 5-2.

TABLE 5-2. RANGE ACCURACY TEST RESULTS

LASER RANGE d_o	THEORETICAL SLANT RANGE	MEASURED SLANT RANGE	MEASUREMENT ERROR
50.04'	52.84'	53.3'	+0.46'
99.94	101.38	102.2	0.82
200.01	200.74	201.4	0.66
349.99	350.41	351.1	0.69

The measurement accuracy results are in general agreement with the preliminary accuracy tests performed in the Bendix parking lot prior to departing for MSFC. The parking lot measurements were made with the $300m^2$ corner reflector on a tripod as the target. The range was established with a tape measure. Even though the error scatter is larger in the parking lot tests, the average error is on the same order of magnitude as the MFSC test results

and the differential in sign is probably due to a bias in the parking lot setup which has not been accounted for.

TABLE 5-3. BENDIX PARKING LOT ACCURACY

TAPE MEASURED RANGE	RADAR MEASURED RANGE	RANGE MEASUREMENT ERROR
26.96 ft	26.8 ft	-.16 ft
50.0	49.7	-.3
75.0	74.9	-.1
100.0	99.85	-.15
150.0	149.69	-.35
175.0	174.7	-.3
200.0	199.6	-.4
250.0	249.5	-.5
300.0	299.3	-.7
350.0	349.6	-.4

5.3 RCS CALIBRATION

RCS calibration was accomplished on-site with a $300m^2$ corner reflector mounted on a 7′ tripod. The tripod was placed 201′ from the radar on the radar range runway. The HST model and positioner were located in the background about 150′ behind the calibration reflector, and situated to yield a minimum A-scope response. The radar was programmed to sweep in range across the reflector. The range sweep was set to obtain a radar response in all the correlators thereby enabling calibration of each correlator channel. Ten seconds of data was recorded for each transmitter power attenuator setting between 0 dB to 50 dB in 5 dB steps.

As a part of the radar setup procedure performed at Bendix prior to the MSFC test series, each of the correlators was calibrated in terms of the correlator output voltage as a function of the receiver input power level. A typical correlator calibration curve is shown in Figure 5-4. The curves were generated by removing the transmitter and receiver antennas and connecting the transmitter directly to the receiver through a calibrated attenuator. The calibration curves were then generated by noting the correlator voltage as the function of the attenuator setting. By monitoring the transmitter power level, the attenuator settings were then converted to received power, P_i.

The calibration curves, in combination with the radar range equation, provide the means of calibrating the radar in terms of RCS (radar cross section).

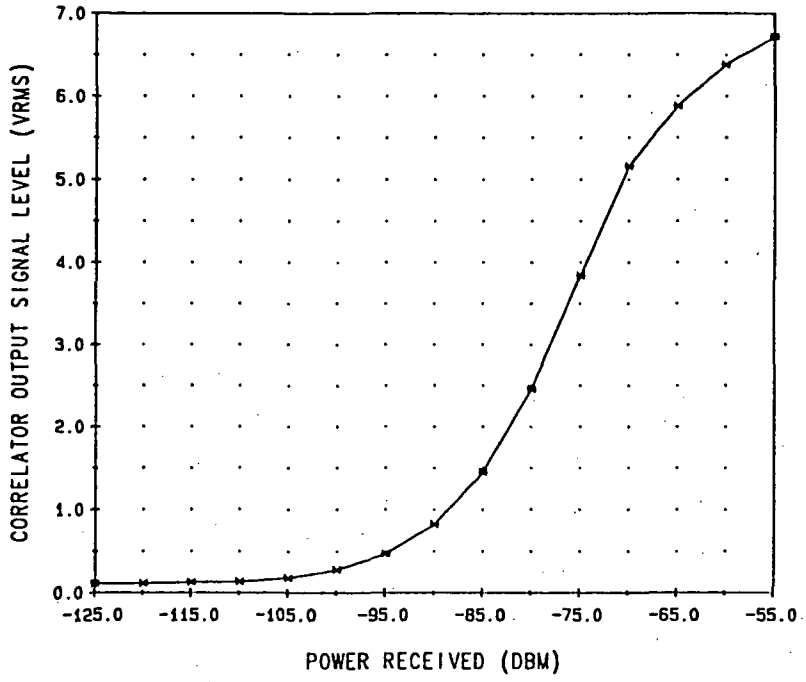

FIGURE 5-4. CORRELATOR CALIBRATION CURVE

The power received from a target with an RCS, σ_T, which is located at a range, R_T, from the radar via the radar range equation,

$$P_i = \frac{P_T G^2 \lambda^2 \sigma_T}{(4\pi)^3 R_T^4} \qquad (5\text{-}11)$$

and solving for σ_T,

$$\sigma_T = \frac{(4\pi)^3 R_T^4 P_i}{P_T G^2 \lambda^2} \qquad (5\text{-}12)$$

Results of the RCS calibration using the $300m^2$ ($24.8\ dBm^2$) corner reflector as the target are listed in Table 5-4.

Received power level adjustement is provided through a programmable variable attenuator in the receiver channel. For the $300m^2$ tests an attenuation on the order of 20 dB was required to avoid saturation.

TABLE 5-4. MEASURED RCS OF 300m^2 REFLECTOR

ATTENUATION	MEASURED RCS
0 dB	21 dBm^2 (saturation)
5	22 "
10	24 "
15	25 "
20	27
25	27
30	27
35	27
40	27
45	27
50	27

Based on the field calibration results, the measured RCS is within 2 dB of the theoretical values.

5.4 MODEL TEST PROCEDURES

The model tests were divided into three major areas: Range Measurements, Radar Cross-Section (RCS) Measurements, and Range-Rate Measurements. Although similar in radar operation, each measurement procedure shall be discussed separately. Due to the target extent and structure complexity, range and doppler acquisiton was maintained throughout the range and rate measurement tests.

5.4.1 HST Model Range Measurements

To illustrate how the measured range can vary with target aspect, this test series allowed the range tracker to lock onto the first prominent scatterer on the model.

Thirty degree (30^o) variations in azimuth from 0^o to 90^o were repeated at each elevation presentation of the model. The elevation angles used wre: 360^o, 355^o, 330^o, 300^o, 275^o, and 270^o.

This progression effectively varies the aspect from horizontal to vertical, with finer cuts around the end-points. Further aspect variation was introduced by varying the radar position: 350', 200', 100', 50', and 25'.

An easily identifiable scatterer is the large end surface; the predicted range should be easiest to compute at that aspect. The elevation required to illuminate the large end was listed in Table 4-1, and is reproduced here as Table 5.5.

TABLE 5-5. ELEVATION - SENSITIVE ORIENTATION

RANGE	ELEVATION ANGLE
350′	359.4°
200′	357.5°
100′	353.3°
50′	345.1°
25′	330.8°

Field experience showed the return off the end wasn't as sensitive as a true flat-plate response would be. The responses were observed to be several degrees wide. The requested angles of 360° and 355° come close to the critical angles at the 350′, 200′ and 100′ points, so the critical angle wasn't requested. At the 50′ and 25′ range points, additional measurements were conducted at requested elevation angles of 345.1° and 330.8° respectively. This procedure was performed at both solar panel positions.

Fifteen seconds of data was recorded for each test. A total of 270 range measurements were made.

5.4.2 HST Model Range Rate Tests

Seven tests were conducted to determine the measurement capabilities of the radar when tracking a moving target. The movement was introduced by backing the van towards the model at a nominal 1 foot/sec rate. The van driver used the laser computer display as a speedometer. Prior to movement, the F/V converter rate output voltage was nulled to zero. The range of movement was limited to 50′ or was terminated if the laser lock on its retro-reflector was lost. An example of the radar range and range rate rate outputs (both are available on the analog tape) compared with the laser outputs is given as Figure 5-5. Note the excellent comparison of radar and laser measured rates. The 5′ differential in radar and laser measured range is due to the radar tracking point being in front of the positioner center. It is actually tracking somewhere on the big end, which is the model feature closest to the radar.

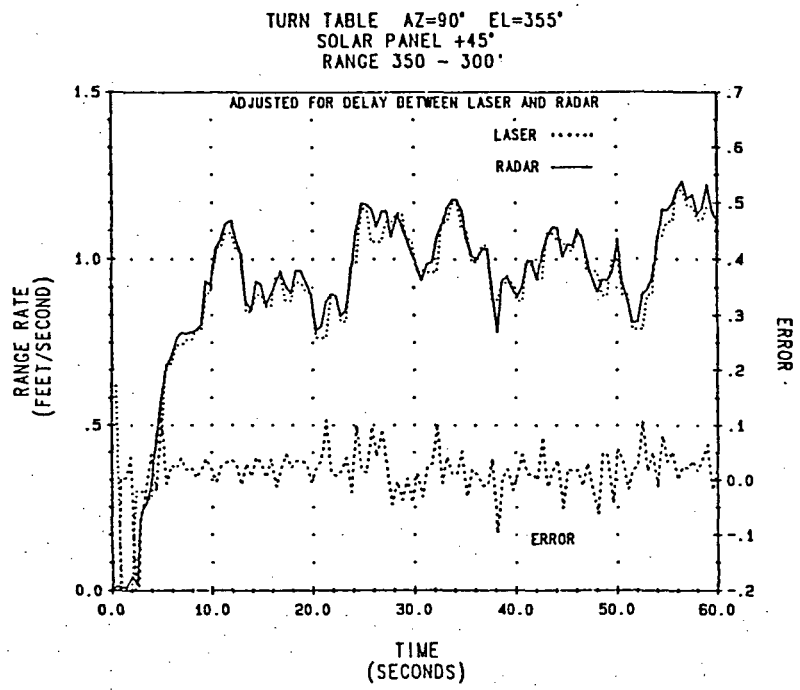

FIGURE 5-5A. RATE COMPARISON RADAR-TO-LASER

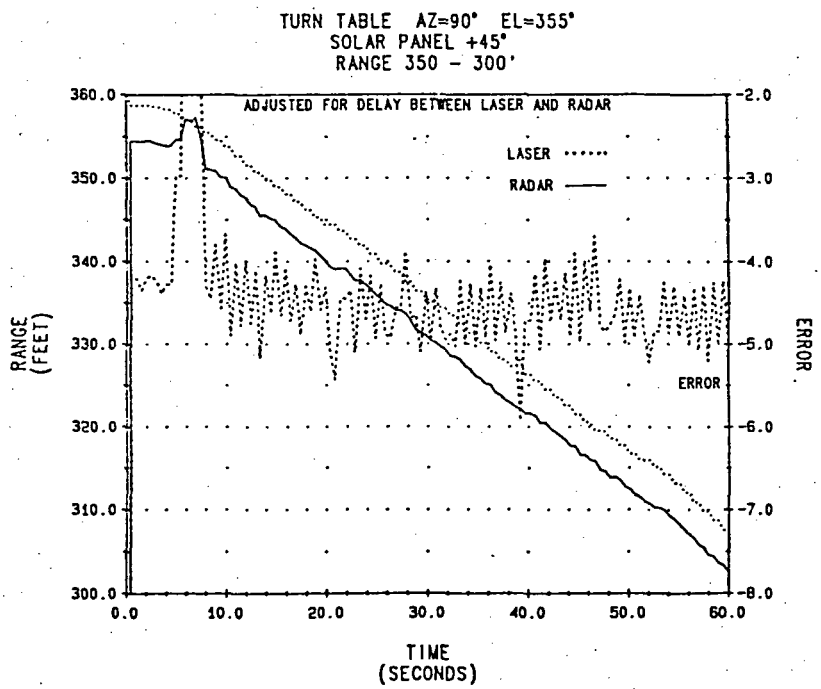

FIGURE 5-5B RANGE COMPARISON RADAR-TO-LASER

5.4.2.1 Video Tape of Rate Test

One rate test from 350′ to 25′ was performed to record the radar range and range rate information on video tape. The HST big end was used as the radar target; the television display of the test simulates a docking with range/rate information super-imposed. No analog recording was made as the data record would have been too long.

The test went very smoothly, the radar tracking the target the entire time. The driver used the laser rate display to aid in maintaining 1′/second speed. A second test person adjusted the radar tripod elevation to maintain the changing elevation angle as the range decreased. This provided a more realistic television display and ensured continuous radar acquisition.

5.4.3 HST Model Signature Tests

Signature tests were performed at all ranges: 350′, 200′, 100′, and 50′. The azimuth turntable was traversed from 0^{o} to 90^{o} at 2.5^{o}/sec and the elevation axis was fixed during each run.

Elevation was changed in 1^{o} increments; total elevation coverage was from 360^{o} to 270^{o}, except at the 350′ site, where elevation coverage was 360^{o} to 180^{o}. Solar panel positions of both 0^{o} and $+45^{o}$ were used at the 350′ and 200′ ranges. At the other ranges, 0^{o} panel position only was used.

The tests were semi-automated: the positioner was completely controlled by a programmed routine which allowed approximately 20 seconds at the azimuth traverse end-points for the radar operator to initialize the radar and recorder via the keyboard for the next run.

5.4.3.1 Range Setting for Signature Testing

To avoid possible confusion over the published radar range setting when studying the data contained in Section 7, a brief explanation of the delay circuitry is in order. Referring to the block diagram of the delay configuration used in the radar data process, Figure 5-6, it becomes evident correlation can only occur when:

$$\text{REF DLY} = \text{Target DLY} + \text{VERN DLY} + \text{Shift Reg DLY} \qquad (5\text{-}13)$$

$$\text{REF DLY} - \text{VERN DLY} = \text{Target DLY} + \text{Shift Reg DLY} \qquad (5\text{-}14)$$

The left hand side of expression of (5-14) is the range setting, and the right hand terms are the variables which affect correlation. The range setting defines the range delay of the acquisition correlator setting between R0 and R1, which correspond to the minimum delay taps on the shift register.

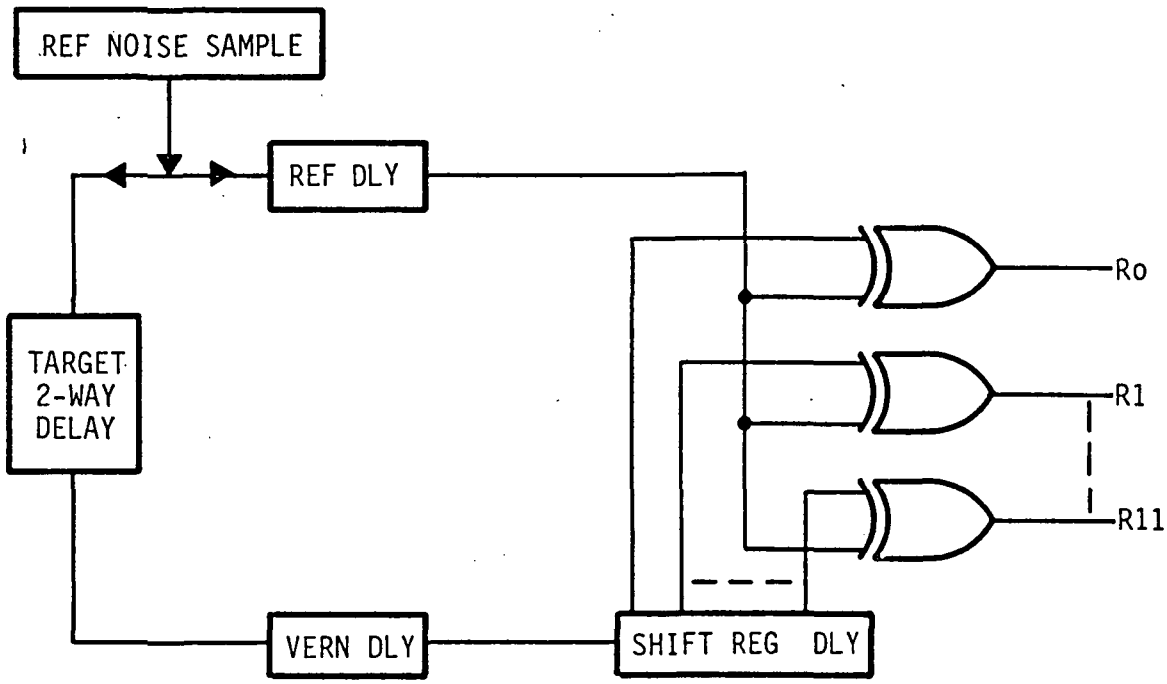

FIGURE 5-6. SYSTEM DELAY ELEMENTS

In comparison to higher-numbered correlators, a larger target delay is required to correlate in the R0 and R1 correlators. As a consequence, when performing the signature tests, the R0 and R1 correlators will be located the furthest from the radar while the highest numbered correlators (R9, R10, etc.) will be closest to the radar as illustrated in Figure 5-7 for the 350' site signature tests.

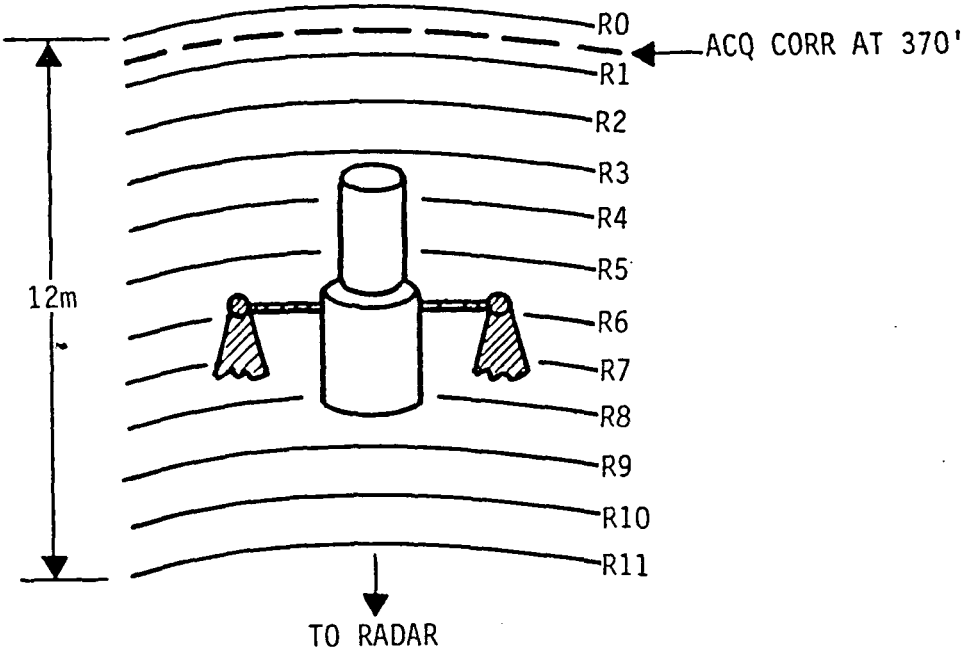

FIGURE 5-7. SIGNATURE TEST RANGE CORRELATOR LAYOUT

SECTION 6.0

TEST LOG

The following is a condensed version of the on-site daily log kept by the test personnel during the September 5 through September 17, 1985 testing period.

TABLE 6-1. CONDENSED TEST LOG

RUN NO.	NO. TESTS	TYPE TEST	RANGE	TAPE NO.
1 - 9	9	Background	350'	1
10 - 26	17	Background w/RAM	All	1
27 - 30	4	Range Acc. w/Reflectors	All	1
31 - 74	44	Range Acc. w/HST Solar Panels = 0^{o}	350'	2
75 - 98	24	Range Acc. w/HST Solar Panels = 0^{o}	200'	2
99 - 122	24	Range Acc. w/HST Solar Panels = 0^{o}	100'	2
123 - 147	25	Range Acc. w/HST Solar Panels = 0^{o}	50'	2
148 - 173	26	Range Acc. w/HST Solar Panels = 0^{o}	25'	3
174 - 199	26	Range Acc. w/HST Solar Panels = 45^{o}	25'	3
200 - 224	25	Range Acc. w/HST Solar Panels = 45^{o}	50'	3
225 - 249	25	Range Acc. w/HST Solar Panels = 45^{o}	100'	3
250 - 275	26	Range Acc. w/HST Solar Panels = 45^{o}	200'	
276 - 300	25	Range Acc. w/HST Solar Panels = 45^{o}	350'	4
301 - 311	11	Range/Range Rate	Variable	4
312 - 495	184	Signature Solar Panels = 45^{o}	350'	5- 8
496 - 677	182	Signature Solar Panels = 0^{o}	350'	8-12
678 - 773	96	Signature Solar Panels = 0^{o}	200'	12-14
774 - 873	100	Signature Solar Panels = 0^{o}	100'	14-16
874 - 970	97	Signature Solar Panels = 0^{o}	50'	16-17
971 -1074	104	Signature Solar Panels = 45^{o}	200'	18-19
1075-1079	5	Signature Solar Panels = 45^{o}	200'	20
	(10^{o} Movement Az/El of HST)			
1080-1091	12	RCS Calibration w/300 M^{2} Reflector Xmit Atten in 5 dB steps	201'	20

The test log (Table 6-1) is shown in matrix form in Table 6-2.

TABLE 6-2. TESTING PERFORMED

TEST POSITION:	350′	200′	100′	50′	25′
TYPE TEST					
RANGE	X[1]	X	X	X	X
RATE	X	X	X		
SIGNATURE	X[2]	X[2]	X	X	

STANDARD CONDITONS

RANGE: El in 30^{o} or 5^{o} steps from 360^{o} to 270^{o}
Az = 0^{o}, 30^{o}, 60^{o}, 90^{o}
Solar Panels = 0^{o}, 45^{o}

RATE: Acquire large end
Move radar at approximately 1 foot/second for (up to) 50′

SIGNATURE: El = 360^{o} to 270^{o} in 1^{o} decrements
Az = 0^{o} to 90^{o} at approximately 3^{o}/second
Solar Panels = 0^{o}

[1] El from 360^{o} to 180^{o}

[2] Solar Panels also at 45^{o}

SECTION 7.0

TEST DATA

This section documents the results of the signature measurements, range accuracy tests, and the range and range rate tracking tests.

The radar signature data was generated by processing the 12 recorded correlator amplitudes. Recorder channel 1 was decoded to derive run number, site location, etc.

For range accuracy and rate tests, only channel 1 was decoded to extract all test information. The correlator channels contain no information other than the early/late correlator amplitudes.

7.1 DATA REDUCTION FACILITY

Data reduction involved playing back the analog test data, inputting this data into an a/d converter to convert to digital data and formatting for tape storage and retrieval. The setup used to reduce the MSFC tapes is illustrated in Figure 7-1.

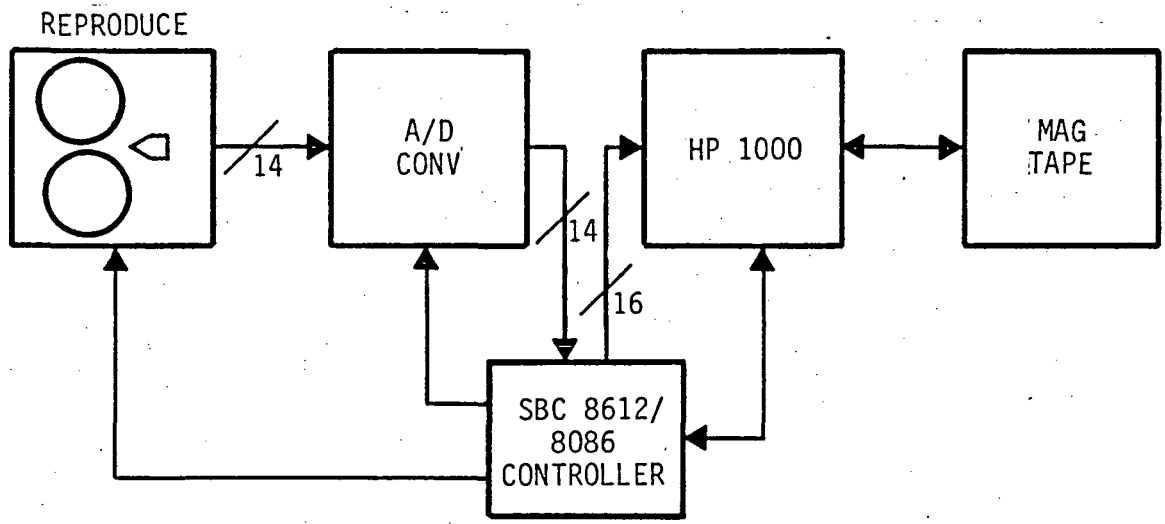

FIGURE 7-1. DATA REDUCTION

A 14-channel analog instrumentation recorder is used to reproduce the data. Playback speed is 1/4 record speed, allowing a reduction of the data rate over the data bus to the HP computer.

The A/D converter samples all 14 channels at 2.5 kHz. The 1/4 playback speed provides an equivalent real-time sample speed at 10 KHz. The raw sampled data is gathered into blocks with the controller; this controller controls the instrumentation recorder under instructions from the HP1000 computer. The HP1000 identifies the data blocks for storage onto the mag tape.

7.2 RCS MEASUREMENT

The largest return is presented as the characteristic RCS determined from the complex radar responses of the model. Other simultaneous returns, though present in the response, are not included in the plots. The plots would be extremely complex and require much greater amounts of data processing time. Some indication of the extended target signature characteristic is evident in the tracking tests discussed in Section 7.3.

7.2.1 RCS Plots, Background Discussion

These plots are generated by first forming a data matrix via these operations:

1. Sequentially input each data block off the mag tape storage.

2. Select those data blocks which contain integer values of azimuth/elevation.

   - Process the correlator responses in the selected data block(s) to arrive at the respective RCS measurement for each correlator.

   - Select the largest RCS measured and note the correlator number.

3. Input the RCS value and correlator identification into the matrix location defined by the azimuth/elevation value.

   - RCS vs. elevation with fixed azimuth angle
   - RCS vs. correlator number
   - RCS distribution throughout the matrix
   - RCS magnitude probability of occurrence

As an aid to understanding the plots, the correlator range coverage layout for the 350′ and 200′ sites is illustrated in Figures 7-2 and 7-3, respectively. These are expanded versions of Figure 5-7, with the HST dimensions superimposed over the correlator range coverage. Three examples of HST model positioning are included in each figure: model broadside to radar, and large or small end closest to radar. For these three orientations, the likely correlator response is:

ASPECT	CORRELATOR
Broadside (Az = 0^{o})	7
Large End on Boresite	8
Small End on Boresite	9
Large End (Small End Closest)	5
Small End (Large End Closest)	4

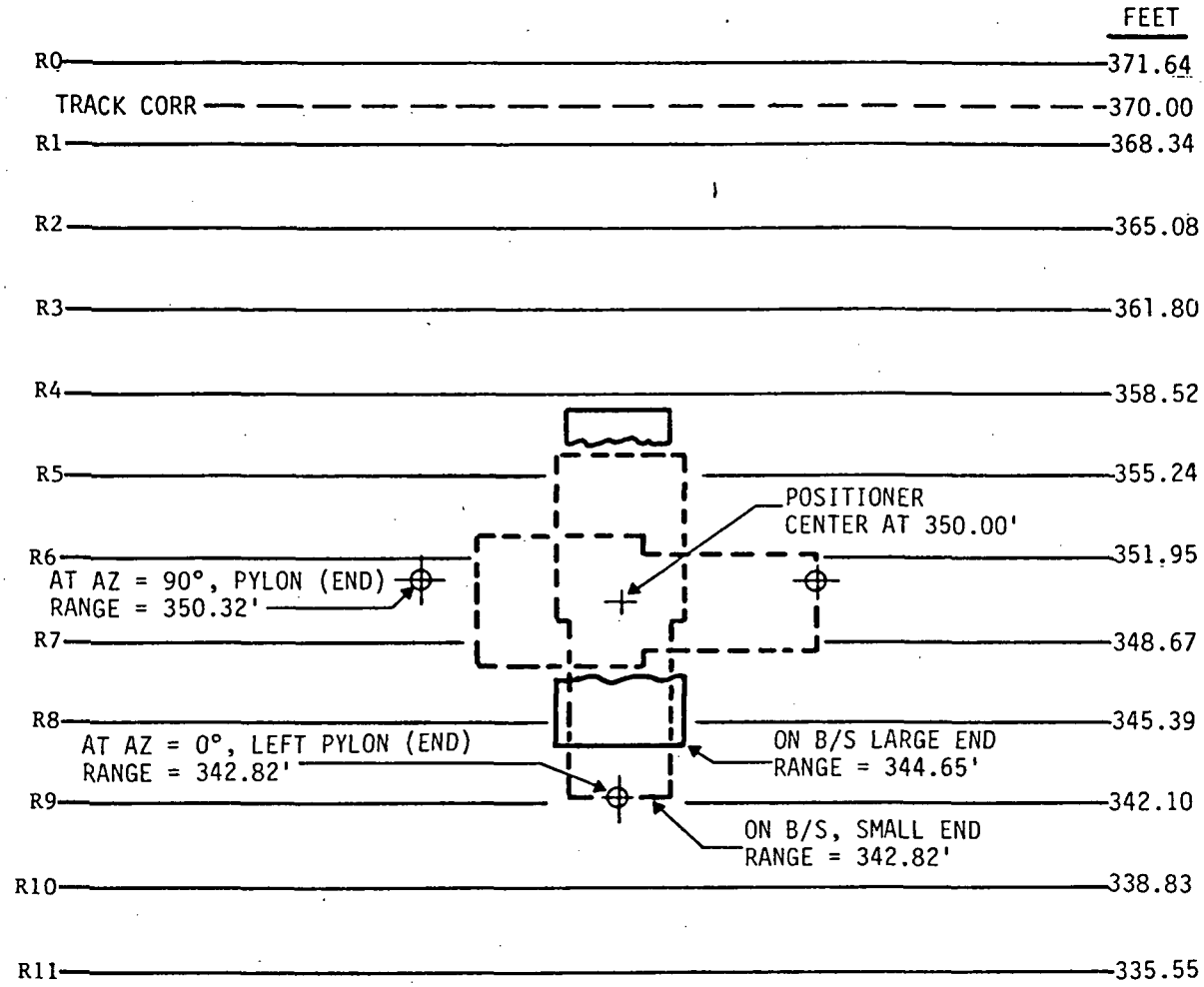

FIGURE 7-2. CORRELATOR RANGE COVERAGE 350' SITE (LASER RANGE = 350.00)

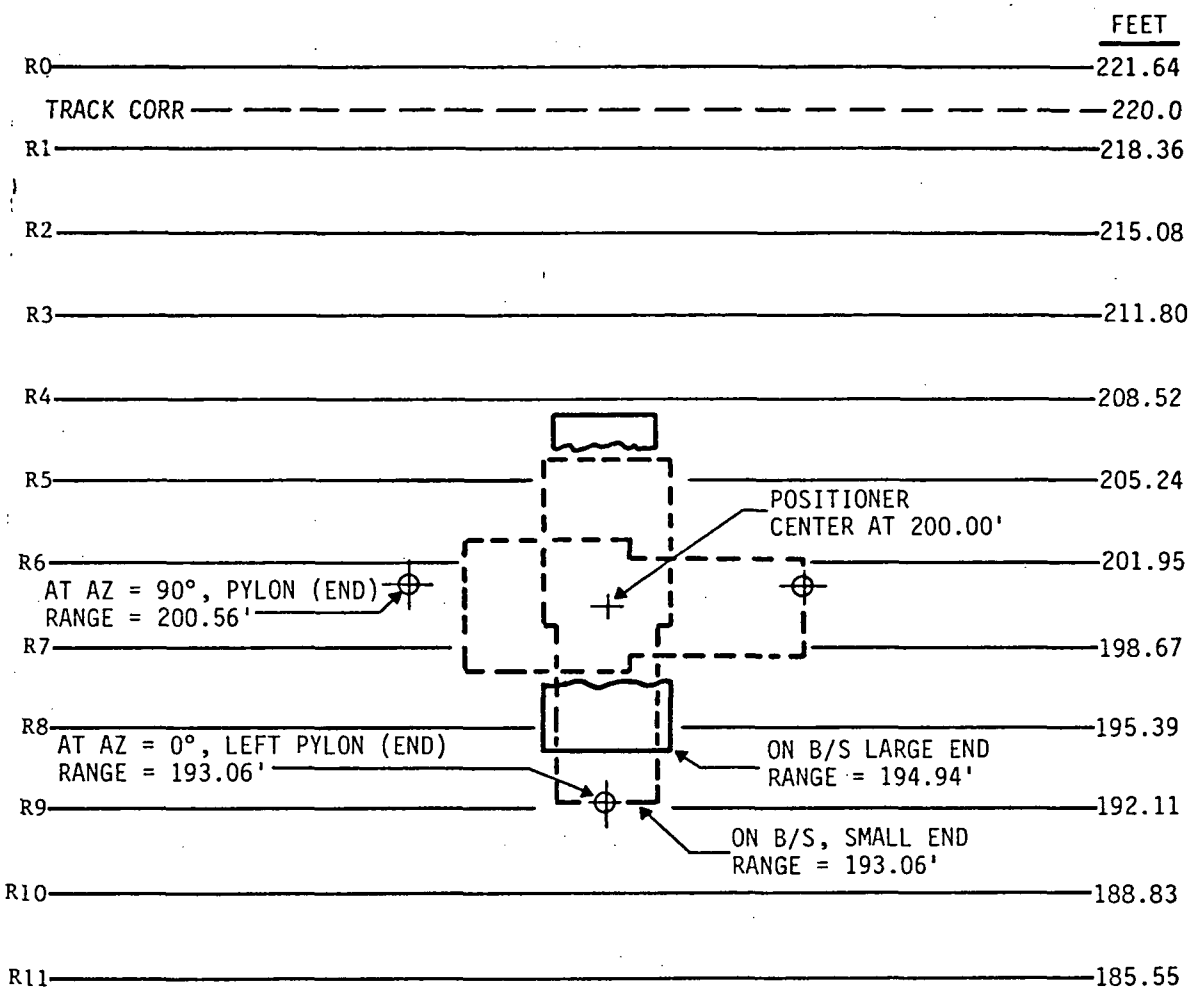

FIGURE 7-3. CORRELATOR RANGE COVERAGE 200' SITE (LASER RANGE = 200.00)

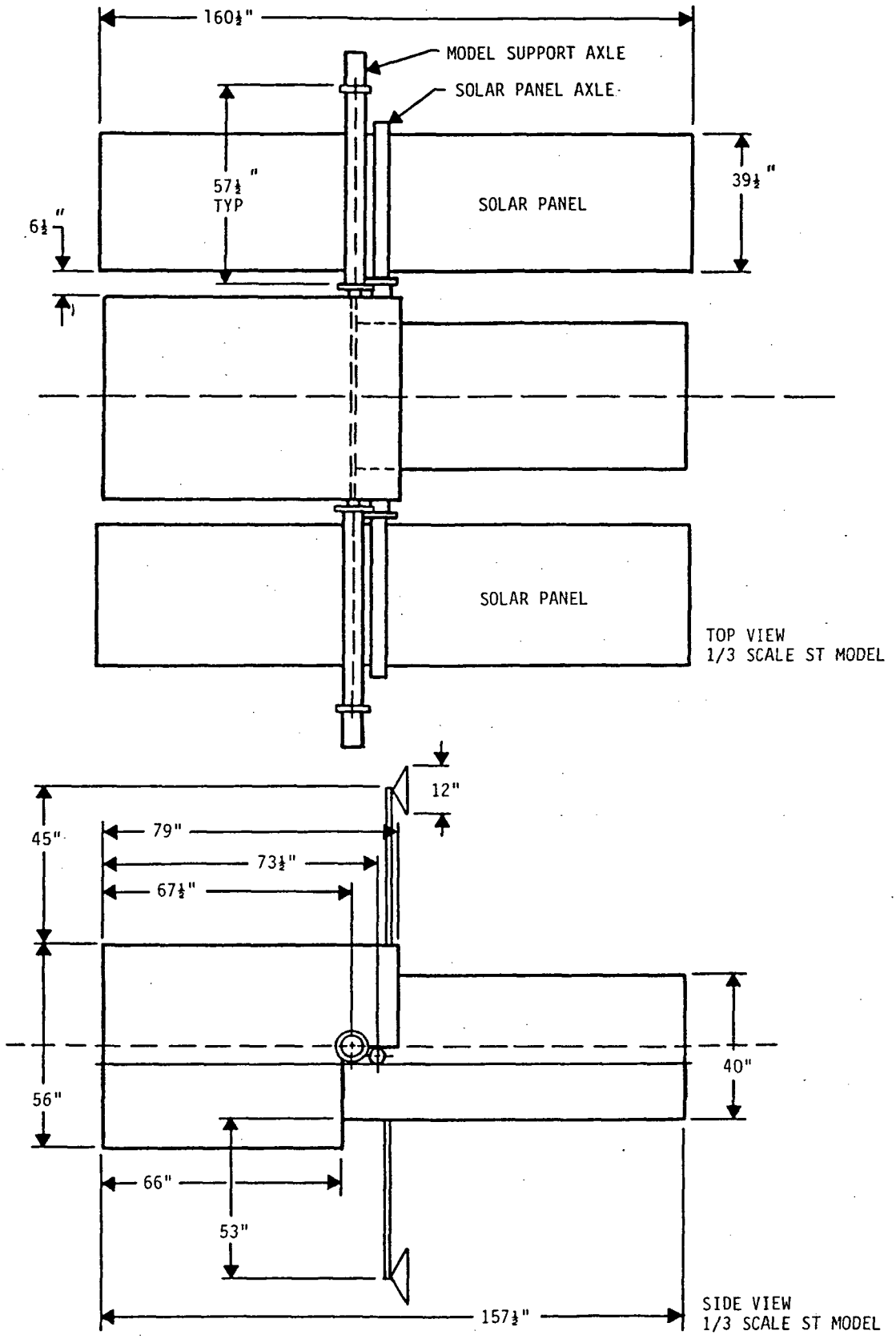

FIGURE 7-4. HST MODEL DIMENSIONS

In other words, the model response will occur in correlators 4-8.

7.2.2. RCS Plots, Specific

Complete sets of RCS plots have been created for the 350' and 200' test sites. Both these sites generated signature data for both solar panel positions, hence, are the most complete. In addition, the 350' site data encompasses 180^{o} of elevation coverage, while all other sites generated 90^{o} of elevation coverage.

The data for these sites is presented as follows:

- The RCS distribution of the entire matrix is generated on one figure as an overview of the RCS distribution

  .. Figure 7-5, 350', solar panels = 0^{o}
  Figure 7-6, 350', solar panels = 45^{o}
  Figure 7-7, 200', Solar panels = 0^{o}
  Figure 7-8, 200', solar panels = 45^{o}

- the largest RCS occurrence, for elevation aspects 1^{o} apart (azimuth is fixed), is plotted

  .. the corresponding correlator number is identified in the subplot directly above the RCS plot

  .. Figure 7-9 to 7-32, 350', solar panels = 0^{o}, 45^{o}

- the RCS density function and distribution for each test site and solar panel setting

  .. Figure 7-33 350', solar panels = 0^{o}
  Figure 7-34 350', solar panels = 45^{o}

7.2.2.1 RCS Distribution, Overview

Because of the large amount of data in each matrix (up to 16,200 points), it is difficult to visualize the RCS distribution as a function of aspect. Figures 7-5 to 7-8 have been produced in an attempt to show the "shift" in the RCS with angle. The symbology has been chosen to make larger RCS appear darker, while smaller RCS appears as the lighter areas. Empty rows are due to corrupted positioner data; the large blank in Figure 7-5, elevations 240 to 245, is because of an erroneous equipment setup - the correlator responses weren't recorded for those five runs.

The RCS distribution appears quite uniform and somewhat independent of solar panel position. The largest RCS (>25 db-m^{2}) exhibits a pattern originating at AZ = 90^{o}, EL = 270^{o} and progressing towards AZ = 0^{o}. The cylinders are vertical at this elevation angle, and we would expect the RCS to be independent of azimuth, because the model is then symmetrical about the vertical

SYMBOL MAGNITUDE

.	< 5 db-m^2
5 < -	< 10
10 < "	< 15
15 < |	< 20
20 < +	< 25
#	> 25

ORIGINAL PAGE IS
OF POOR QUALITY

FIGURE 7-5. RCS DISTRIBUTION

SOLAR PNLS = 45°

ORIGINAL PAGE IS
OF POOR QUALITY

SYMBOL MAGNITUDE

. < 5 db-m^2
5 < - < 10
10 < " < 15
15 < | < 20
20 < + < 25
> 25

MODEL ELEVATION

0° 45° 90°

MODEL AZIMUTH

FIGURE 7-6. RCS DISTRIBUTION

ORIGINAL PAGE IS
OF POOR QUALITY

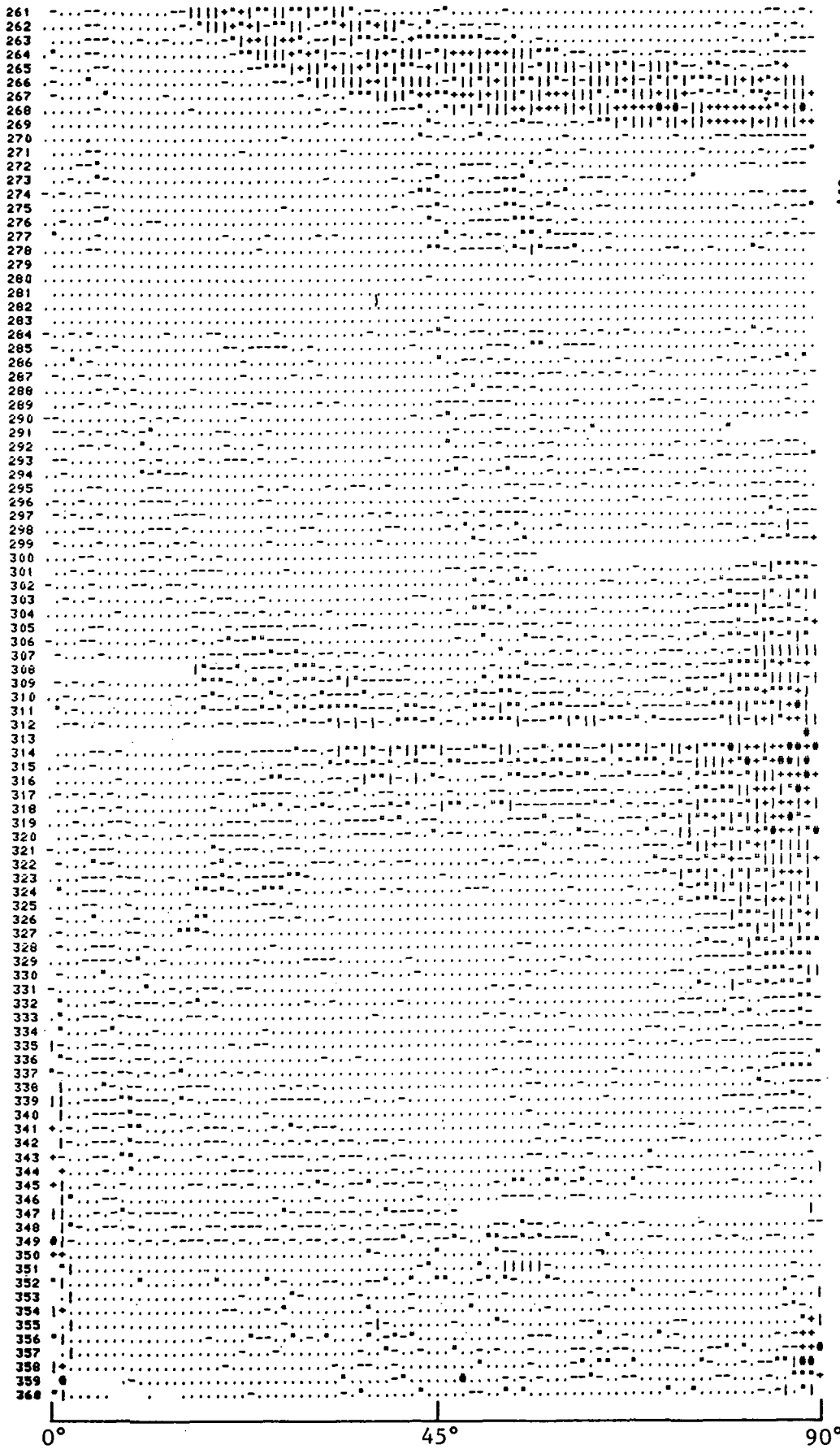

FIGURE 7-7 RCS DISTRIBUTION, 200' SITE

SOLAR PANELS = 0^{o} DATA NOT AVAILABLE

SITE DATA TAPE IS DEFECTIVE

FIGURE 7-8. RCS DISTRIBUTION, 200´ SITE

axis. The feature which contributes to the large RCS close to AZ = 0^{o} from EL = 270^{o} to 180^{o} could (perhaps) be the dihedral reflector at the junction of the two cylinders.

Referring to Figure 7-6, in the region where AZ = 90^{o}, EL = 315^{o}, a darker region occurs than is present in Figure 7-5. This is due to the solar panels; the response for solar panels = 0^{o} (Figure 7-5), is still apparent at the end of the body response where AZ = 90^{o}, EL = 270^{o}. This will be discussed further in the next section.

7.2.2.2 RCS Distribution, RCS Function vs. EL

The plots included in this report have been selected to show:

- solar panel RCS characteristic
- model main body RCS characteristic
- overall trends

All plots at AZ = 0^{o} or 90^{o} contain invalid data, indicated by the "no data" entry in the correlator identification subplot. This is due to the positioner outputting some previous data point held in its controller prior to and for a short time after startup. The data is correct for passage through the end points from the middle, e.g., in a decreasing direction through 0^{o} or in an increasing direction through 90^{o}. The data is incorrect for passage through the end points from a dead stop, e.g., in an increasing direction from an initial startup at 0^{o} or decreasing direction from a startup at 90^{o}.

This means half the RCS data at the end points is lost, the rest is available and appears on the plots. For example, refer to Figure 7-9, AZ = 0^{o}. The RCS characteristic around EL = 270^{o} (solar panel = 0^{o}) and EL = 315^{o} (solar panel = 45^{o}) is still evident.

This particular characteristic of maxima separated by EL = 45^{o} is still evident for azimuths up to 85^{o} or so, and is evidently caused by the solar panels. Based upon this assumption, the RCS of the solar panels is approximately 30 db-m^{2}. With further decreases in azimuth, the solar panel contribution becomes less evident. However, a response is always present at EL 270^{o}. Because this response is relatively insensitive to azimuth orientation, with a maximum response > 40 db-m^{2}, it is attributed to the main body of the model. Why the overall response decreases to 5-10 db-m^{2} for most azimuths, then rises to 10 - 20 db-m^{2} at azimuths close to 0^{o} is unknown at this time. At azimuth = 0^{o}, the model should be blocked somewhat by the pylon, but as illustrated at AZ = 1^{o} or 0^{o} (Figure 7-31 and 7-32), the main responses are still in correlators 6, 7, and 8. Pylon response would occur in correlator 9.

7.2.2.3 RCS Probability

Both solar panel positions used indicate the most likely RCS measured to be around 5 db-m^{2}, with a slight skew towards RCS around 1.5 - 4 db-m^{2}. In general, the function approaches a gaussian distribution with RCS between -5 to +25 db-m^{2}. The RCS distribution for the 350' site is given in Figure 7-33 and 7-34.

ORIGINAL PAGE IS
OF POOR QUALITY

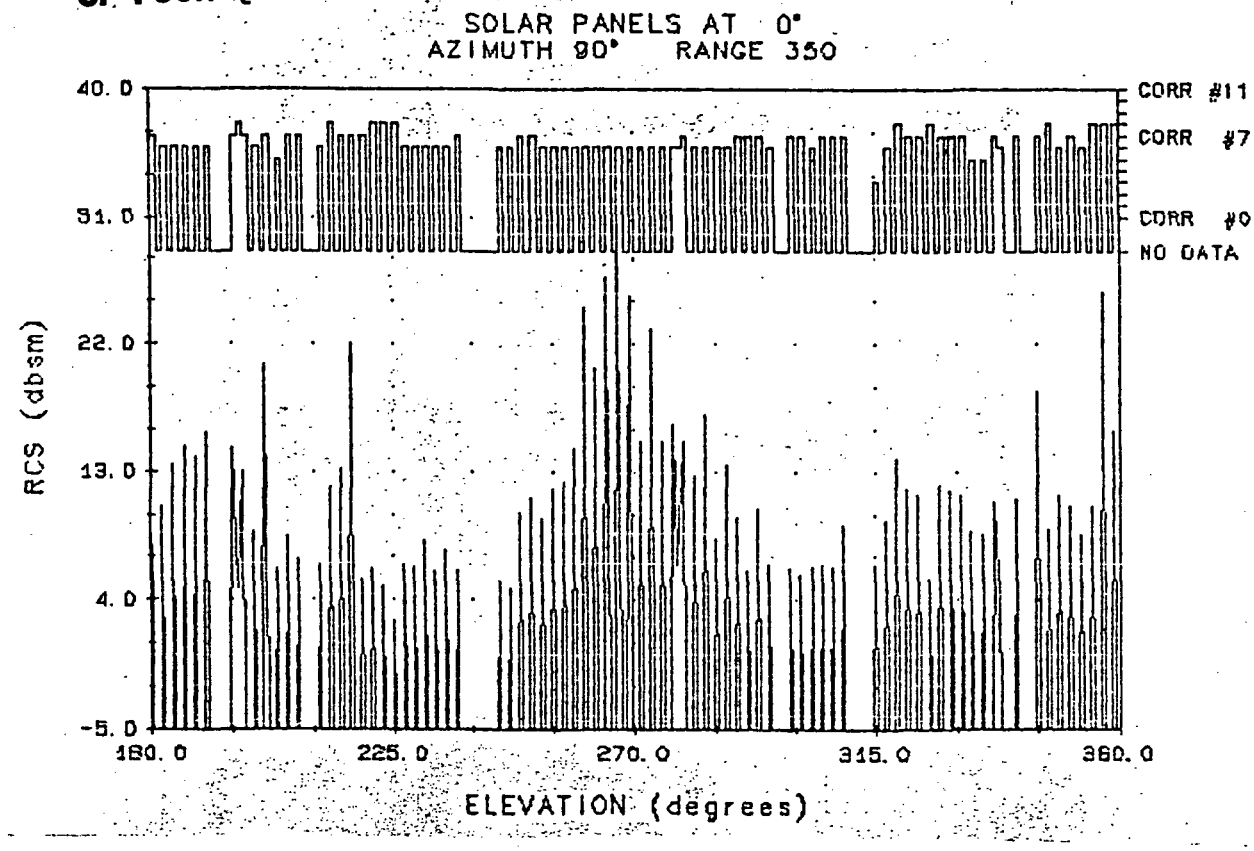

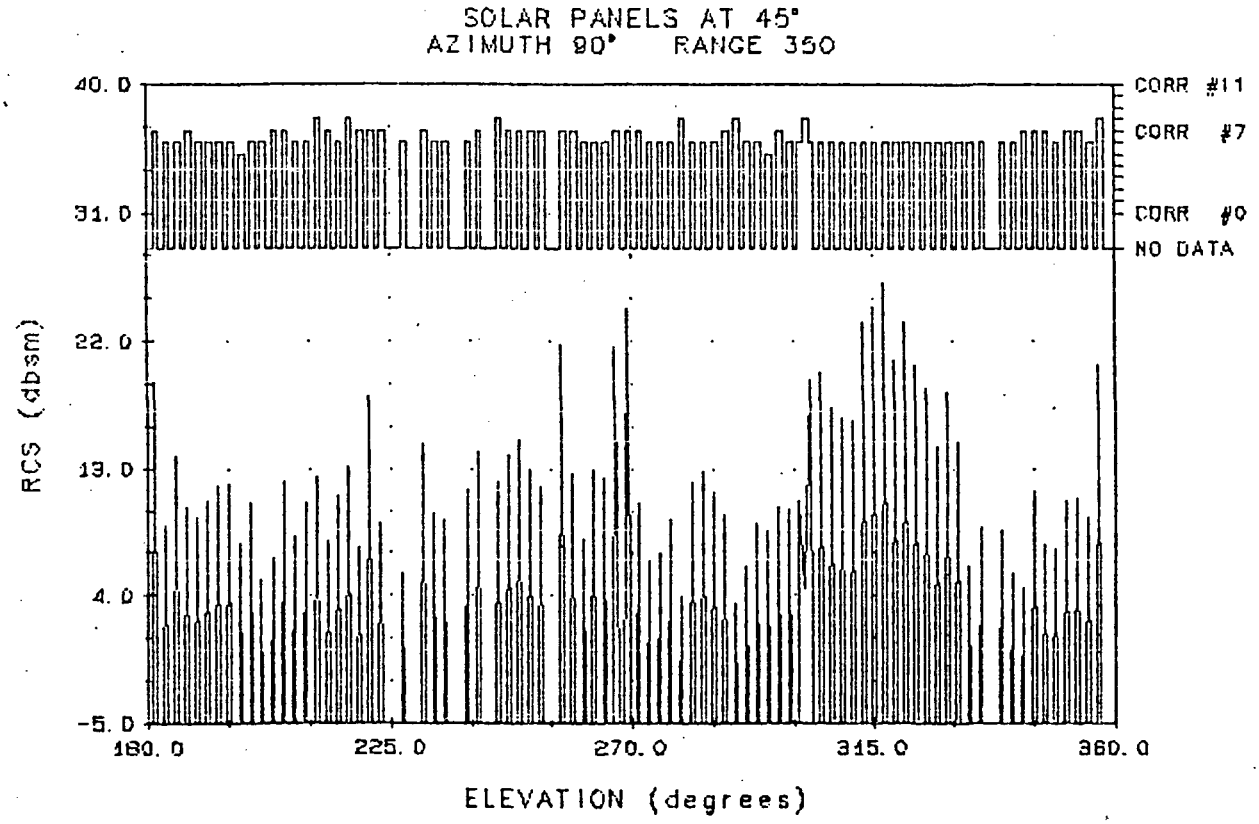

FIGURE 7-9. HST MODEL RCS

ORIGINAL PAGE IS
OF POOR QUALITY

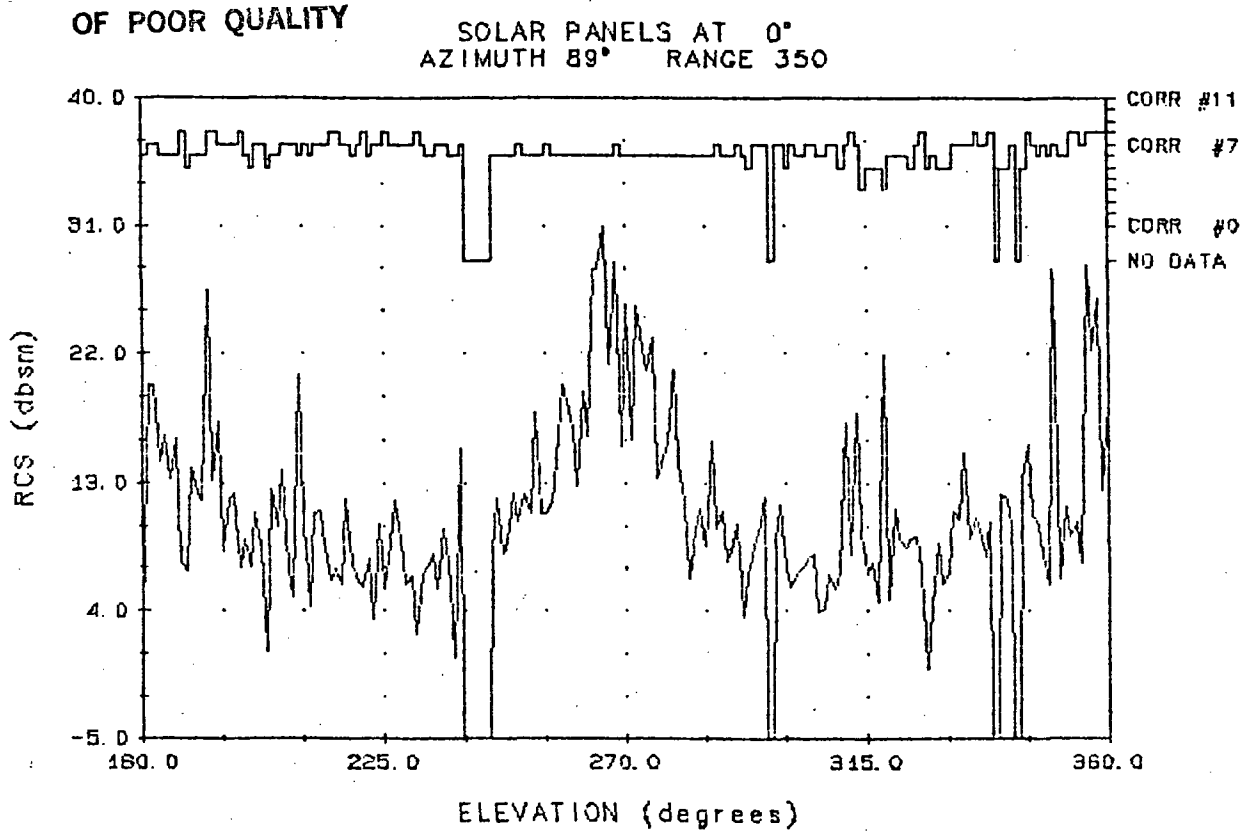

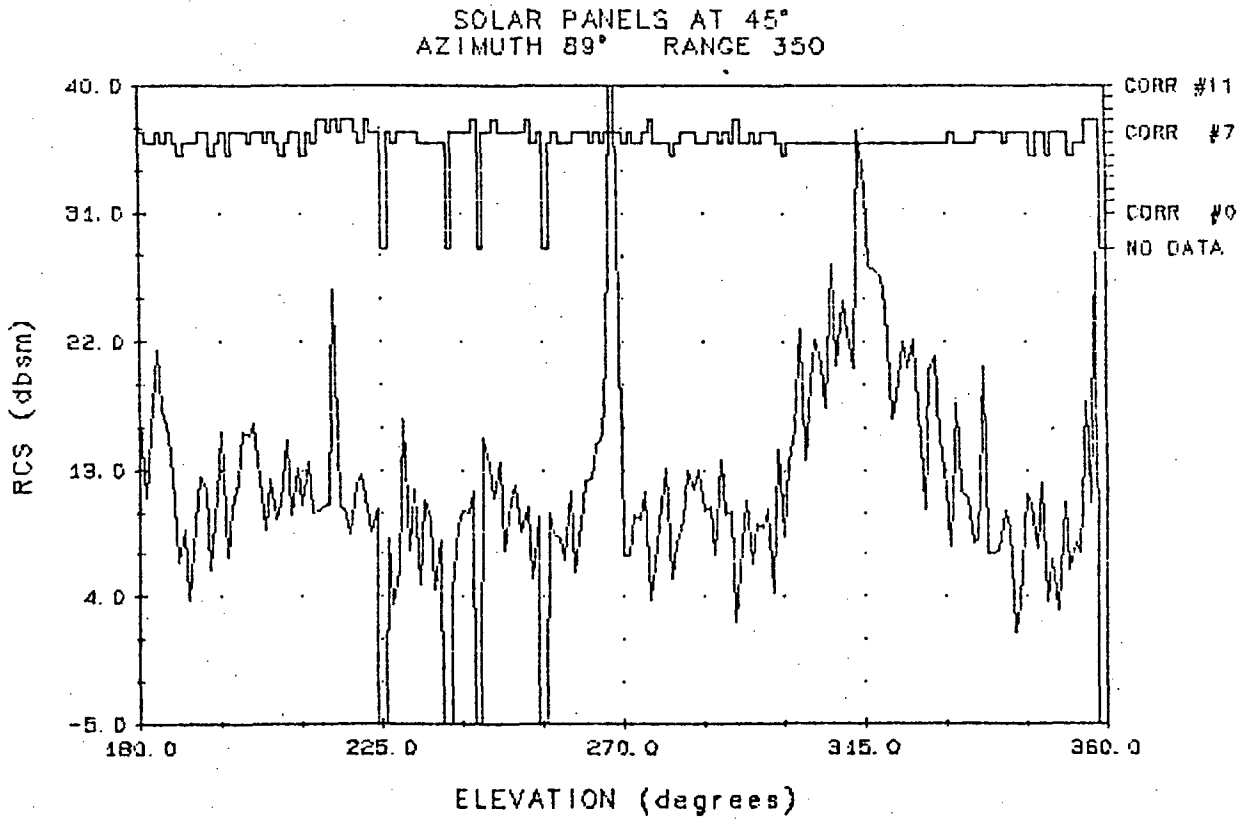

FIGURE 7-10. HST MODEL RCS

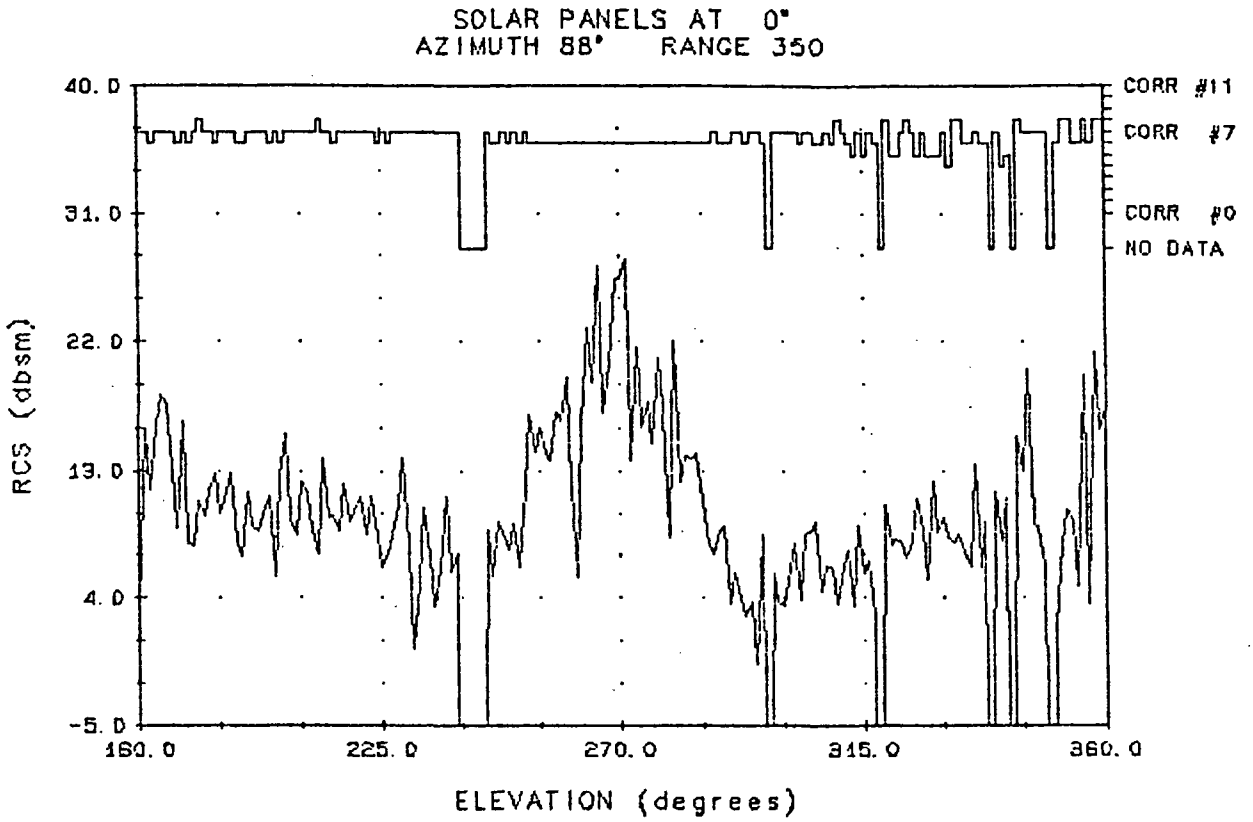

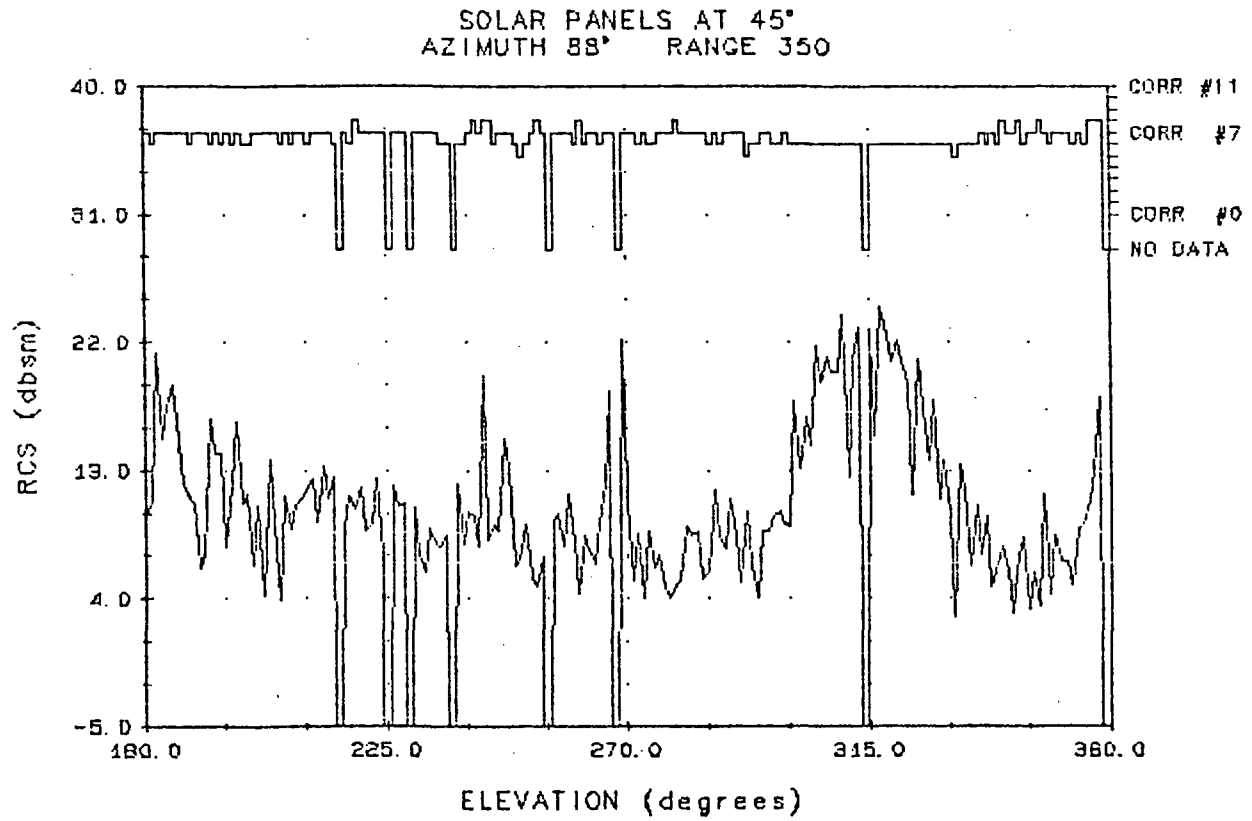

FIGURE 7-11. HST MODEL RCS

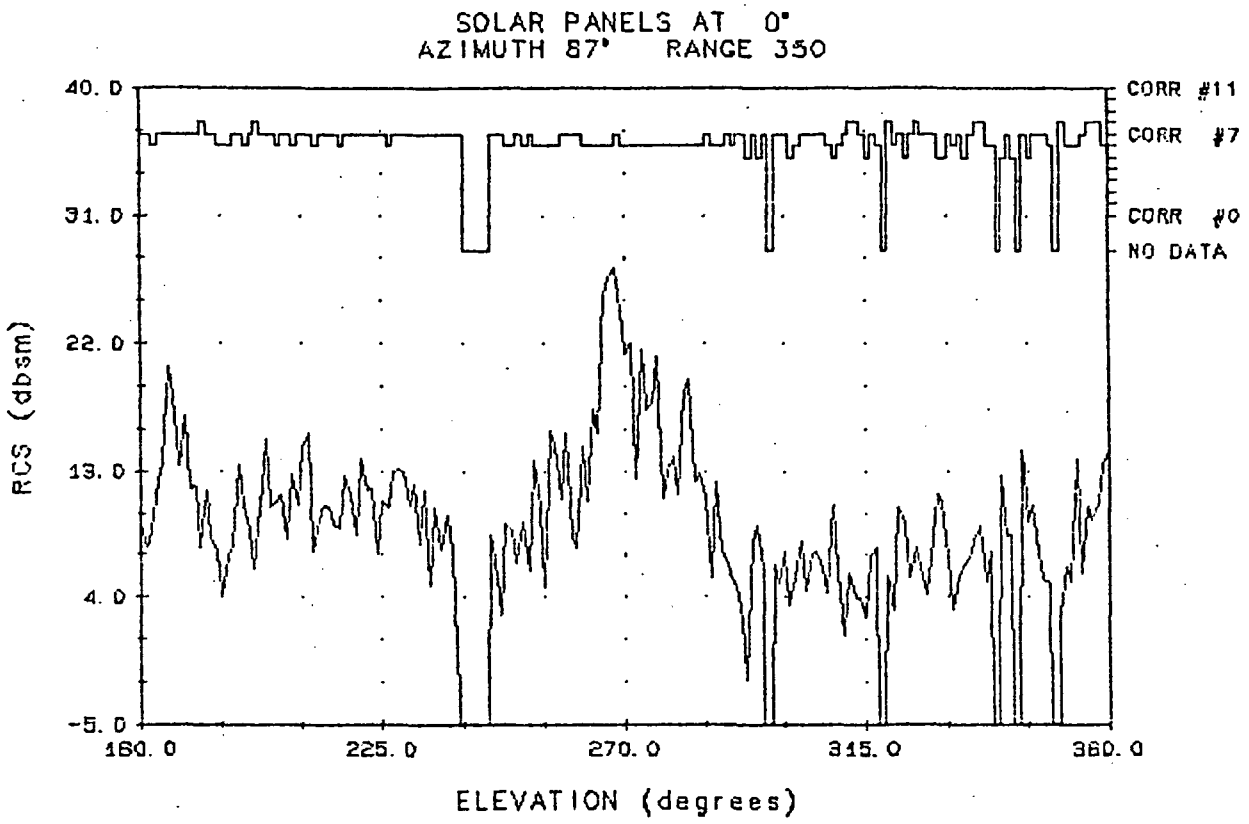

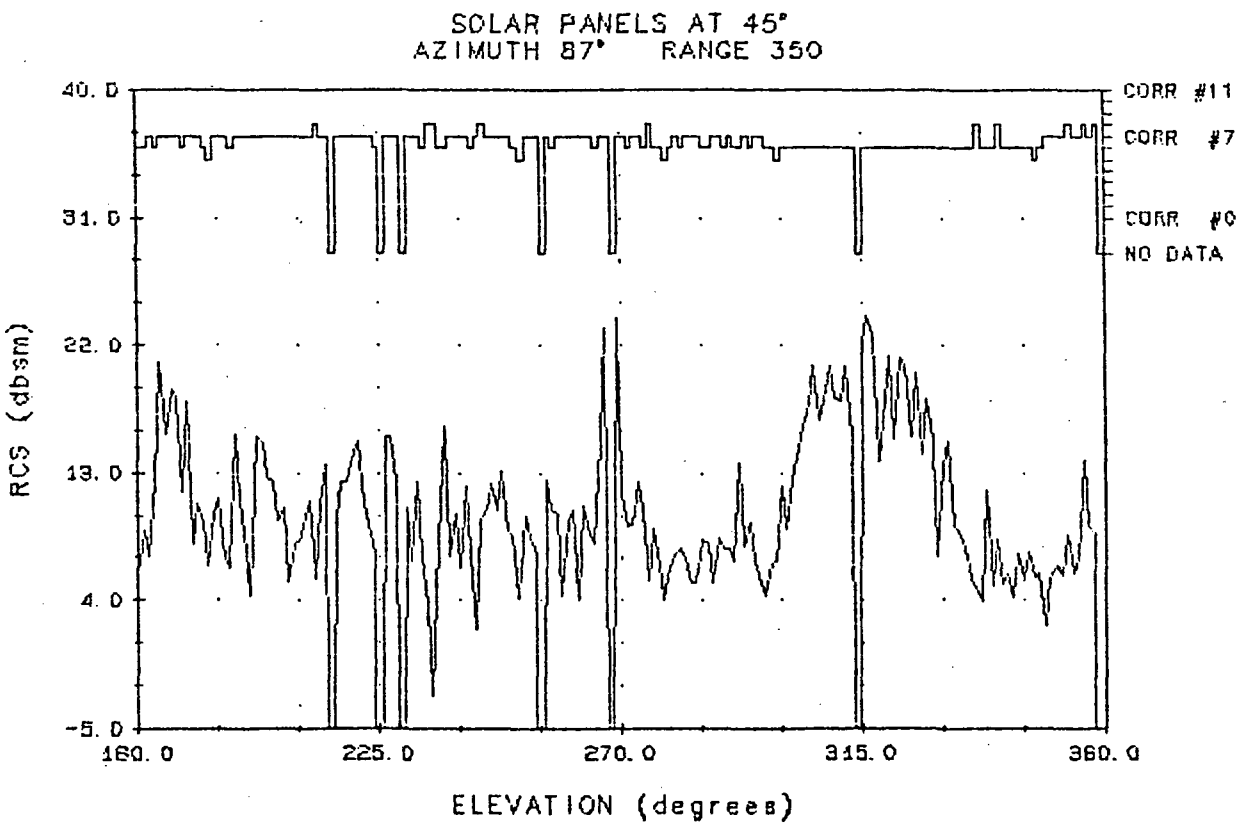

FIGURE 7-12. HST MODEL RCS

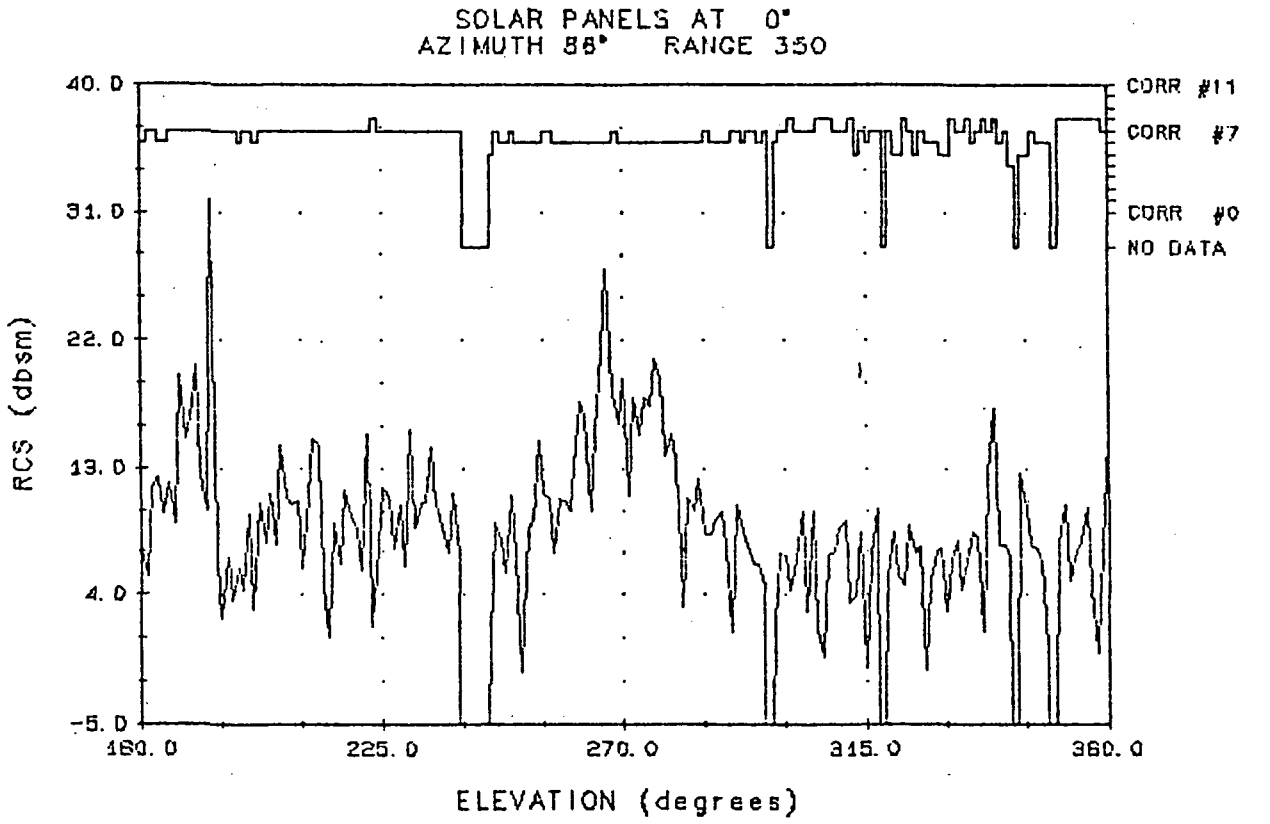

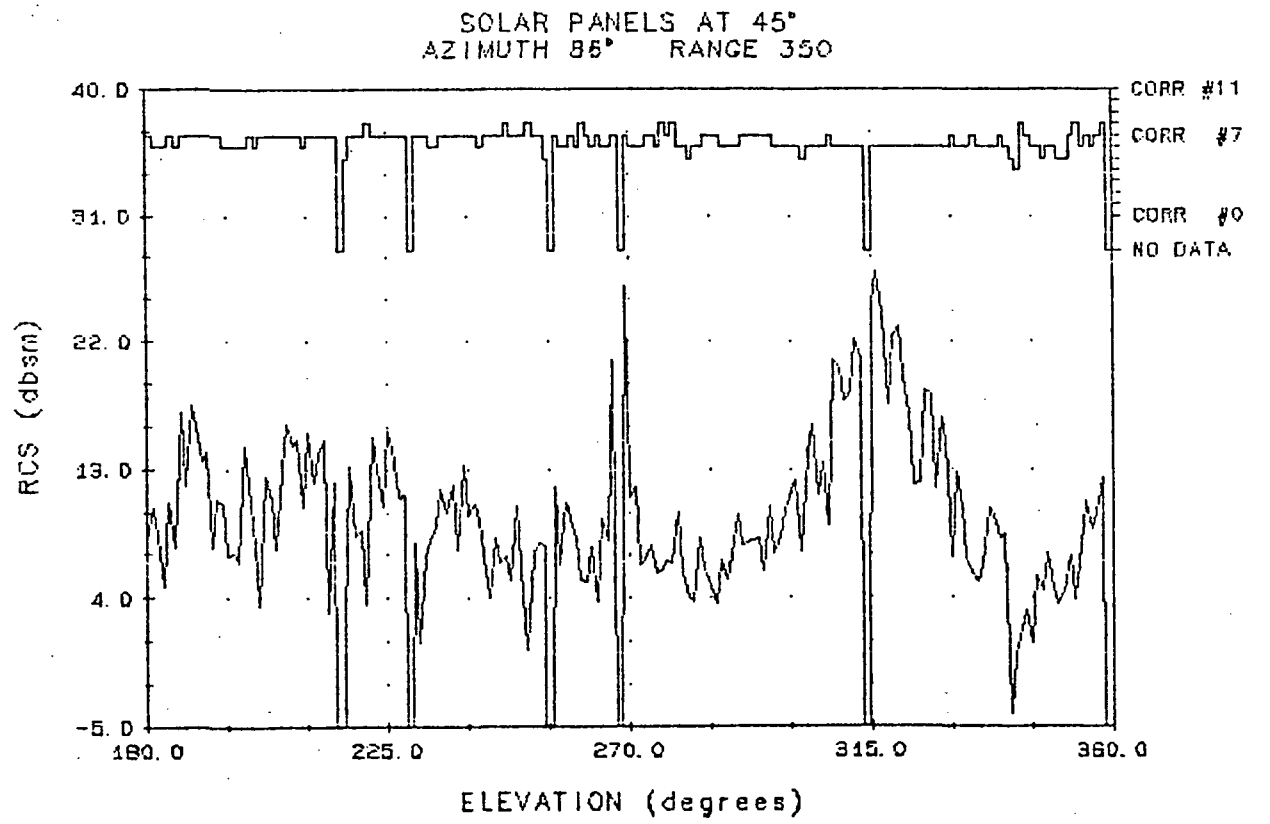

FIGURE 7-13. HST MODEL RCS

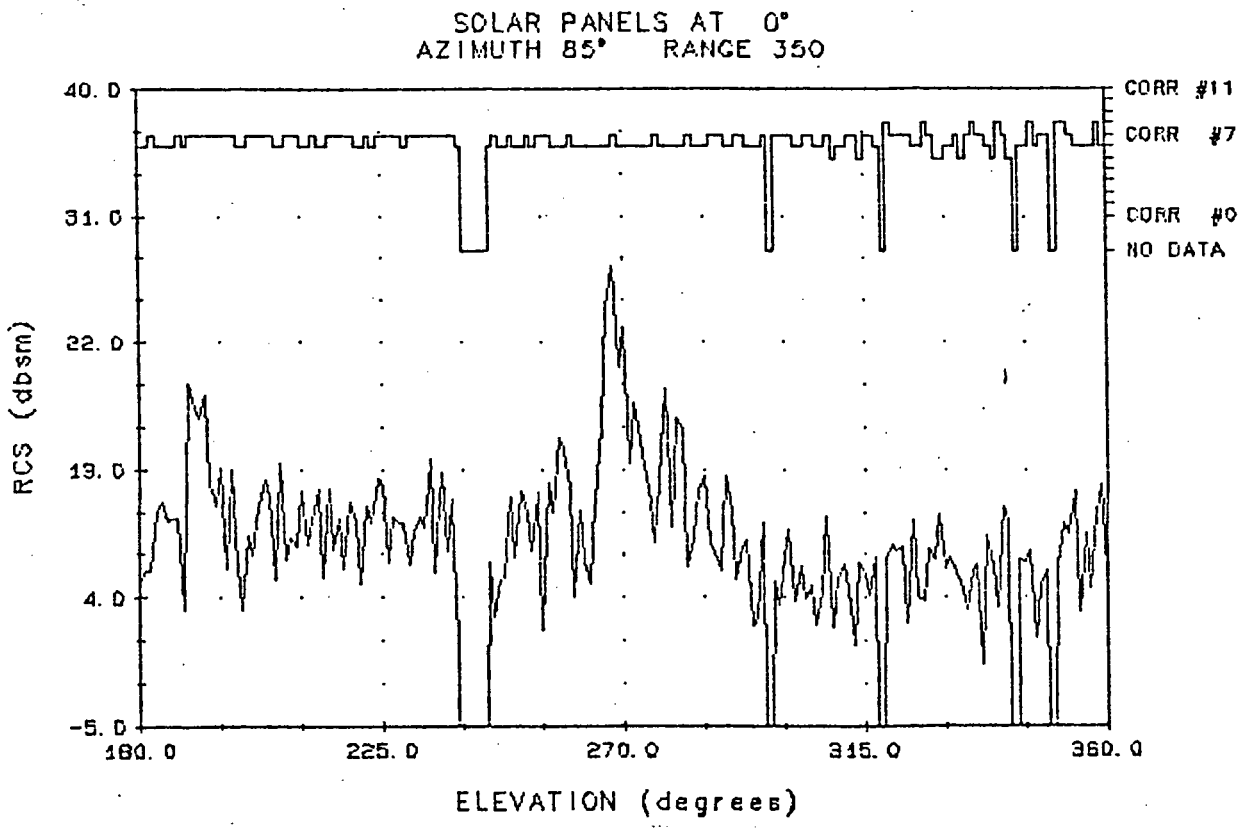

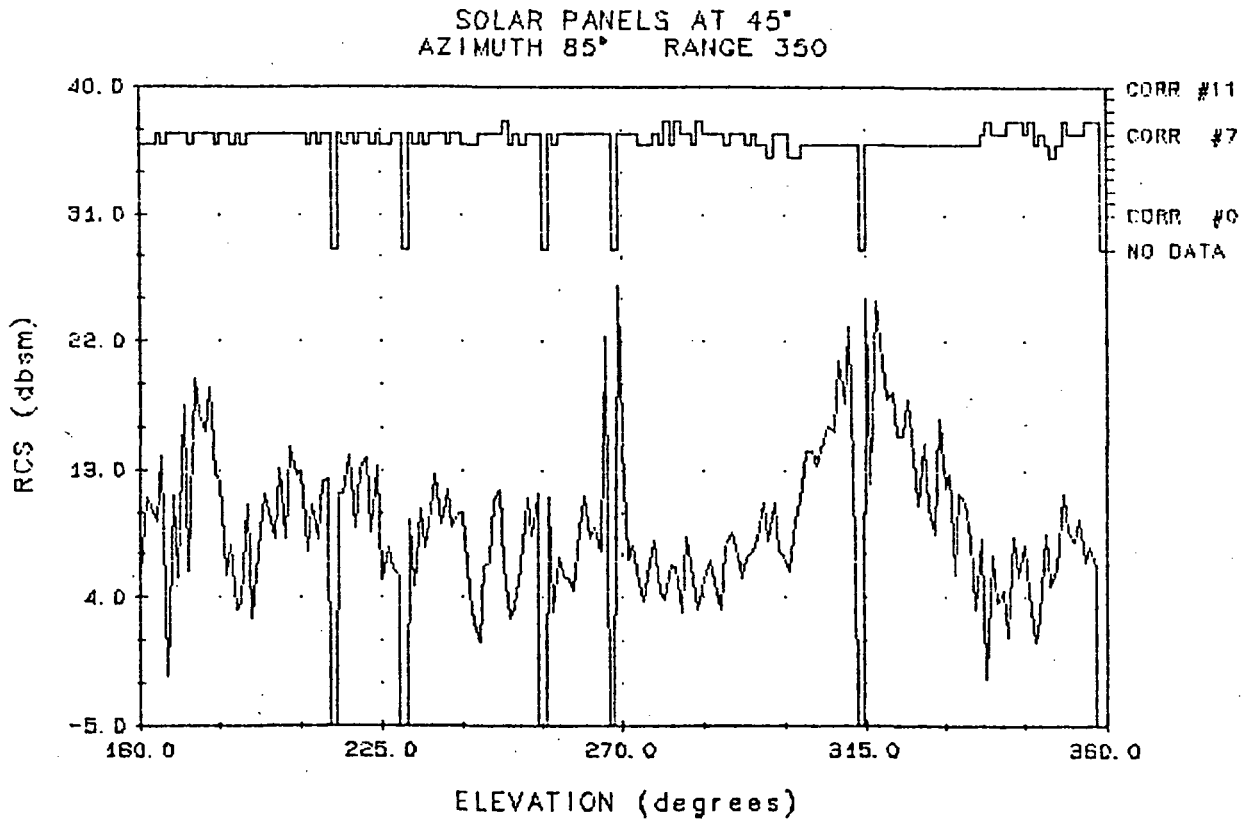

FIGURE 7-14. HST MODEL RCS

ORIGINAL PAGE IS
OF POOR QUALITY

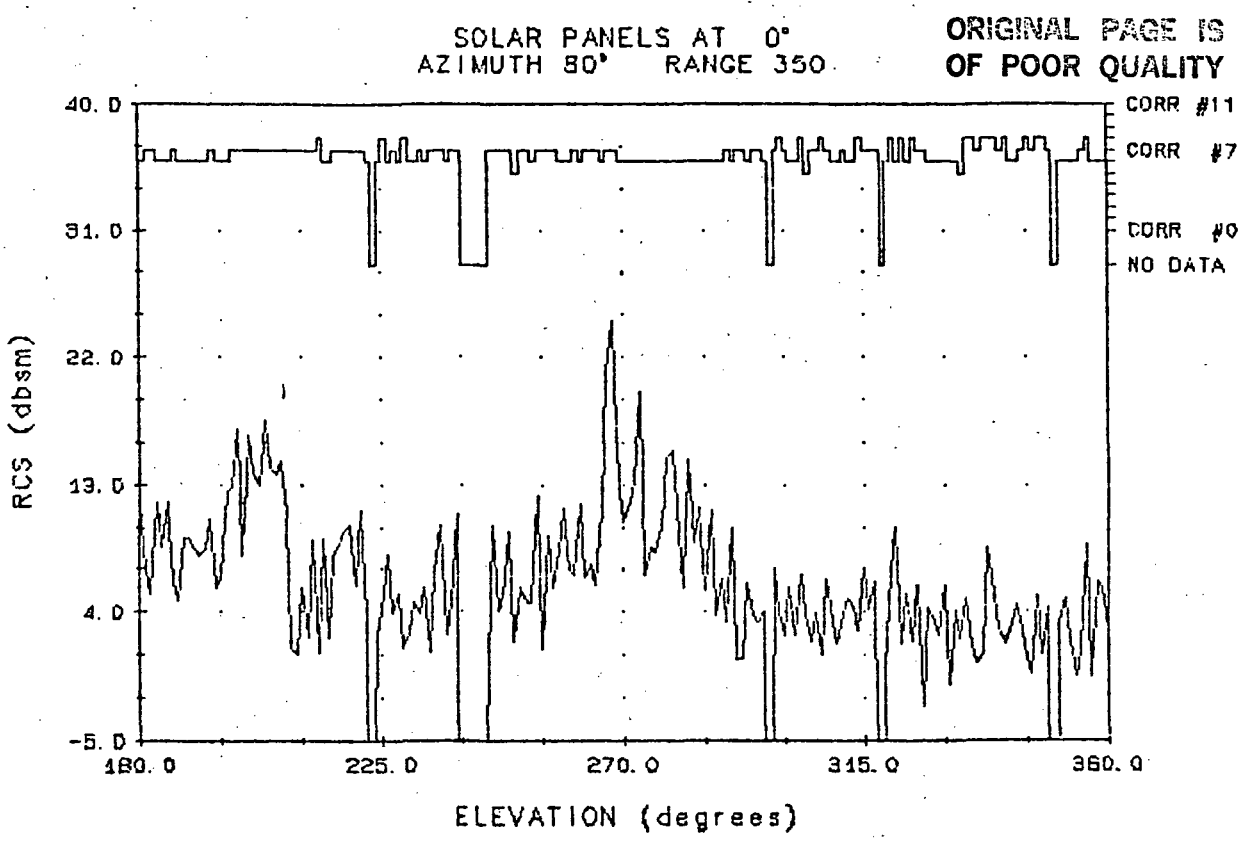

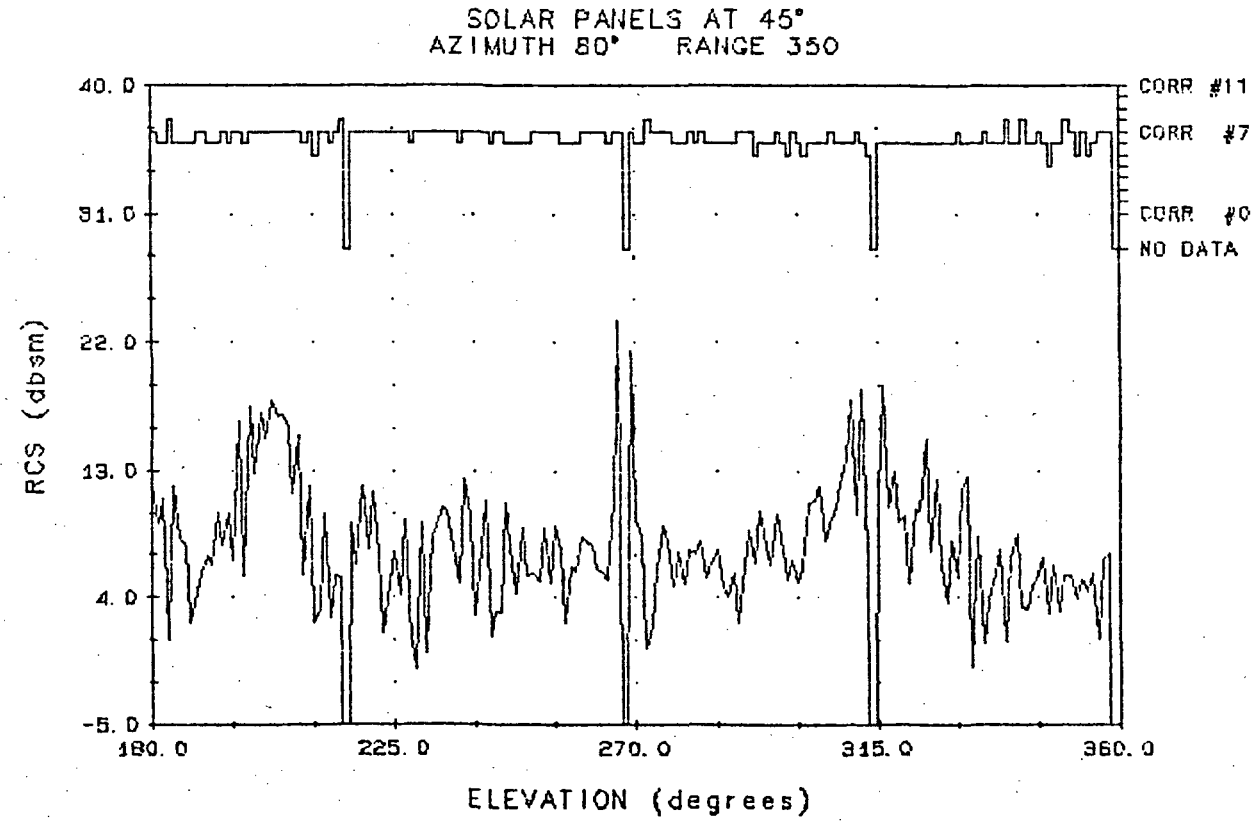

FIGURE 7-15. HST MODEL RCS

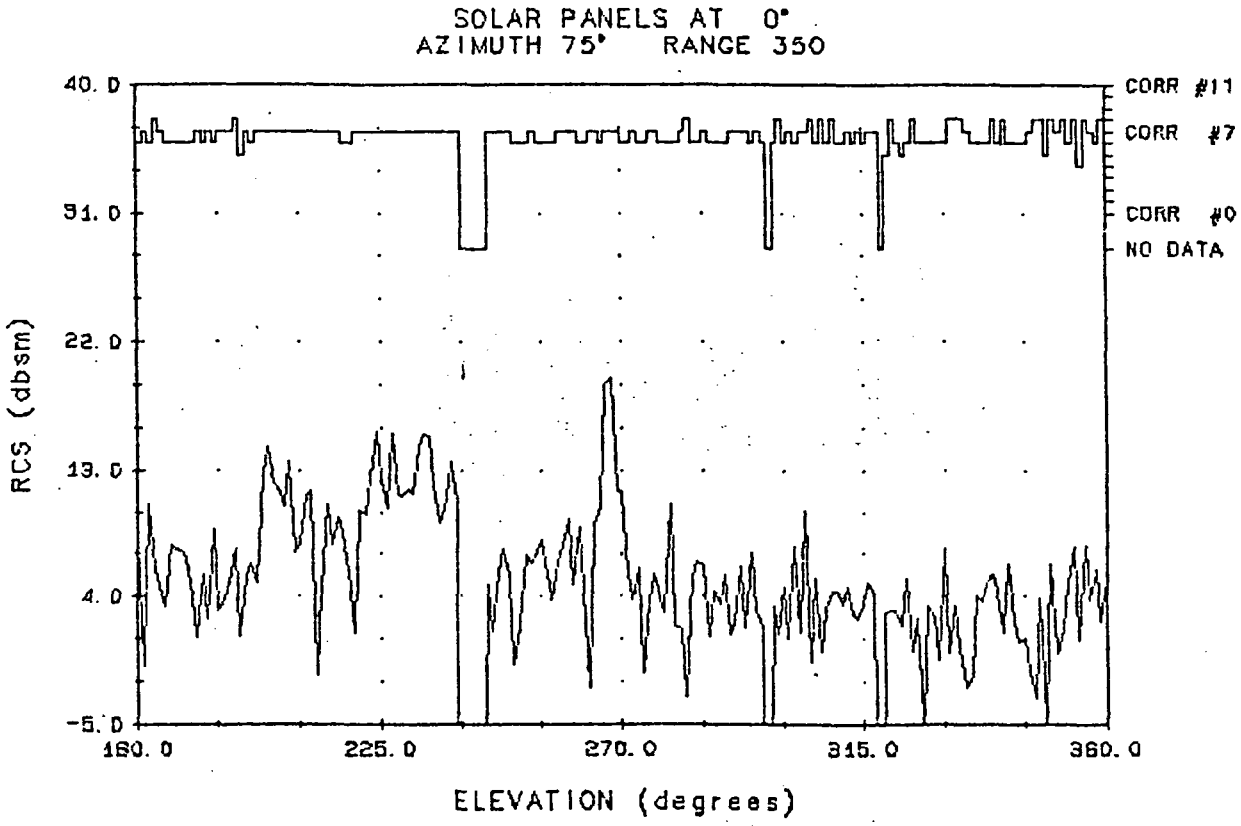

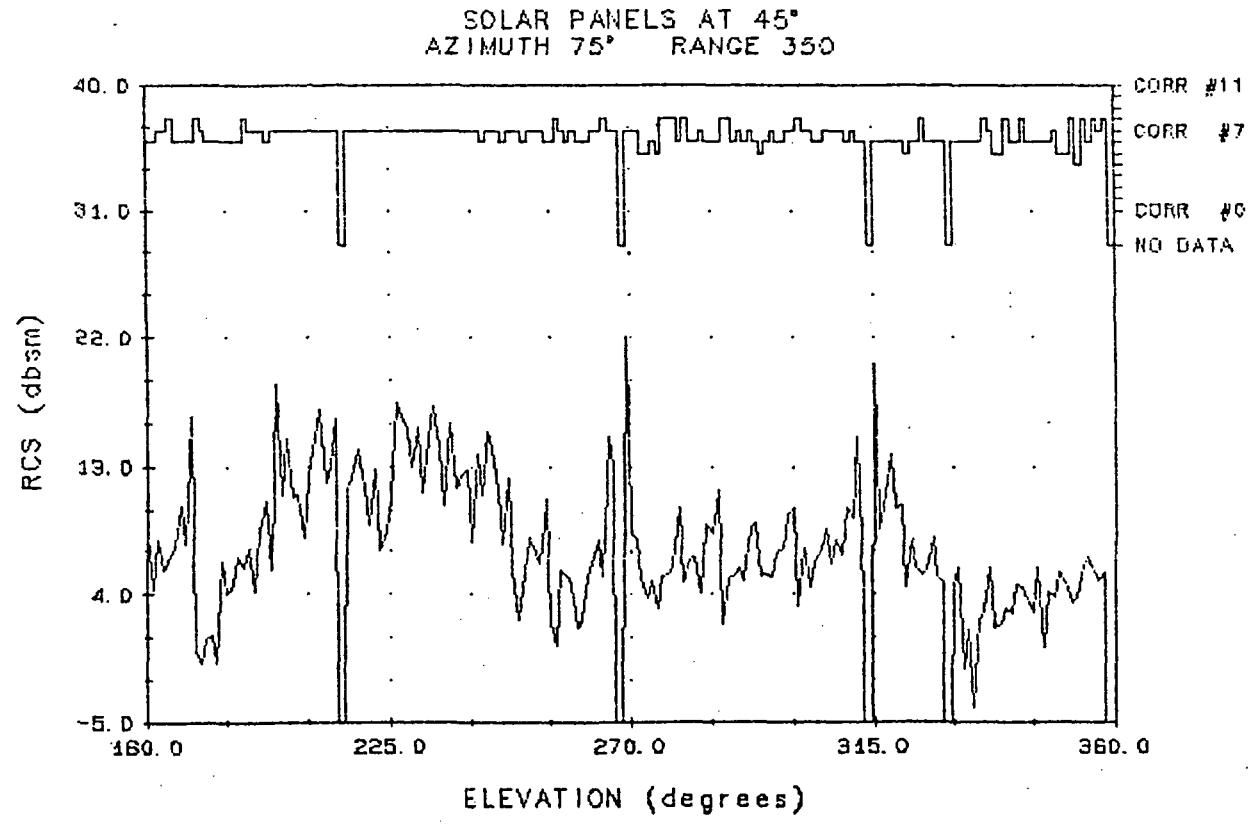

FIGURE 7-16. HST MODEL RCS

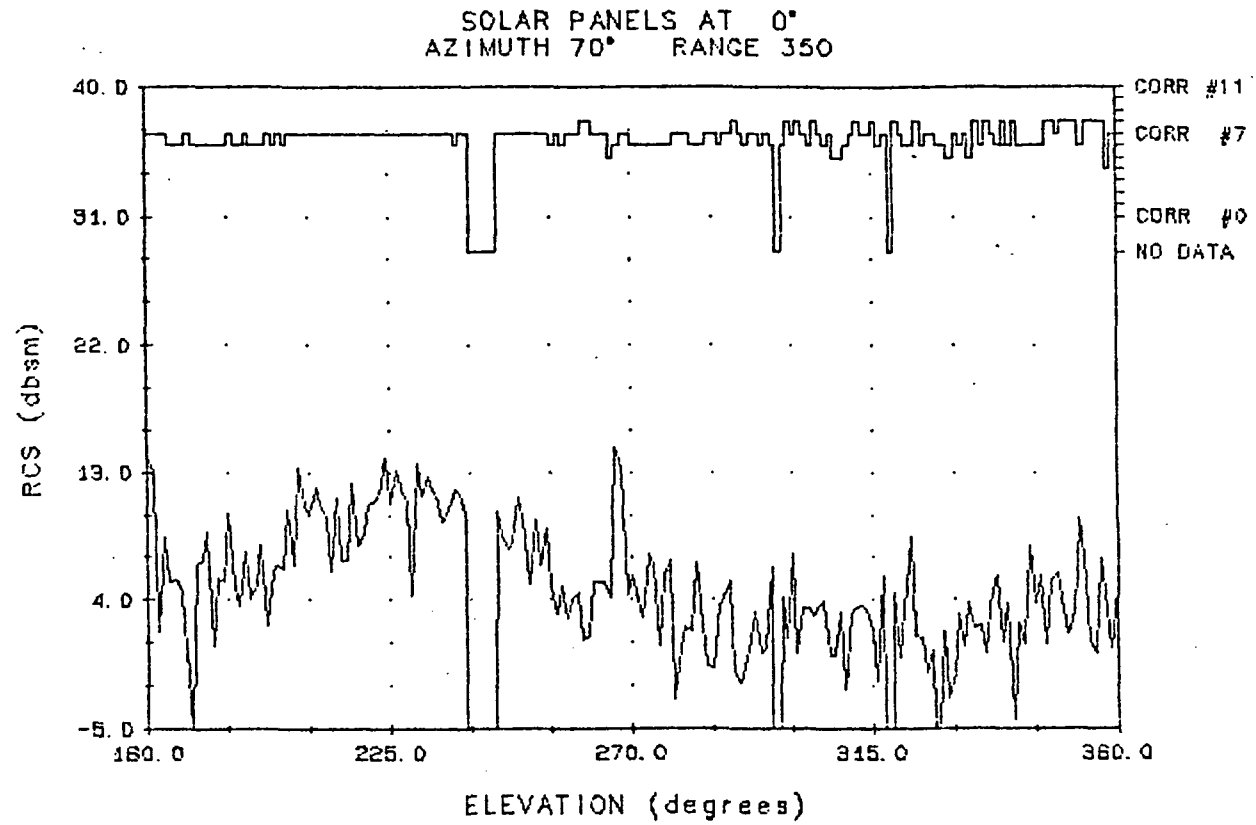

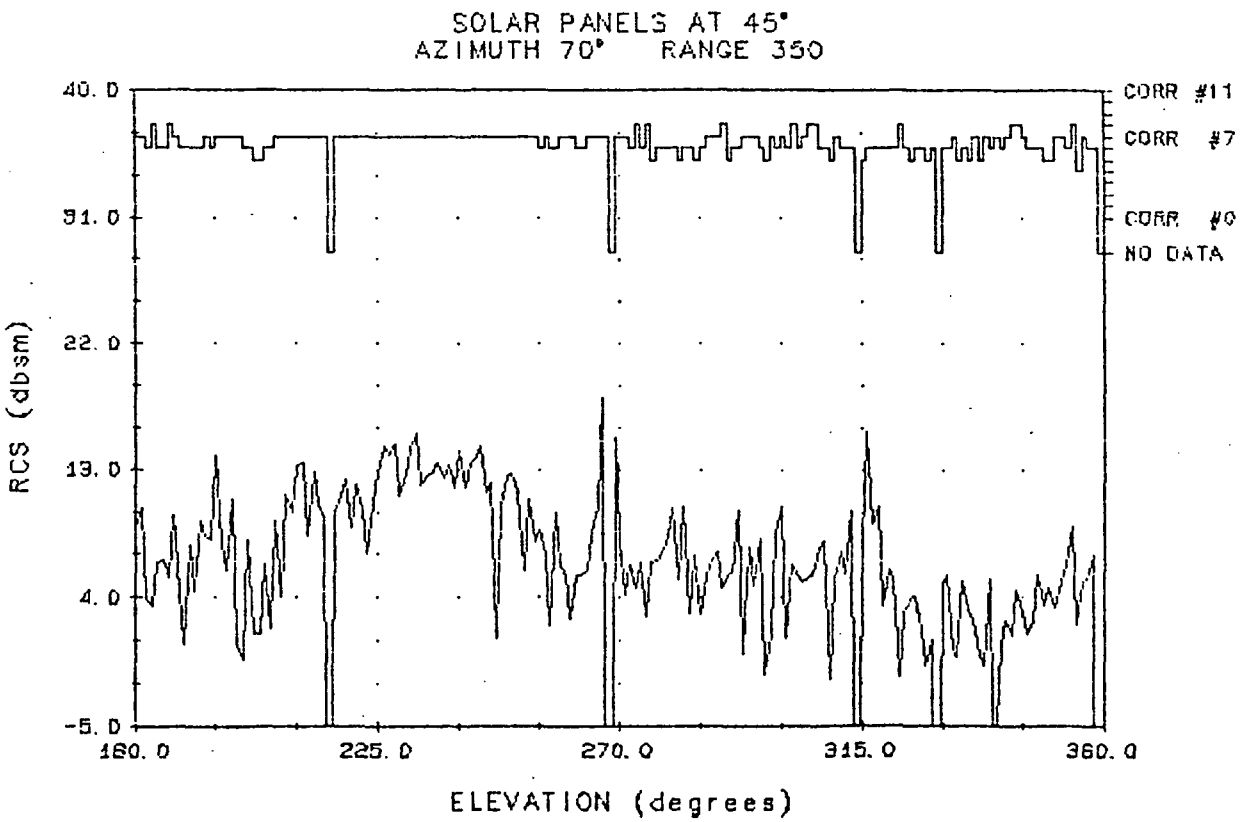

FIGURE 7-17. HST MODEL RCS

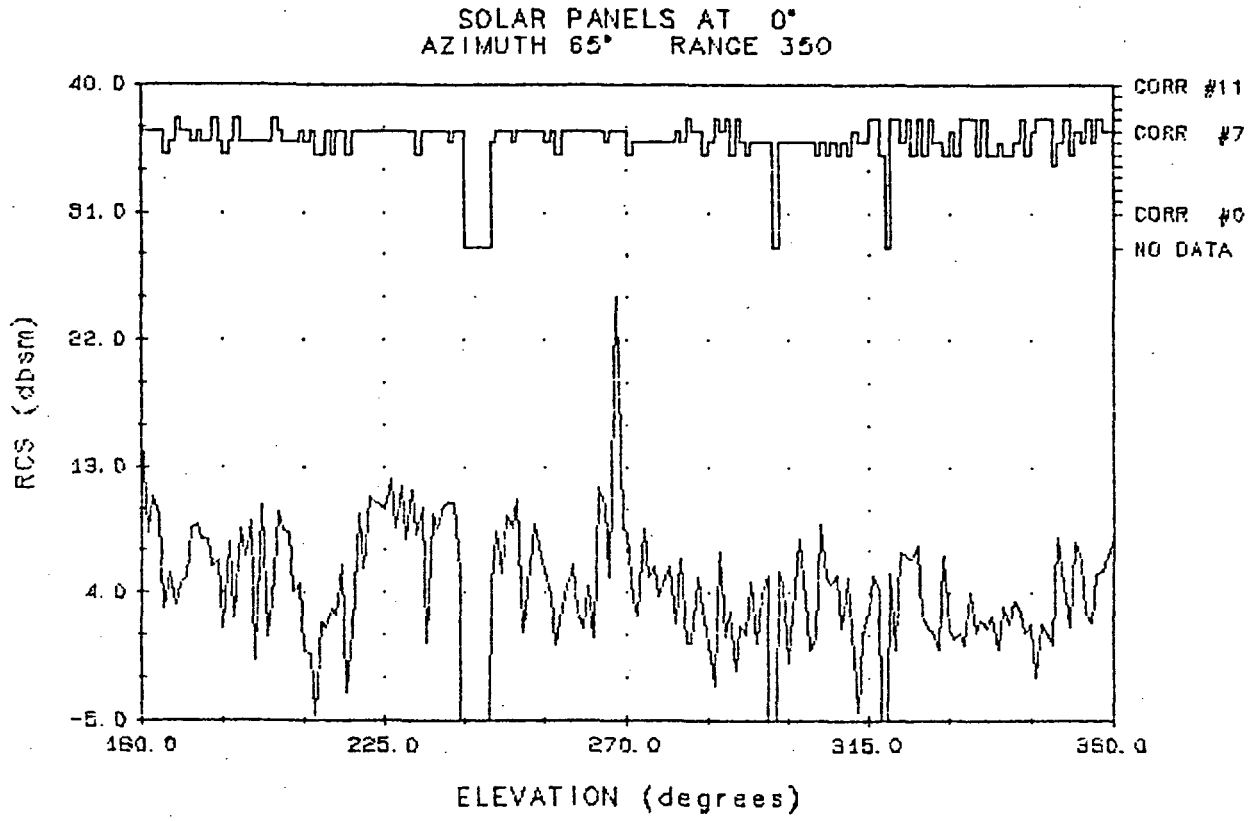

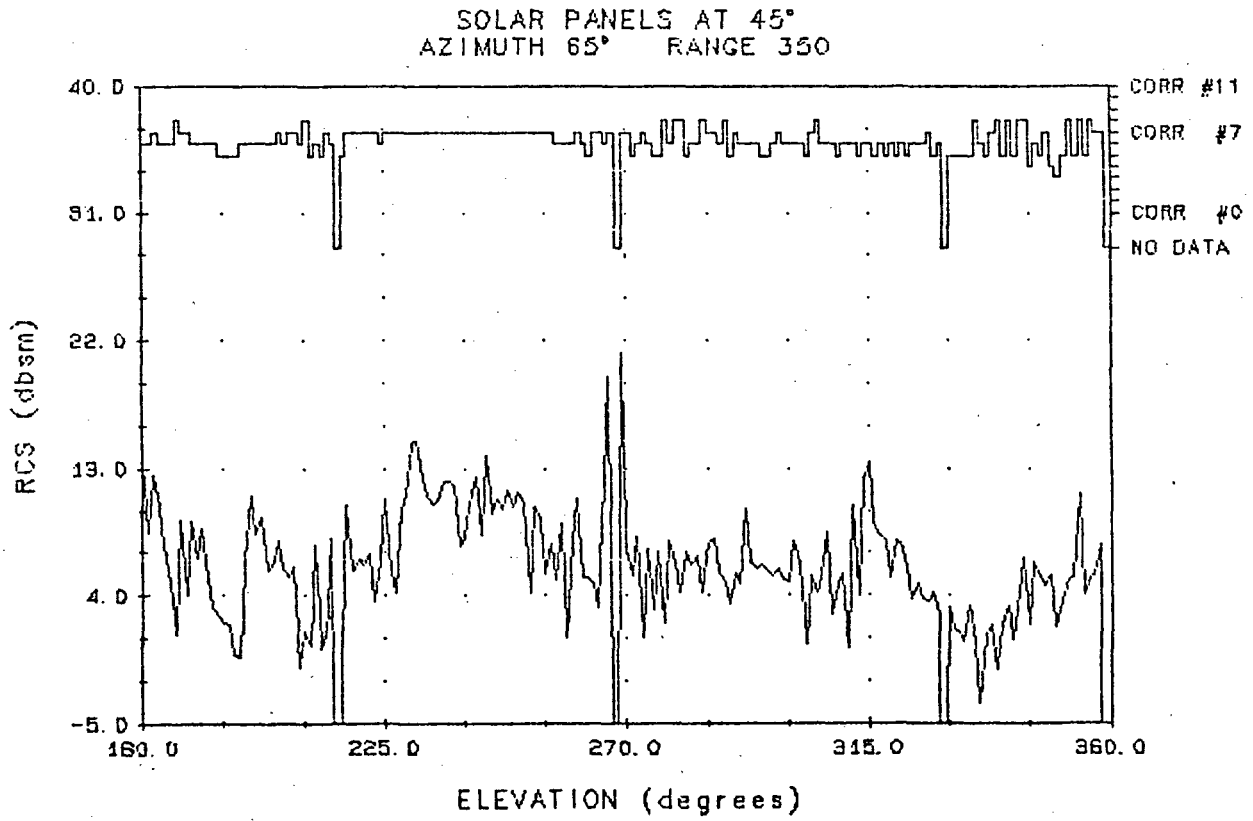

FIGURE 7-18. HST MODEL RCS

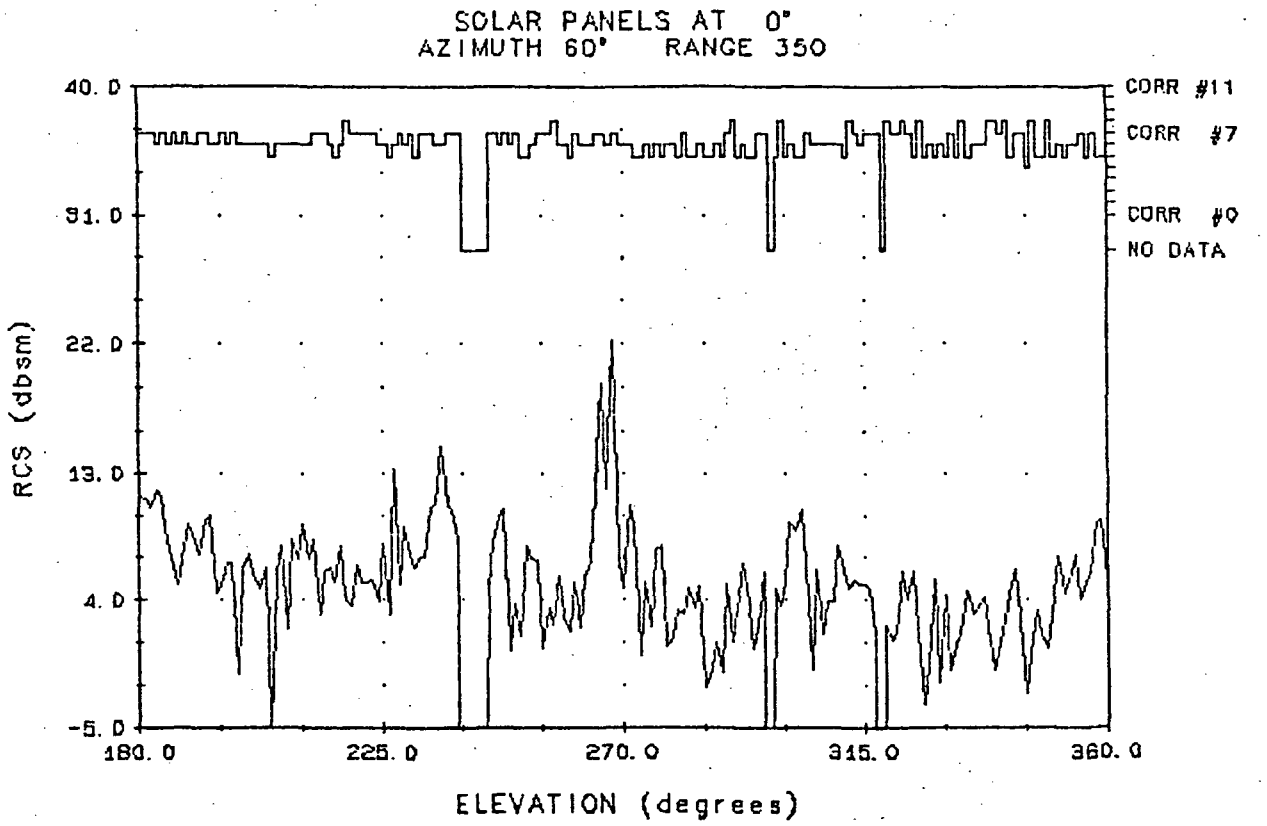

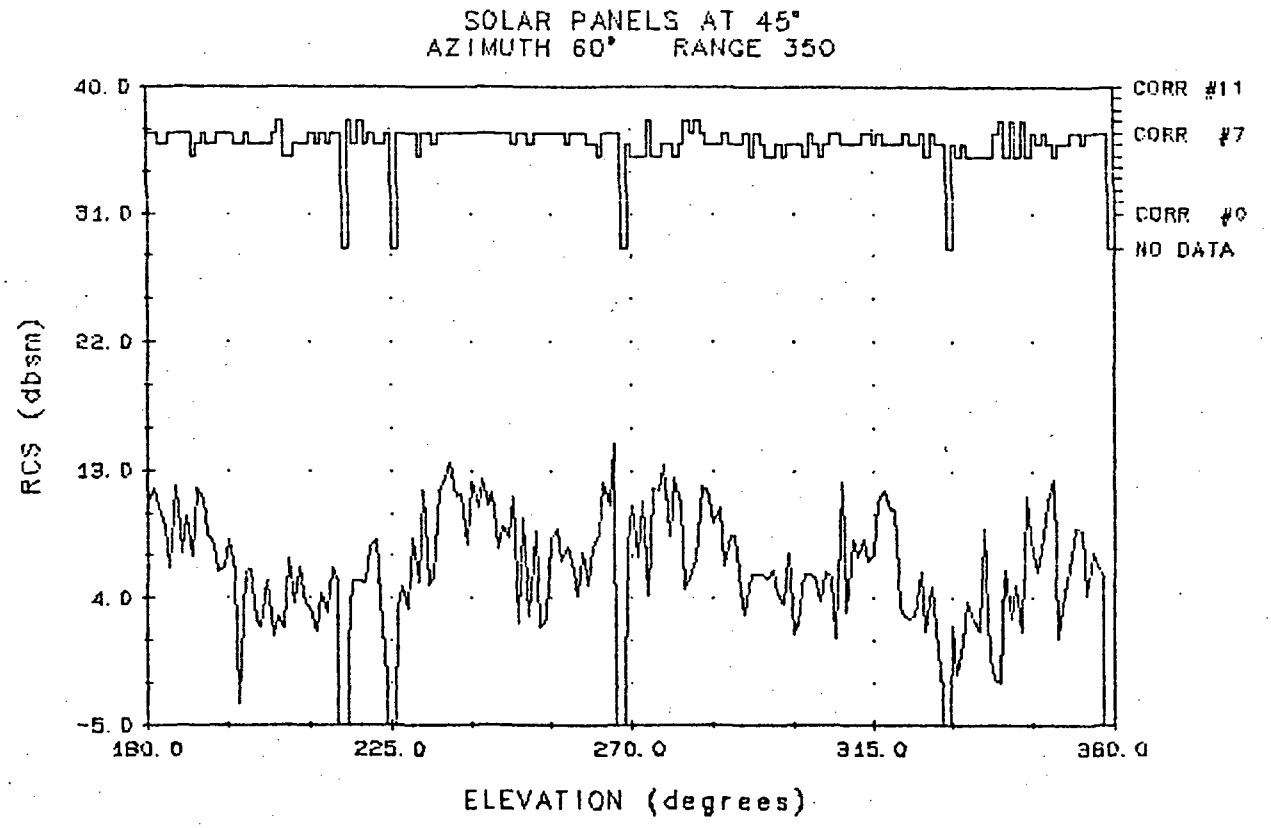

FIGURE 7-19. HST MODEL RCS

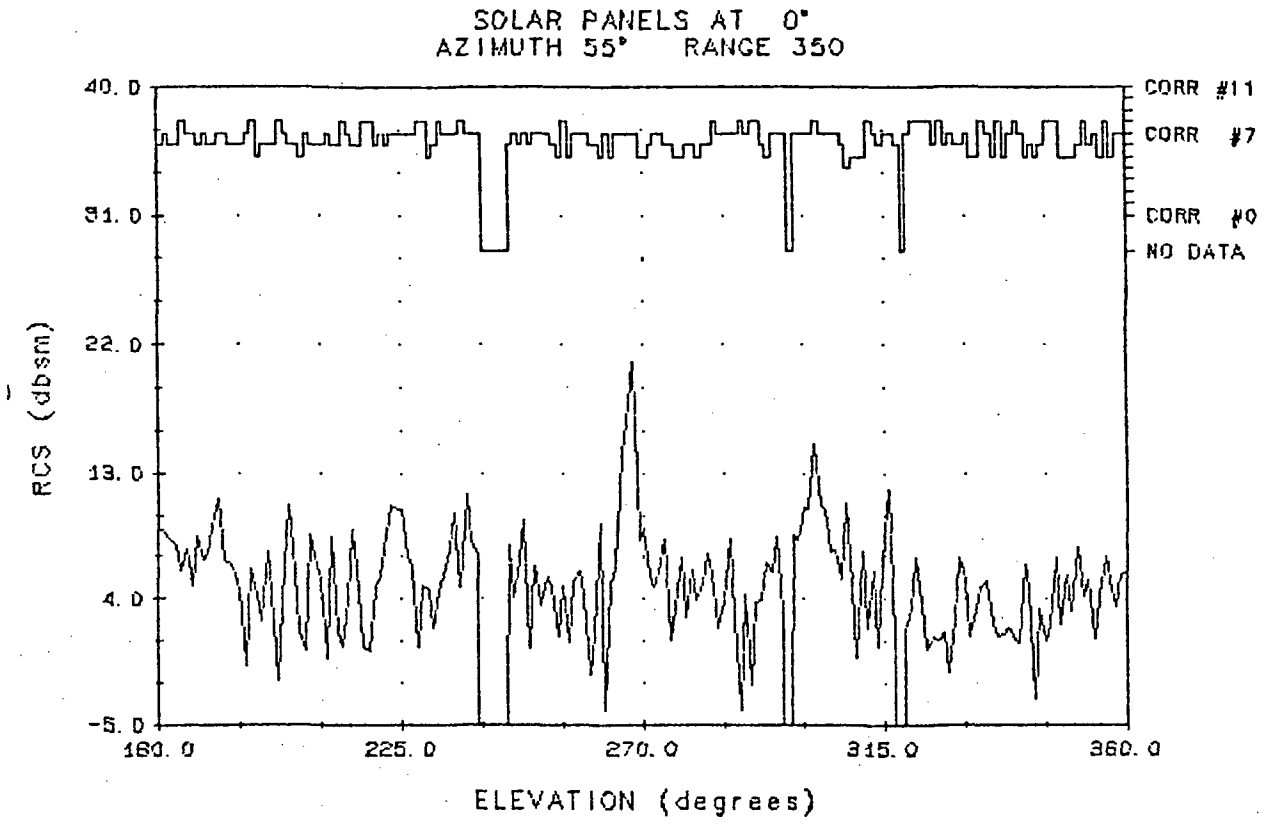

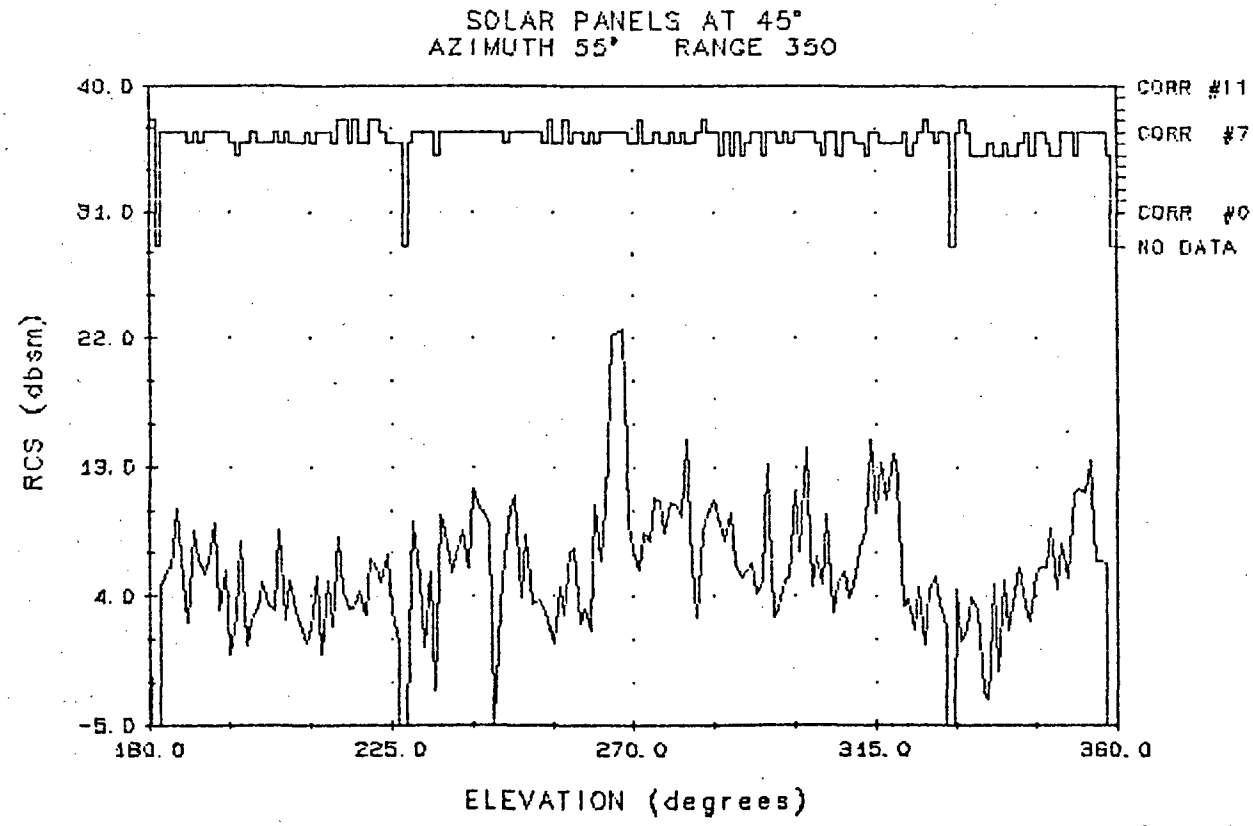

FIGURE 7-20. HST MODEL RCS

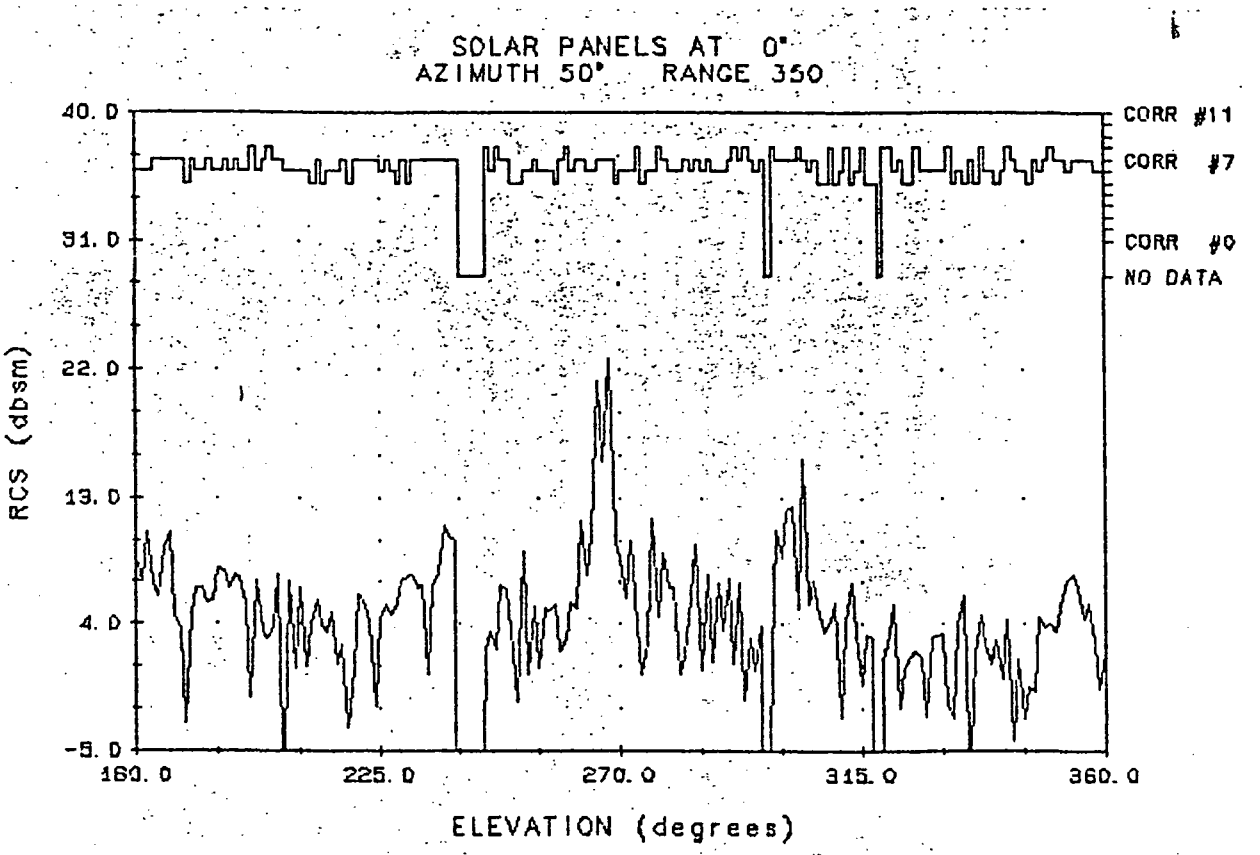

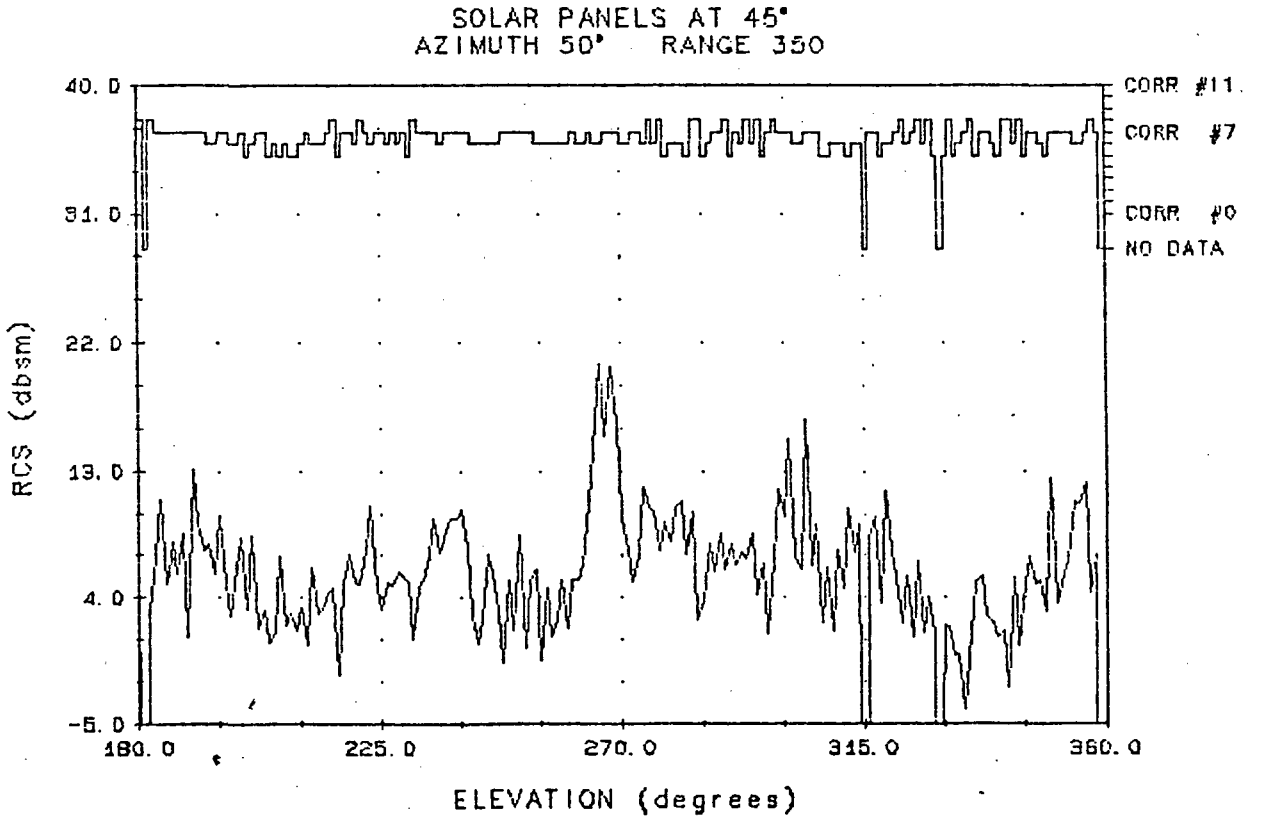

FIGURE 7-21. HST MODEL RCS

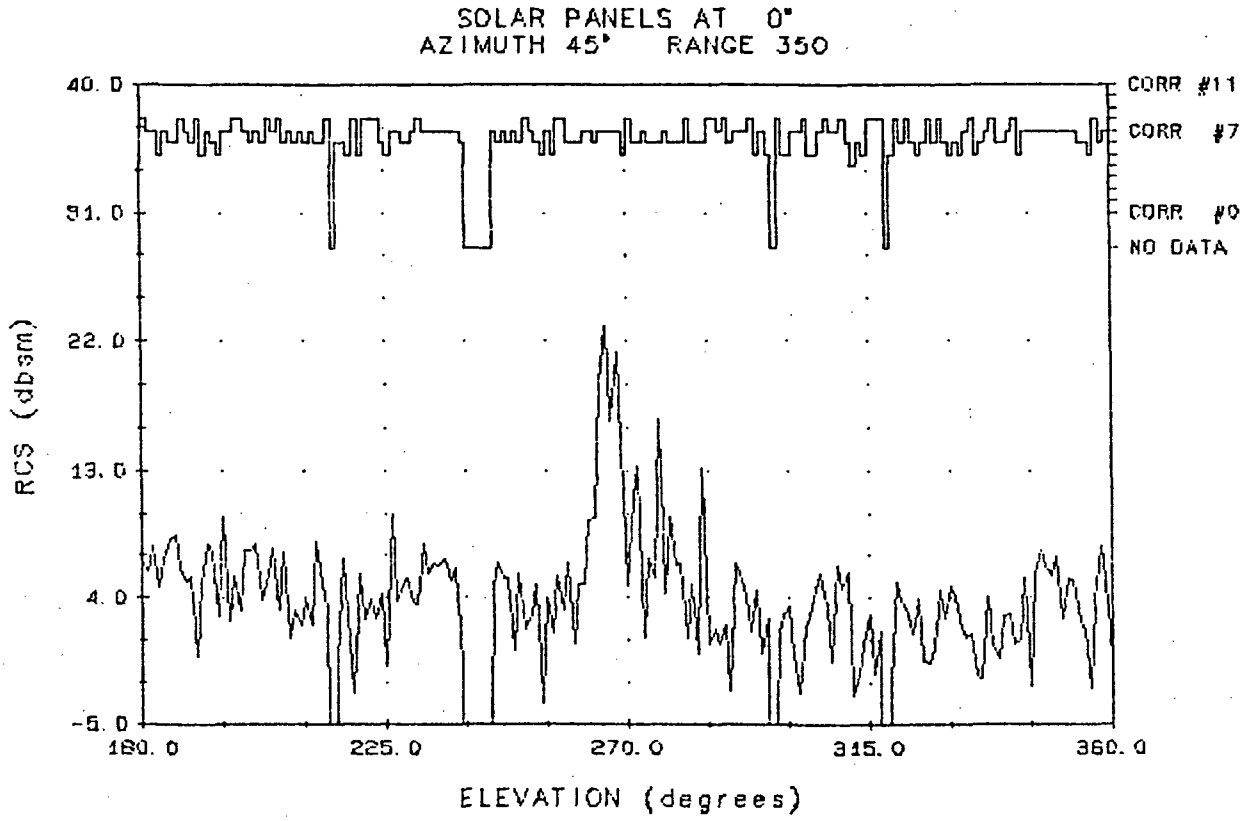

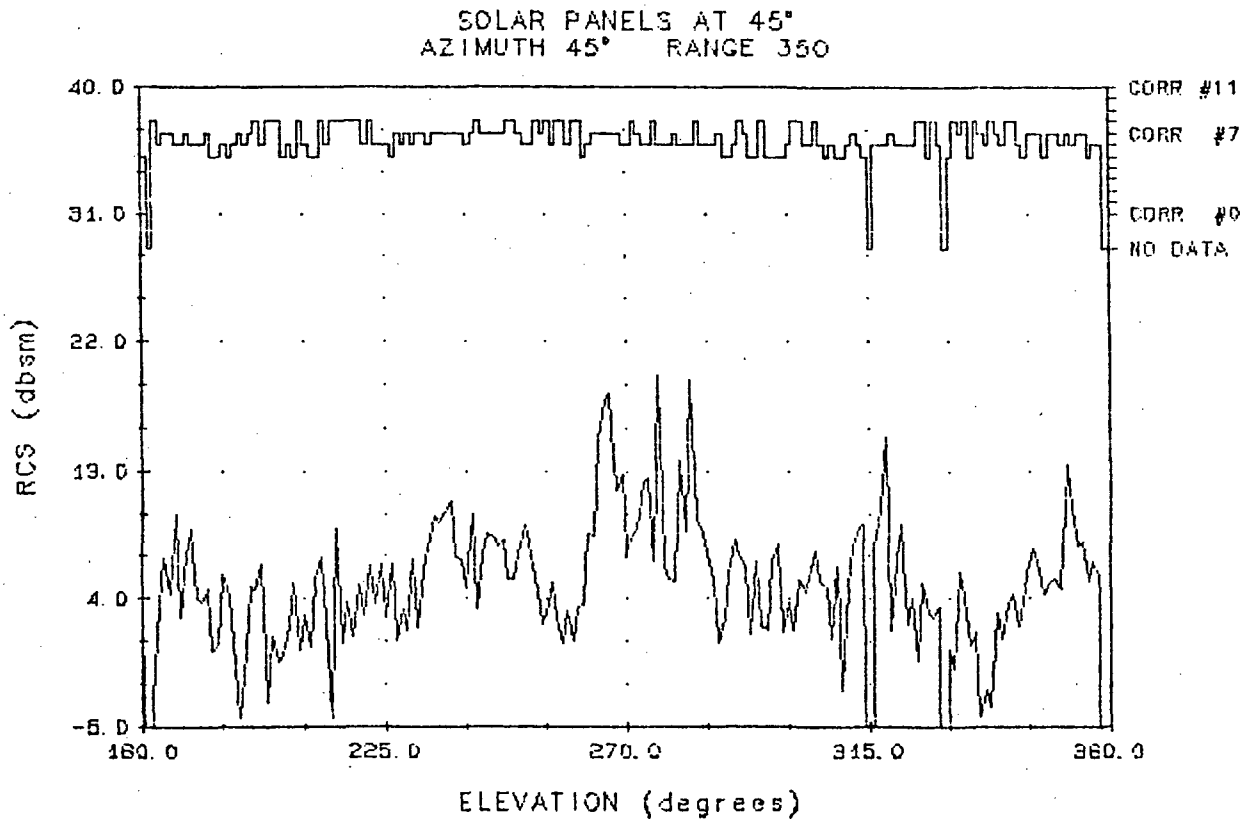

FIGURE 7-22. HST MODEL RCS

ORIGINAL PAGE IS
OF POOR QUALITY

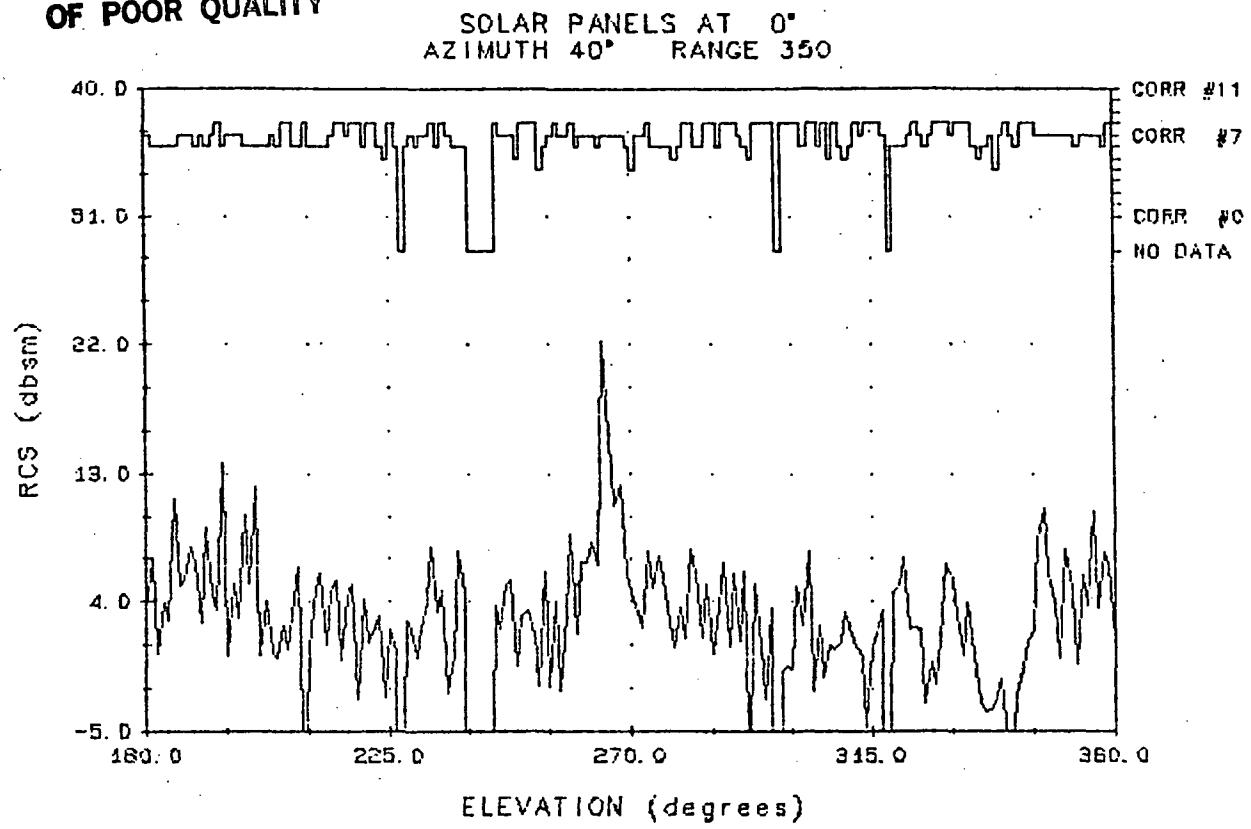

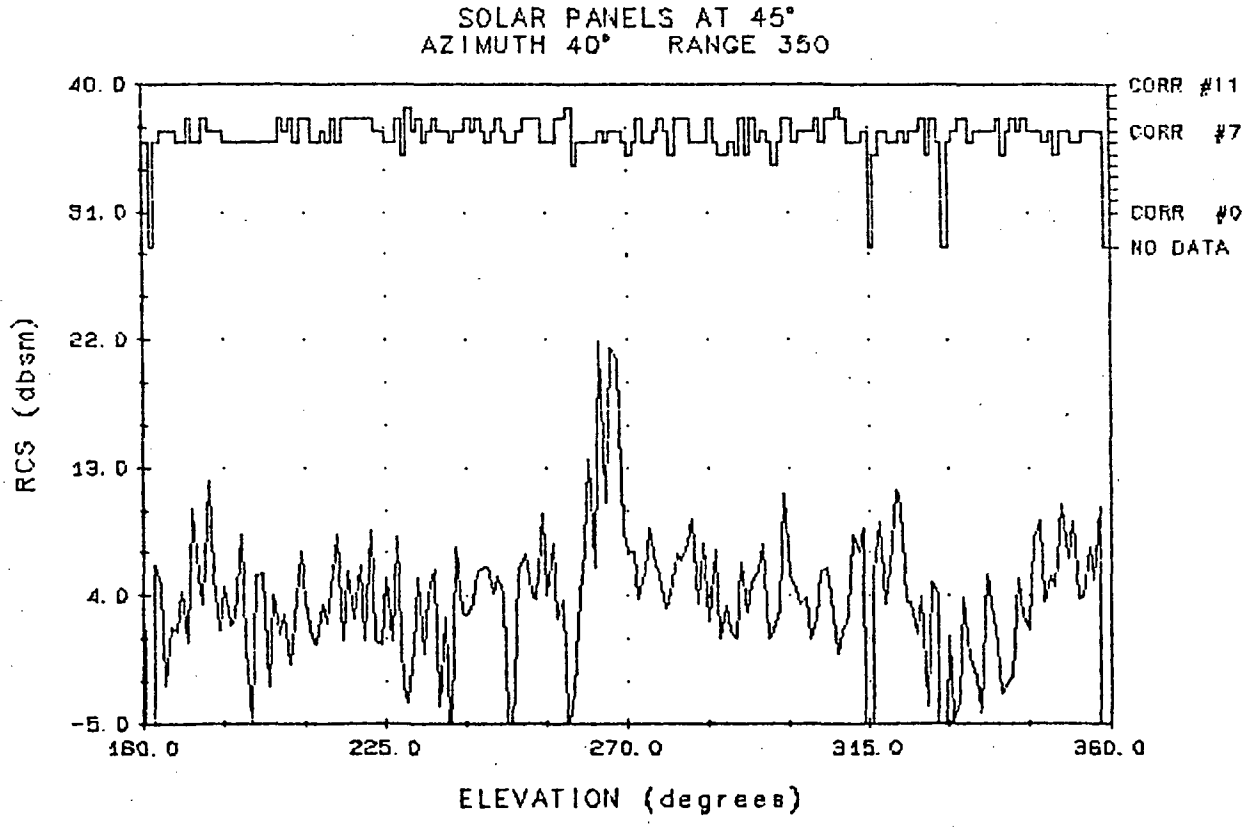

FIGURE 7-23. HST MODEL RCS

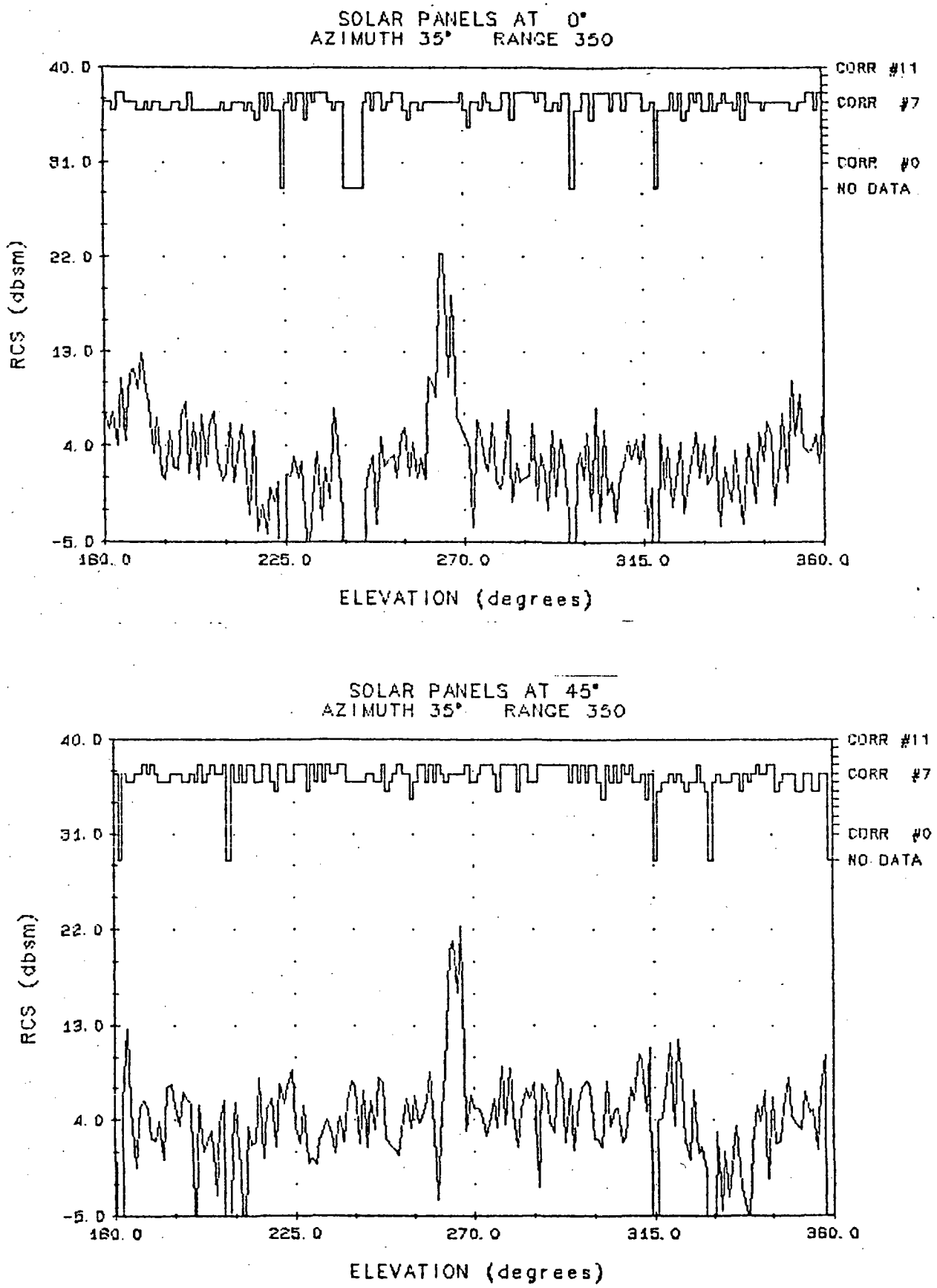

FIGURE 7-24. HST MODEL RCS

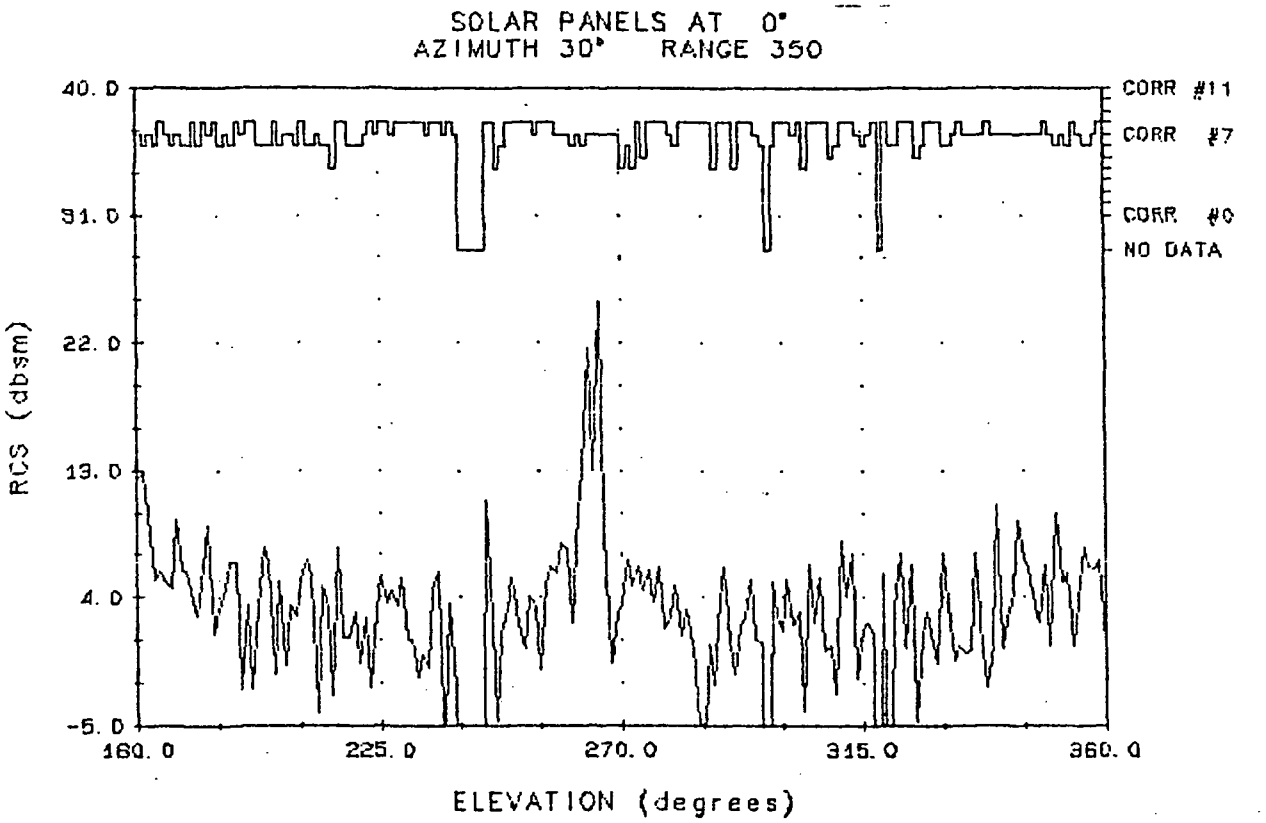

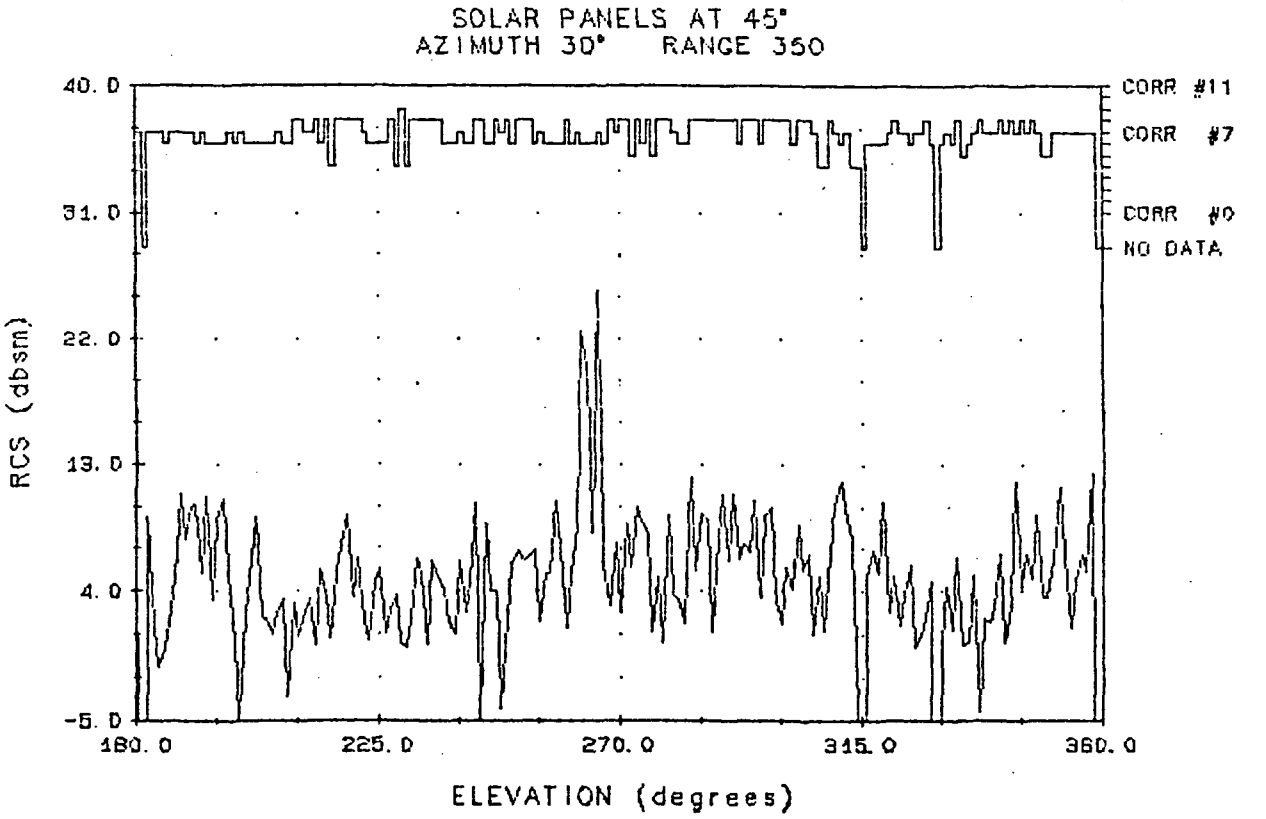

FIGURE 7-25. HST MODEL RCS

ORIGINAL PAGE IS
OF POOR QUALITY

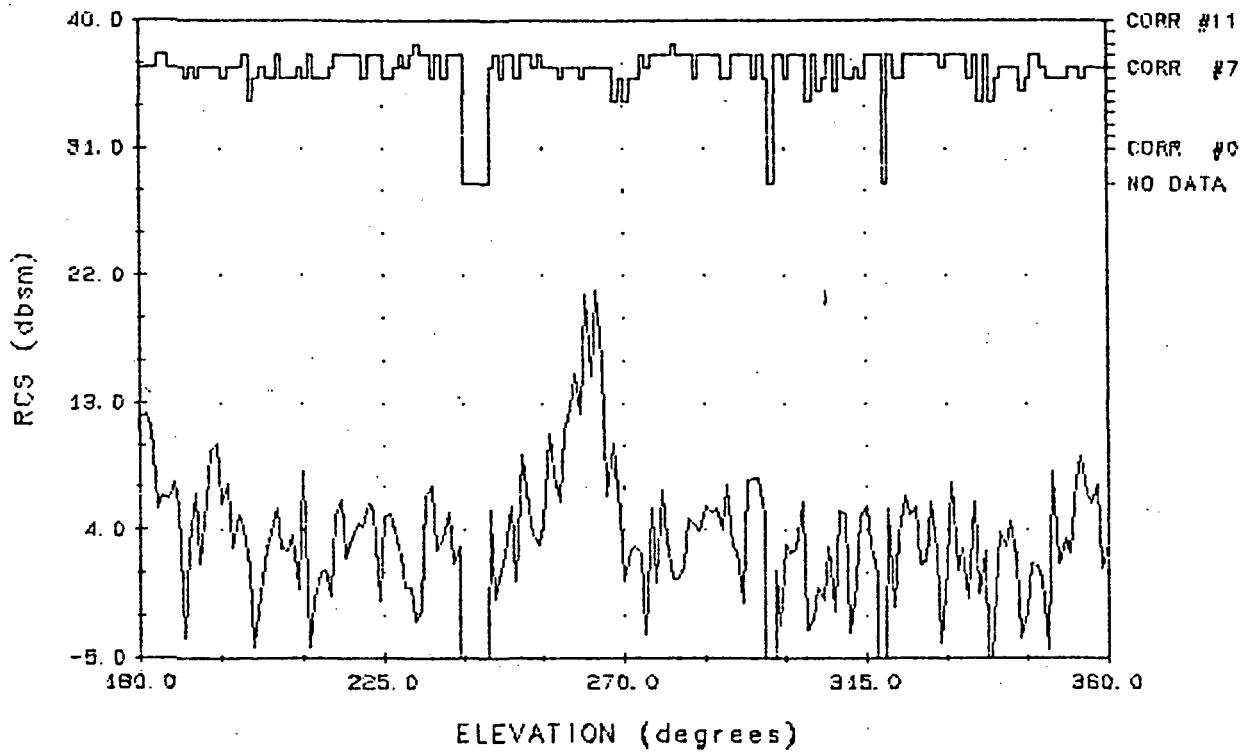

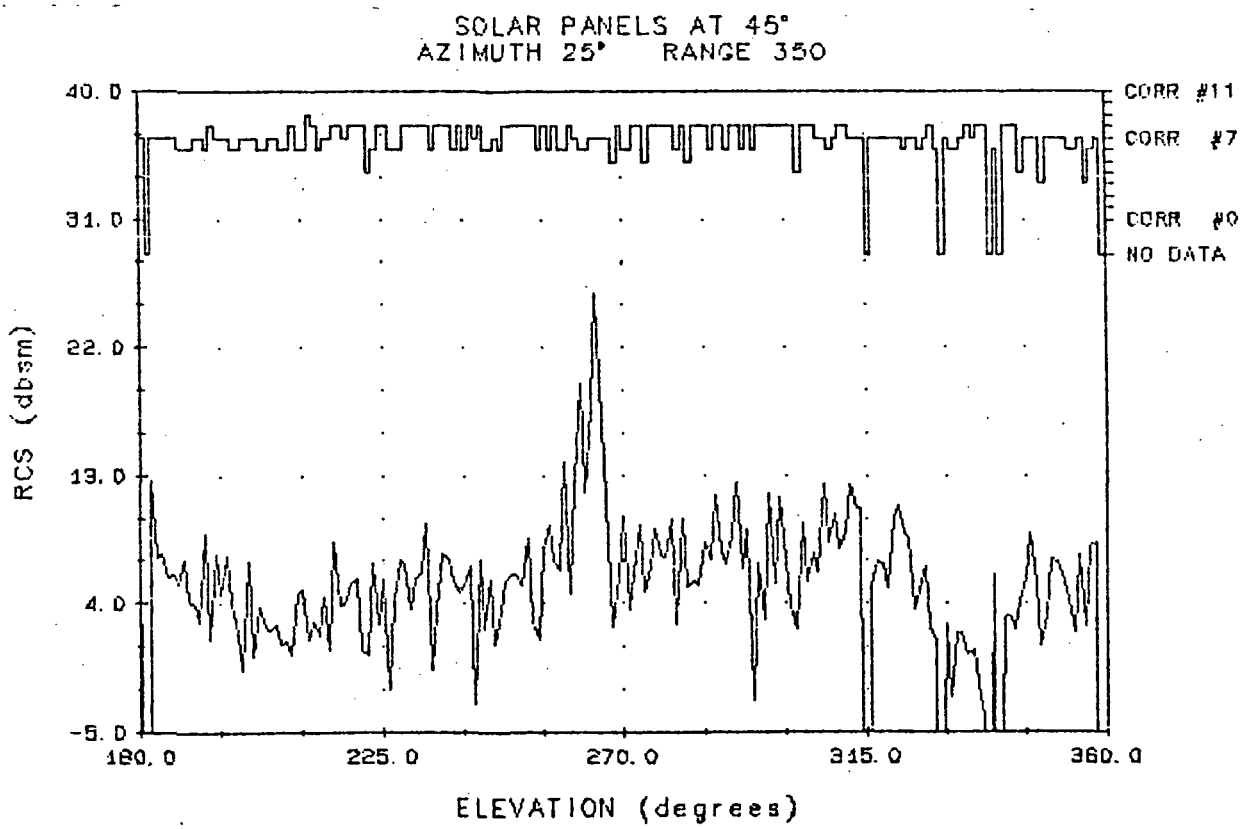

FIGURE 7-26. HST MODEL RCS

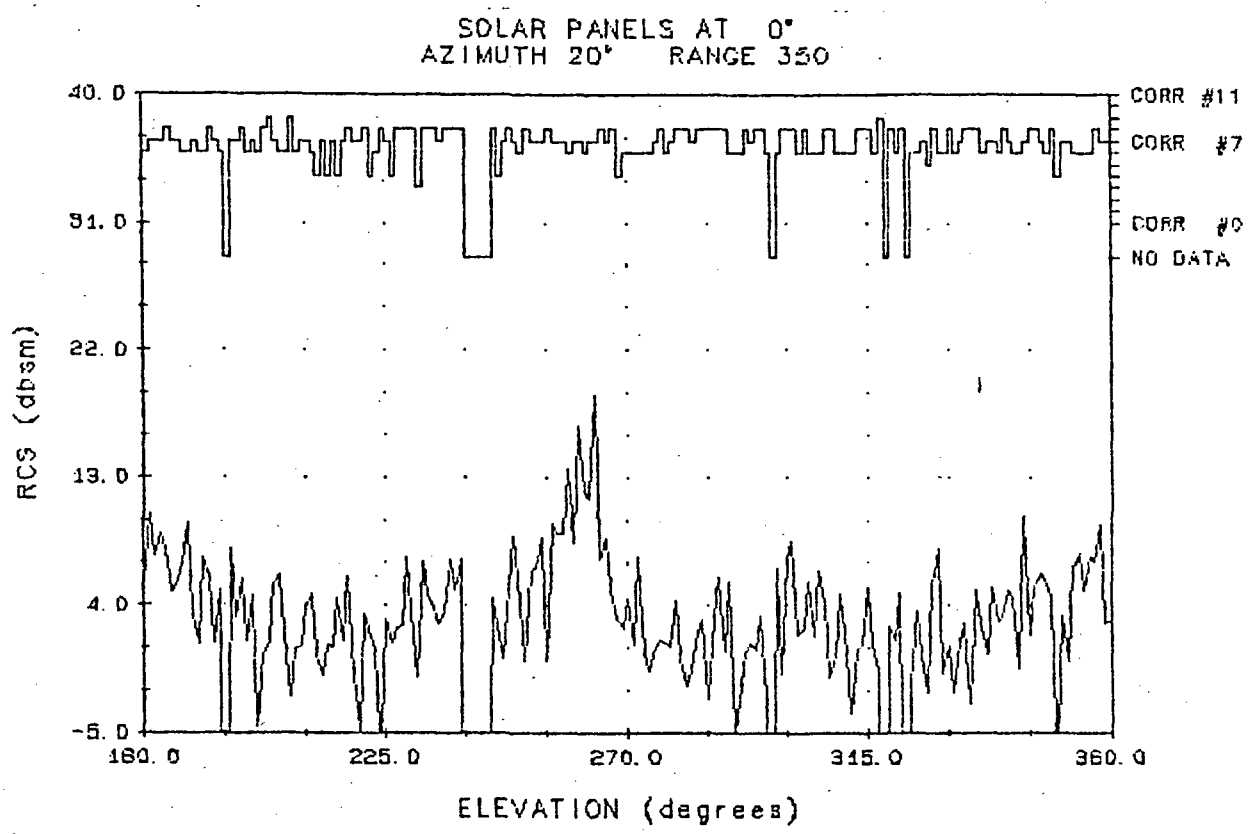

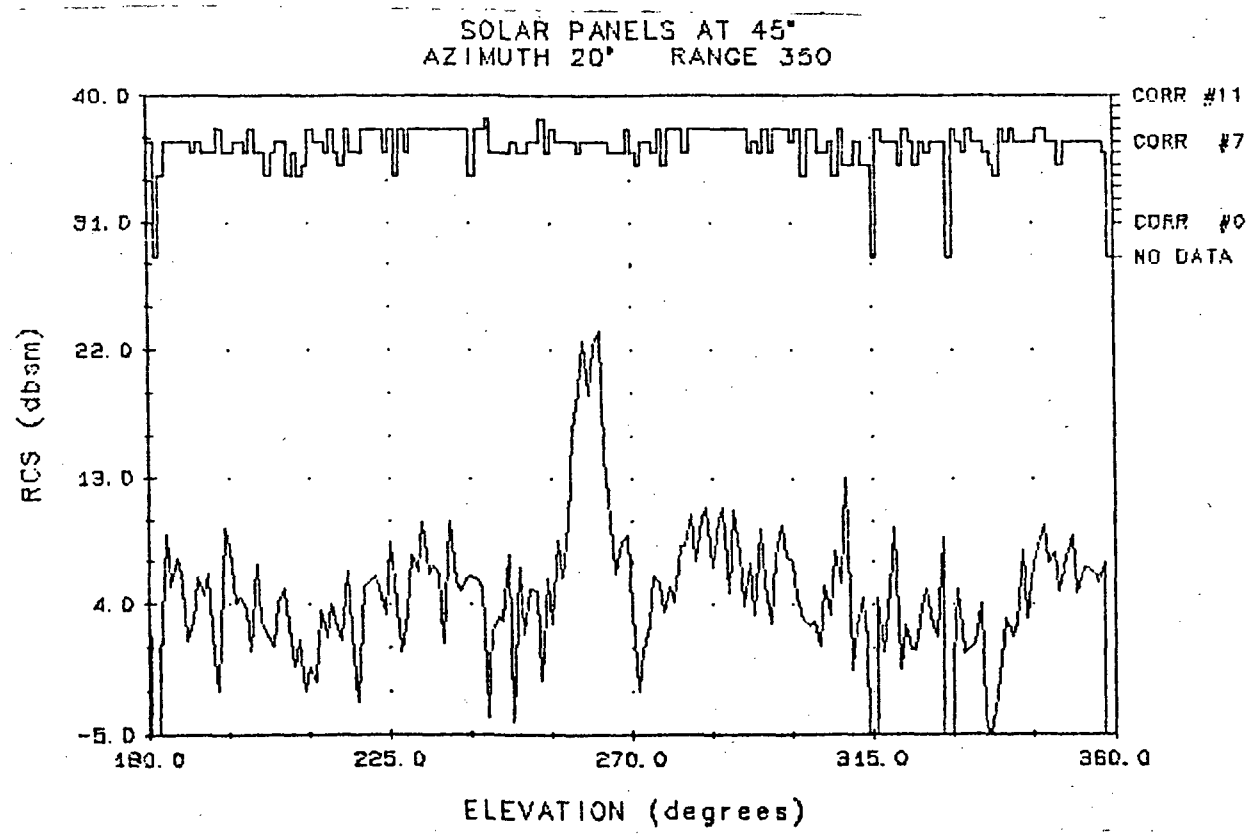

FIGURE 7-27. HST MODEL RCS

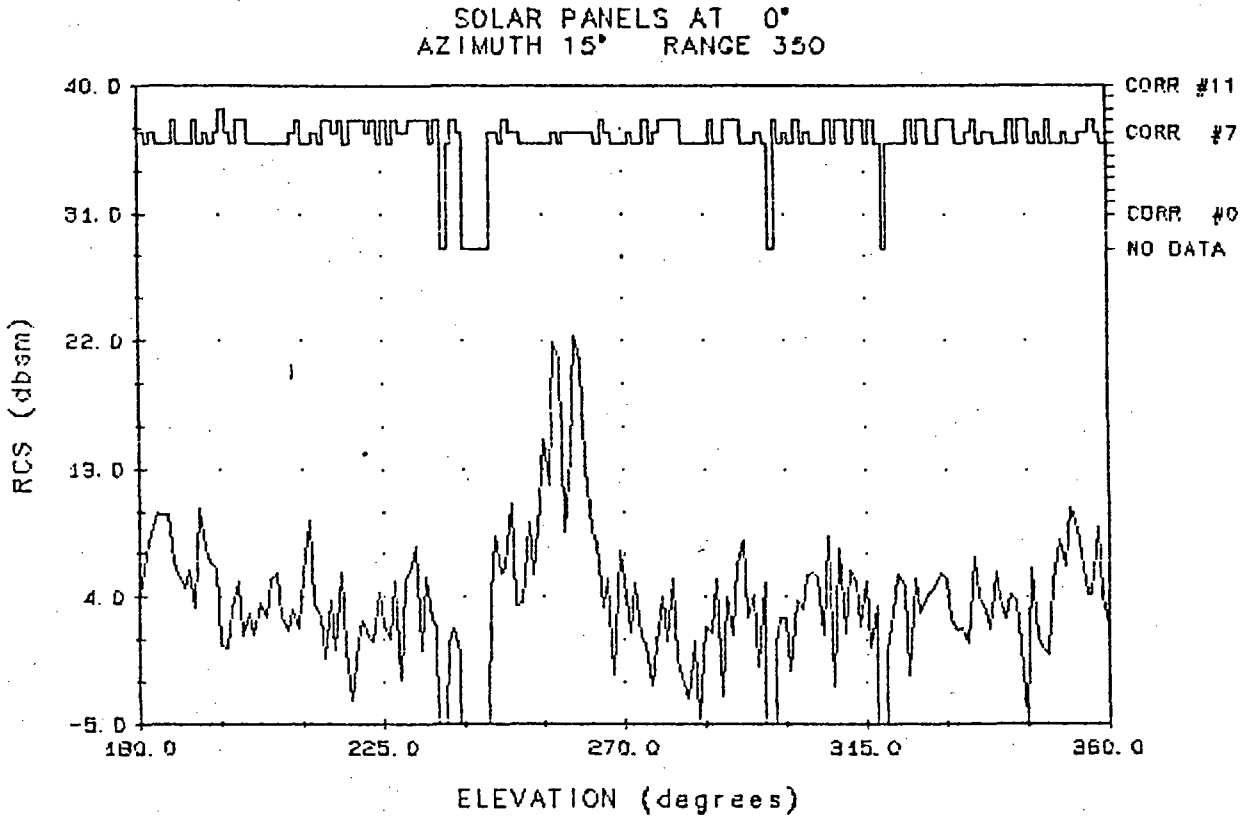

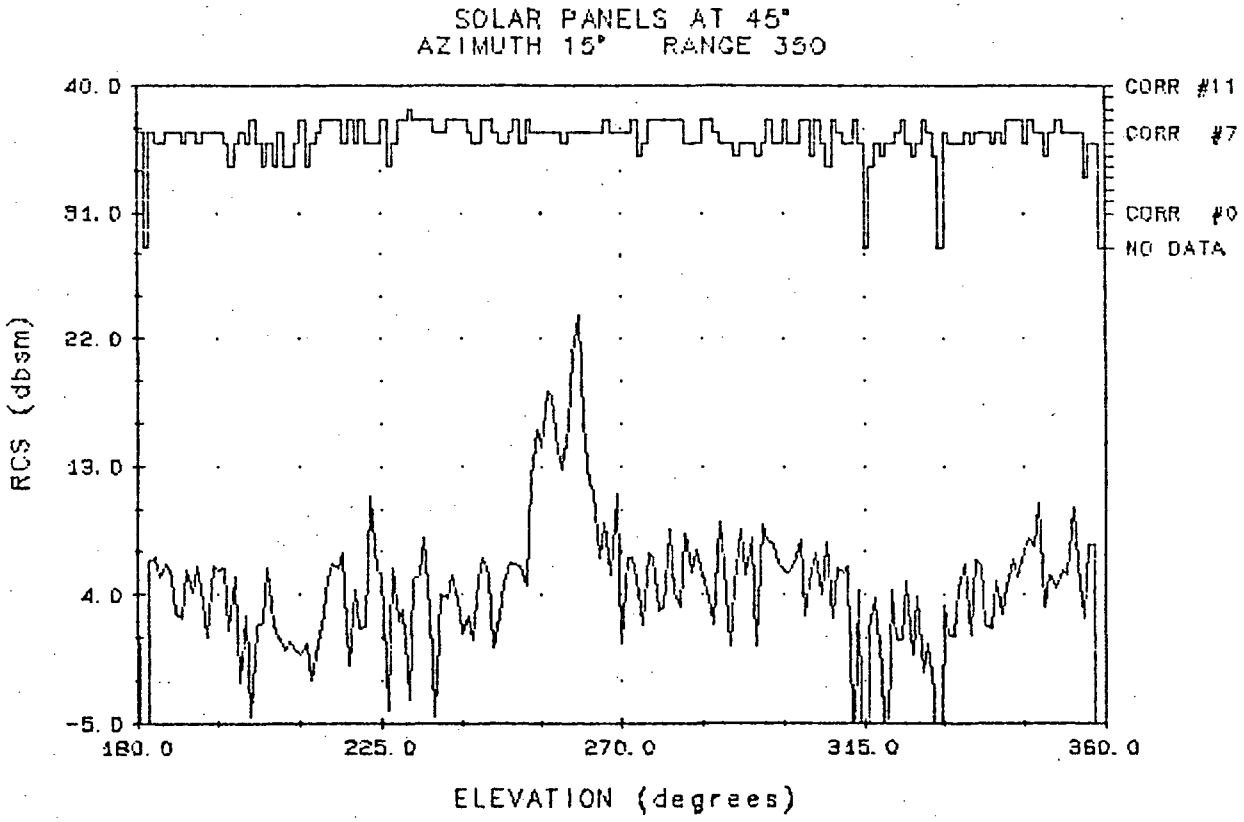

FIGURE 7-28. HST MODEL RCS

ORIGINAL PAGE IS
OF POOR QUALITY

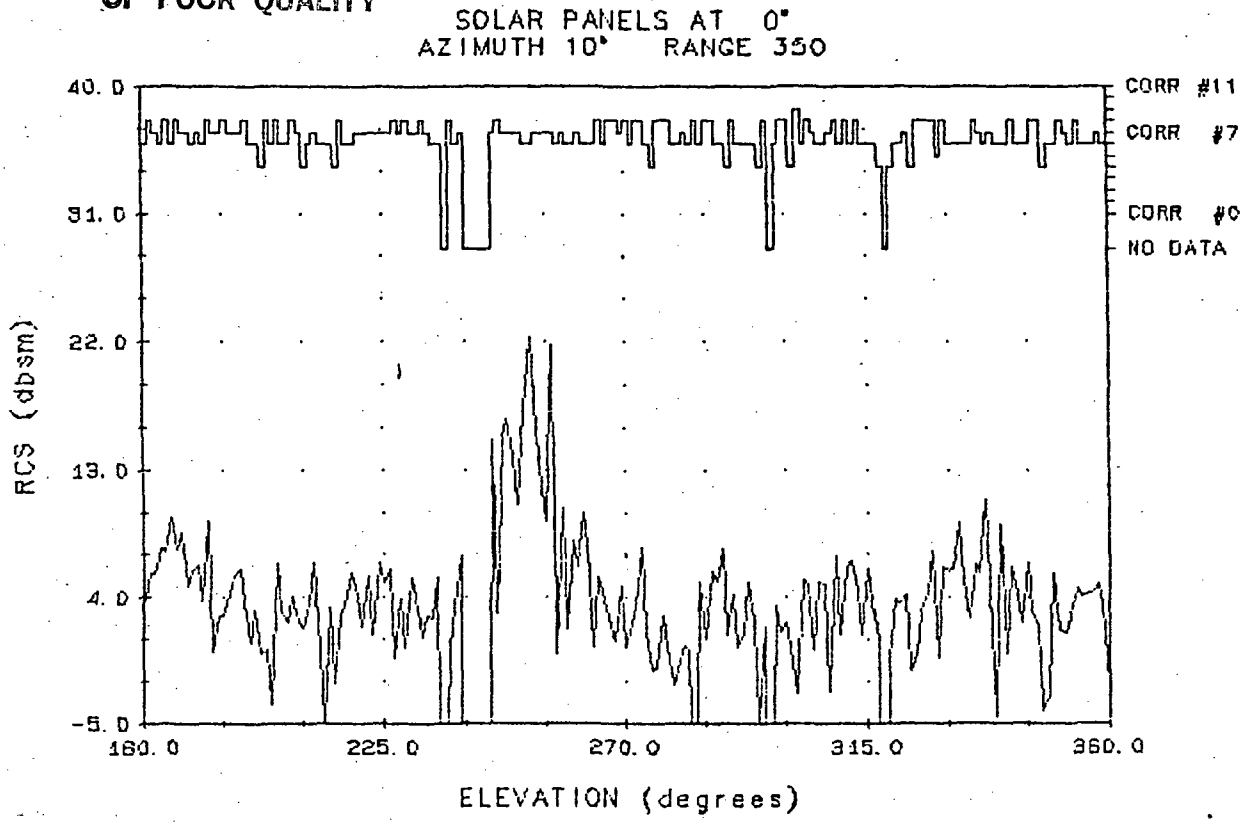

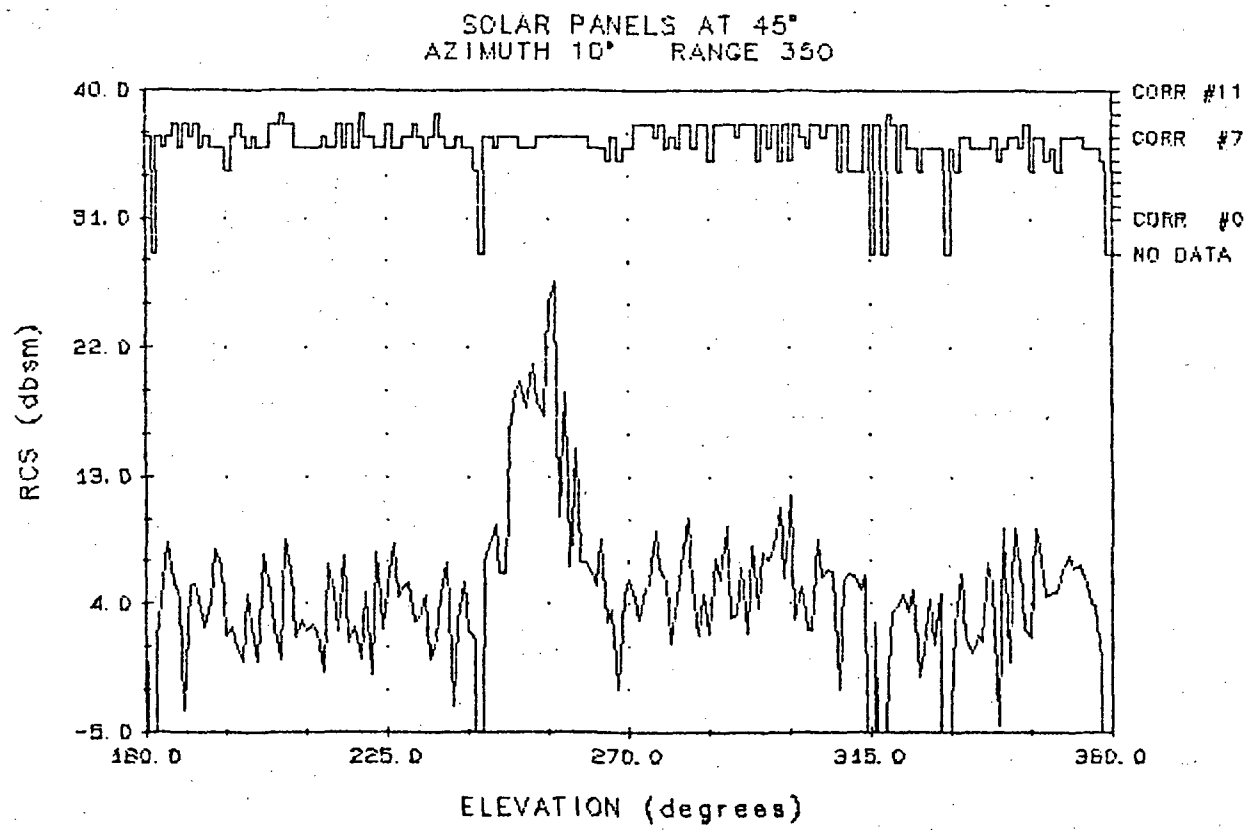

FIGURE 7-29. HST MODEL RCS

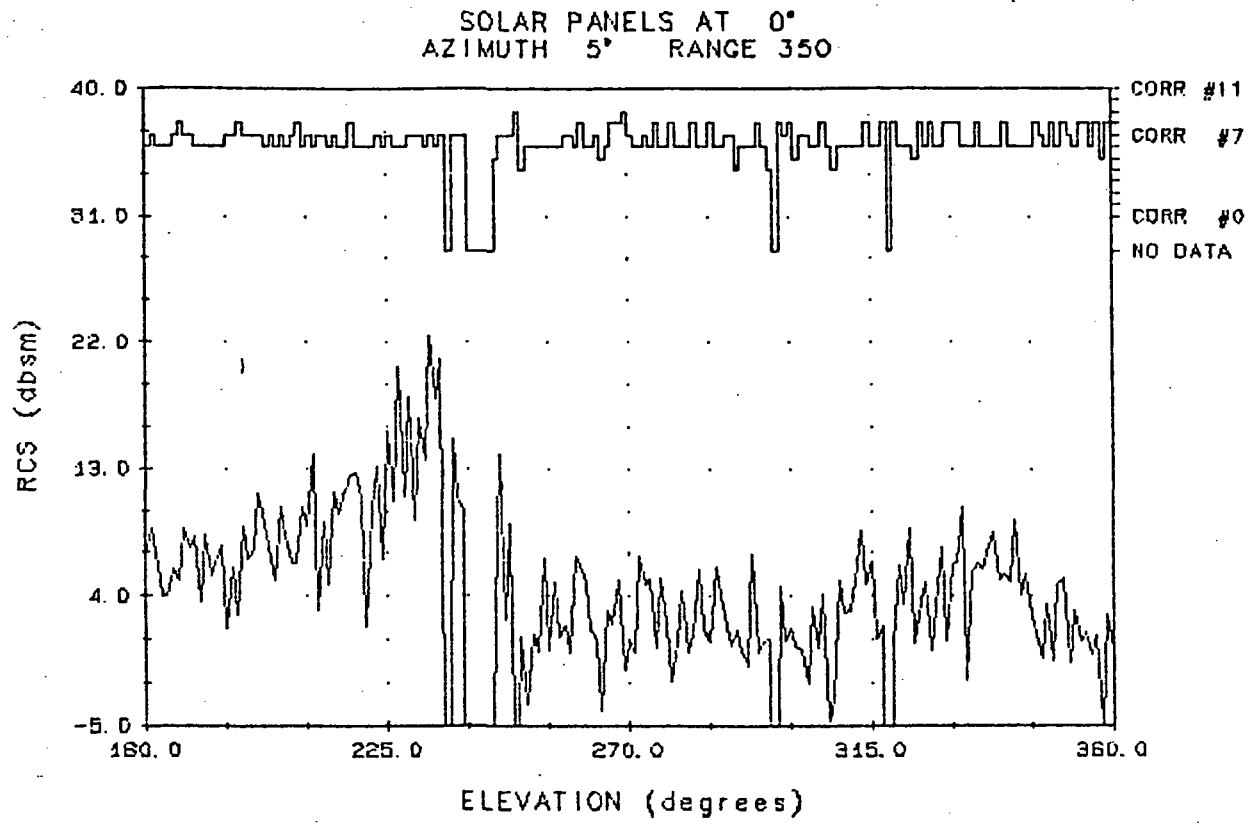

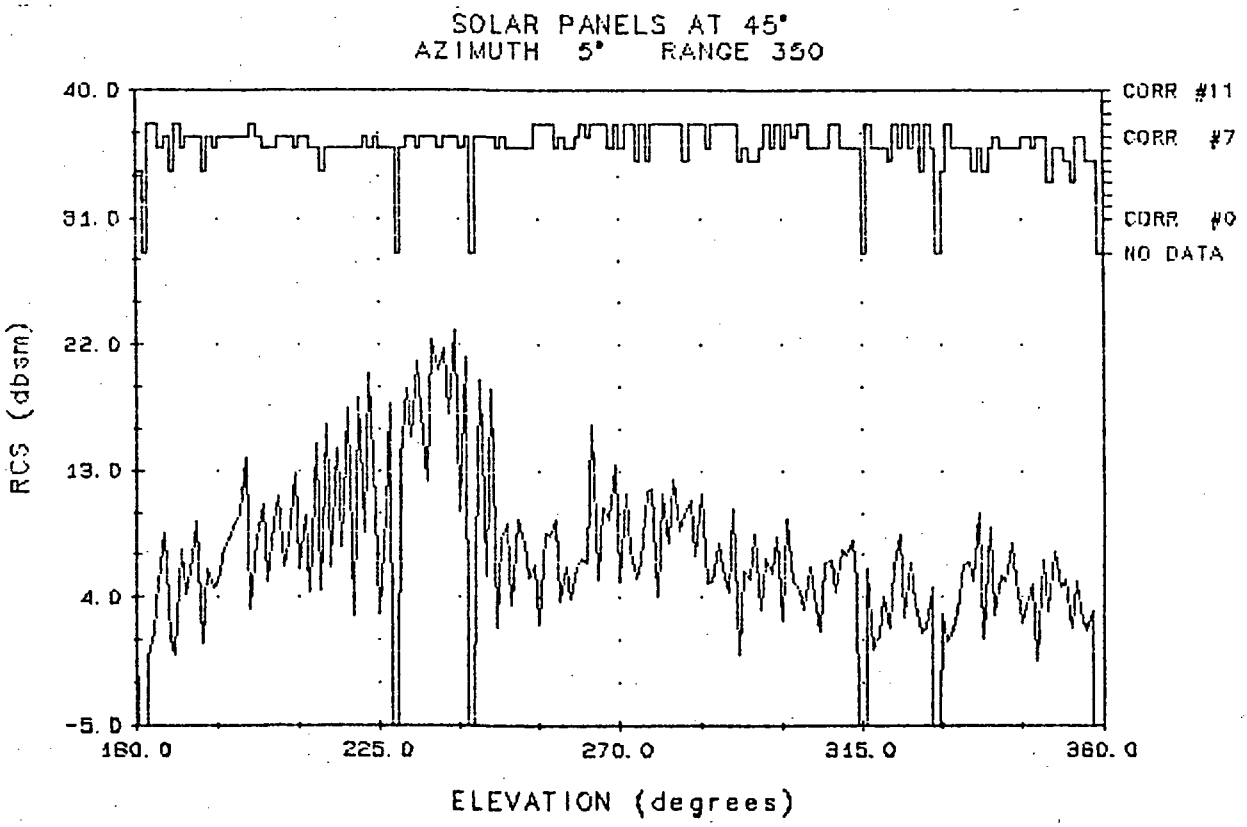

FIGURE 7-30. HST MODEL RCS

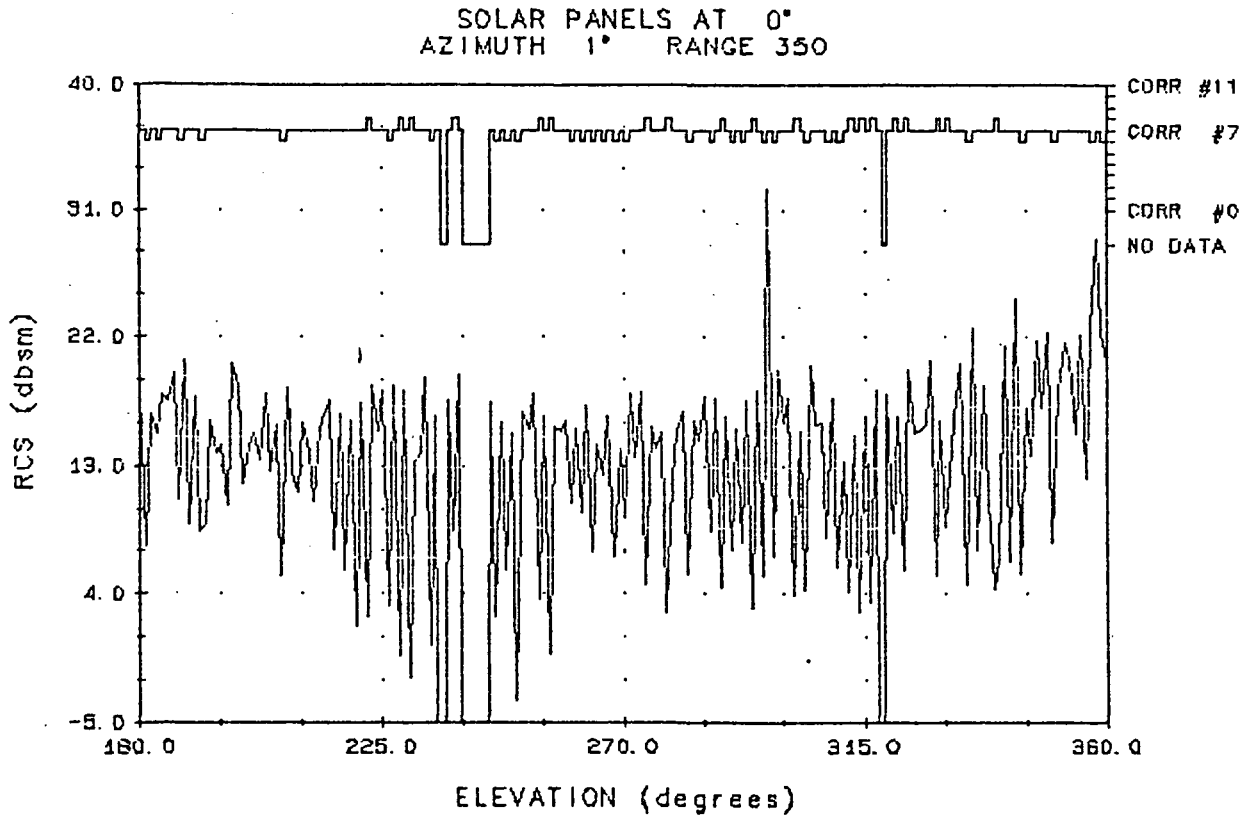

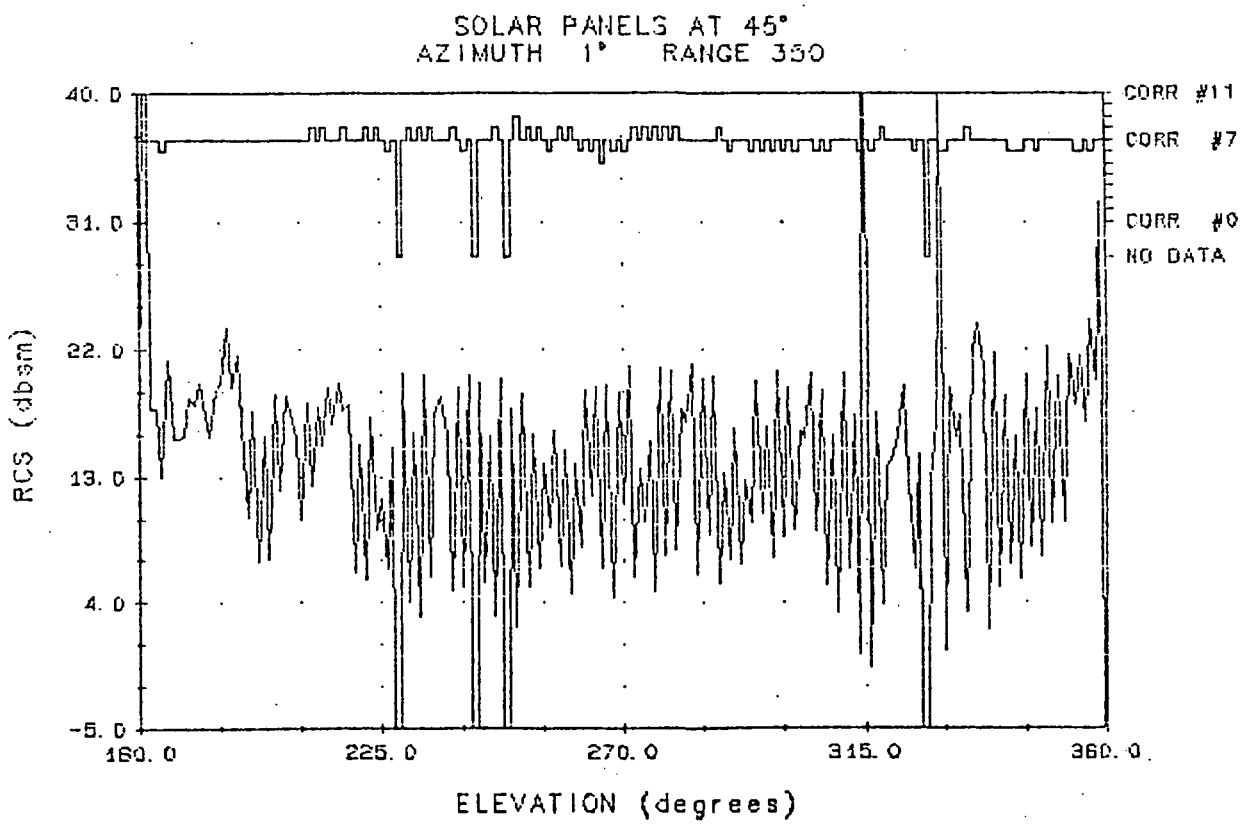

FIGURE 7-31. HST MODEL RCS

ORIGINAL PAGE IS
OF POOR QUALITY

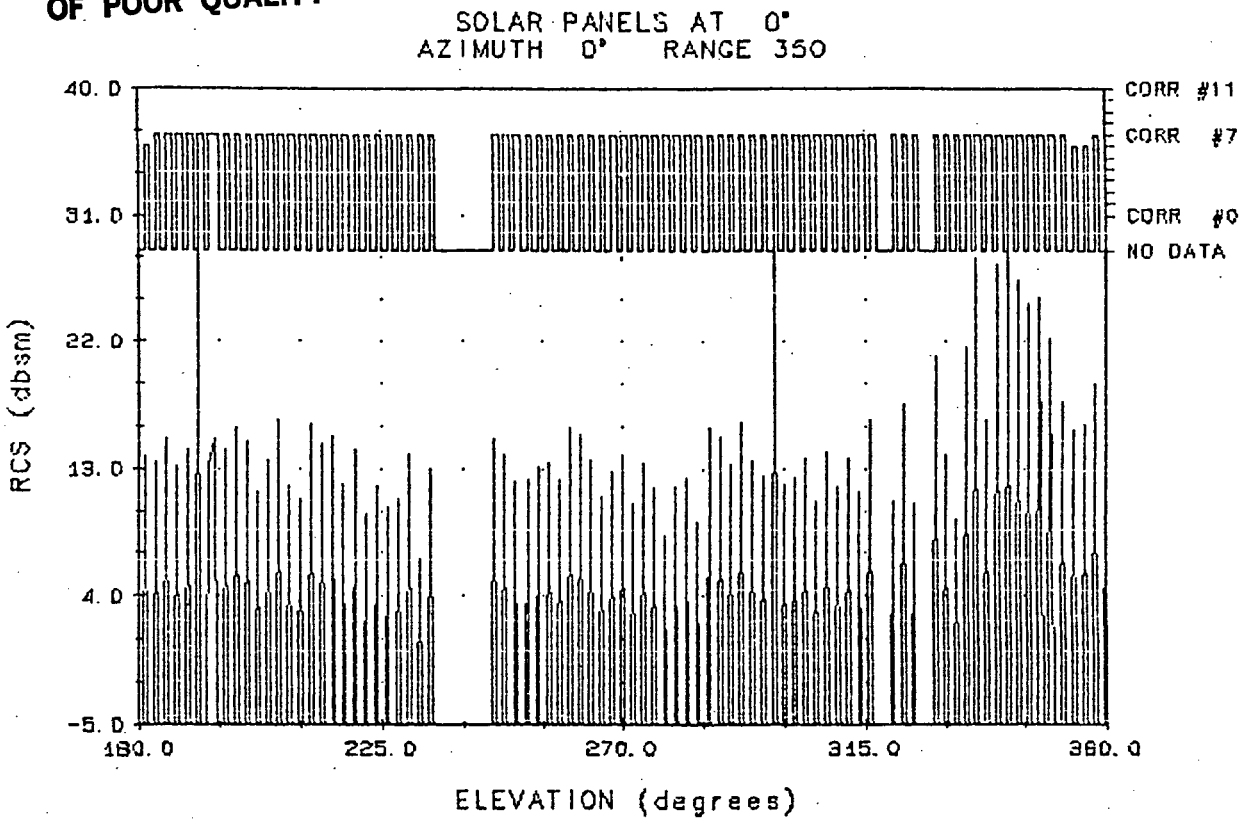

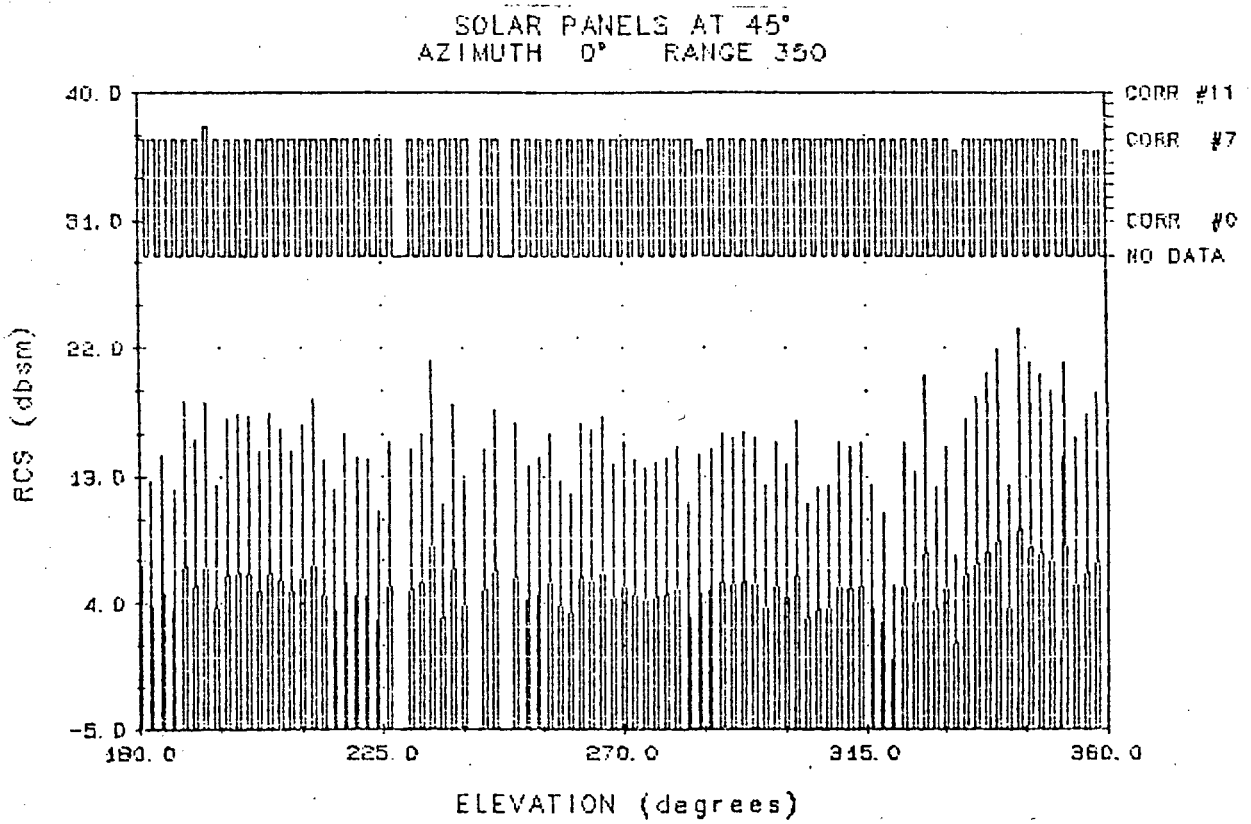

FIGURE 7-32. HST MODEL RCS

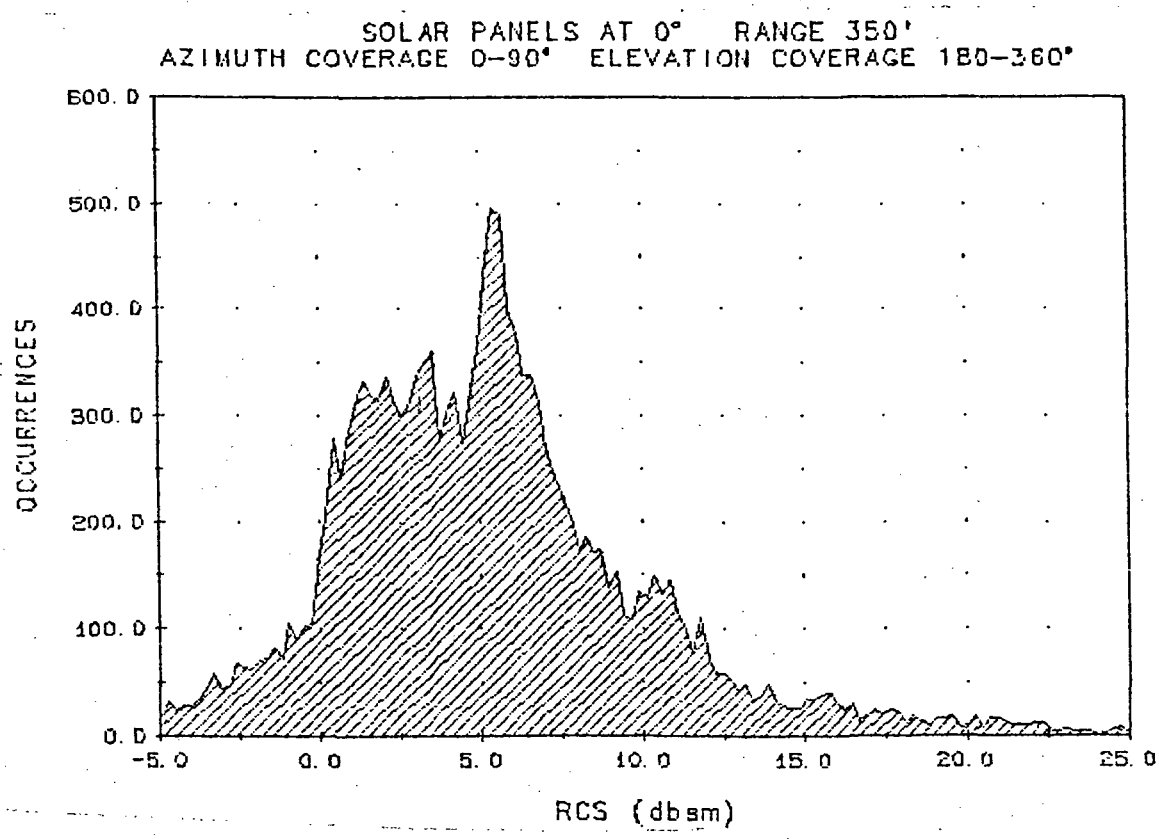

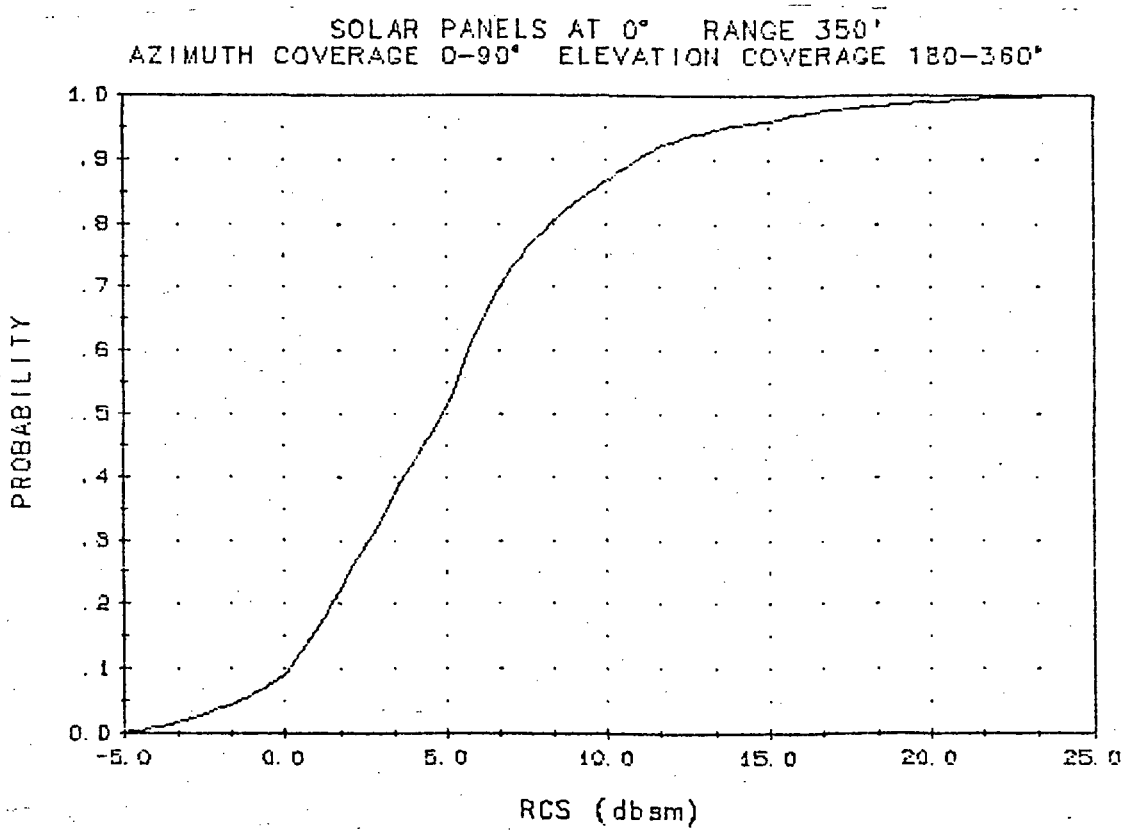

FIGURE 7-33. RCS DISTRIBUTION, 350', 0° SOLAR PANELS

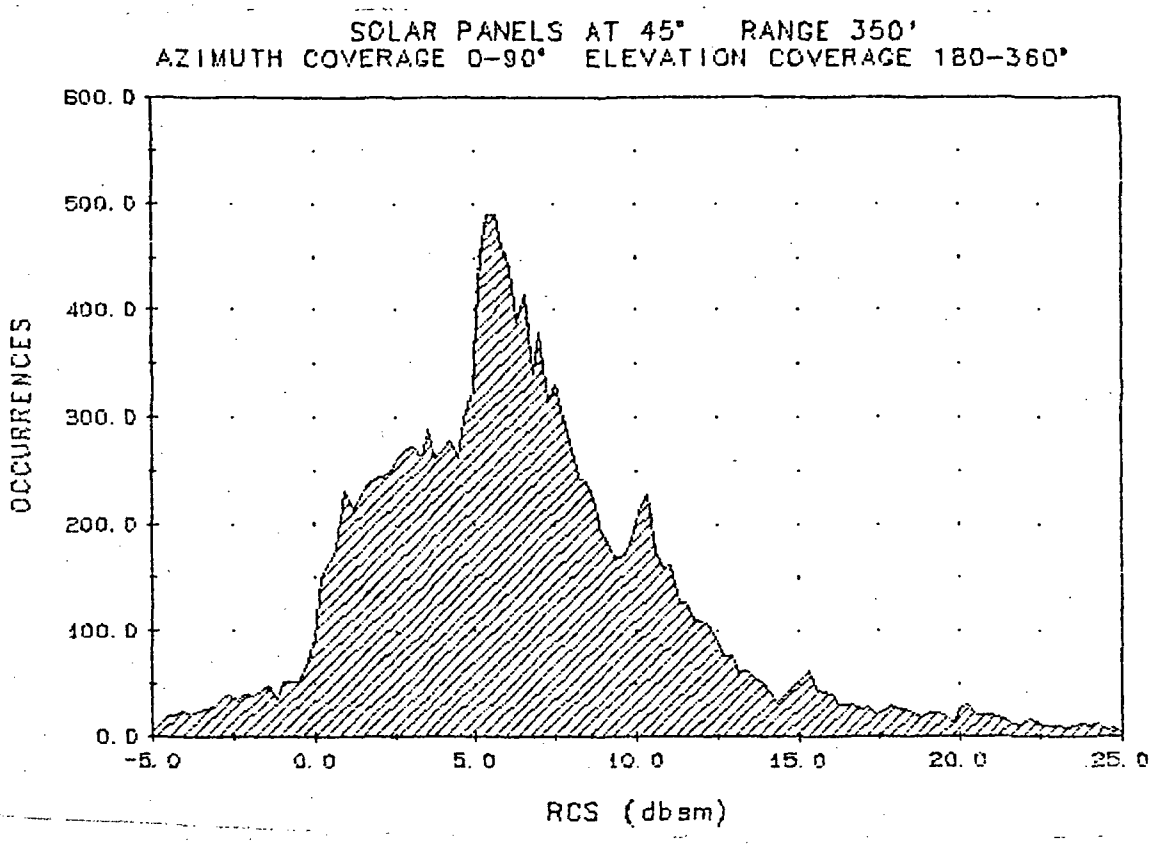

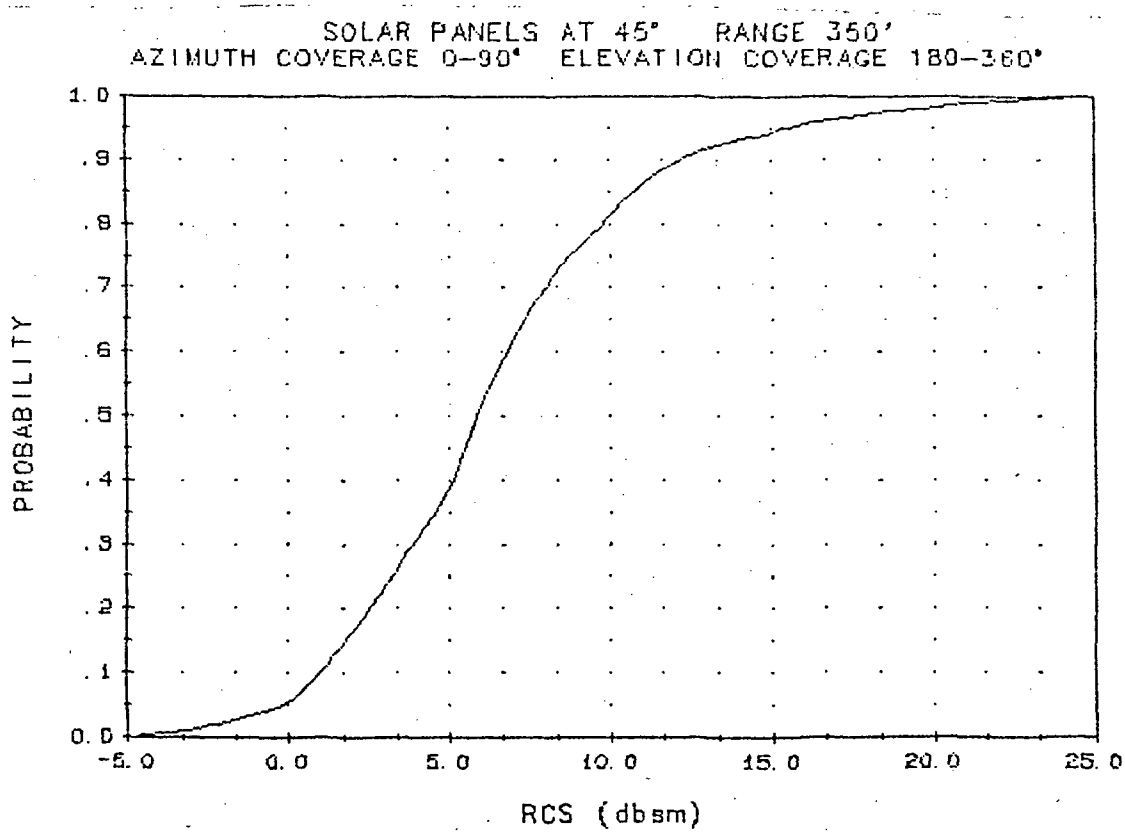

FIGURE 7-34. RCS DISTRIBUTION, 350', 45° SOLAR PANEL

7.3 RANGE MEASUREMENT

The range word, which is the reference and vernier delay setting recorded on tape, is extracted and plotted. The mean and standard deviation is computed for each test.

7.3.1 Reference Point

Obviously the indicated range will vary with the tracking point on the model. The tracking point is influenced by the aspect, hence it is difficult to predict the tracking point beforehand, except for simple situations like the big end on boresite.

It is simplest to define the model support axle as the range measurement reference. All radar range measurements can then be visualized with respect to the axle. This reference point range calculation was derived as a consequence of the range calibration discussed in Section 5.2, Range Accuracy Calibration. The range to the axle midway between the pylons is listed in Table 7-1 for the various ranges.

TABLE 7-1. REFERENCE RANGE

SITE	RANGE
25′	29.2′
50′	52.3′
100′	101.1′
200′	200.6′
350′	350.3′

The pertinent range is included on each plot as the reference line.

7.3.2 Range Correction

The range accuracy calibration, discussed in Section 5.2, resulted in an average error of +.66 feet. The plots of radar range do not incorporate any correction; the correction is to be applied by the reader. This correction may be required to firmly establish the result.

A fine example of a radar range test result is run 173, shown in Figure 7-35. The model was positioned to put the big end on boresite.

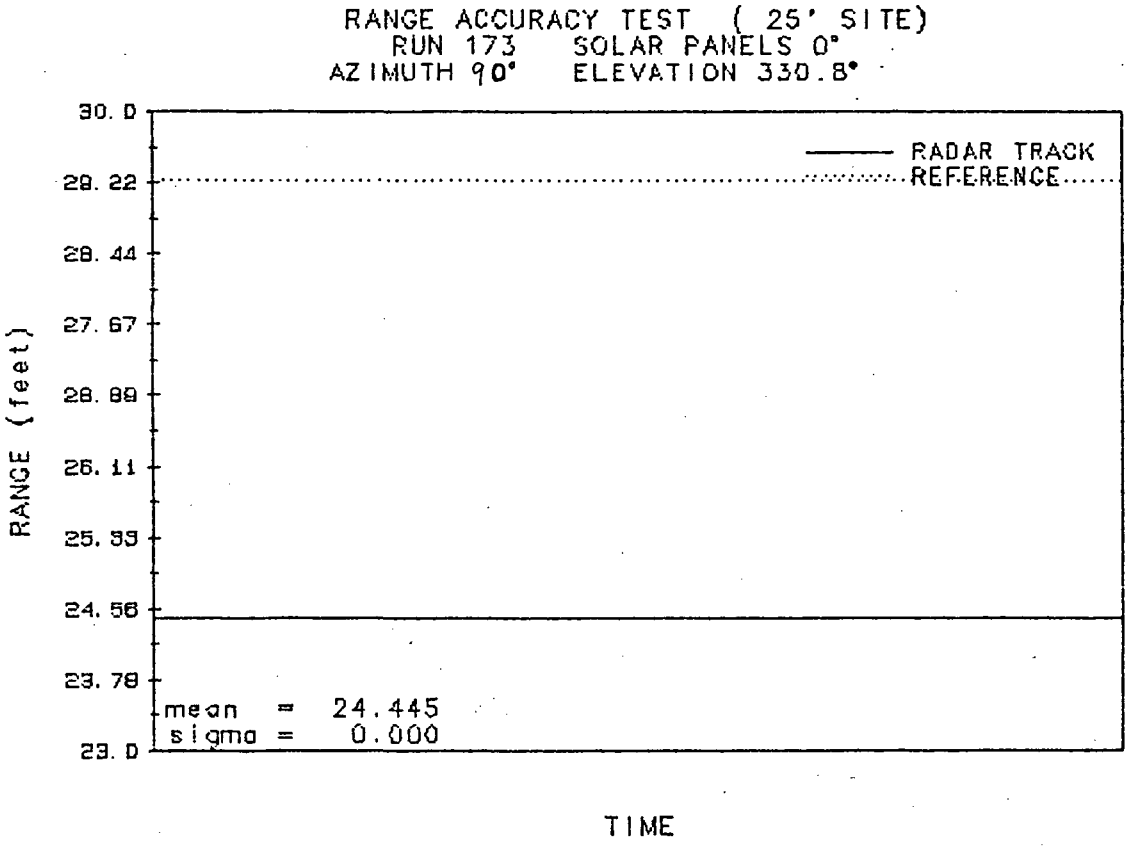

FIGURE 7-35. RUN 173 RANGE MEASUREMENT

The range measured should be the reference range minus 5.625′ (67.5", the dimension from the axle to the big end surface), or 29.2′ -5.625′ = 23.575′. The radar measurement of 24.445′ minus the .66′ factor gives a resulting measurement of 23.785′, which is within 1 vernier step of the calculated range.

7.3.3 Apparent Quantization Level

Increased precision is obtained by quantizing the range error into smaller steps than the vernier step size. The recorded range word is also quantized to 1/2 the vernier step size. This is illustrated in Figure 7-36, test run 200.

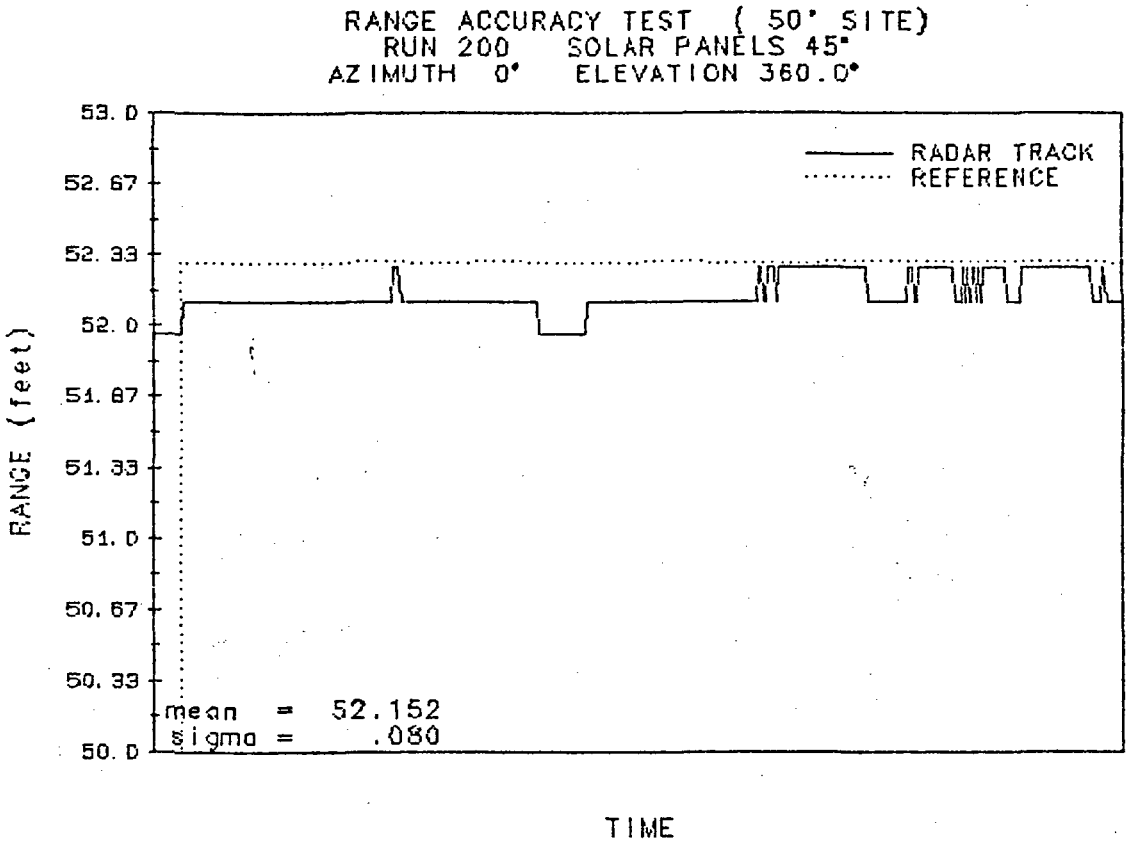

FIGURE 7-36. QUANTIZING EXAMPLE

The range measurement appears to vary between 51.98′ and 52.30′, with two distinct levels; the step size is .156′. The finer steps are due to the plotter and not the range word.

7.3.4 Measurement Results

All measurements taken at the five sites have the same general characteristics:

- Measurement to the big end on boresite yields a stable return with good match to predicted range.
  - Measurements at farther ranges include more competing scatterers in the return, hence are noisier than close-in ranges.
- Measurements with the model positioned to include two or more scatterers of the same approximate magnitude can result in a range measurement which hops from one scatterer to another.
  - The size of the range hop can be as large as 6′ or more
  - The frequency of the hops may vary from 1 per 15 second test run to 3-4 per second. The vibration frequency of the model, due to the wind environment, is the driving factor in the hop rate.

- Momentary loss-of-track, though very seldom, is indicated by large output excursions of 30´ or more.

- Best performance is obtained when a single surface is presented to the radar.

  .. The big end

  .. The side of the model with the longitudinal axis orthogonal to the radar.

The 200´ site results are representative of the radar performance, because the entire model is illuminated. The range measurements for both solar panel positions are included as Figure 7-37 to Figure 7-60. The measurements may differ because of differing wind conditions as well as the change in the solar panels.

All test runs have been processed and the range mean and deviation are tabulated in Table 7-2. The largest possible range hop from the reference is 90", the distance from the axle to the small end, so only indicated ranges with less than a 10´ difference from the reference range are included in the calculation of mean and deviation.

7.4 TRACKING ACCURACY TESTS

Four tests were successfully conducted to measure the range and rate tracking accuracy of the radar. The tests were conducted over 50 foot intervals from 350´ to 130´ ranges to the model. The tests were conducted at 1 to 5 feet per second rates and required roughly one minute to perform.

Because the previous rate test, wherein the video tape was made, established that solid track of the model could be maintained without changing the model aspect, its position remained the same for all tests. The position AZ = 90^{o} and EL = 355^{o} put the big end within 4.4^{o} of boresite for all ranges used.

All tests proceeded smoothly; each test was terminated to limit the data record to one minute.

7.4.1 Tracking Plots (Figure 7-61 to 7-64)

The plots show the difference between the laser and the radar range and rate measurements. The range measurements differ in magnitude because the reference point for each differs: the laser reference is the positioner center, while the radar measurement point is somewhere on the big end. Each plot has been adjusted for the time delay generated in the laser circuitry before its range measurement result is transmitted over the RS 232 bus to the instrumentation computer. The amount of delay was selected for "best fit" in the rate comparisons.

All plots show the test sequence of: start recorder, wait 5 seconds until the record mode is activated, then start van movement to achieve 1´/second rate. The plot for run 302 show a radar tracking point shift, probably due to a "lurch" in the van orientation which changed the radar aimpoint enough to cause track of something closer to the positioner center. The overall test results are tabulated in Table 7-3 on page 7-72.

TABLE 7-2. HST MODEL RANGE MEASUREMENTS, RUNS 31-300

SITE	SOLAR PANEL	RUN NO.	AZ POS.	EL POS.	R_{MEAN}	σ_R
350	0	31	0.0	360.0	349.78	.342
350	0	32	30.0	360.0	346.41	.371
350	0	33	60.0	360.0	346.95	.068
350	0	34	90.0	360.0	345.04	.349
350	0	35	0.0	355.0	348.57	.098
350	0	36	30.0	355.0	346.12	.080
350	0	37	60.0	355.0	348.64	1.007
350	0	38	90.0	355.0	345.69	.312
350	0	39	0.0	330.0	349.93	.588
350	0	40	30.0	330.0	346.52	.163
350	0	41	60.0	330.0	346.51	.127
350	0	42	90.0	330.0	346.58	1.254
350	0	43	0.0	300.0	348.42	.116
350	0	44	30.0	300.0	347.95	2.353
350	0	45	60.0	300.0	347.32	1.347
350	0	46	90.0	300.0	347.17	1.086
350	0	47	0.0	275.0	348.49	.104
350	0	48	30.0	275.0	354.24	1.575
350	0	49	60.0	275.0	355.27	.259
350	0	50	90.0	275.0	351.19	.517
350	0	51	0.0	270.0	348.40	.096
350	0	52	30.0	270.0	347.70	1.734
350	0	53	60.0	270.0	347.32	2.538
350	0	54	90.0	270.0	349.82	.652
350	0	55	90.0	265.0	348.49	.121
350	0	56	30.0	265.0	350.11	.501
350	0	57	60.0	265.0	346.76	1.184
350	0	58	90.0	265.0	351.19	.273
350	0	59	0.0	240.0	348.37	.061
350	0	60	30.0	240.0	350.84	5.161
350	0	61	60.0	240.0	348.01	.731
350	0	62	90.0	240.0	348.05	2.122
350	0	63	0.0	210.0	348.47	.109
350	0	65	60.0	210.0	350.83	.461
350	0	66	90.0	210.0	346.55	.991
350	0	67	0.0	185.0	348.57	.097
350	0	68	30.0	185.0	349.77	.147
350	0	69	60.0	185.0	350.13	.082
350	0	70	90.0	185.0	345.53	3.493
350	0	71	0.0	180.0	348.28	.103
350	0	72	30.0	180.0	349.81	1.370
350	0	73	60.0	180.0	351.40	.120
350	0	74	90.0	180.0	344.29	2.909
200	0	75	0.0	360.0	198.17	.307
200	0	76	30.0	360.0	197.76	1.798
200	0	77	60.0	360.0	199.59	.850
200	0	78	90.0	360.0	197.38	1.681
200	0	79	0.0	355.0	199.60	.380

TABLE 7-2. HST MODEL RANGE MEASUREMENTS, RUNS 31-300 (CONTINUED)

SITE	SOLAR PANEL	RUN NO.	AZ POS.	EL POS	R_{MEAN}	σ_R
200	0	80	30.0	355.0	200.12	.992
200	0	81	60.0	355.0	202.70	.911
200	0	82	90.0	355.0	195.87	.054
200	0	83	0.0	330.0	198.90	.135
200	0	84	30.0	330.0	197.06	1.084
200	0	85	60.0	330.0	197.60	1.235
200	0	86	90.0	330.0	197.70	1.915
200	0	87	0.0	300.0	201.94	.555
200	0	88	30.0	300.0	208.06	.282
200	0	89	60.0	300.0	200.51	2.967
200	0	90	90.0	300.0	200.58	3.150
200	0	91	0.0	275.0	201.95	.101
200	0	92	30.0	275.0	195.96	.252
200	0	93	60.0	275.0	201.05	1.675
200	0	94	90.0	275.0	201.57	.596
200	0	95	0.0	270.0	201.00	.178
200	0	96	30.0	270.0	200.02	1.414
200	0	97	60.0	270.0	201.29	1.624
200	0	98	90.0	270.0	201.51	.365
200	0	99	90.0	265.0	101.16	.178
100	0	100	30.0	360.0	97.56	1.320
100	0	101	60.0	360.0	96.89	.353
100	0	102	90.0	360.0	101.90	.715
100	0	103	0.0	355.0	100.82	.098
100	0	104	30.0	355.0	101.71	.245
100	0	105	60.0	355.0	97.97	.181
100	0	106	90.0	355.0	96.51	.131
100	0	107	0.0	330.0	100.18	.119
100	0	108	30.0	330.0	99.65	.808
100	0	109	60.0	330.0	104.17	2.842
100	0	110	90.0	330.0	102.79	.238
100	0	111	0.0	300.0	100.60	.120
100	0	112	30.0	300.0	101.42	2.499
100	0	113	60.0	300.0	98.62	1.530
100	0	114	90.0	300.0	105.72	.367
100	0	115	0.0	275.0	102.50	.074
100	0	116	30.0	275.0	100.60	.109
100	0	117	60.0	275.0	100.42	.339
100	0	118	90.0	275.0	102.34	.709
100	0	119	0.0	270.0	93.32	.030
100	0	120	30.0	270.0	101.08	.939
100	0	121	60.0	270.0	100.01	.280
100	0	122	90.0	270.0	102.38	.525
50	0	123	90.0	330.8	47.71	.124
50	0	124	30.0	265.0	52.43	.048
50	0	125	60.0	265.0	49.13	.310
50	0	126	90.0	265.0	47.98	.403
50	0	127	0.0	240.0	47.60	.113

TABLE 7-2. HST MODEL RANGE MEASUREMENTS, RUNS 31-300 (CONTINUED)

SITE	SOLAR PANEL	RUN NO.	AZ POS.	EL POS	R_{MEAN}	σ_R
50	0	128	30.0	240.0	51.67	.107
50	0	129	60.0	240.0	50.63	.970
30	0	130	90.0	240.0	52.83	.153
50	0	131	0.0	210.0	46.86	.061
50	0	132	30.0	210.0	51.22	.097
50	0	133	60.0	210.0	51.77	.126
50	0	134	90.0	210.0	47.70	.181
50	0	136	30.0	185.0	47.37	.118
50	0	137	60.0	185.0	50.69	1.431
50	0	138	90.0	185.0	57.73	.389
50	0	139	0.0	180.0	47.07	.056
50	0	140	30.0	180.0	47.19	.156
50	0	141	60.0	180.0	52.90	1.124
50	0	142	90.0	180.0	53.47	1.196
50	0	143	0.0	270.0	54.37	.145
50	0	144	30.0	270.0	49.06	1.786
50	0	145	60.0	270.0	51.58	.217
50	0	146	90.0	270.0	53.21	1.102
50	0	147	90.0	345.1	47.66	.015
25	0	148	0.0	360.0	21.52	.002
25	0	149	30.0	360.0	29.32	.292
25	0	150	60.0	360.0	25.16	.100
25	0	151	90.0	360.0	24.53	.079
25	0	152	0.0	355.0	28.41	.110
25	0	153	30.0	355.0	27.76	.154
25	0	154	60.0	355.0	29.52	.001
25	0	155	90.0	355.0	24.46	.038
25	0	156	0.0	330.0	22.77	.125
25	0	157	30.0	330.0	27.86	.193
25	0	158	60.0	330.0	29.42	.074
25	0	159	90.0	330.0	24.29	.001
25	0	160	0.0	300.0	22.54	.076
25	0	161	30.0	300.0	29.40	1.498
25	0	162	60.0	300.0	35.92	.177
25	0	163	90.0	300.0	24.04	.077
25	0	164	0.0	275.0	22.90	.041
25	0	165	30.0	275.0	26.05	.629
25	0	166	60.0	275.0	27.69	.374
25	0	167	90.0	275.0	28.27	.316
25	0	168	0.0	270.0	24.37	.077
25	0	169	30.0	270.0	26.56	1.298
25	0	170	60.0	270.0	29.35	.846
25	0	171	90.0	270.0	29.41	.083
25	0	172	90.0	330.8	24.29	.001
25	45	175	0.0	360.0	22.50	.086
25	45	176	30.0	360.0	28.83	.111
25	45	177	60.0	360.0	29.03	.490
25	45	178	90.0	360.0	24.57	.061

ORIGINAL PAGE IS
OF POOR QUALITY

TABLE 7-2. HST MODEL RANGE MEASUREMENTS, RUNS 31-300 (CONTINUED)

SITE	SOLAR PANEL	RUN NO.	AZ POS.	EL POS	R_{MEAN}	σ_R
25	45	179	0.0	355.0	22.82	.076
25	45	180	30.0	355.0	28.90	.500
25	45	181	60.0	355.0	29.26	.166
25	45	182	90.0	355.0	24.45	.028
25	45	183	0.0	330.0	23.21	.032
25	45	184	30.0	330.0	29.14	1.013
25	45	185	60.0	330.0	29.41	.119
25	45	186	90.0	330.0	24.29	.001
25	45	187	0.0	300.0	22.85	.074
25	45	188	30.0	300.0	28.76	.079
25	45	189	60.0	300.0	36.45	.460
25	45	190	90.0	300.0	24.29	.001
25	45	191	0.0	275.0	22.29	.011
25	45	192	30.0	275.0	29.48	.880
25	45	193	60.0	275.0	28.97	.247
25	45	194	90.0	275.0	28.74	1.021
25	45	195	0.0	270.0	25.03	.066
25	45	196	30.0	270.0	29.10	.324
25	45	197	60.0	270.0	28.79	.195
25	45	198	90.0	270.0	29.06	.773
25	45	199	90.0	330.8	24.29	.001
50	45	200	0.0	360.0	52.15	.081
50	45	201	30.0	360.0	52.11	.149
50	45	202	60.0	360.0	52.62	.066
50	45	203	90.0	360.0	48.80	.079
50	45	204	0.0	355.0	52.56	.051
50	45	205	30.0	355.0	47.94	.301
50	45	206	60.0	355.0	50.10	1.520
50	45	207	90.0	355.0	47.89	.077
50	45	208	0.0	330.0	47.81	.029
50	45	209	30.0	330.0	51.06	1.339
50	45	210	60.0	330.0	47.83	.188
50	45	211	90.0	330.0	47.77	.068
50	45	212	0.0	300.0	46.75	.037
50	45	213	30.0	300.0	50.71	1.878
50	45	214	60.0	300.0	52.98	1.309
50	45	215	90.0	300.0	53.72	.195
50	45	216	0.0	275.0	47.38	.082
50	45	217	30.0	275.0	51.64	1.306
50	45	218	60.0	275.0	52.20	.474
50	45	219	90.0	275.0	52.10	.597
50	45	220	0.0	270.0	47.25	.079
50	45	221	30.0	270.0	51.67	.856
50	45	222	60.0	270.0	50.90	.887
50	45	223	90.0	270.0	51.49	.300
50	45	224	90.0	345.1	47.52	.134
100	45	225	0.0	360.0	101.15	.042
100	45	226	30.0	360.0	99.78	.634

TABLE 7-2. HST MODEL RANGE MEASUREMENTS, RUNS 31-300 (CONTINUED)

SITE	SOLAR PANEL	RUN NO.	AZ POS.	EL POS	R_{MEAN}	σ_R
100	45	227	60.0	360.0	97.93	.070
100	45	228	90.0	360.0	98.74	3.806
100	45	229	0.0	355.0	100.00	1.173
100	45	230	30.0	355.0	100.46	.496
100	45	231	60.0	355.0	99.56	3.699
100	45	232	90.0	355.0	96.17	.159
100	45	233	0.0	330.0	98.58	2.275
100	45	234	30.0	330.0	96.76	1.613
100	45	235	60.0	330.0	98.12	1.842
100	45	236	90.0	330.0	96.44	.191
100	45	237	0.0	300.0	94.64	.671
100	45	238	30.0	300.0	100.35	.126
100	45	239	60.0	300.0	100.11	1.817
100	45	240	90.0	300.0	102.37	.640
100	45	241	0.0	275.0	95.84	.190
100	45	242	30.0	275.0	96.31	.101
100	45	243	60.0	275.0	103.19	2.472
100	45	244	90.0	275.0	100.91	.684
100	45	245	0.0	270.0	96.98	.164
100	45	246	30.0	270.0	95.84	.130
100	45	247	60.0	270.0	104.17	2.592
100	45	248	90.0	270.0	100.73	.422
200	45	251	.0	*****	200.45	.141
200	45	252	0.0	360.0	199.92	.365
200	45	253	30.0	360.0	200.30	1.225
200	45	254	60.0	360.0	201.41	.380
200	45	255	90.0	360.0	199.31	.190
200	45	256	0.0	355.0	199.75	1.015
200	45	257	30.0	355.0	196.58	.107
200	45	258	60.0	355.0	195.85	.089
200	45	259	90.0	355.0	200.36	.172
200	45	260	0.0	330.0	197.08	.990
200	45	261	30.0	330.0	197.60	.121
200	45	262	60.0	330.0	201.57	.894
200	45	263	90.0	330.0	198.47	.014
200	45	264	0.0	300.0	196.97	.298
200	45	265	30.0	300.0	198.92	1.176
200	45	266	60.0	300.0	201.86	.762
200	45	267	90.0	300.0	198.88	.093
200	45	268	0.0	275.0	198.16	2.283
200	45	269	30.0	275.0	202.06	2.727
200	45	270	60.0	275.0	199.33	2.016
200	45	272	0.0	270.0	196.95	1.564
200	45	273	30.0	270.0	199.84	.606
200	45	274	60.0	270.0	199.94	.799
200	45	275	90.0	270.0	195.74	.074
350	45	276	0.0	360.0	349.85	.416
350	45	277	30.0	360.0	349.61	.725

TABLE 7-2. HST MODEL RANGE MEASUREMENTS, RUNS 31-300 (CONTINUED)

SITE	SOLAR PANEL	RUN NO.	AZ POS.	EL POS	R_{MEAN}	σ_R
350	45	278	60.0	360.0	348.21	2.617
350	45	279	90.0	360.0	346.75	2.322
350	45	280	0.0	355.0	348.78	.326
350	45	281	30.0	355.0	348.73	1.237
350	45	282	60.0	355.0	346.73	.571
350	45	283	90.0	355.0	345.54	.406
350	45	284	0.0	330.0	349.81	.273
350	45	285	30.0	330.0	346.48	.914
350	45	286	60.0	330.0	349.00	3.105
350	45	287	90.0	330.0	351.23	1.446
350	45	288	0.0	300.0	348.75	.089
350	45	289	30.0	300.0	346.16	.127
350	45	290	60.0	300.0	348.29	.916
350	45	291	90.0	300.0	351.11	2.375
350	45	292	0.0	275.0	348.73	.082
350	45	293	30.0	275.0	349.74	1.611
350	45	294	60.0	275.0	346.19	.233
350	45	295	90.0	275.0	350.80	.832
350	45	296	0.0	270.0	348.92	.112
350	45	297	30.0	270.0	347.40	1.429
350	45	298	60.0	270.0	349.16	2.095
350	45	299	90.0	270.0	349.25	.213

TESTS CONDUCTED WITH
DOCKING END ON BORESITE

SITE	SOLAR PANEL	RUN NO.	AZ POS.	EL POS	R_{MEAN}	σ_R
50	0	147	90.0	345.1	47.66	.015
25	0	172	90.0	330.8	24.29	.001
25	45	199	90.0	330.8	24.29	.001
50	45	224	90.0	345.1	47.52	.134
100	45	249	90.0	353.3	96.24	0.000
200	45	275	90.0	357.5	195.74	.074
350	45	300	90.0	359.4	345.27	.331

C-2

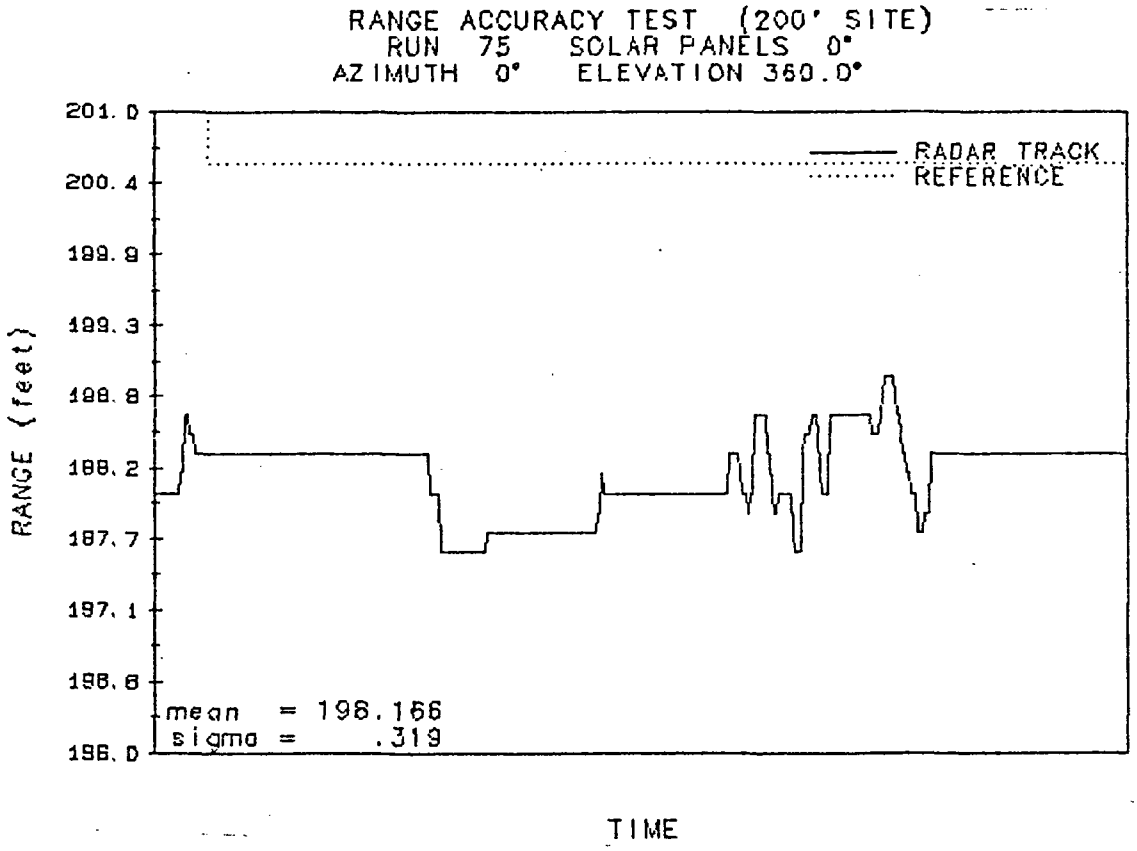

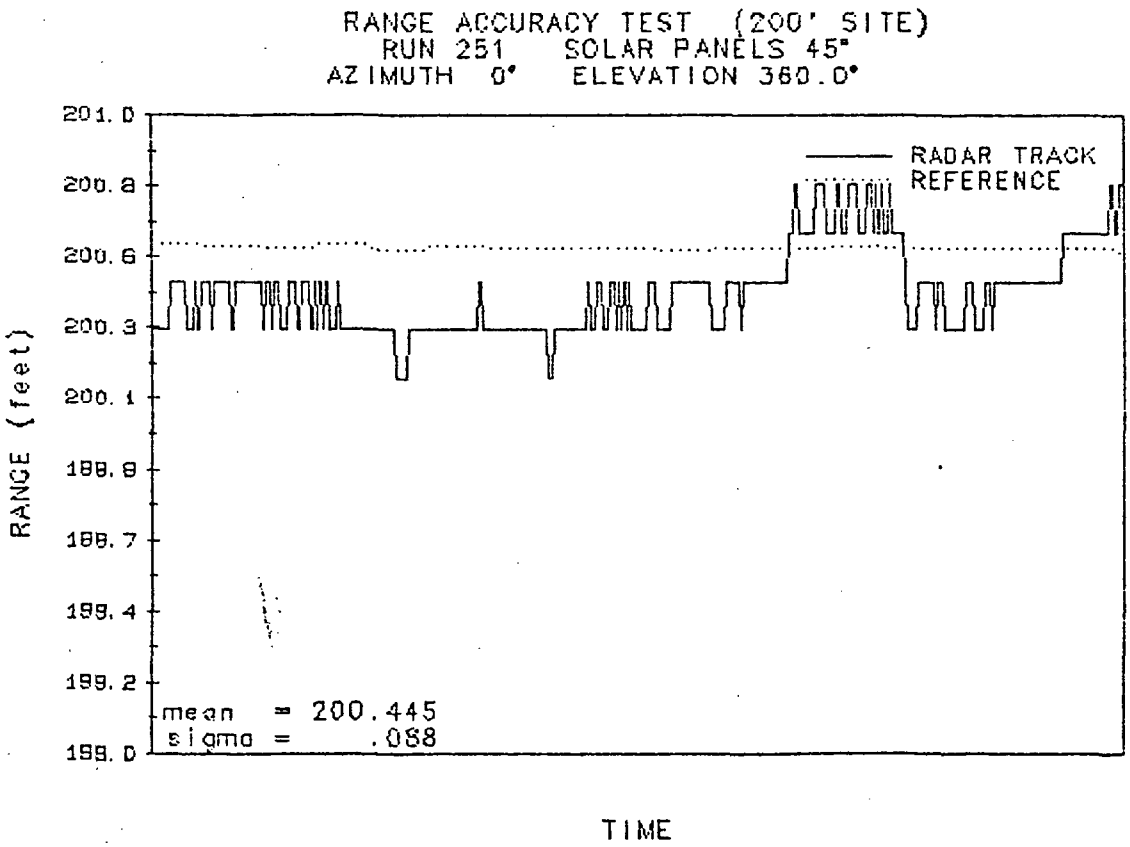

FIGURE 7-37. RANGE ACCURACY PLOTS, 200' SITE

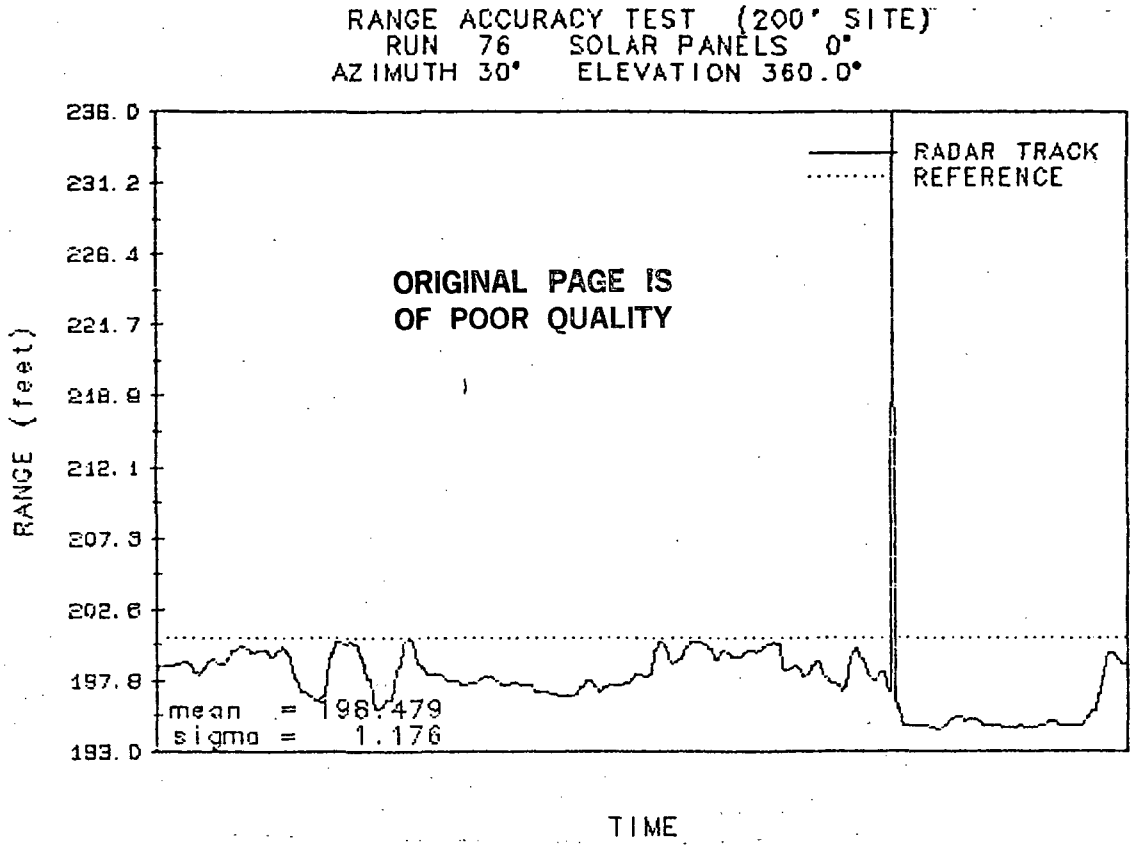

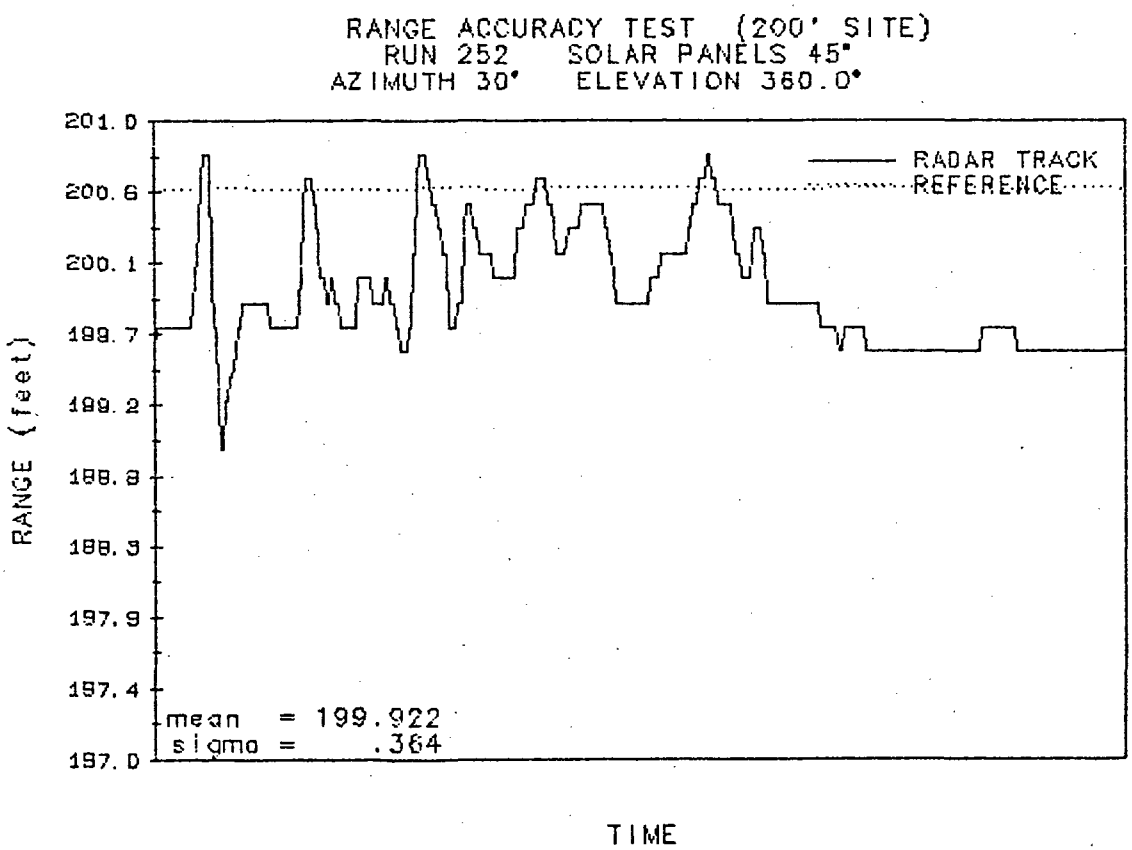

FIGURE 7-38. RANGE ACCURACY PLOTS, 200' SITE

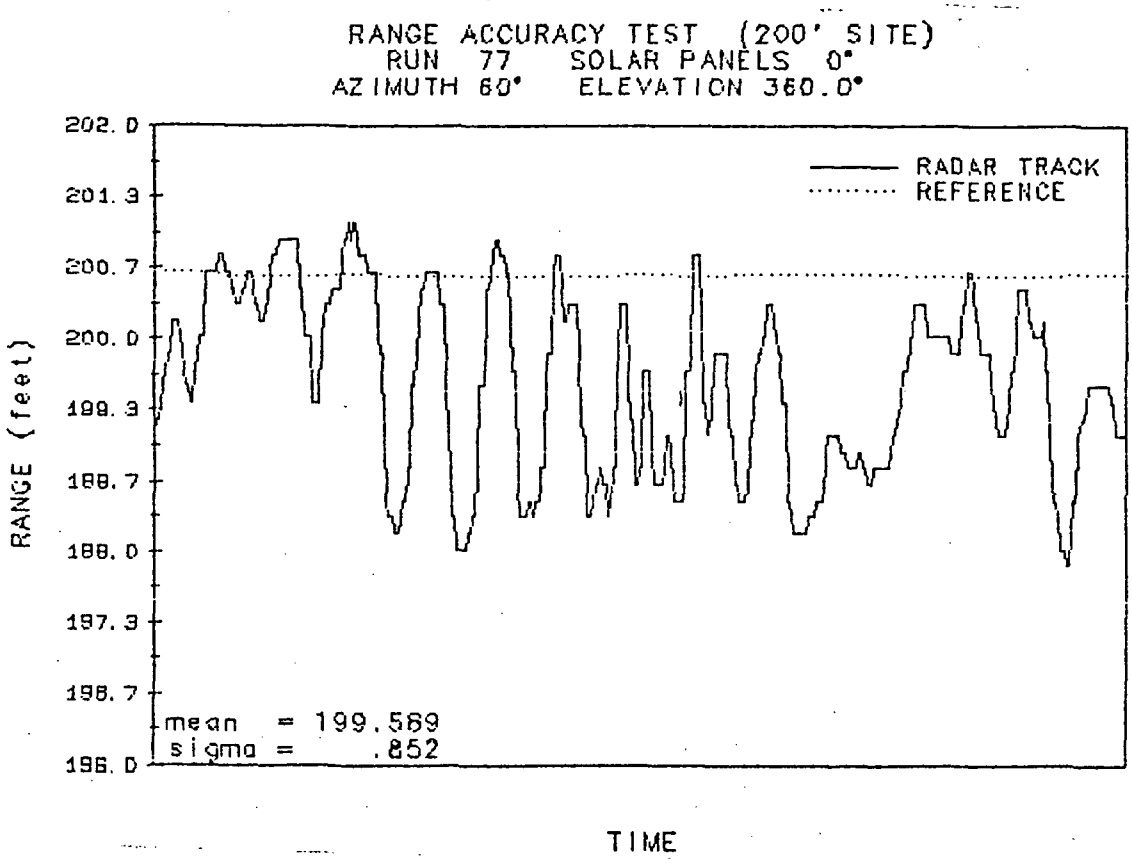

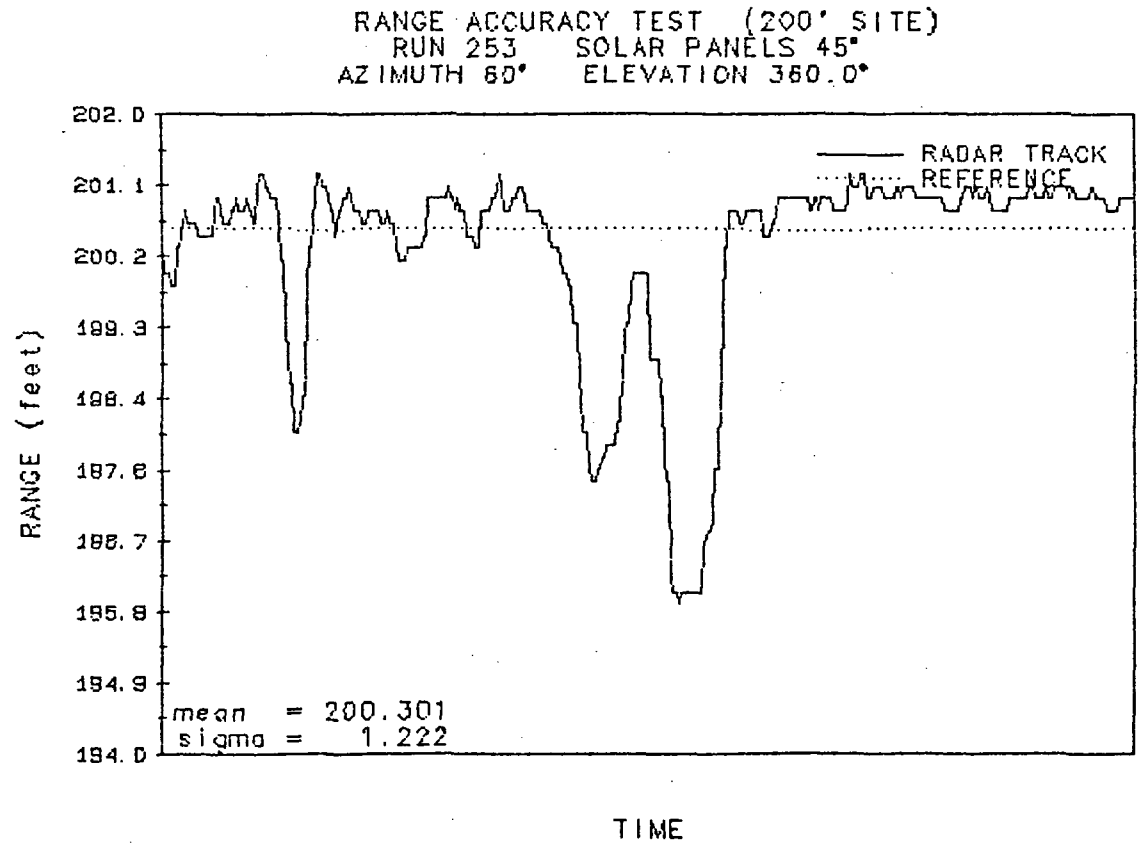

FIGURE 7-39. RANGE ACCURACY PLOTS, 200' SITE

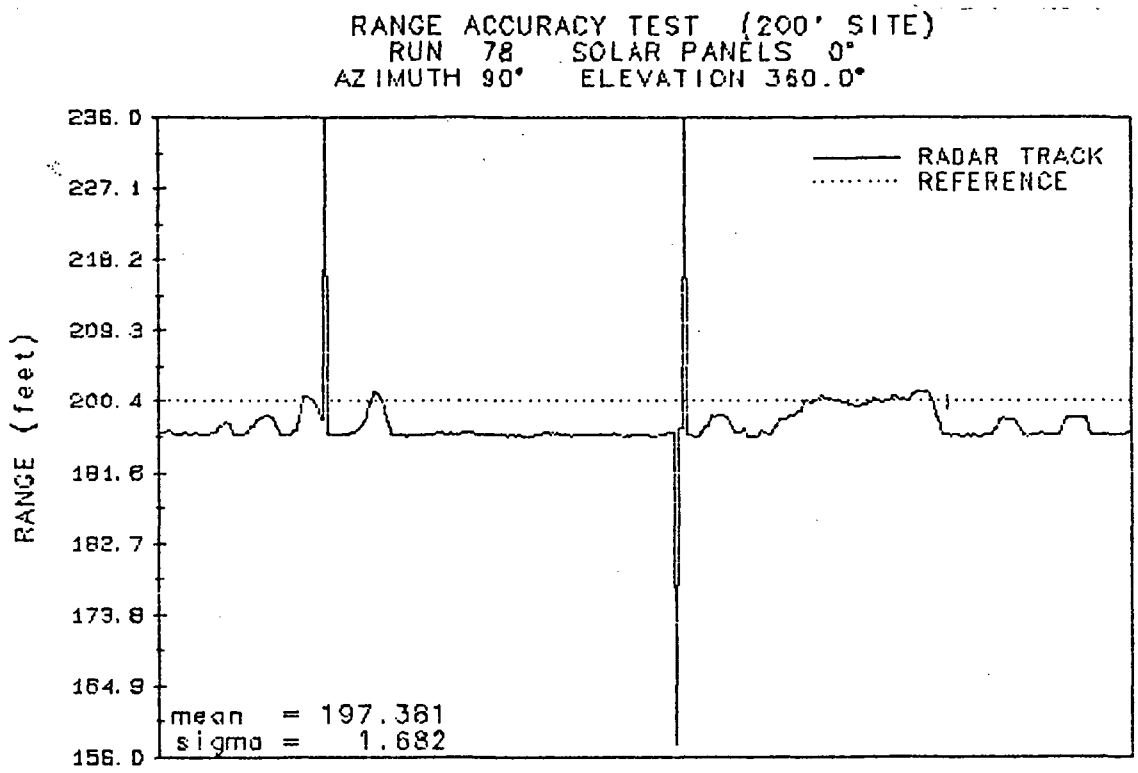

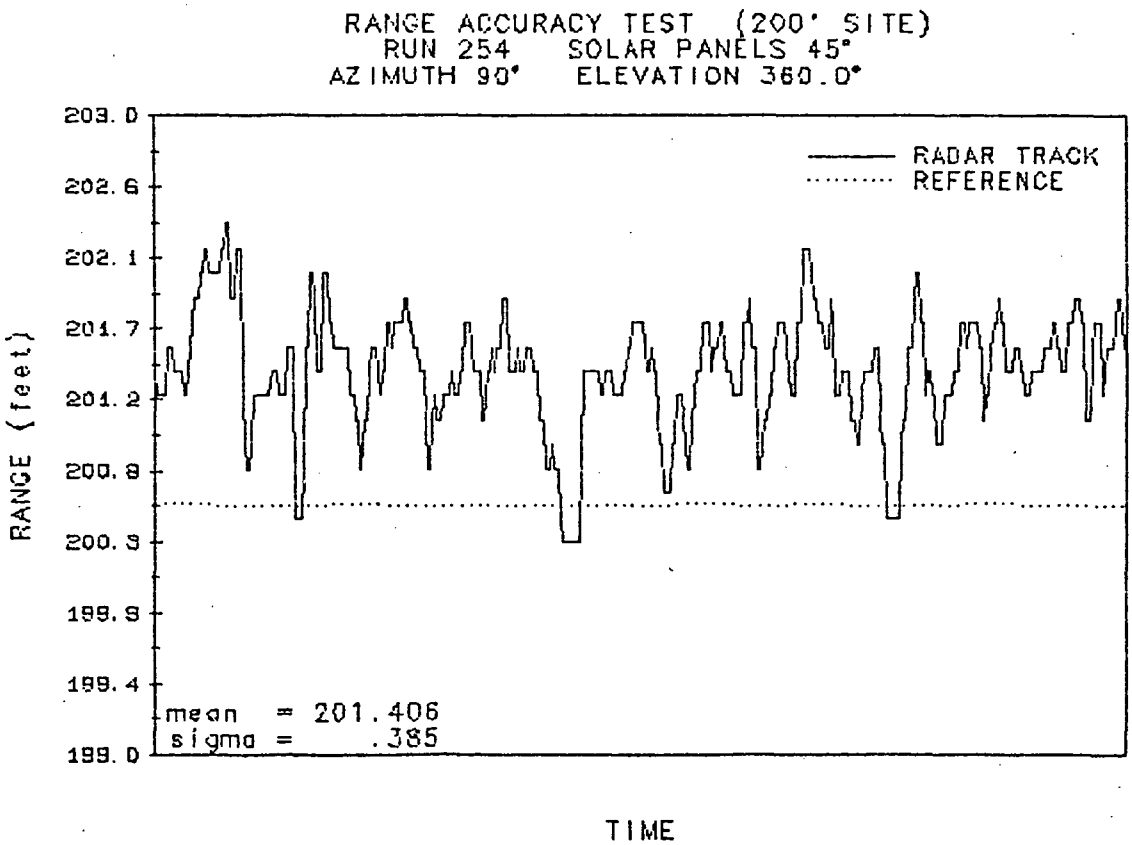

FIGURE 7-40. RANGE ACCURACY PLOTS, 200' SITE

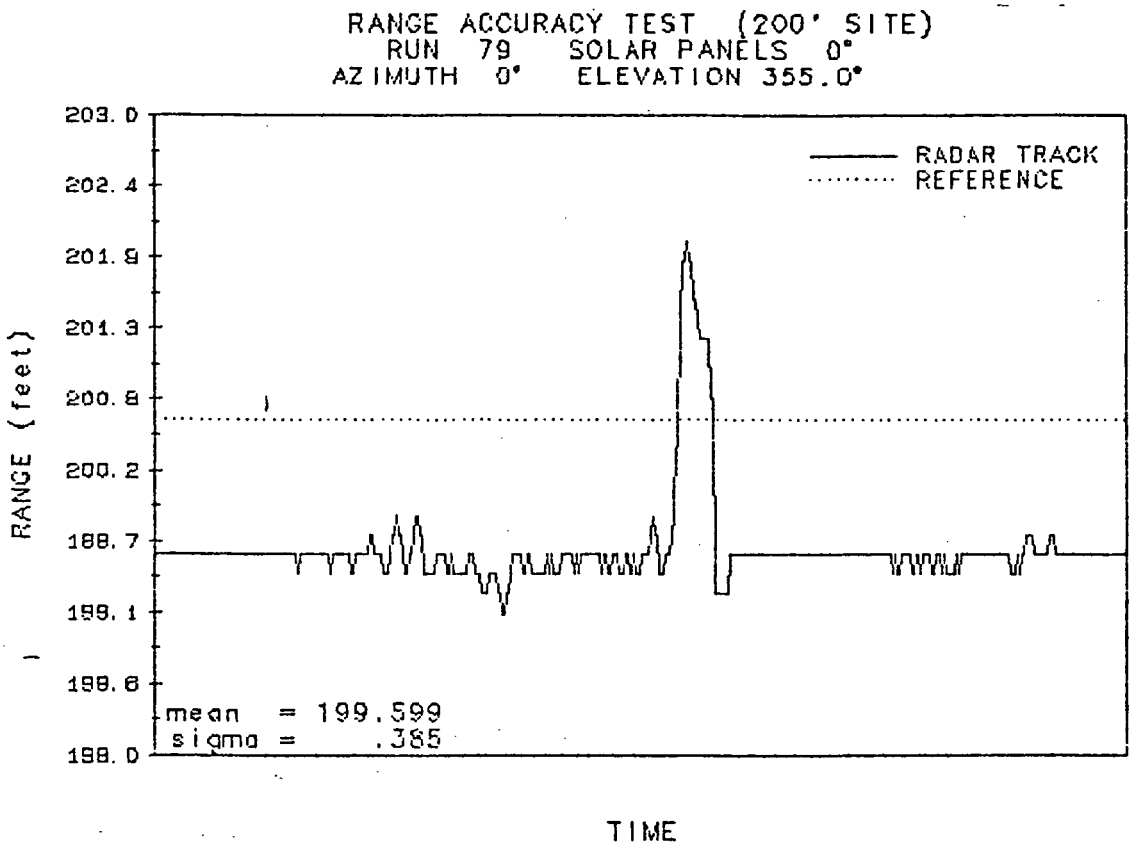

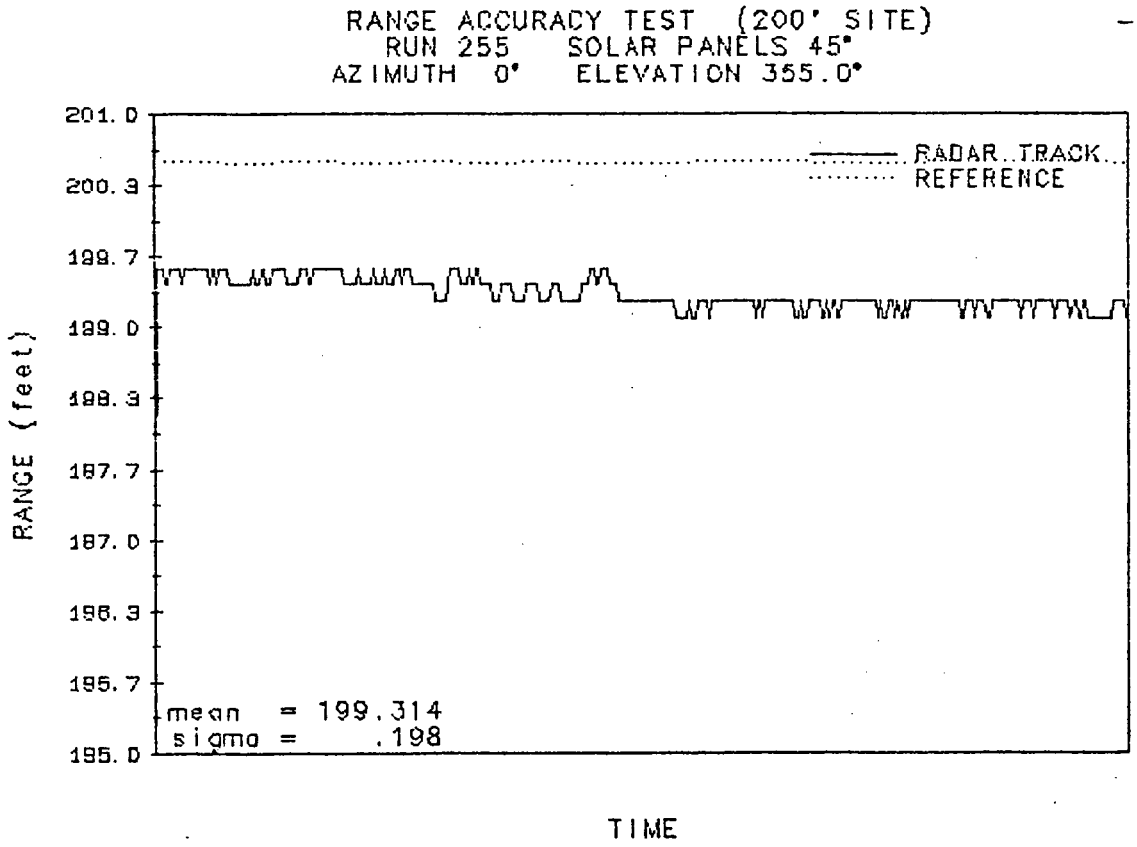

FIGURE 7-41. RANGE ACCURACY PLOTS, 200' SITE

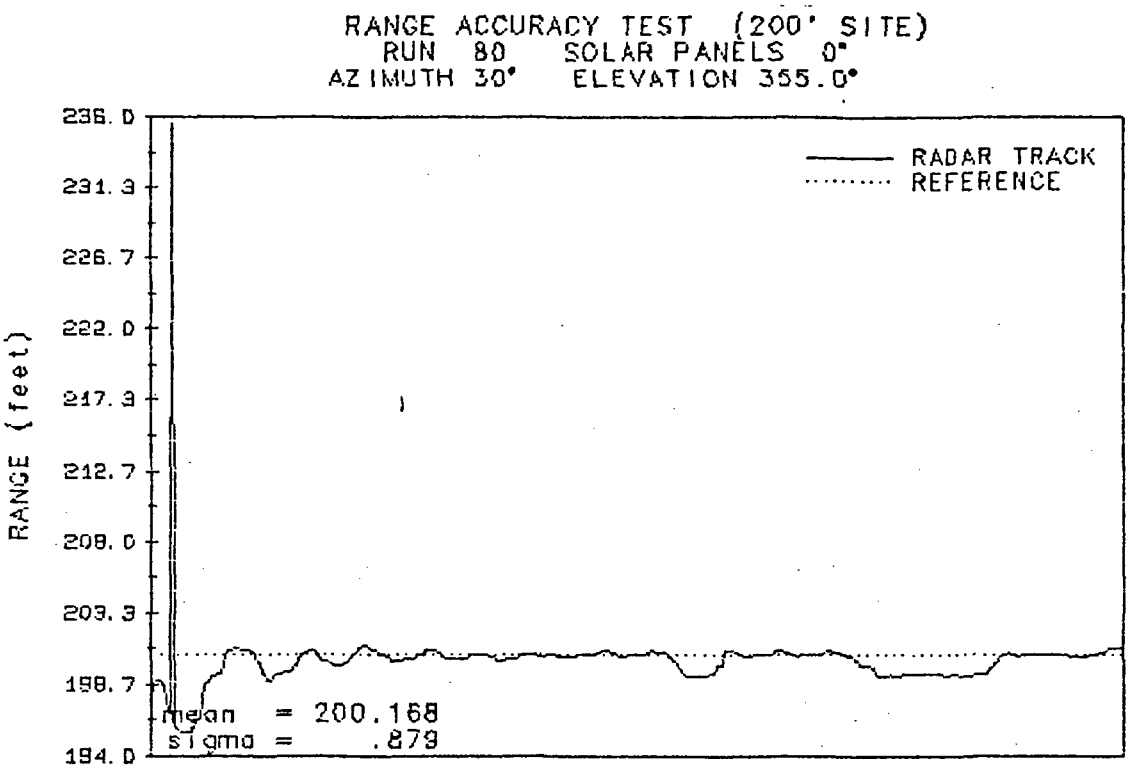

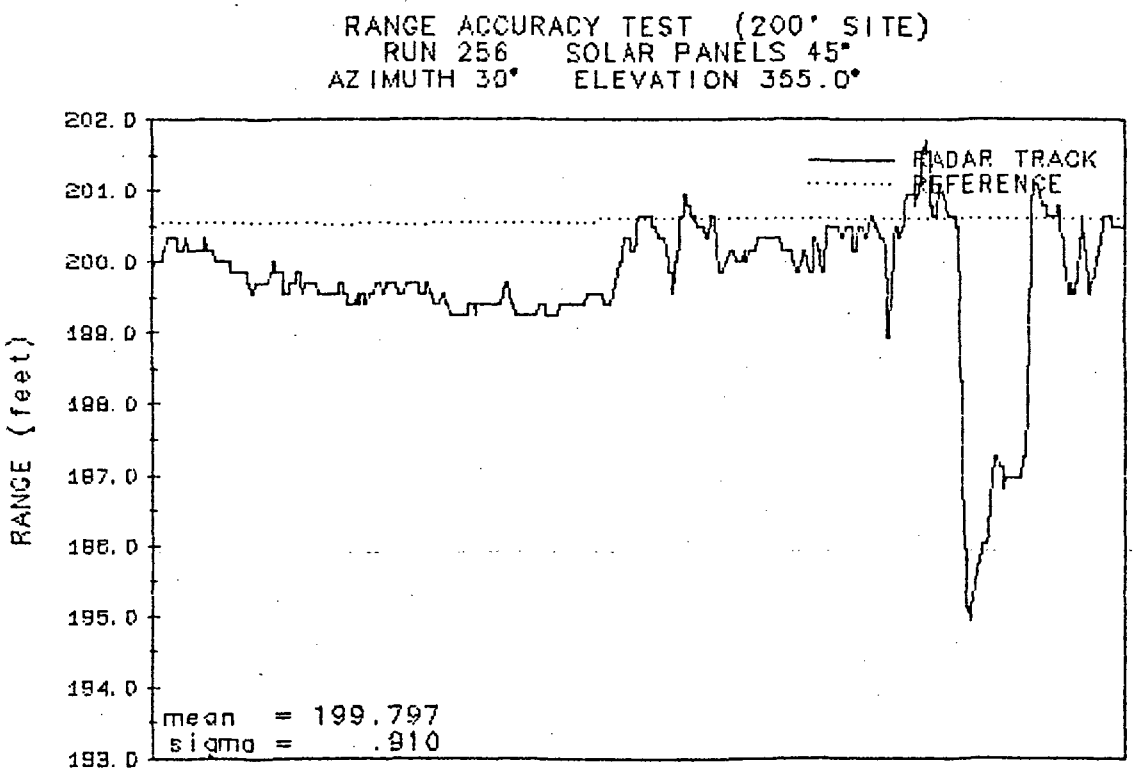

FIGURE 7-42. RANGE ACCURACY PLOTS, 200' SITE

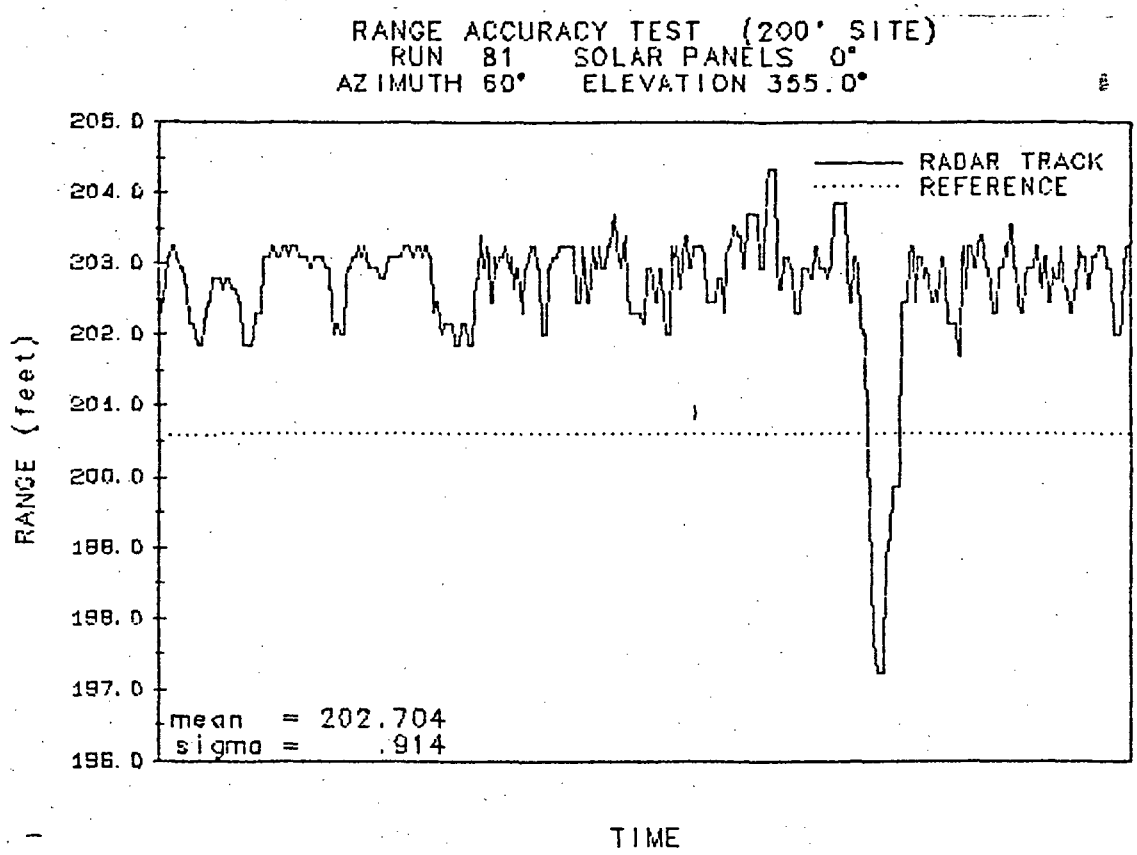

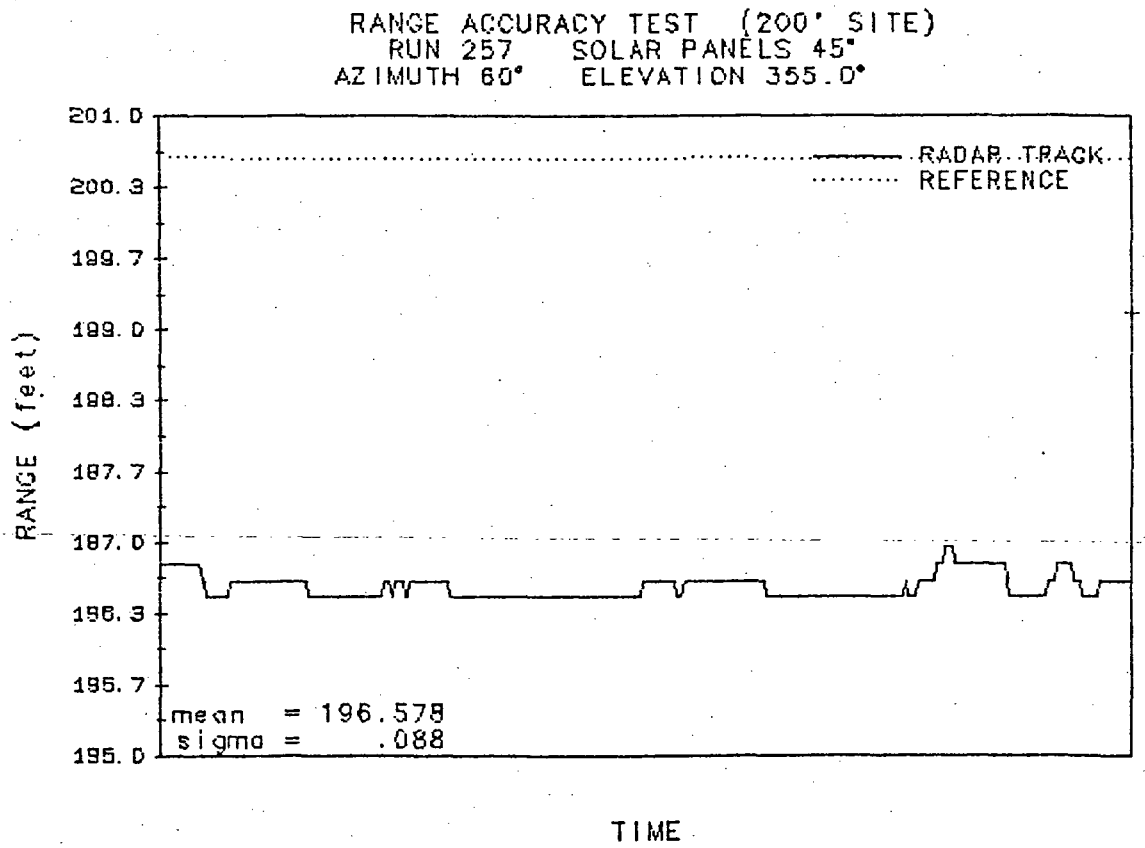

FIGURE 7-43. RANGE ACCURACY PLOTS, 200' SITE

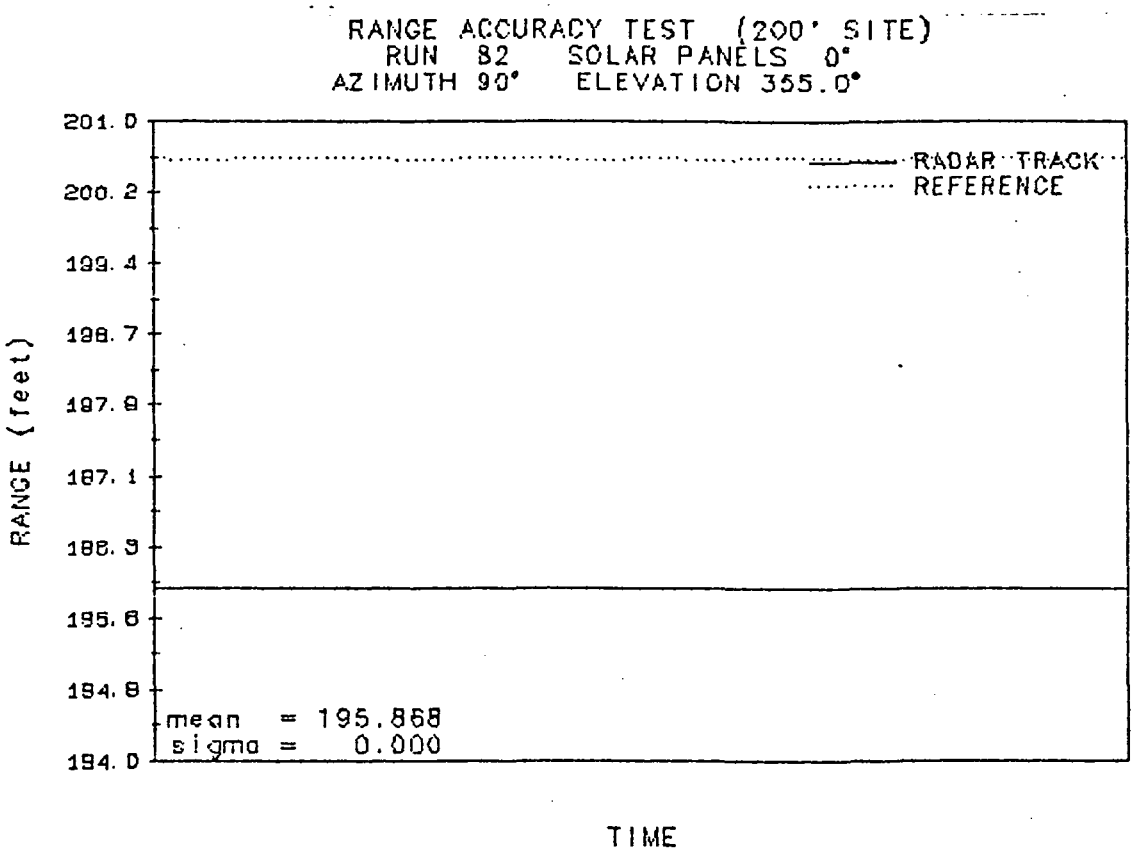

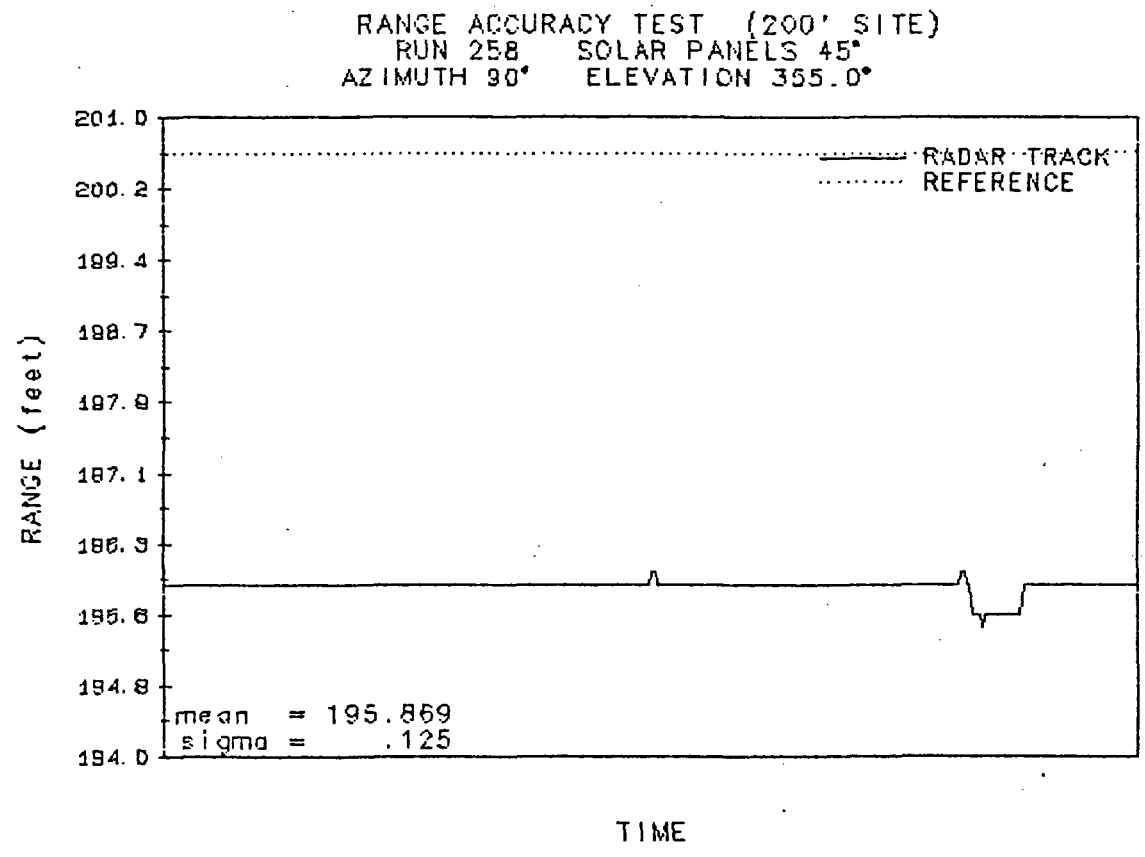

FIGURE 7-44. RANGE ACCURACY PLOTS, 200' SITE

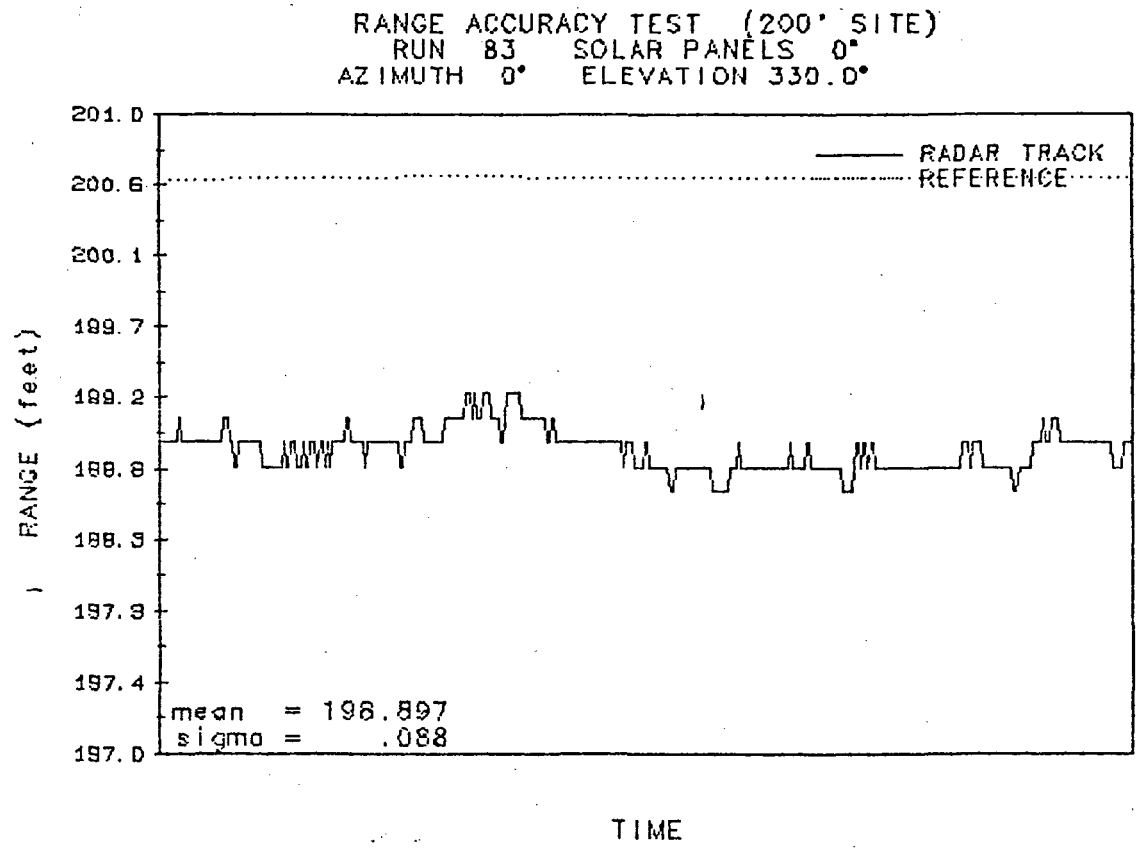

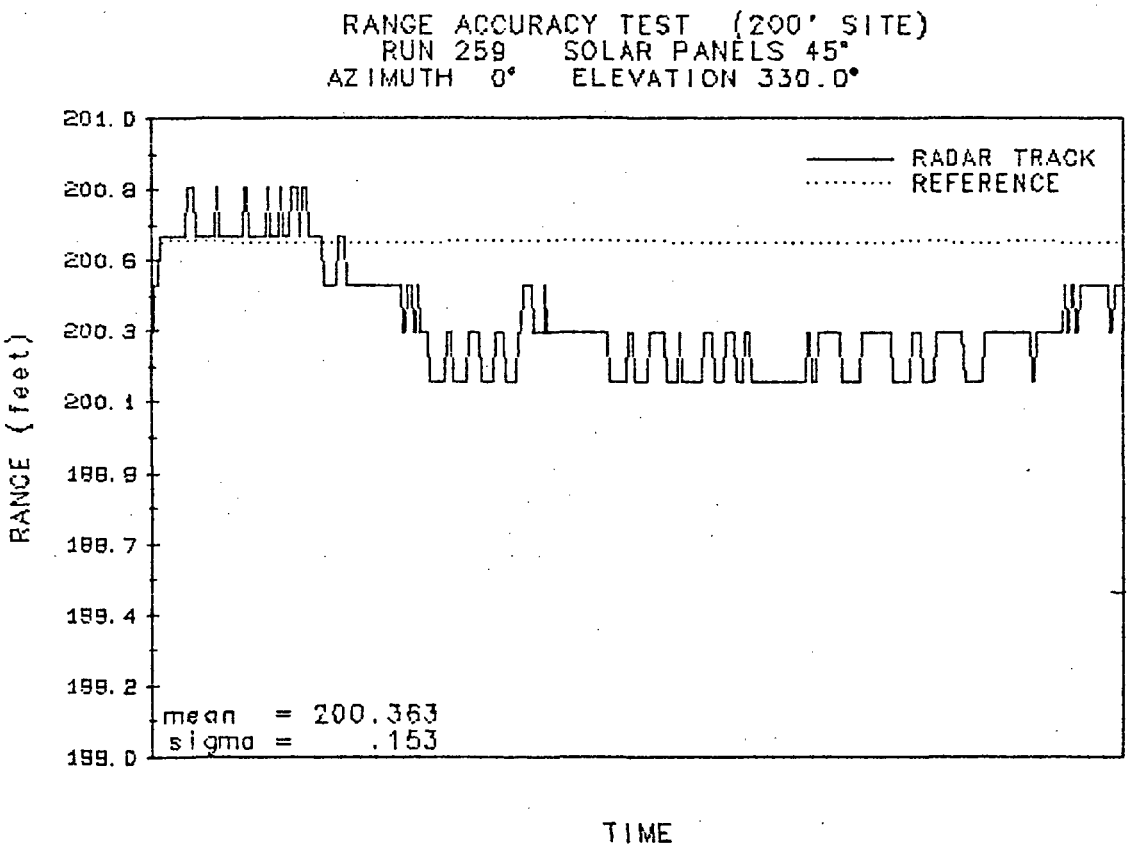

FIGURE 7-45. RANGE ACCURACY PLOTS, 200' SITE

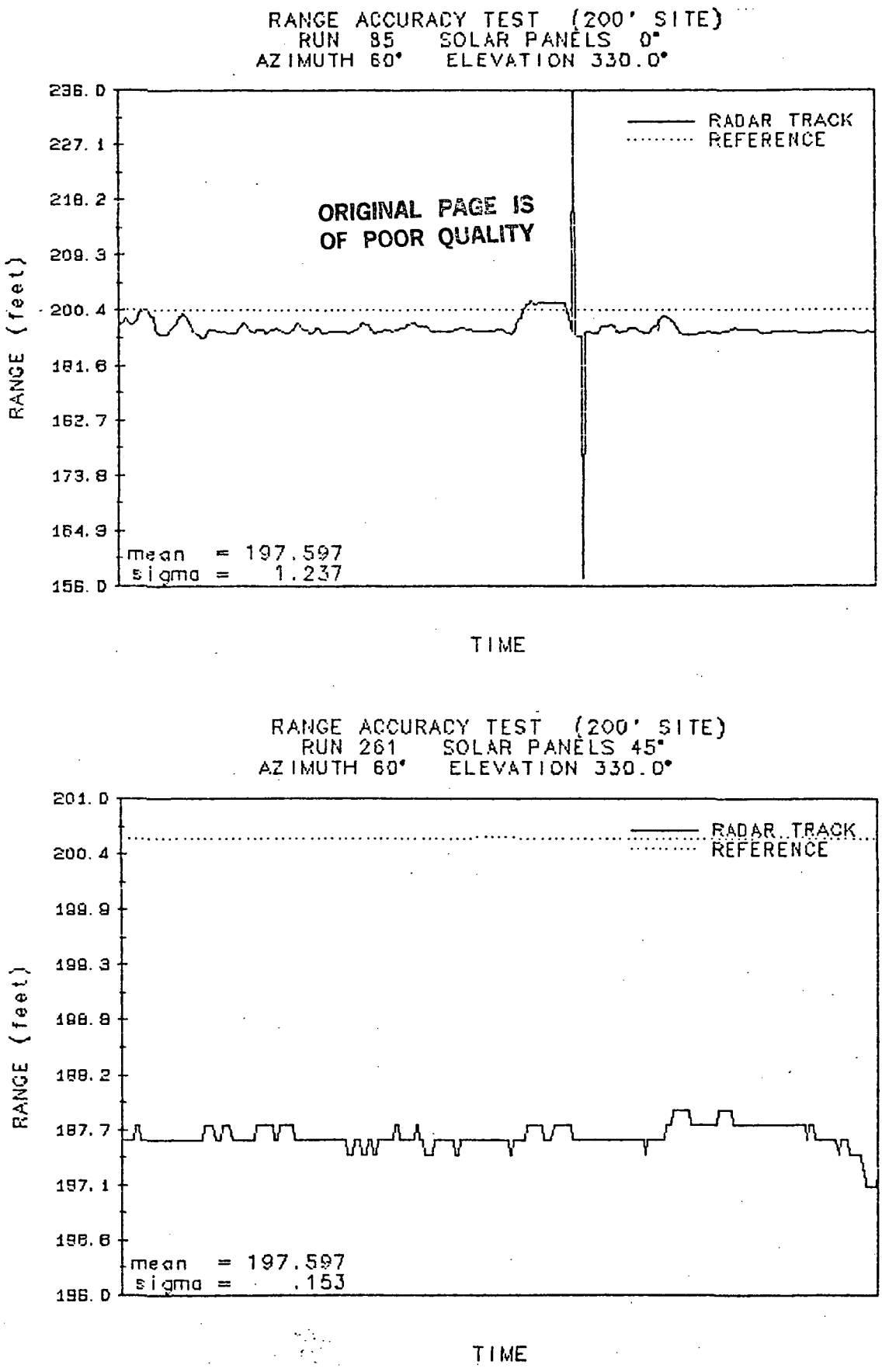

FIGURE 7-46. RANGE ACCURACY PLOTS, 200' SITE

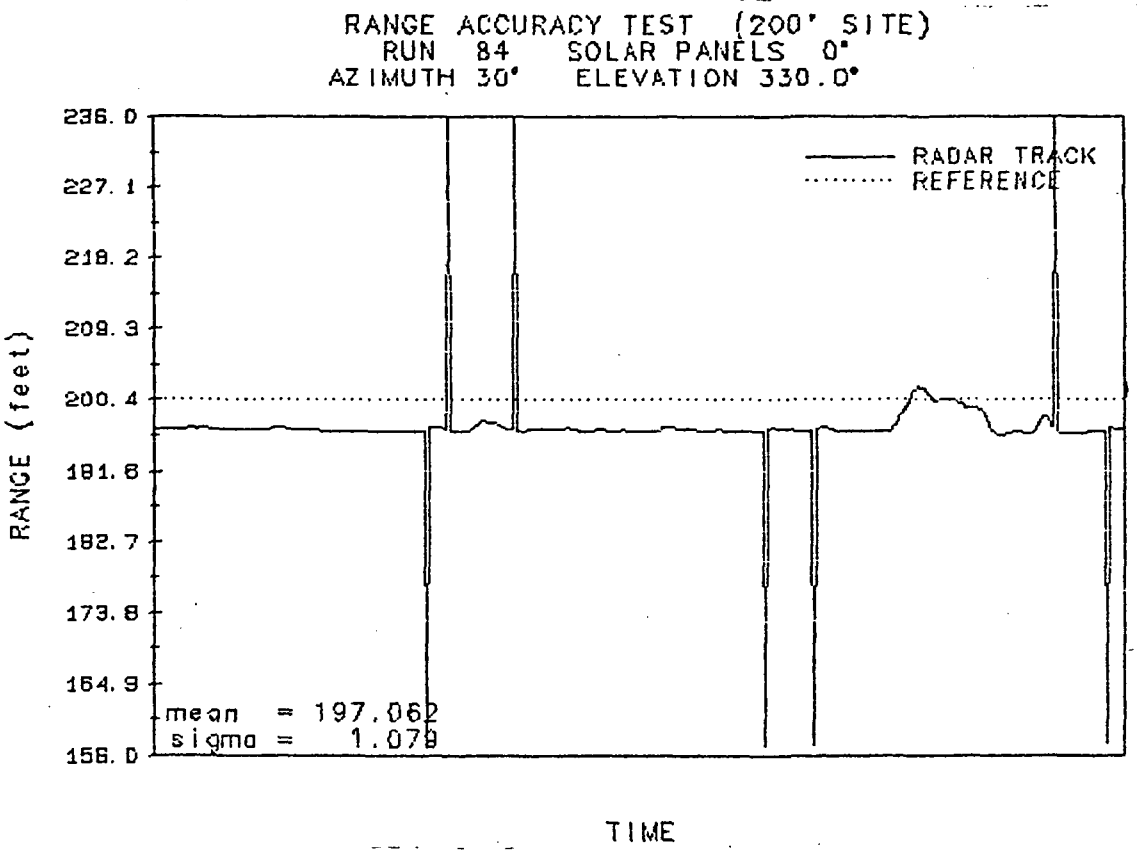

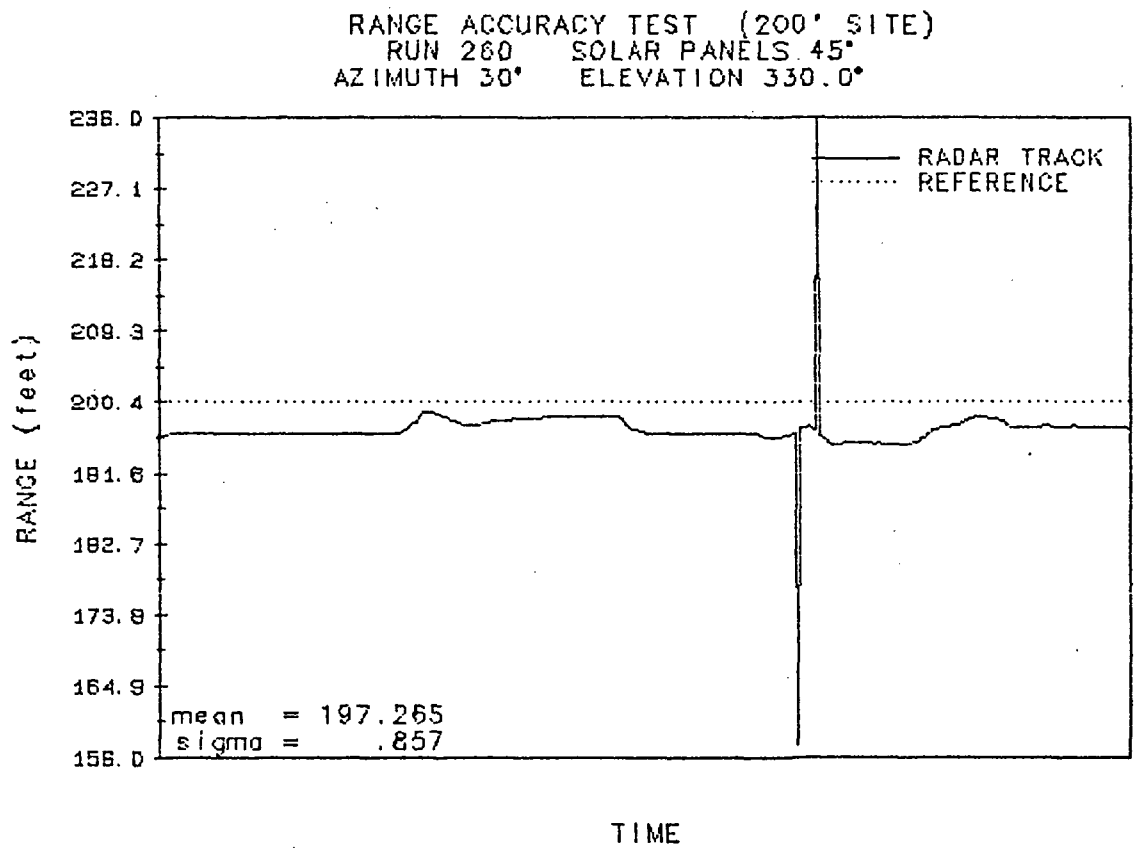

FIGURE 7-47. RANGE ACCURACY PLOTS, 200' SITE

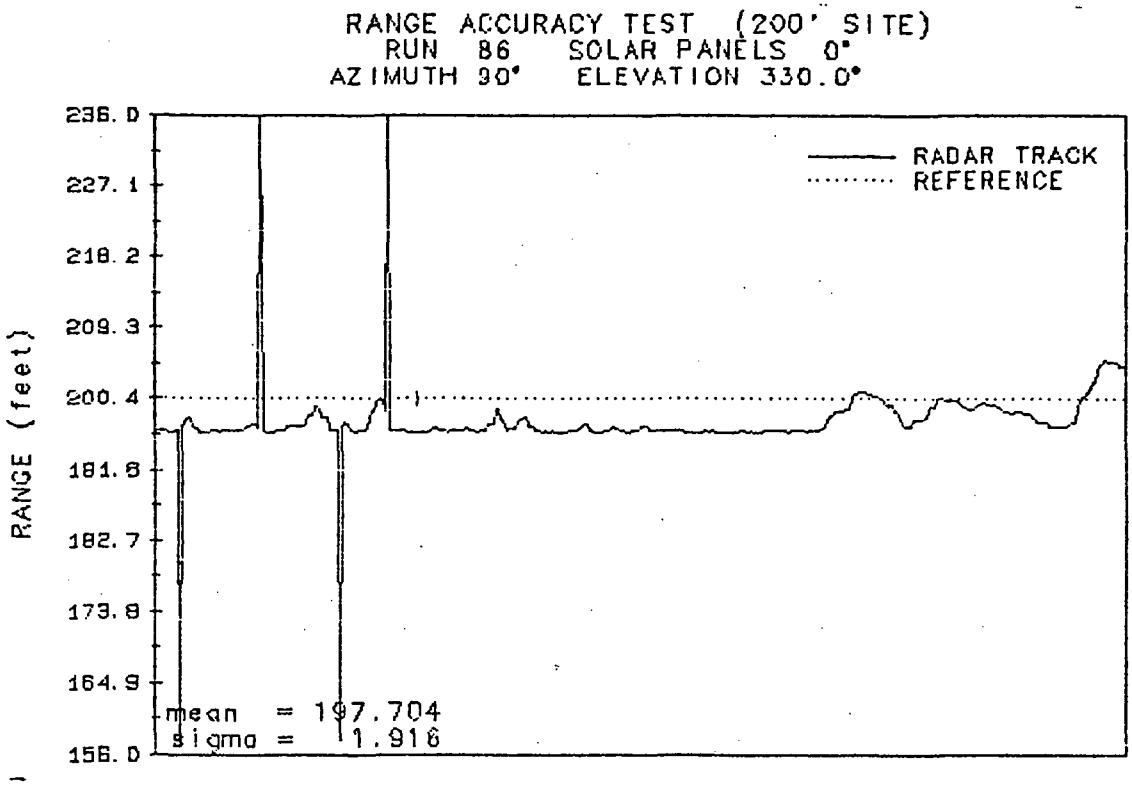

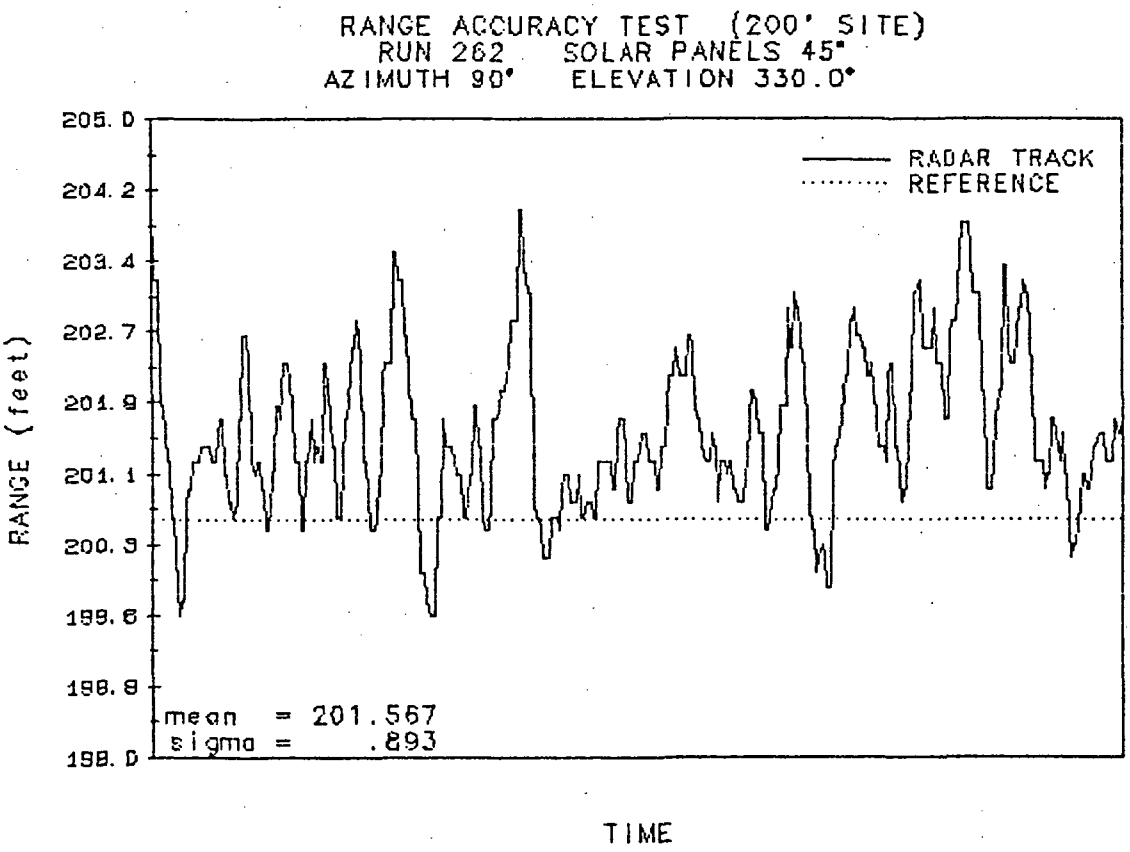

FIGURE 7-48. RANGE ACCURACY PLOTS, 200' SITE

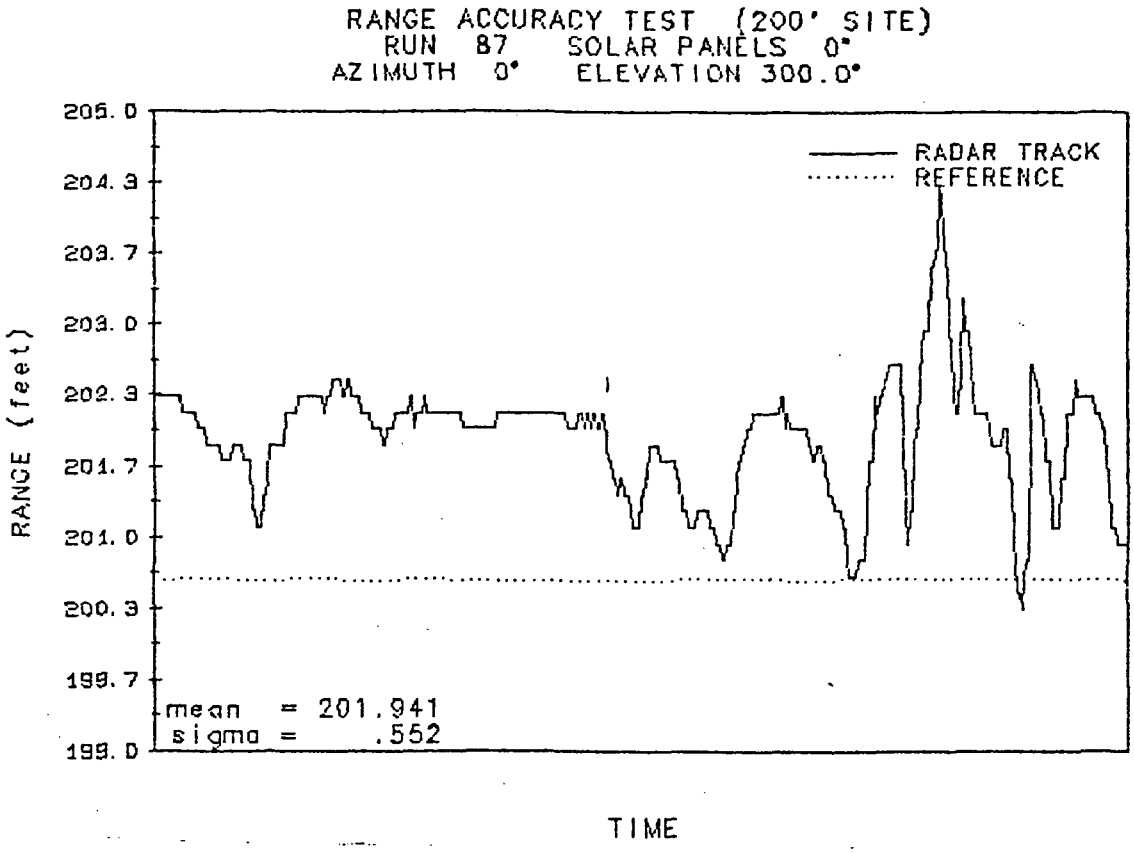

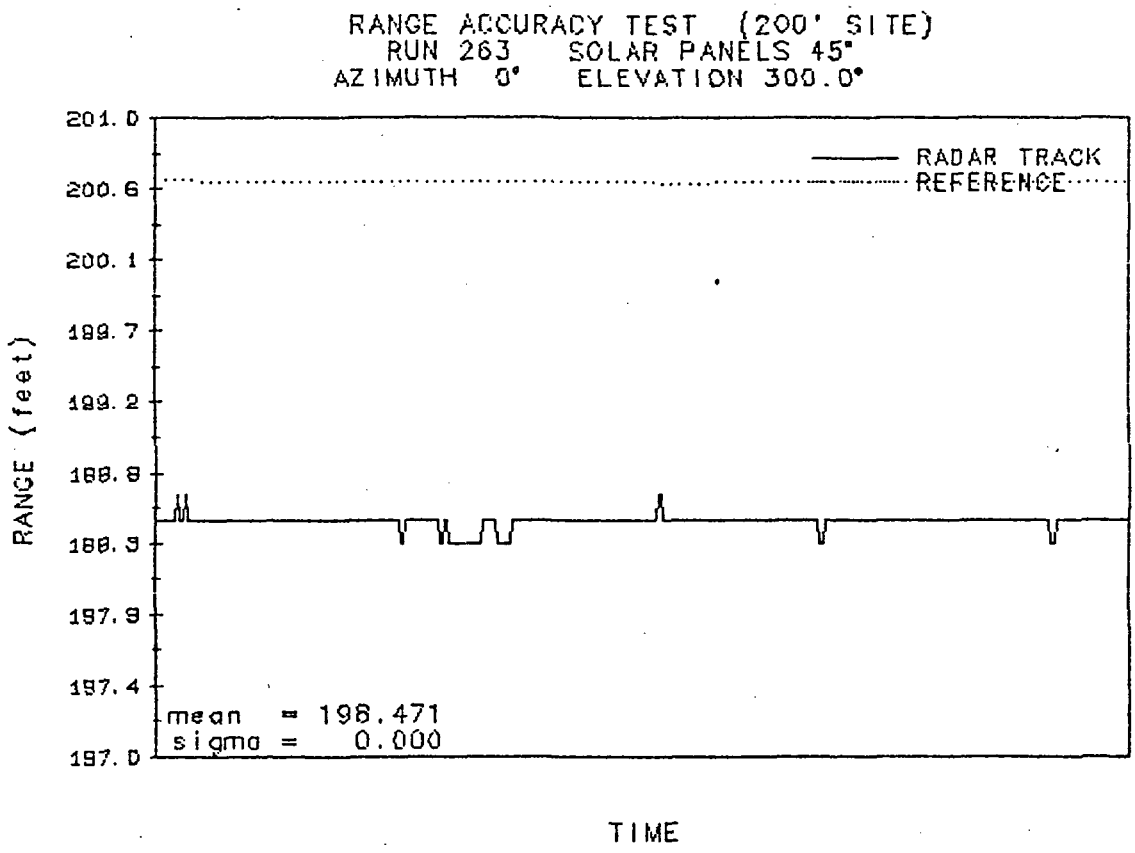

FIGURE 7-49. RANGE ACCURACY PLOTS, 200' SITE

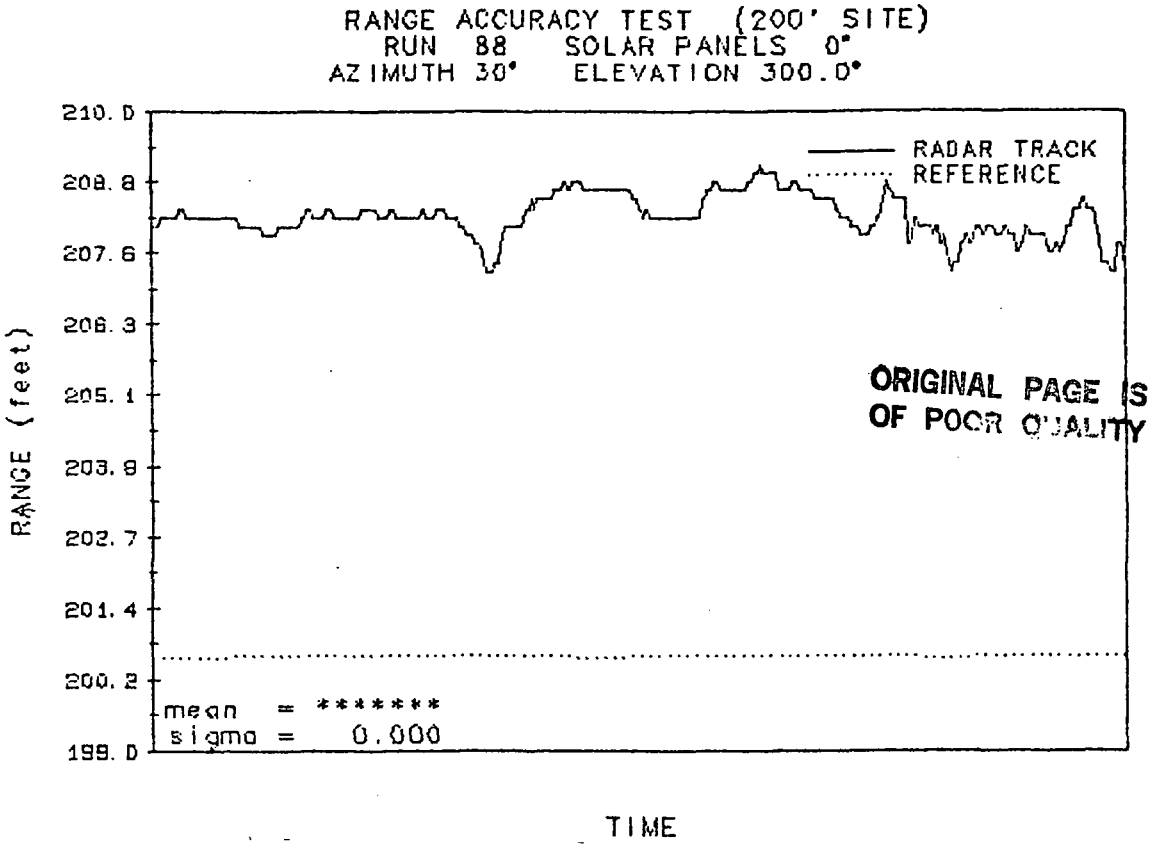

ORIGINAL PAGE IS
OF POOR QUALITY

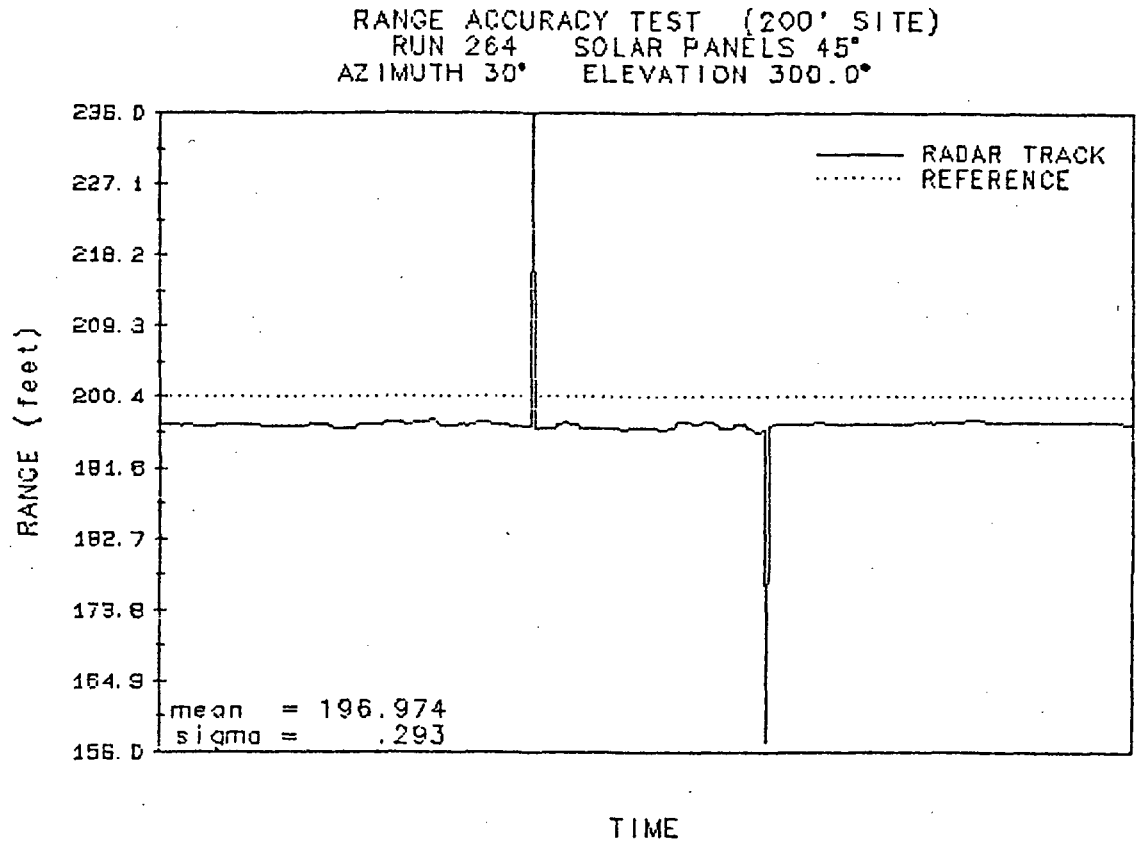

FIGURE 7-50. RANGE ACCURACY PLOTS, 200' Site

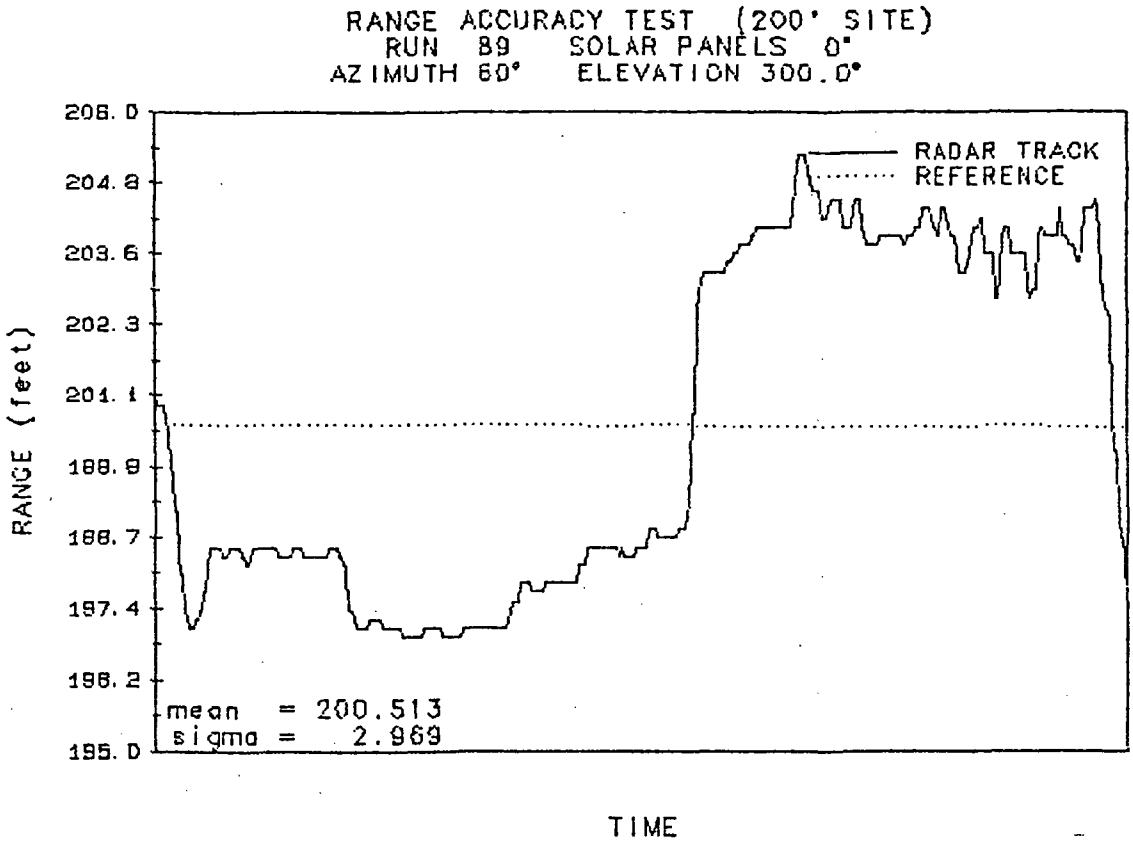

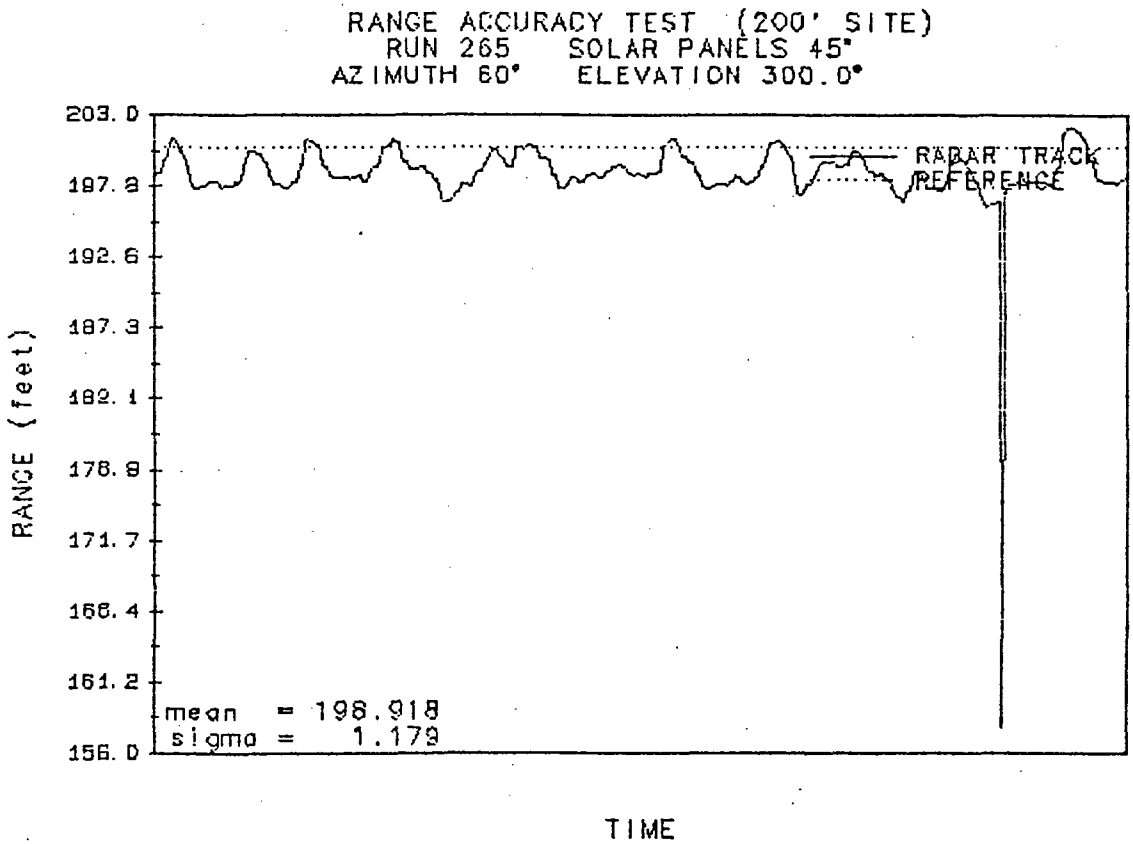

FIGURE 7-51. RANGE ACCURACY PLOTS, 200' SITE

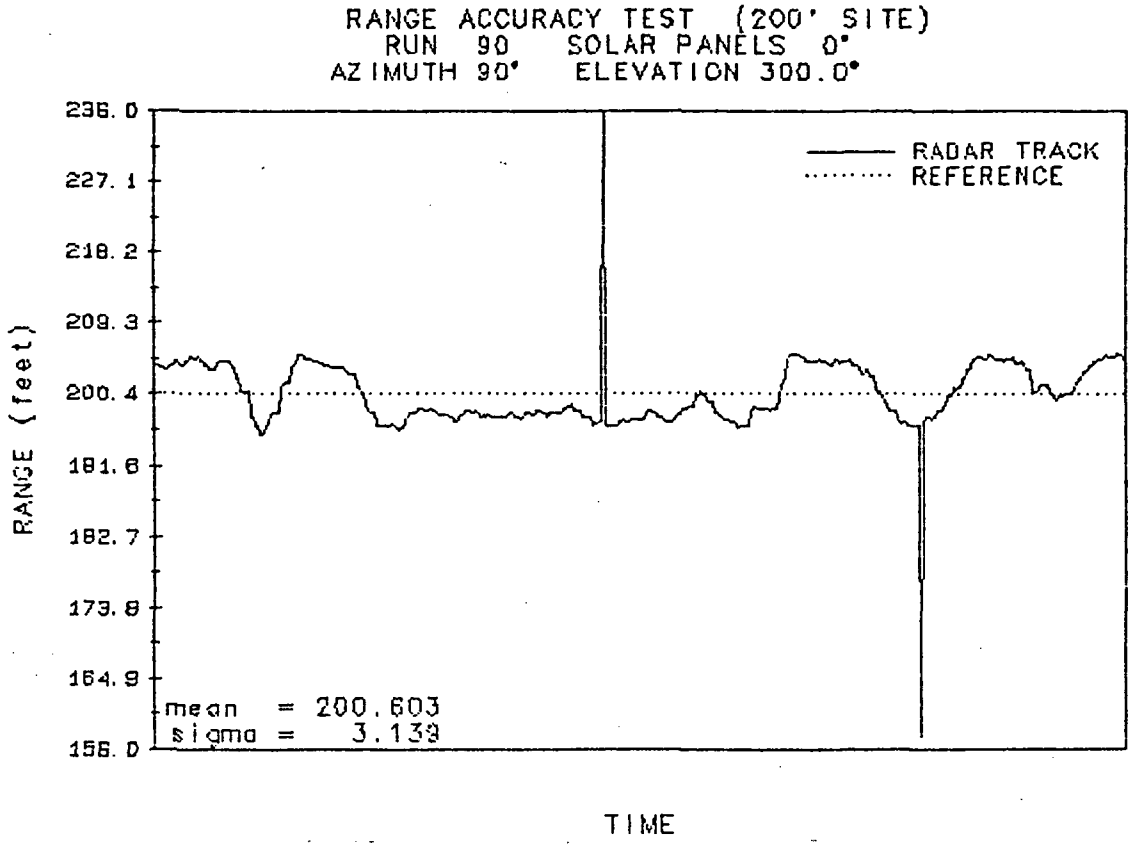

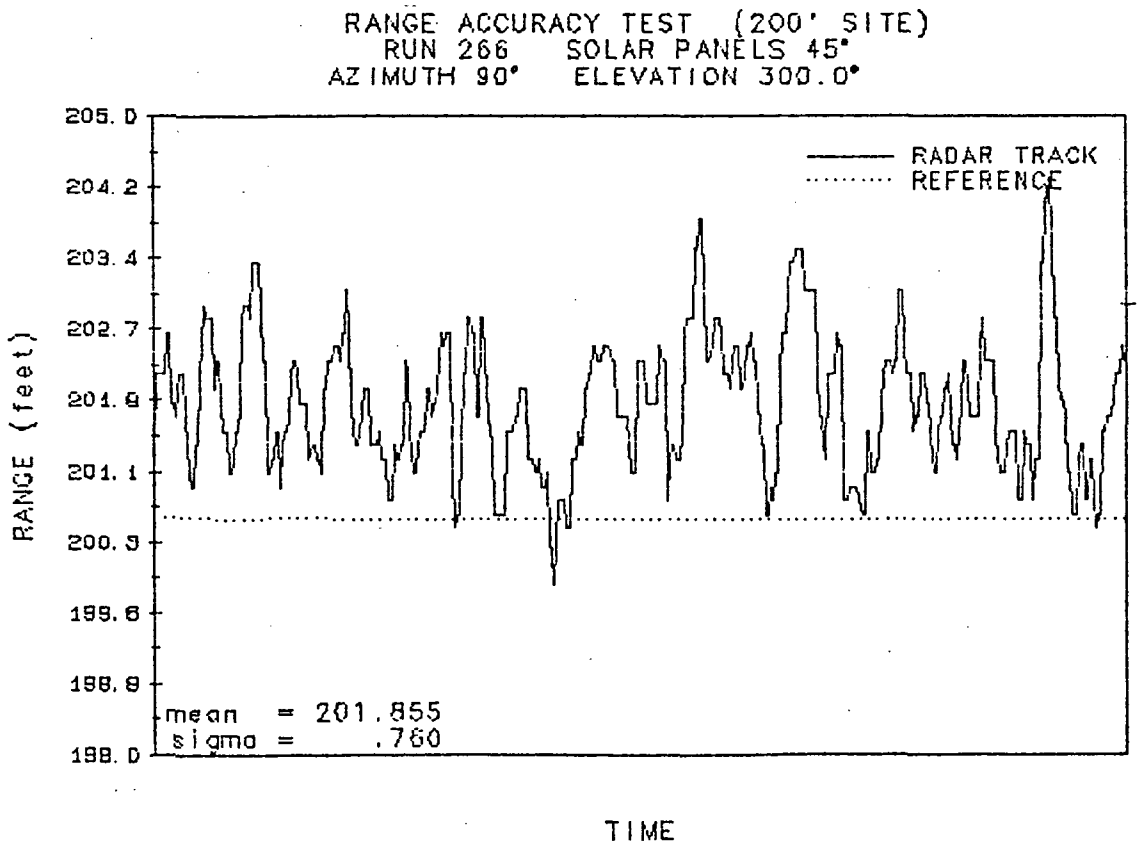

FIGURE 7-52. RANGE ACCURACY PLOTS, 200' SITE

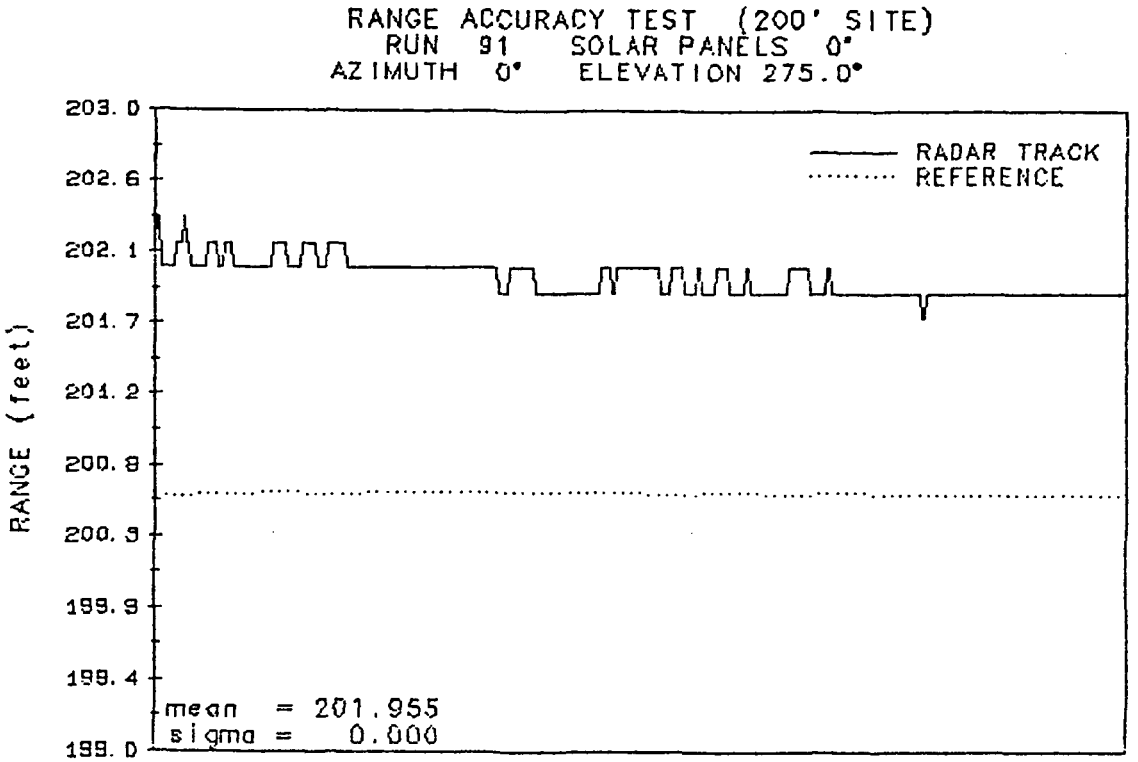

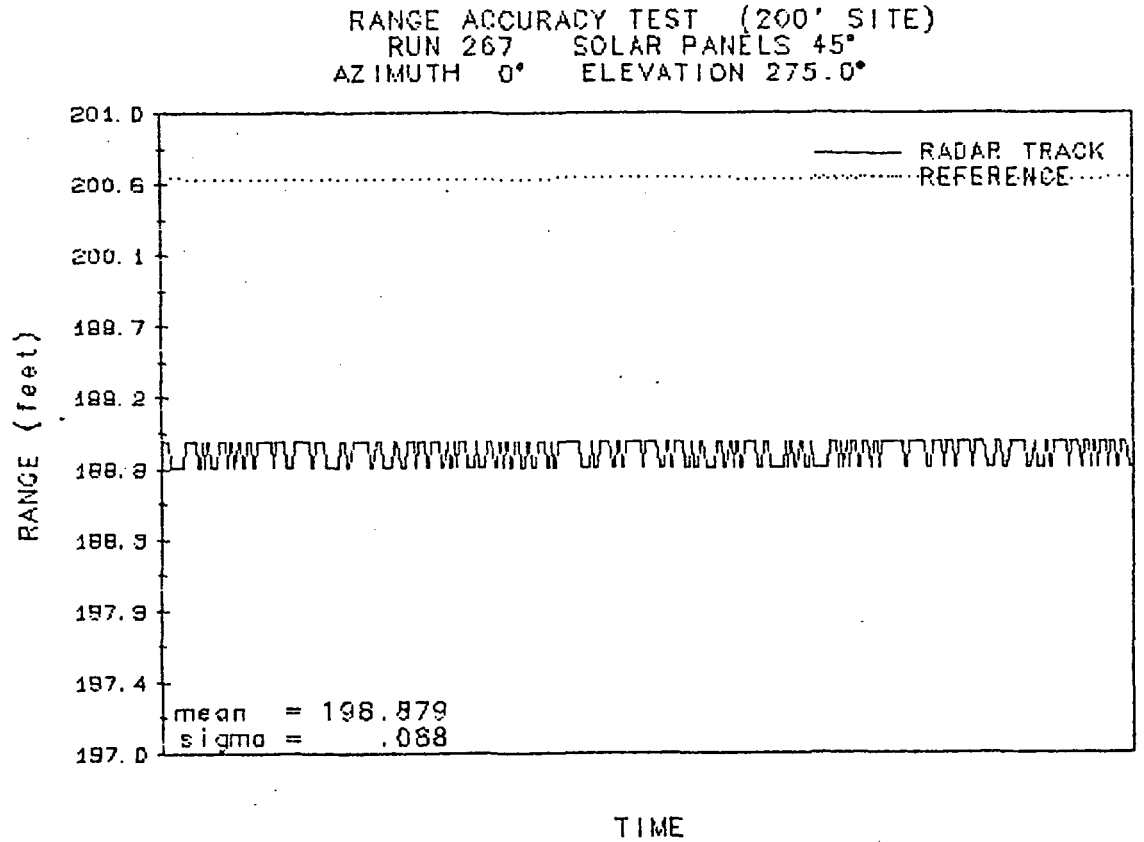

FIGURE 7-53. RANGE ACCURACY PLOTS, 200' SITE

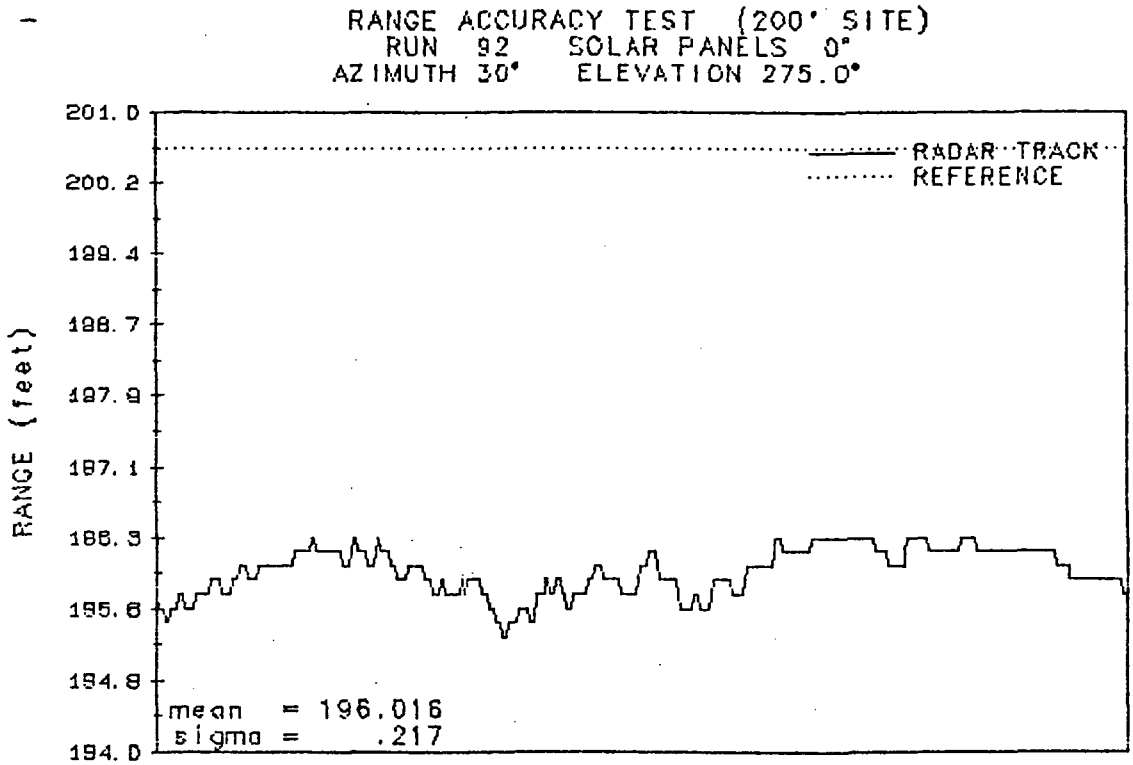

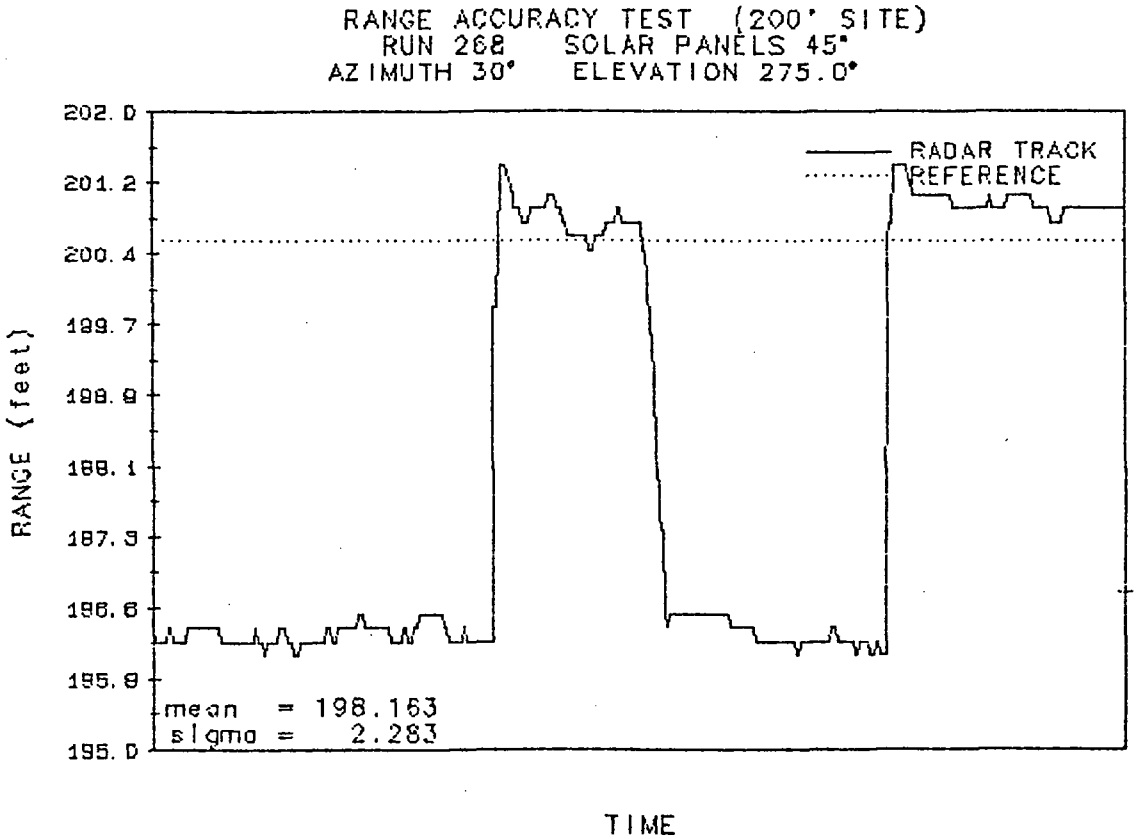

FIGURE 7-54. RANGE ACCURACY PLOTS, 200' SITE

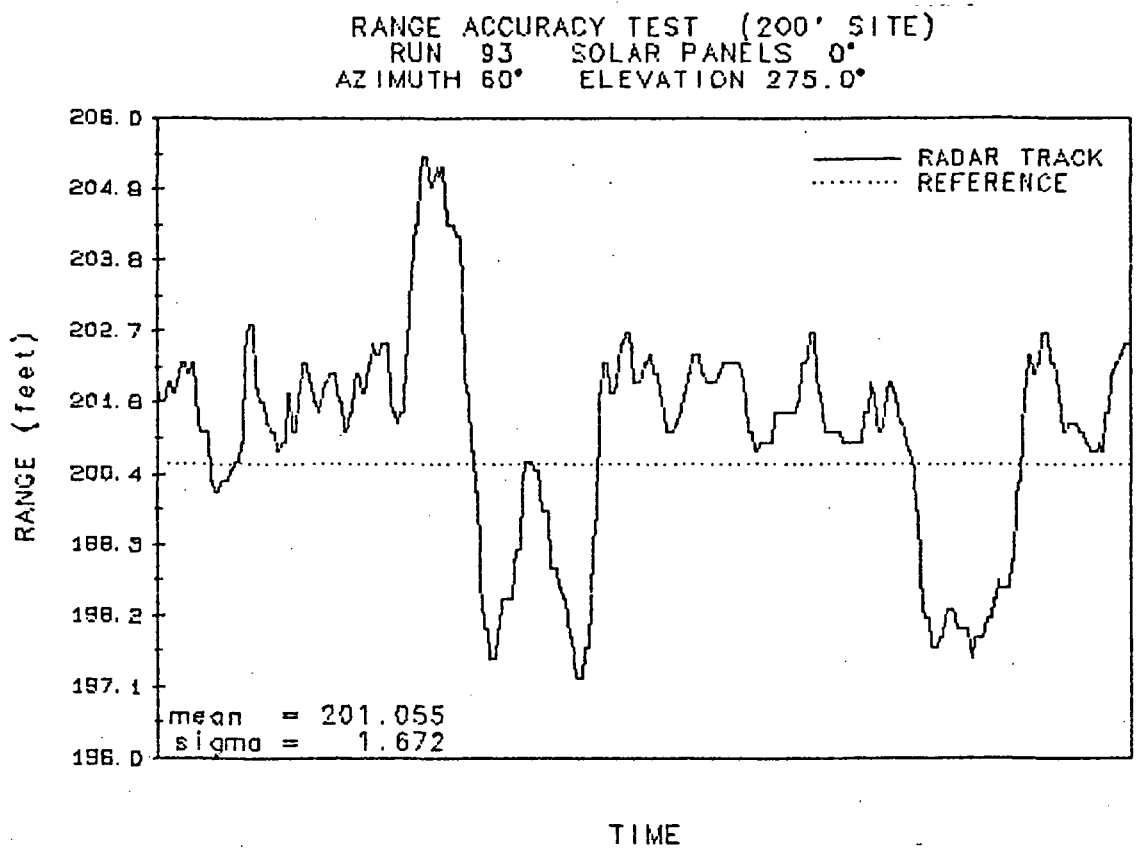

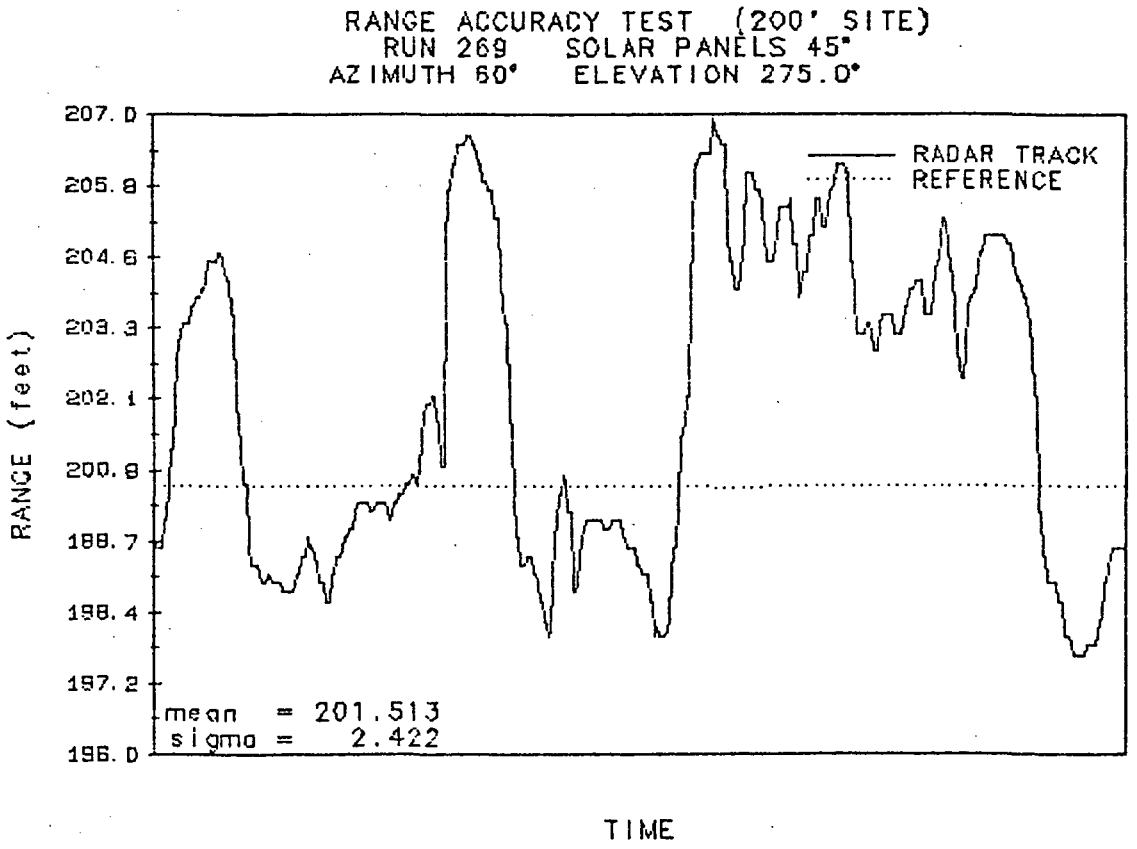

FIGURE 7-55. RANGE ACCURACY PLOTS, 200' SITE

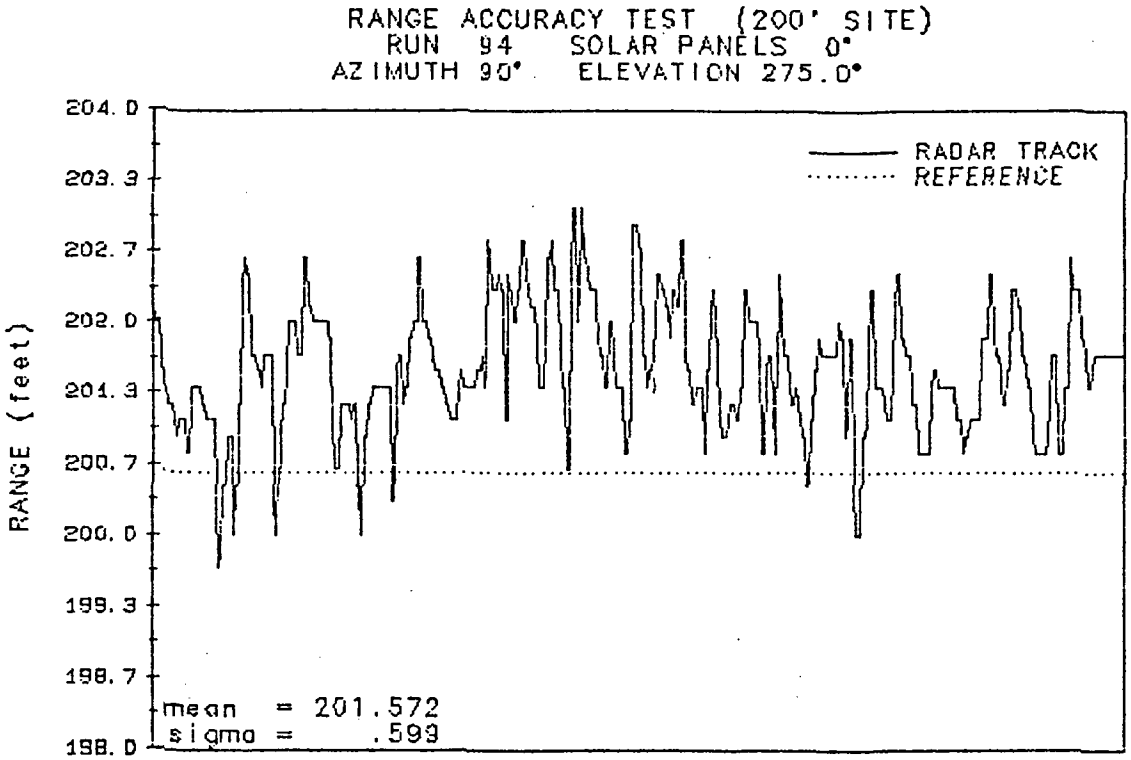

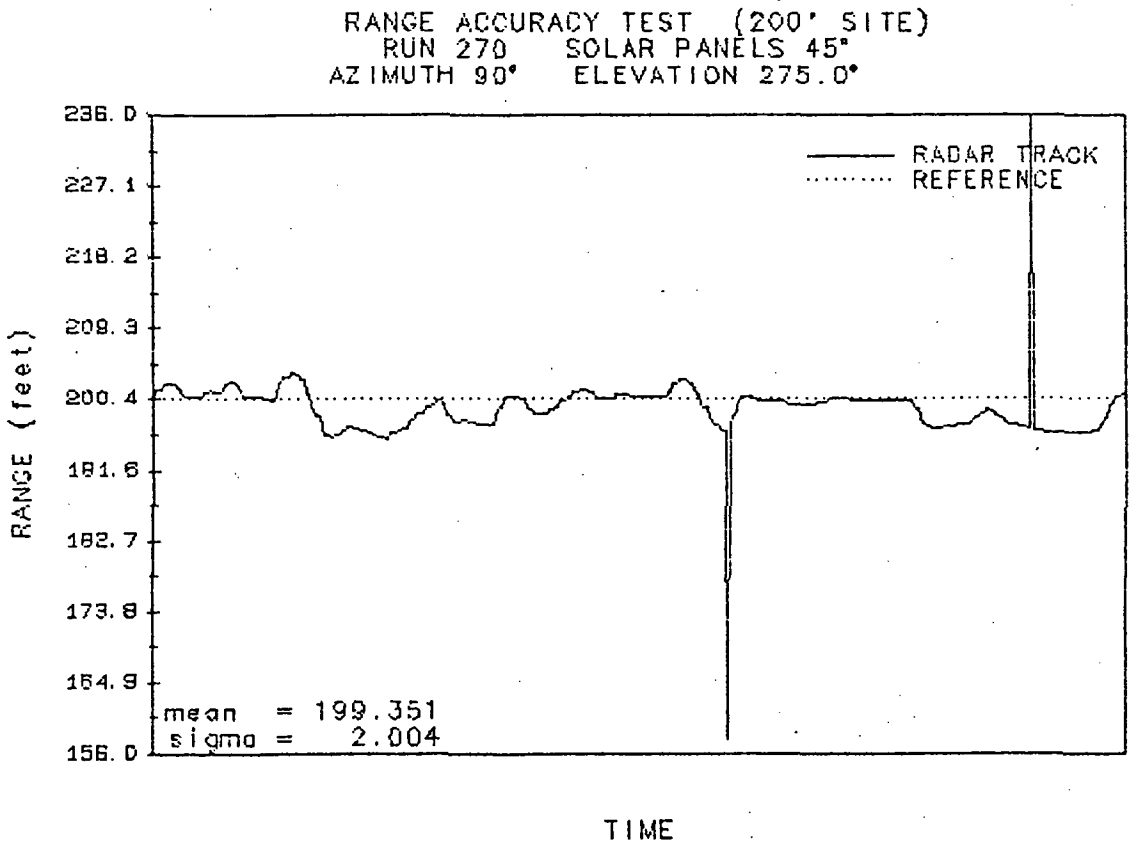

FIGURE 7-56. RANGE ACCURACY PLOTS, 200' SITE

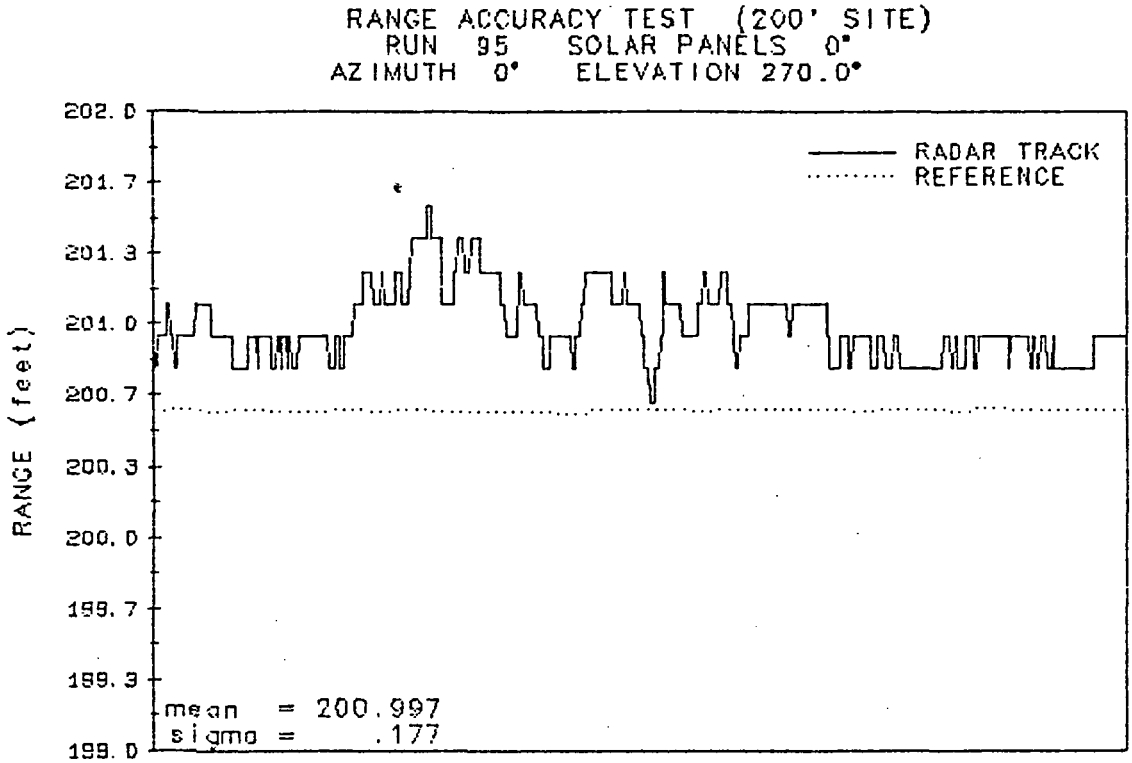

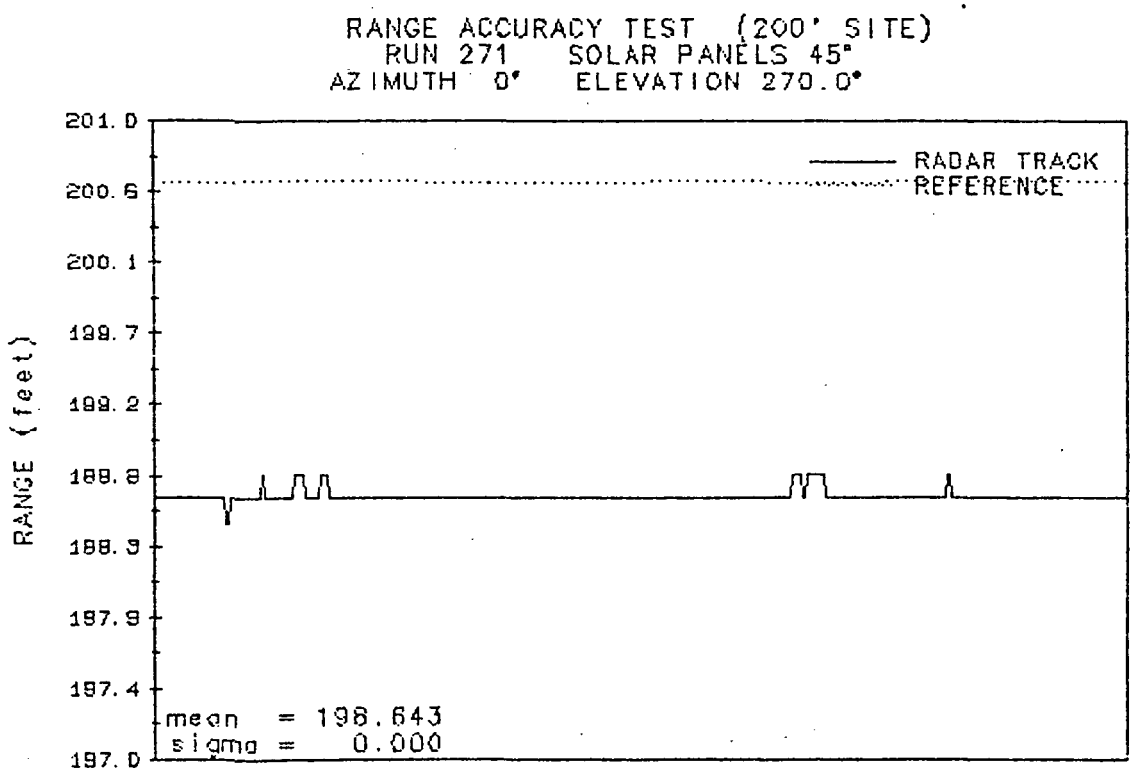

FIGURE 7-57. RANGE ACCURACY PLOTS, 200' SITE

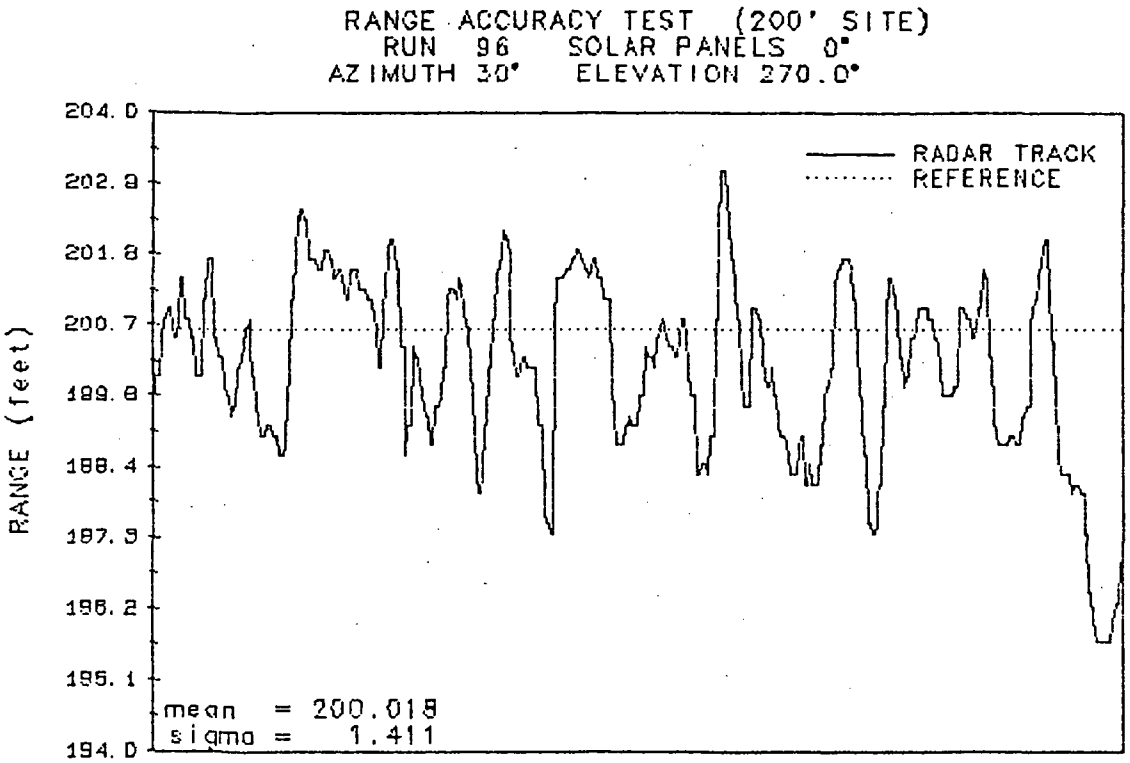

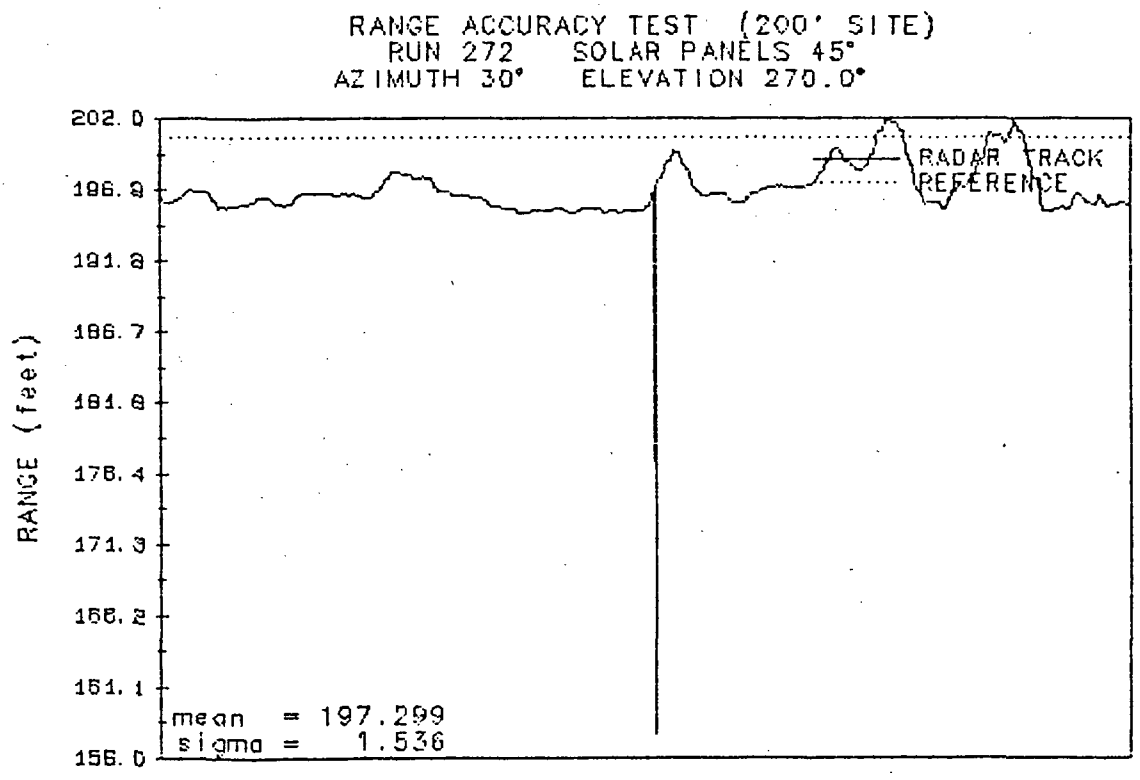

FIGURE 7-58. RANGE ACCURACY PLOTS, 200' SITE

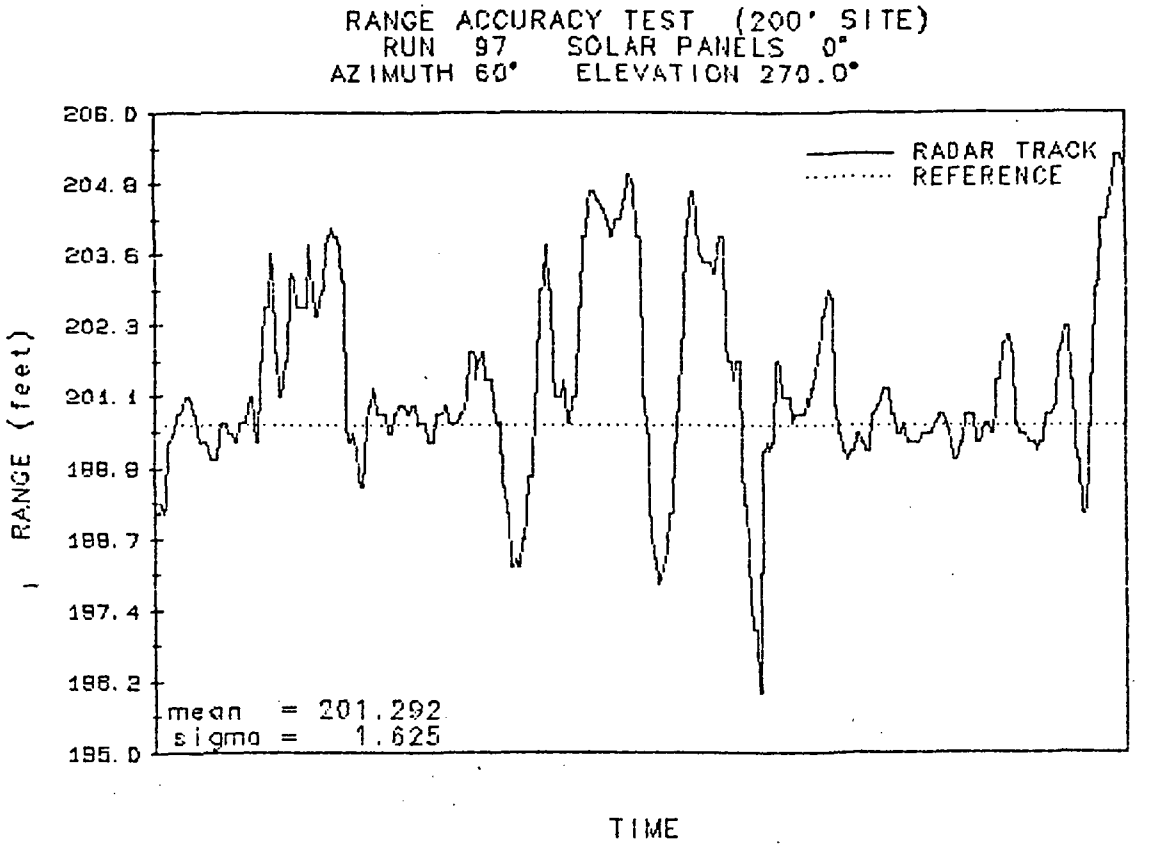

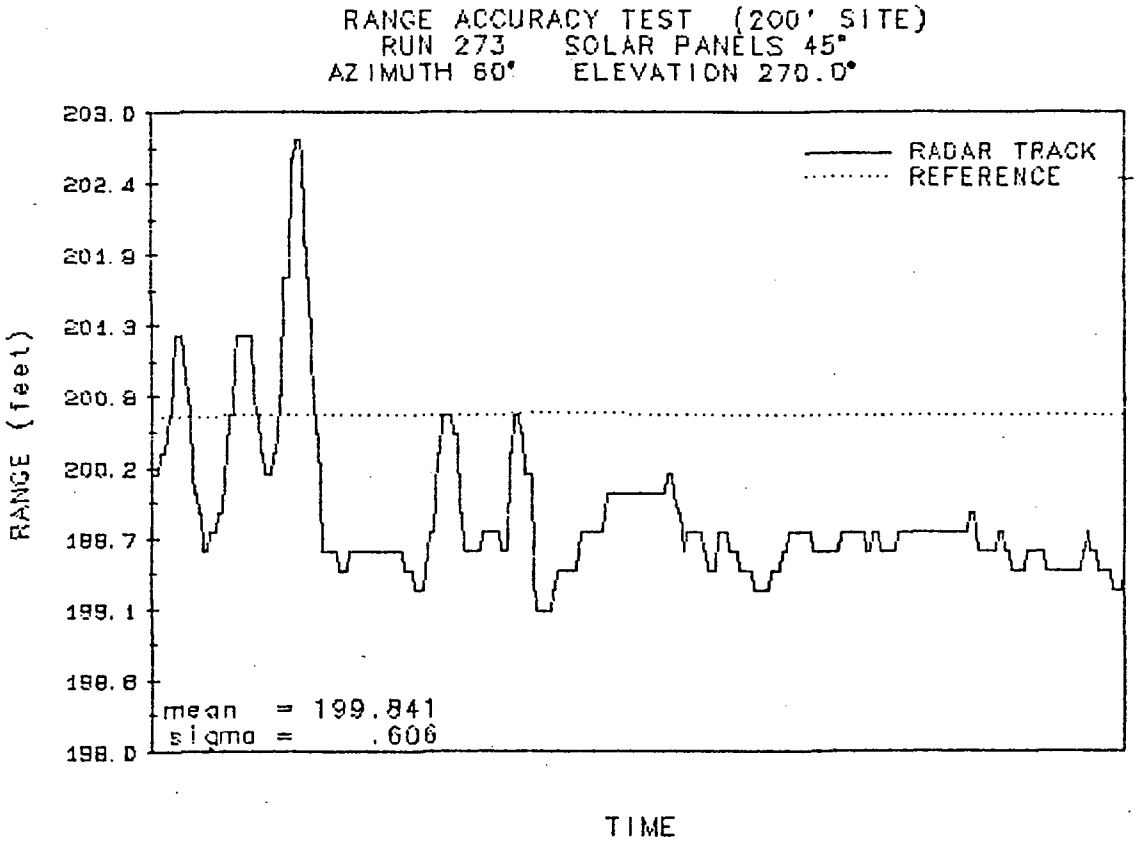

FIGURE 7-59. RANGE ACCURACY PLOTS, 200' SITE

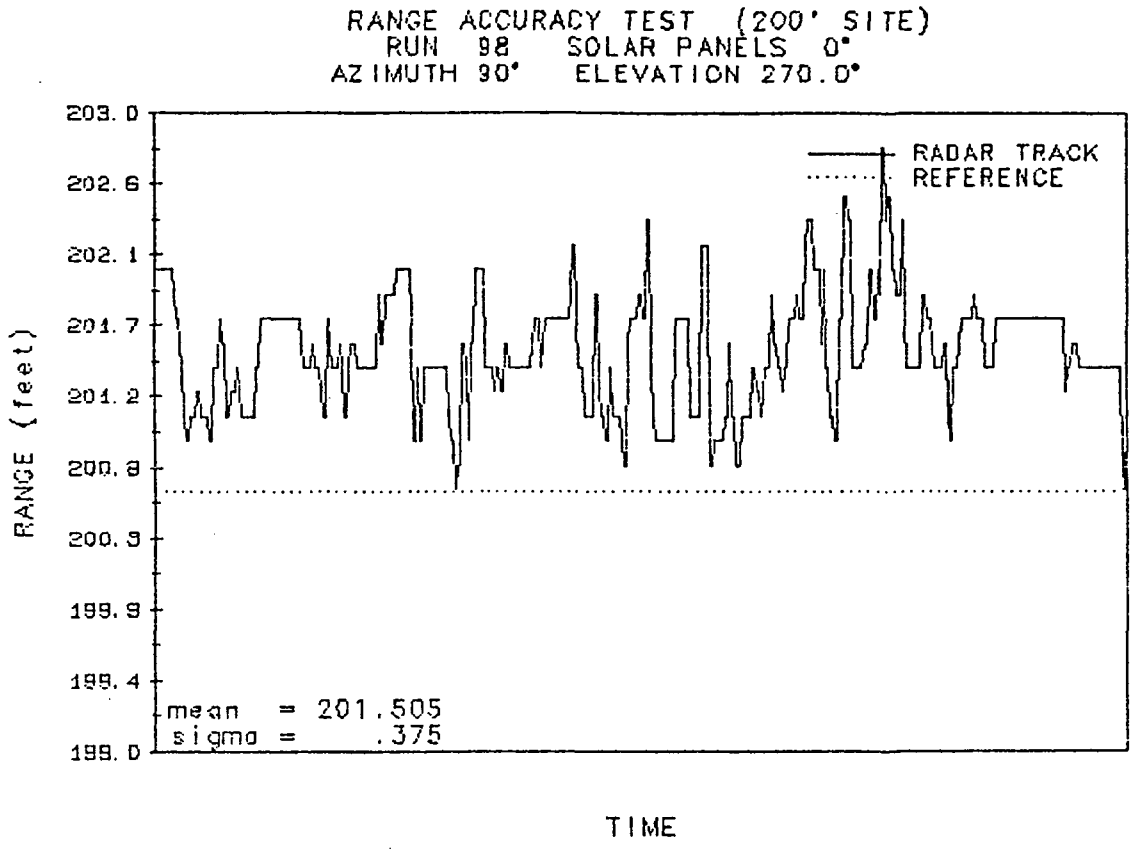

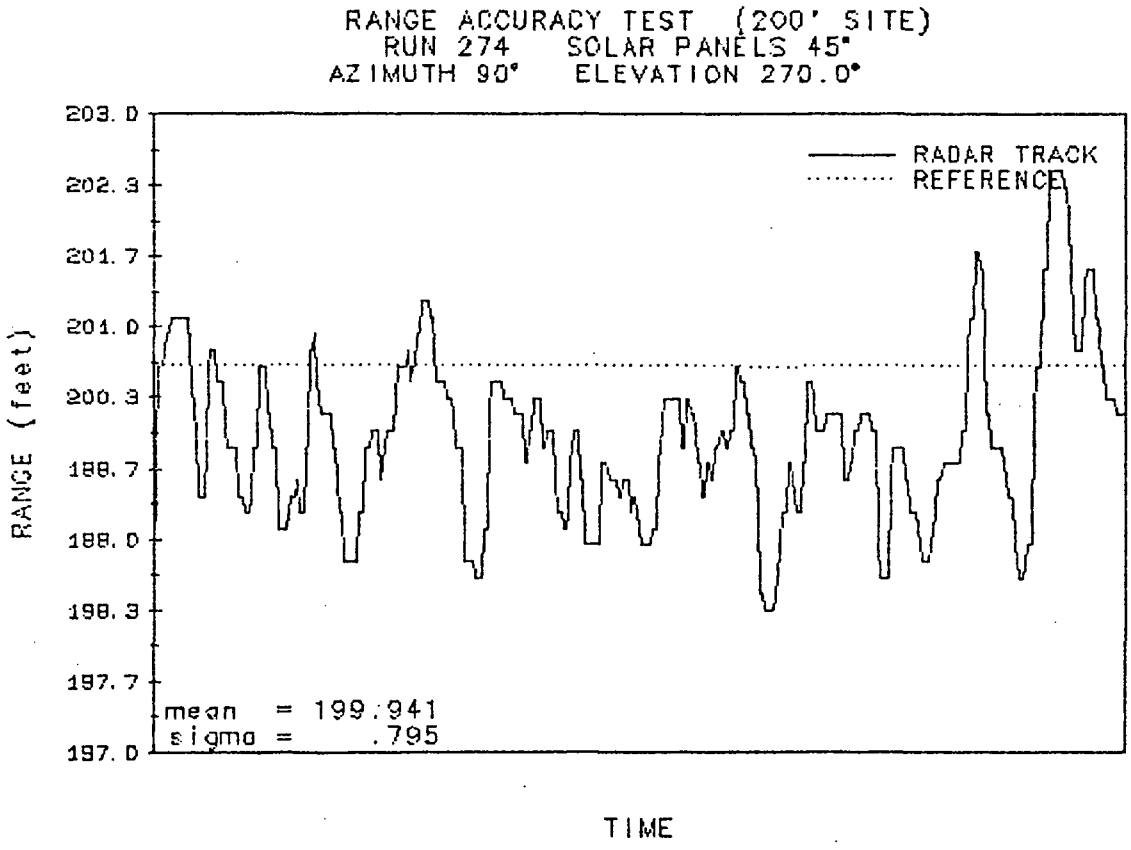

FIGURE 7-60. RANGE ACCURACY PLOTS, 200' SITE

Other plot characteristics noted:

Run 303 - Blank area is caused by loss of laser acquisition and subsequent loss of laser range data

Run 304 - The peak rate achieved was 2 fps. The low laser update rate causes "notchy" difference computation result

Run 305 - The peak rate achieved was 5 fps, with acceleration of up to .55 ft/sec^2. Solid radar track is indicated. The laser update rate is apparent in the rate plot

TABLE 7-3. TRACKING TEST RESULTS

TEST RUN	TEST RANGE	RANGE Δ, MEAN	RANGE σ	RATE ERROR, MEAN	RATE σ
302	350-300	-4.6′	.42	.016′/sec.	.039
303	300-250	-4.9′	.56	.025	.056
304	250-200	-5.2′	.61	.009	.085
305	200-130	-5.4′	.89	.009	.105

The trend in Table 7-3, Δ column, indicates the difference between the laser and radar range mesurements is increasing at the shorter ranges. Applying the geometric considerations derived in Section 5.2 for the range calibration, the difference in range measurements is calculated at the nominal midpoint of each test range using the center of the big end as the track point. The results of these calcultions are listed in Table 7-4.

TABLE 7-4. RANGE DIFFERENCES DUE TO SETUP GEOMETRY

RANGE	R DIFFERENCE
325	-5.25′
275	-5.19′
225	-5.10′
175	-4.97′

Per Table 7-4, the data trends for measured and calculated range differences have opposite slopes, apparently crossing over somewhere around the 250′ range point. This result seems to indicate a tracking point shift is also occurring. The shift would have to shorten the radar range; the tracking point must shift into the lower half of the big end.

The apparent increase in the rate error deviation with decreasing test range is coincidental. The higher testing rates, with attendant "notchy" laser rate updates in these test runs, produce larger steps in the rate error computation.

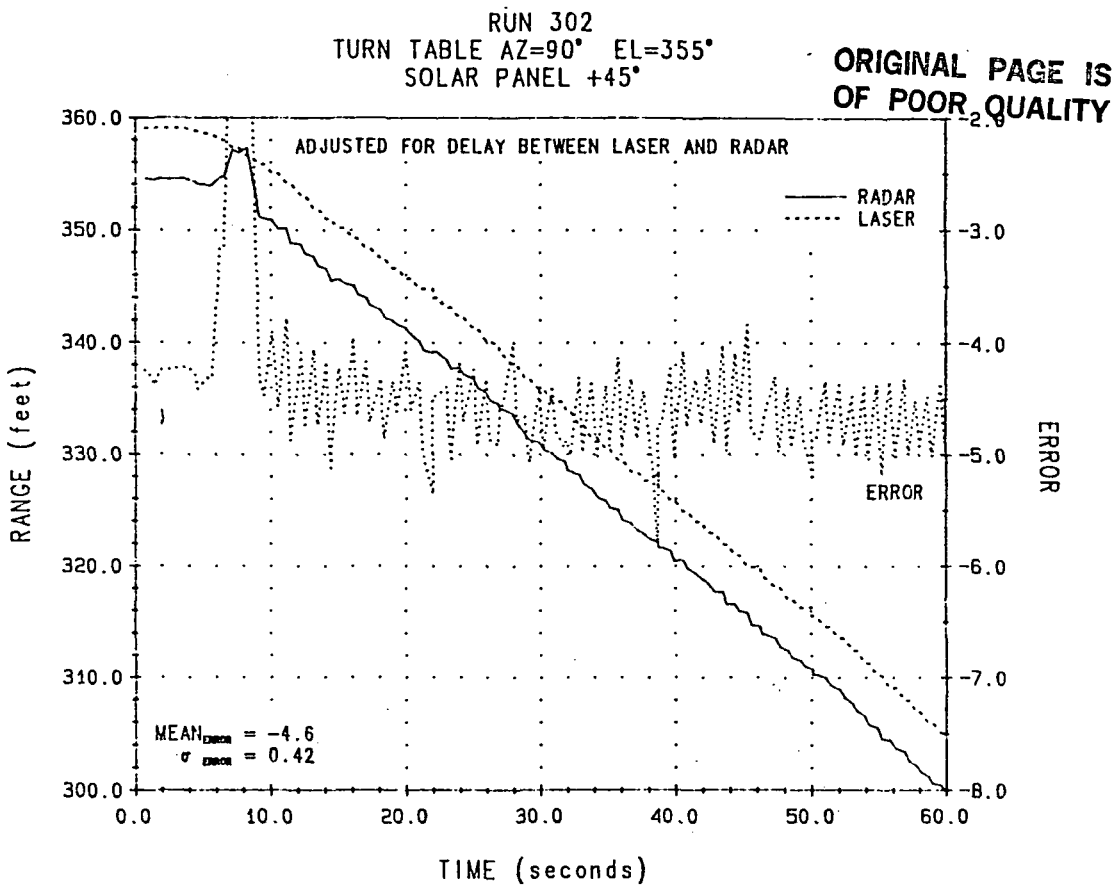

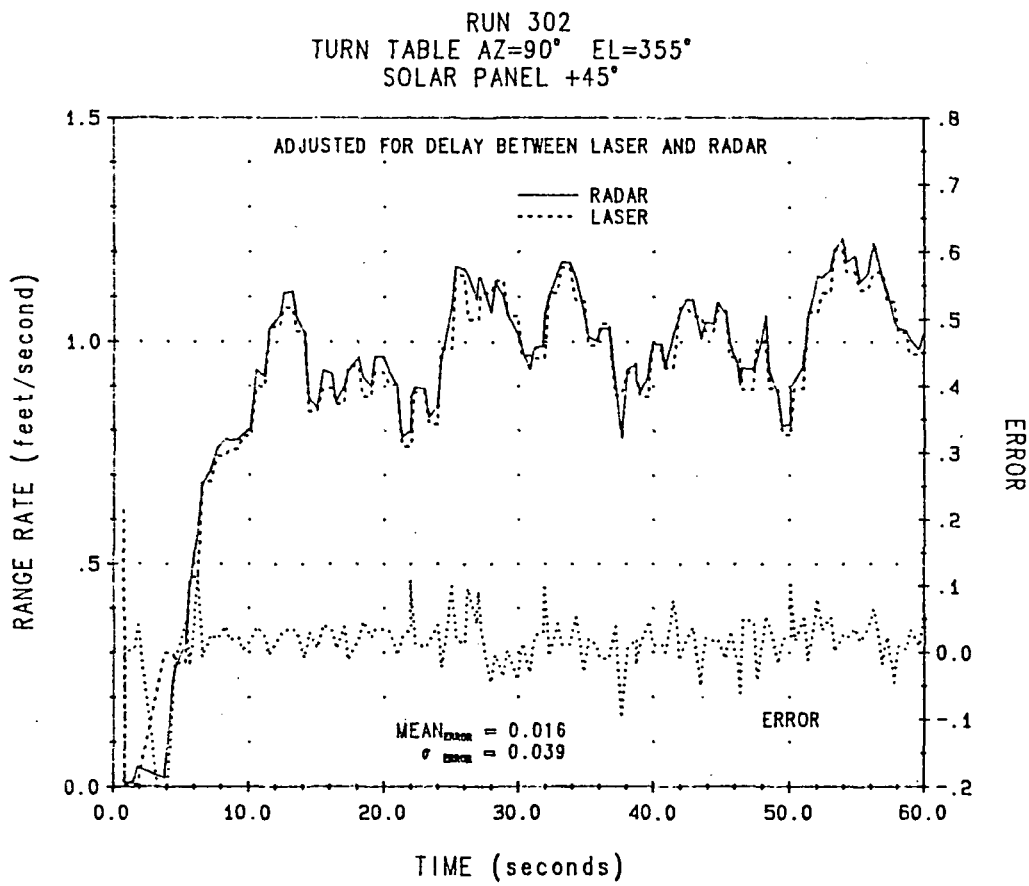

FIGURE 7-61. TRACKING TEST RUN 302

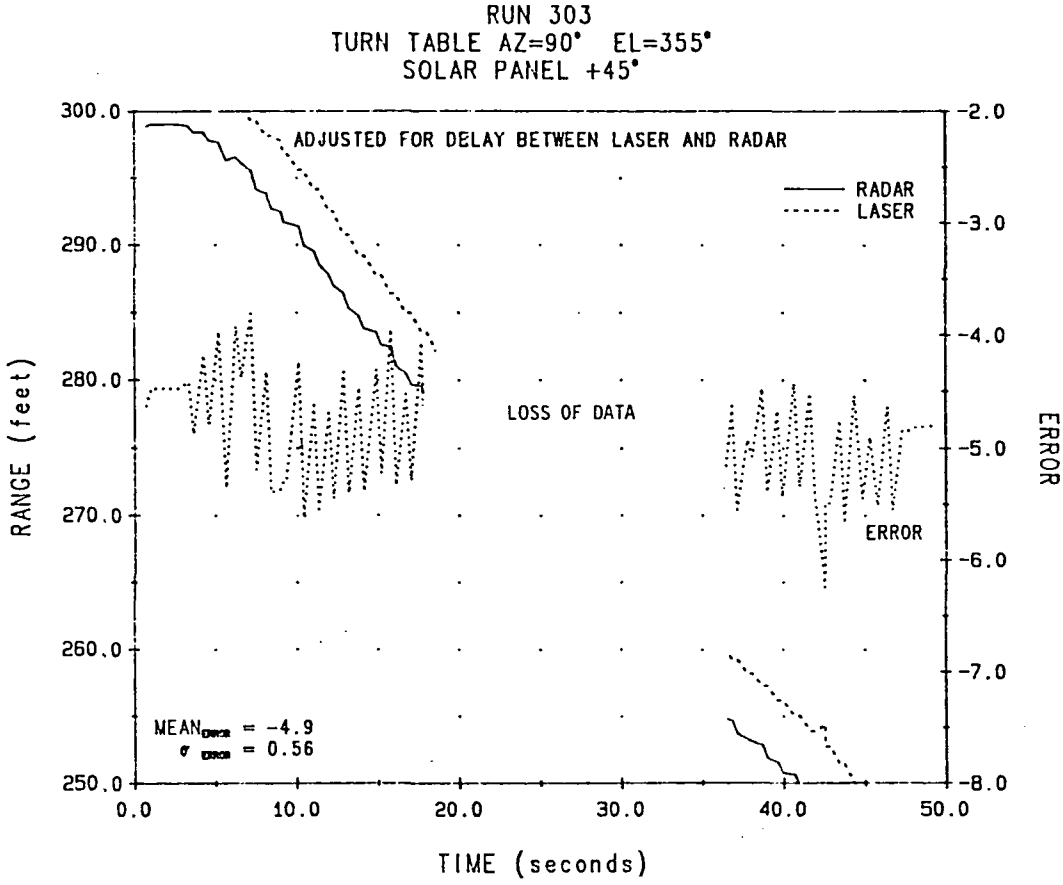

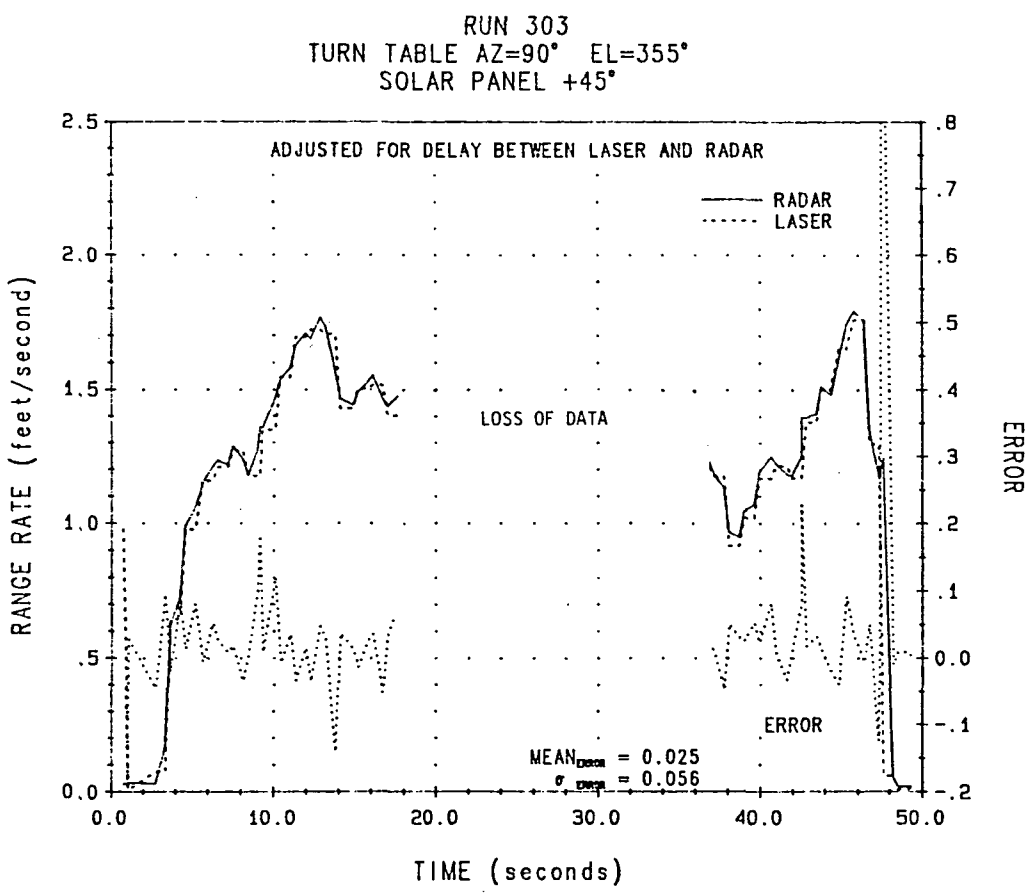

FIGURE 7-62. TRACKING TEST RUN 303

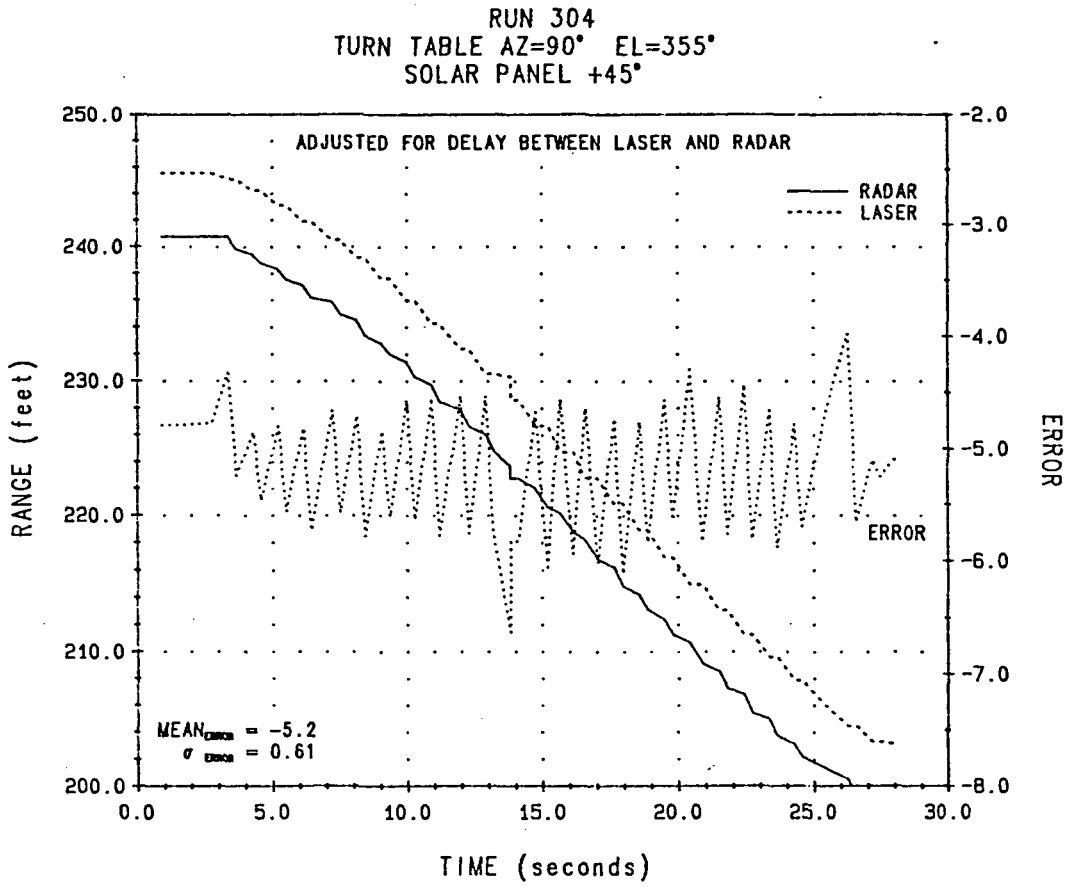

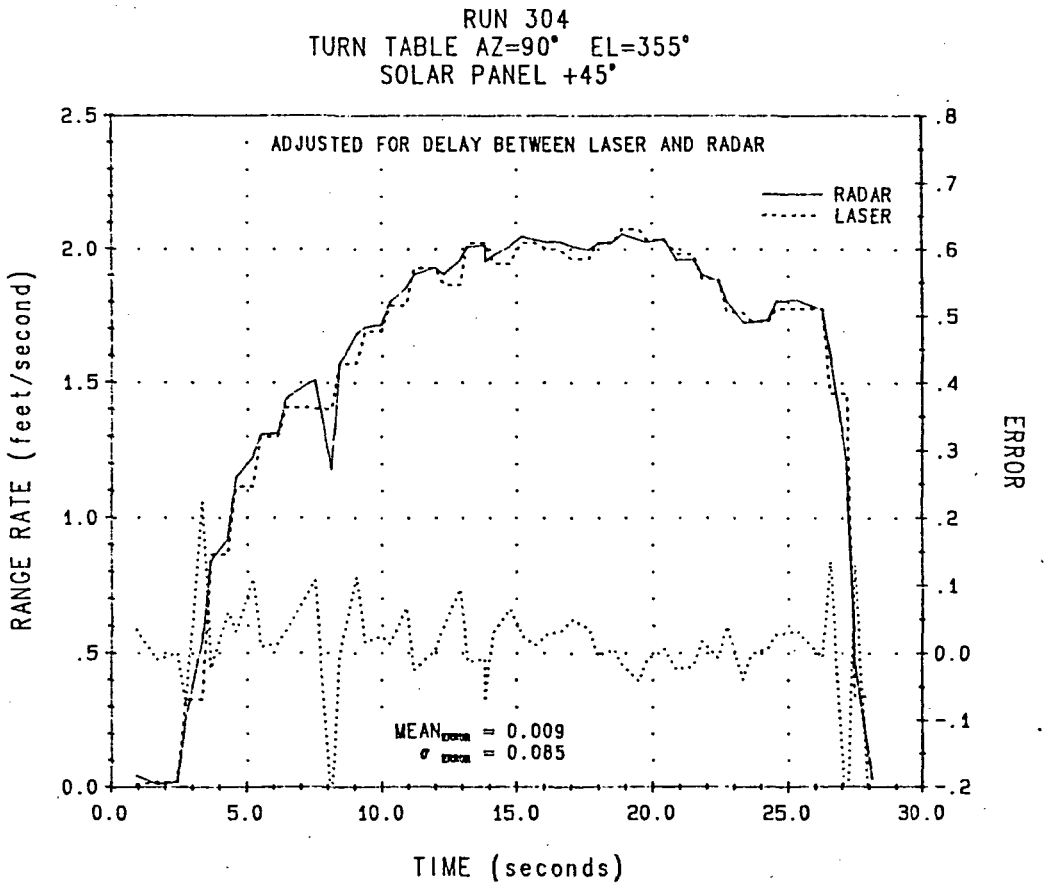

FIGURE 7-63. TRACKING TEST RUN 304

ORIGINAL PAGE IS
OF POOR QUALITY

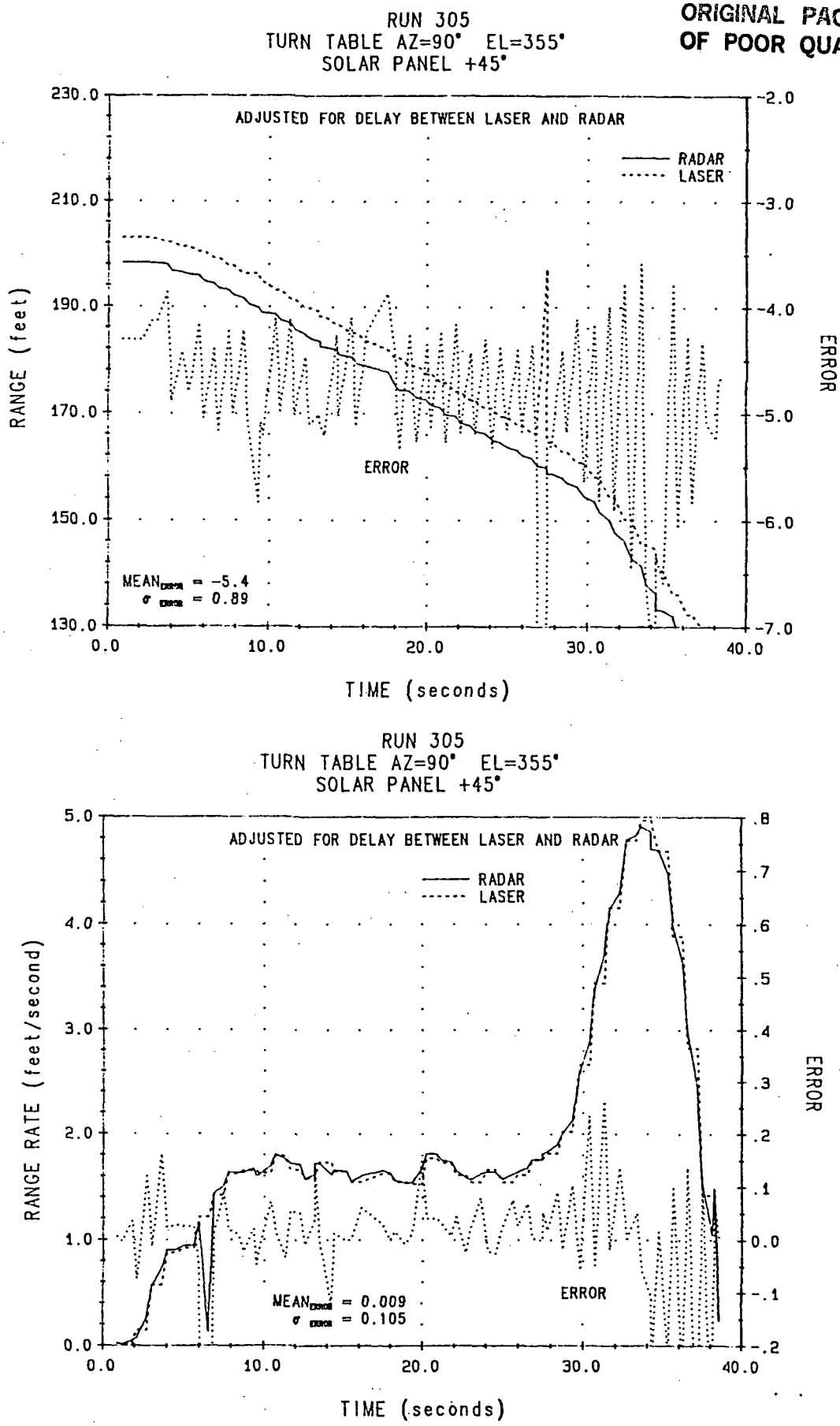

FIGURE 7-64. TRACKING TEST RUN 305